

Quorum sensing dynamics
in the α -proteobacterium *Sinorhizobium meliloti*
at the single-cell and population level

Kumulative Dissertation
zur Erlangung des Grades eines
Doktor der Naturwissenschaften
(Dr. rer. nat.)

dem Fachbereich Biologie
der Philipps-Universität Marburg

vorgelegt von
Diplom-Biologin
Vera Bettenworth
aus Siegen

Marburg an der Lahn, 2022

Originaldokument gespeichert auf dem Publikationsserver der
Philipps-Universität Marburg
<http://archiv.ub.uni-marburg.de>

Dieses Werk bzw. sein Inhalt steht unter einer
Creative Commons
Namensnennung
Keine kommerzielle Nutzung
Weitergabe unter gleichen Bedingungen
3.0 Deutschland Lizenz.

Die vollständige Lizenz finden Sie unter:
<http://creativecommons.org/licences/by-nc-sa/3.0/de/>

Die Arbeiten zur vorliegenden Dissertation wurden von November 2015 bis Januar 2022 unter der Betreuung von Frau Prof. Dr. Anke Becker an der Philipps-Universität Marburg in der Arbeitsgruppe „Vergleichende Genomik“ durchgeführt.

Tag der Einreichung: 4. März 2022

Vom Fachbereich Biologie der Philipps-Universität Marburg
(Hochschulkennziffer 1180) als Dissertation angenommen am 8. Juni 2022

Erstgutachter(in):	Prof. Dr. Anke Becker
Zweitgutachter(in):	Prof. Dr. Erhard Bremer
Drittgutachter(in):	Prof. Dr. Gert Bange

Tag der Disputation: 22. Juli 2022

Weitere Mitglieder der Prüfungskommission:

Prof. Dr. Michael Bölker
Prof. Dr. Victor Sourjik

Die in dieser Arbeit vorgestellten Ergebnisse sind im Rahmen folgender Artikel in Fachzeitschriften veröffentlicht oder zur Publikation eingereicht worden:

V. Bettenworth, M. McIntosh, A. Becker, B. Eckhardt. **Front-propagation in bacterial inter-colony communication.** *Chaos: An Interdisciplinary Journal of Nonlinear Science* 28, 106316 (2018).

V. Bettenworth, S. van Vliet, B. Turkowyd, A. Bamberger, H. Wendt, M. McIntosh, W. Steinchen, U. Endesfelder, A. Becker. **Frequency modulation of a bacterial quorum sensing response.** *Under review at Nature Communications.*

Des Weiteren wurde ein zentraler Aspekt des Forschungsgebiets in folgendem, ebenfalls in einer Fachzeitschrift veröffentlichten Übersichtsartikel behandelt:

V. Bettenworth, B. Steinfeld, H. Duin, K. Petersen, W. R. Streit, I. Bischofs, A. Becker. **Phenotypic heterogeneity in bacterial quorum sensing systems.** *Journal of Molecular Biology* 431, 4530-4546 (2019).

Table of Contents

Zusammenfassung	6
Summary.....	7
Abbreviations.....	8
1 Introduction	9
1.1 Quorum sensing – gene regulation by “hormone-like cell products”	9
1.2 “The languages of bacteria”: diversity in autoinducers and cognate receptors	10
1.3 Biotic and abiotic factors influencing quorum sensing processes	12
1.4 An unexpected discovery: phenotypic heterogeneity in quorum sensing	14
1.5 The model organism <i>S. meliloti</i> and its Sin quorum sensing system	17
2 Aim of this work: a better understanding of quorum sensing dynamics.....	19
3 Results	20
3.1 Front-propagation in bacterial inter-colony communication.....	20
3.2 Frequency modulation of a bacterial quorum sensing response	32
4 Discussion	89
4.1 Spreading the news: signal propagation over a distance	89
4.2 Stochastic pulsing in <i>sinI</i> expression	94
4.3 The mechanism: a regulatory system based on low probabilities.....	97
4.4 Postulated roles: information integration and collective decision-making	102
5 Conclusions	105
6 References	107
Appendix.....	122
Eidesstattliche Erklärung / <i>Statutory declaration</i>	122
Acknowledgements.....	123
Curriculum vitae.....	124

Zusammenfassung

Im Quorum Sensing produzieren Bakterien kleine Moleküle, die sich in der Umgebung anreichern, während die Population wächst. Erreichen die Moleküle eine Schwellenwertkonzentration, induzieren sie in den Zellen größere Verhaltensänderungen; sie werden deshalb als Autoinduktoren bezeichnet. Da man davon ausgeht, dass die entsprechenden Verhaltensweisen nur effektiv sind, wenn sie von einer großen Zahl von Zellen gemeinsam ausgeführt werden, gelten die Moleküle als Indikatoren für die Zelldichte. Quorum-Sensing-Systeme wurden in den meisten Bakterien identifiziert und umfassen eine Vielzahl an Autoinduktoren, Rezeptoren und Netzwerk-Architekturen. Hingegen ist nur wenig darüber bekannt, wie diese Komponenten dynamisch auf Einzelzellebene interagieren, um ihre Rolle in der Zell-Zell-Kommunikation zu erfüllen. Zudem wird Quorum Sensing oft in Flüssigkulturen studiert, die kontinuierlich geschüttelt werden, aber über die Ausbreitung von Autoinduktoren etwa in der Rhizosphäre, wo aktive Durchmischung vernachlässigbar ist, ist ebenfalls nur wenig bekannt. Ziel dieser Arbeit war es, diese Aspekte im Modellorganismus *Sinorhizobium meliloti* zu untersuchen.

In (Bettenworth et al., 2018) wurde die Ausbreitung von Autoinduktoren durch Diffusion in einer zweidimensionalen Umgebung erforscht. Auf den ersten Blick sollte Diffusion zu einer Verdünnung der Moleküle führen und die Geschwindigkeit, mit der sich die Schwellenwertkonzentration von der Quelle entfernt, stetig verlangsamen. In unseren Experimenten allerdings bewegte sich die Schwellenwertkonzentration mit konstanter Geschwindigkeit, vergleichbar der Frontausbreitung in musterbildenden Systemen. Dies ist unserem mathematischen Modell zufolge im exponentiellen Wachstum der Senderzellen begründet, das zu einer Überlagerung einer exponentiell wachsenden Zahl von Konzentrationsprofilen führt und so den Verdünnungseffekt der Diffusion kompensiert. In der Folge kann selbst eine einzelne Senderkolonie eine Antwort in mehr als 7 mm entfernten Empfängerzellen auslösen (Bettenworth et al., 2018).

In (Bettenworth et al., n.d.) wurde die Quorum-Sensing-Dynamik im Hinblick auf die Expression des Autoinduktor-Synthese-Gens in einzelnen Zellen und den zeitlichen Verlauf der Antwort in den entsprechenden Kolonien untersucht. Wir konnten zeigen, dass das Autoinduktor-Synthese-Gen in *S. meliloti* nicht kontinuierlich, sondern in asynchronen stochastischen Pulsen exprimiert wird, und dass die Stochastizität auf der Seltenheit und vermutlich auch der geringen Affinität des Transkriptionsaktivators für den Promotor beruht. Physiologische Faktoren modulieren die Häufigkeit dieses Aktivators oder seine Affinität zum Promotor und damit die Frequenz der Genexpressionspulse. Höhere oder niedrigere Pulsfrequenz wiederum führt zu einer Quorum-Sensing-Antwort bei niedrigeren beziehungsweise höheren Zellzahlen. Mit anderen Worten: Quorum Sensing in *S. meliloti* basiert auf einem stochastischen Regelkreis, der den physiologischen Zustand der einzelnen Zellen in der Pulsfrequenz kodiert, mit der das Autoinduktor-Synthese-Gen exprimiert wird. Die Pulsfrequenzen aller Zellen werden im gemeinsamen Autoinduktor-Pool integriert, und nur wenn dieses Votum den Schwellenwert überschreitet, wird das Antwort-Verhalten ausgelöst. Folglich dient Quorum Sensing in *S. meliloti* weniger der Zellzahlbestimmung, wie es die Analogie des Quorums suggeriert, sondern ähnelt eher einer Abstimmung innerhalb der Gemeinschaft (Bettenworth et al., n.d.).

Summary

In quorum sensing, bacteria produce and release so-called autoinducers that accumulate in the environment while the cells grow. Once these molecules reach a threshold concentration, they trigger major behavioral changes in the population. Since the triggered behaviors are thought to be effective only when performed by a large enough group, autoinducers are generally taken to indicate when this sufficient cell density has been reached. Quorum sensing systems have been identified in most bacterial species, comprising a variety of autoinducers, receptors and network architectures. However, little is known about how these components interact dynamically at the single-cell level to fulfill their task of cell-cell communication. Furthermore, quorum sensing is often studied in well-shaken liquid cultures, but little is known about autoinducer dispersal and response dynamics over larger distances in physiological niches like the rhizosphere where active mixing is negligible. The aim of this work therefore was to investigate these aspects in the model organism *Sinorhizobium meliloti*.

In (Bettenworth et al., 2018), the dynamics of autoinducer dispersal by diffusion in a two-dimensional environment were explored. At first sight, diffusive spreading should yield a dilution of the molecules and, with increasing distance from the source, slow down progression of the concentration level necessary to trigger a response in distantly located receiver cells. In contrast to this expectation, however, this threshold concentration did not decelerate in our experiments, but instead travelled with constant speed, comparable to front propagation in pattern-forming systems. According to our mathematical model, this effect was due to the exponential growth of the sender cells which yielded adding-up of an exponentially growing number of autoinducer concentration profiles, thus compensating for the thinning effect of diffusion. Consequently, even a single sender colony could induce a response in receiver cells up to 7 mm away (Bettenworth et al., 2018).

In (Bettenworth et al., n.d.), quorum sensing dynamics were investigated on a smaller scale, namely with respect to autoinducer synthase gene expression in single cells and the timing of the response in the respective colonies. We could show that in *S. meliloti* the autoinducer synthase gene is not expressed continuously, but in discrete stochastic pulses, and that stochasticity stems from scarcity and, presumably, low binding affinity of the essential transcription activator. Physiological factors modulate abundance of this activator or its binding affinity to the autoinducer synthase gene promoter and thereby modulate gene expression pulse frequency. Higher or lower pulse frequencies in turn trigger the onset of the quorum sensing response at lower or higher cell numbers, respectively. In other words: *S. meliloti* quorum sensing is based on a stochastic regulatory system that encodes each cell's physiological condition in the pulse frequency with which it expresses its autoinducer synthase gene; pulse frequencies of all members of a population are then integrated in the common pool of autoinducers. Only if this vote crosses the threshold, the response behavior is initiated. Consequently, *S. meliloti* quorum sensing is not so much a matter of counting cell numbers as suggested by the analogy of the quorum, but more comparable to a voting in a local community, or the collective decision-making described for social insects (Bettenworth et al., n.d.).

Abbreviations

AHL	<i>N</i> -acyl-homoserine lactone
AI-2	autoinducer-2
bp	base pairs
cAMP	3',5'-cyclic adenosine monophosphate, cyclic AMP
c-di-GMP	3',5'-cyclic dimeric guanosine monophosphate, cyclic di-GMP
cfu	colony forming units
CRP	cAMP receptor protein; also CAP (catabolite activator protein) or CLR (CRP-like protein)
CSP	competence-stimulating peptide
DNA	deoxyribonucleic acid
EMSA	electrophoretic mobility shift assay
EPS	exopolysaccharide
GB1	immunoglobulin-binding domain of streptococcal protein G (a solubility tag)
HL	homoserine lactone; also HSL
IPTG	isopropyl β -D-thiogalactopyranoside (synthetic inducer of the <i>lac</i> promoter)
mRNA	messenger ribonucleic acid
ppGpp	guanosine-3'-diphosphate-5'-diphosphate, guanosine tetraphosphate
pppGpp	guanosine-3'-diphosphate-5'-triphosphate, guanosine pentaphosphate
wt	wild type or wild-type

Standardized abbreviations, SI units and one letter or three letter codes for amino acids are used without further reference.

1 Introduction

Bacteria are typically well-equipped for adapting to environmental changes or different stages of life: With the exception of specialists like endosymbionts or parasites that live in unusually constant environments and often possess less than a dozen regulatory genes, they frequently harbor hundreds of genes whose products have sensory or regulatory functions, accounting for up to 10% of their genomes (Unden, 2014). Some of the respective regulatory systems are very specific and have only a narrow sphere of action. But there are several others that have a multitude of targets and coordinate major systematic transitions in gene expression and behavior. E.g., the stringent response alarmones guanosine tetraphosphate and guanosine pentaphosphate (ppGpp and pppGpp, respectively) target key enzymes in nucleotide synthesis, DNA replication, transcription and translation, collectively procuring a slow-growing phenotype (Irving et al., 2020; Steinchen & Bange, 2016); the nucleotide second messenger cyclic-AMP (cAMP) is bound by the cAMP receptor protein (CRP) or homologs thereof that can then interact with numerous target promoters, primarily redirecting transcription towards alternative catabolic pathways (Botsford & Harman, 1992; Gancedo, 2013); the nucleotide second messenger cyclic-di-GMP (c-di-GMP) in turn binds to enzymes, transcription factors and riboswitches, amongst other things promoting a motile-to-sessile lifestyle switch (Jenal et al., 2017; Römling et al., 2013); and various alternative sigma factors can replace the housekeeping sigma factor in the RNA polymerase holoenzyme, thereby redirecting transcription to their particular sets of target genes (Feklistov et al., 2014; Lonetto et al., 2019; Paget, 2015). Quorum sensing – the reaction to small diffusible or secreted molecules that the cells themselves beforehand produced – is yet another bacterial way of altering gene expression on a larger scale, inducing far-reaching behavioral changes towards, e.g., virulence or biofilm formation.

1.1 Quorum sensing – gene regulation by “hormone-like cell products”

Quorum sensing regulatory systems per definition exhibit a strong influence of population density: The molecules mediating the effect are produced by the bacteria, accumulate in the environment while the population grows, and trigger activation of target genes and behaviors once they reach a threshold concentration correlating with higher cell densities (Fig. 1).

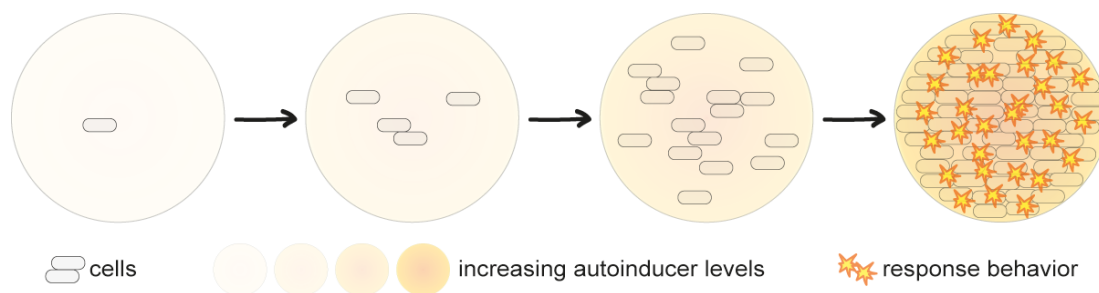


Figure 1. Cell density and quorum sensing. The cells produce so-called autoinducers, and autoinducer concentrations rise with cell density. Once autoinducer levels reach a threshold concentration, they trigger species-specific response behavior, e.g., bioluminescence (Keller & Surette, 2006).

The connection between cell density and behavior was first discovered in the early 1960s when two groups independently reported that genetic competence in streptococci (Pakula & Walczak, 1963) and pneumococci (now *Streptococcus pneumoniae*) (Tomasz & Hotchkiss, 1964) was governed by a macromolecular factor produced by cultures of a certain density and transferable via sterile culture supernatants or crude extracts. As this factor propagated a physiological state within the population, it was interpreted as a “hormone-like cell product” and thus a form of intercellular communication allowing a population of physically distinct cells to behave as a biological unit – analogous to the hormonal control of differentiation processes until then only associated with higher organisms (Tomasz, 1965).

Shortly after, it was shown that the lag phase preceding the production of bioluminescence by *Photobacterium fischeri* (now *Aliivibrio fischeri*) in liquid cultures could be abolished by growing cells not in fresh medium, but in medium that had been “conditioned” by preliminary exposure to bacteria (Kempner & Hanson, 1968); the higher the optical density of the cultures conditioning the medium, the shorter the bioluminescence-lag of the ensuing cultures turned out to be (Eberhard, 1972). Since the conditioning of the medium was attributed to the bacteria, and since bioluminescence was thus regarded as self-induced by the cells, the phenomenon was termed “autoinduction” (Neelson et al., 1970), and the corresponding activators were termed “autoinducers”.

Autoinduction, it was later concluded, allowed *A. fischeri* to discriminate between its free-living state in the ocean where the bacterium is found at densities of less than 10^2 cells per ml, and its host-associated state in the light organs of squids where it reaches cell densities of 10^8 or more and where the bacteria are provided with nutrients in return for their light emission camouflaging the host (Fuqua et al., 1994; Neelson, 1977; Ruby & McFall-Ngai, 1992). As by then several homologous or potentially homologous regulatory systems from other, sometimes only distantly related Gram-negative bacteria had been reported whose target behaviors likewise appeared to be linked to high cell densities, a common theme was deduced: Certain bacterial behaviors, it was argued, could only be performed efficiently by large enough groups, and autoinduction provided the means to determine when this “minimum behavioral unit” or “quorum” was reached (Fuqua et al., 1994). Subsequently, “quorum sensing” (Fuqua et al., 1994) became the far more popular term for the process.

1.2 “The languages of bacteria”: diversity in autoinducers and cognate receptors

Today quorum sensing is regarded as almost omnipresent in bacteria – for many species, at least one such regulatory system has been described, and even several quorum sensing systems operating in parallel are not unusual (Hense & Schuster, 2015; Keller & Surette, 2006; Whiteley et al., 2017). Both the regulatory circuits governing synthesis of and response to autoinducers and the chemical nature of the respective autoinducer molecules are highly diverse (Keller & Surette, 2006; Whiteley et al., 2017). Nevertheless, certain patterns are discernable: Gram-positive bacteria typically produce oligopeptide autoinducers for intra-species communication (Fig. 2A, upper left) whose precursors are encoded by short open reading frames, cleaved and

often post-translationally modified (Bassler & Losick, 2006; Monnet et al., 2014; Neiditch et al., 2017). In Gram-negative bacteria, *N*-acyl homoserine lactones (AHLs) produced from *S*-adenosyl-methionine and an acyl chain presented by an acylated acyl carrier protein are the most prevalent class of intra-species autoinducers (Fig. 2A, lower left) (Bassler & Losick, 2006; Pappenfort & Bassler, 2016; Watson et al., 2002). And in both Gram-negative and Gram-positive bacteria, the so-called autoinducer-2 (AI-2) (Fig. 2A, right), a family of molecules which in many bacteria spontaneously arise from a by-product of the activated methyl cycle, has been suggested for inter-species communication (Bassler & Losick, 2006; Hardie & Heurlier, 2008).

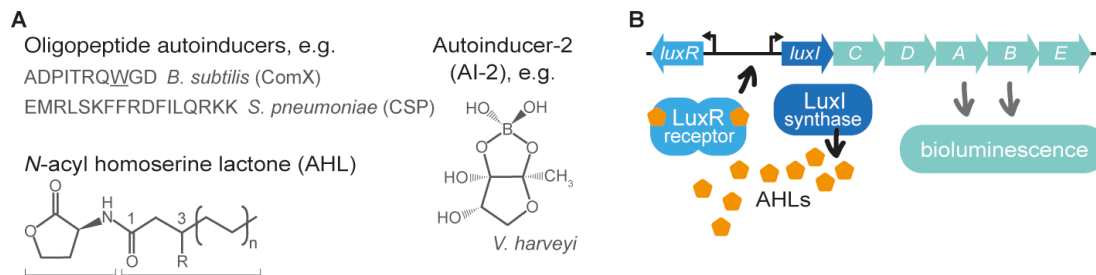


Figure 2. “The languages of bacteria” (Schauder & Bassler, 2001) and canonical Gram-negative quorum sensing. (A) Gram-positive bacteria typically communicate via oligopeptide autoinducers (upper left; letters indicate amino acids in single letter code, the underlined tryptophan is post-translationally modified; CSP, competence-stimulating peptide). In Gram-negative bacteria, *N*-acyl homoserine lactones (AHLs, lower left; brackets indicate the homoserine lactone ring and the acyl chain, respectively; R, hydrogen-, oxo- or hydroxy-substituent) are most common for intra-species communication. The so-called autoinducer-2 (AI-2, right) has been suggested for inter-species communication in both Gram-negative and Gram-positive bacteria. Oligopeptide autoinducers redrawn from (Monnet et al., 2014), AHL from (Keller & Surette, 2006), AI-2 from (Whiteley et al., 2017). (B) In the Lux quorum sensing system of *A. fischeri*, the synthase LuxI produces AHLs that bind to the transcription factor LuxR. LuxR then boosts transcription of *luxI*, and of the *luxCDABE* genes required for bioluminescence (Whiteley et al., 2017).

The paradigmatic quorum sensing system for Gram-negative intra-species communication is the Lux system of *A. fischeri* (Fig. 2B): Here, the synthase LuxI produces short-chain AHLs that bind to the receptor LuxR. The LuxR-AHL complex then facilitates expression of the *lux* operon comprising the AHL synthase gene – thus exerting a positive feedback on AHL production – and the *luxCDABE* genes required for bioluminescence (Dunlap, 1999).

Quorum sensing systems homologous to the Lux system have been described for many other Gram-negative species (Case et al., 2008; Pappenfort & Bassler, 2016). Their AHLs share the homoserine lactone ring, but differ in their acyl chains with respect to length and modifications like oxo- or hydroxy substituents on the third carbon of the acyl chain, or the presence of one or more double bonds (Fig. 2A, lower left) (Churchill & Chen, 2011; Frederix & Downie, 2011; Watson et al., 2002). AHLs with shorter chain length have been found to easily diffuse into and out of the cell (Kaplan & Greenberg, 1985; Pearson et al., 1999), whereas impeded diffusion and active transport have been described for AHLs with longer acyl chains (Krol & Becker, 2014; Pearson et al., 1999). AHLs are typically bound with high specificity by their cognate LuxR-type transcription regulators; the latter commonly operate as homodimers, binding the autoinducers at the N-terminal domains, and their usually palindromic DNA recognition sites

by helix-turn-helix motifs at the C-termini (Churchill & Chen, 2011; Papenfort & Bassler, 2016; Vannini, 2002; R. Zhang et al., 2002).

Besides LuxR-type receptors, two-component systems consisting of membrane-bound histidine sensor kinases and corresponding response regulators triggering the downstream cascade are common in autoinducer sensing: They recognize, e.g., harveyi autoinducer 1, a short canonical AHL in *Vibrio harveyi*, but also atypical autoinducers in Gram-negative bacteria like cholera autoinducer 1 in *Vibrio cholerae* (Milton, 2006; Papenfort & Bassler, 2016). Furthermore, they govern the response to AI-2 in both Gram-negative and Gram-positive bacteria (Bassler & Losick, 2006; Hardie & Heurlier, 2008). Last but not least, many of the oligopeptide autoinducers in Gram-positive bacteria are detected by two-component systems (Bassler & Losick, 2006; Kleerebezem et al., 1997; Monnet et al., 2014). Other oligopeptide autoinducers, however, are imported into the cell where they bind to specific peptide receptors; the latter often are transcription factors or phosphatases whose activity is controlled by autoinducer binding, both ultimately regulating target gene expression (Monnet et al., 2014; Neiditch et al., 2017).

1.3 Biotic and abiotic factors influencing quorum sensing processes

Almost since the advent of quorum sensing research, effects of various environmental and endogenous factors on autoinducer-regulated processes have been described (Fig. 3). Addition of glucose to the medium, for instance, extends the lag phase preceding luciferase synthesis and bioluminescence in *A. fischeri*, an effect that has been linked to catabolite repression and the ensuing lack of stimulation of *luxR* and *luxICDABE* expression by CRP-cAMP (Dunlap & Greenberg, 1985, 1988; Friedrich & Greenberg, 1983; Lyell et al., 2013; Neelson et al., 1972). In *Escherichia coli*, expression of the *lsr* operon encoding the AI-2 transporter is likewise subject to catabolite repression (Xavier & Bassler, 2005), and import is furthermore directly inhibited by binding of unphosphorylated HPr, a protein of the phosphotransferase system, to the AI-2 kinase LsrK (Ha et al., 2018). Accordingly, nutrient limitation has been suggested to promote competence development and production of the CSP pheromone in *S. pneumoniae* (Alloing et al., 1998; Claverys et al., 2000), and antibiotic stress induces expression of the respective *com* regulon (Prudhomme et al., 2006).

Factors secreted by host cells or other microorganisms in the vicinity also impact quorum sensing: Opines, low molecular weight compounds produced by plant cells transfected with the *Agrobacterium tumefaciens* T-DNA fragment in the course of infection, induce expression of *traR*, the gene encoding the LuxR-type AHL receptor gene, and thereby enable TraR-AHL-controlled replication and conjugation of the Ti plasmid (Fuqua & Winans, 1994; Lang & Faure, 2014; Piper et al., 1999). Other plant-produced compounds like flavonoids or furanones, in contrast, specifically suppress quorum sensing-controlled virulence factor production by plant-pathogenic bacteria (Joshi et al., 2021; Paczkowski et al., 2017; Smith et al., 2004). Moreover, a variety of so-called quorum quenching enzymes counteract autoinducer accumulation by active degradation (Grandclément et al., 2016; Horswill et al., 2007; Smith et al., 2004).

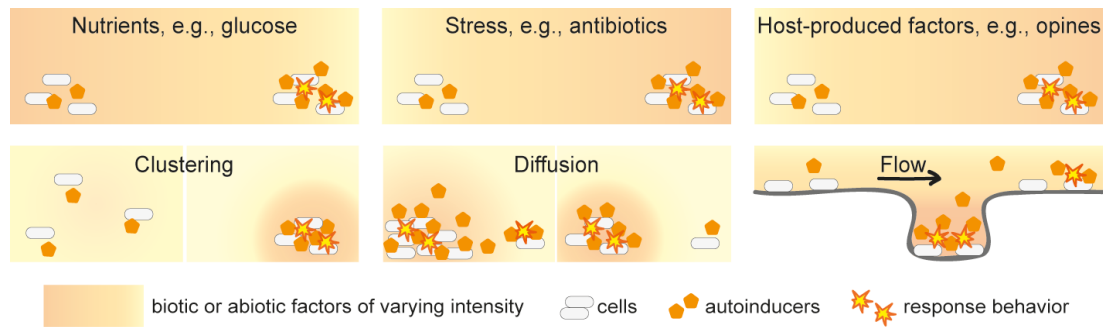


Figure 3. Biotic and abiotic influences on quorum sensing systems or quorum sensing-regulated processes. Various environmental and endogenous factors have been shown to affect autoinducer production, stability, accumulation, uptake, or the reaction to them. Not shown are, e.g., temperature and pH, both of which alter autoinducer stability (Byers et al., 2002; Decho et al., 2010; Horswill et al., 2007; Yates et al., 2002), or quorum quenching enzymes like lactonases or acylases that actively degrade autoinducers.

How fast autoinducers produced by some cells reach potential kin, inducing them to show response behavior, furthermore depends on the distance the molecules have to cover, and on their travelling speed. Autoinducer-producing cells growing in clusters can reach the threshold concentration necessary to trigger a response more easily than the same number of cells randomly distributed over the same surface, especially if the regulatory system includes a positive feedback of autoinducers on their own production (Egland et al., 2004; Hense et al., 2007; Müller et al., 2006). Spreading of autoinducers in cell-free space by diffusion in turn will dilute the molecules (Alberghini et al., 2009); limiting diffusion by growing *Pseudomonas putida* on dry instead of wet leaves thus triggered a response at comparatively smaller cell numbers (Dulla & Lindow, 2008). Last but not least, flow can suppress quorum sensing over short distances by washing away autoinducer molecules, but lead to autoinducer accumulation downstream or in crevices, and thus produce localized responses (M. K. Kim et al., 2016; Kirisits et al., 2007; Meyer et al., 2012; Mukherjee & Bassler, 2019).

The well-documented impact of all of these biotic and abiotic factors has repeatedly provoked criticism on either the classification of specific molecules as means of inter-cellular communication, or on the concept of “quorum sensing” in general. For instance, based on the above-described induction of the *S. pneumoniae com* regulon by antibiotics, Prudhomme et al. proposed that “CSP is not an effector of quorum sensing but is an alarmone that conveys a stress signal” (Prudhomme et al., 2006). Redfield universally criticized the view of autoinducer-signaling as a means to detect cell density and promote group behavior, and instead suggested that “quorum sensing” might only be a side effect of “diffusion sensing”; autoinducer-based regulatory systems, the author argued, might have just as well evolved to convey information about environmental factors like diffusion or flow, limiting secretion of degradative enzymes or other costly exofactors to conditions under which they would remain in close proximity to their respective producers (Redfield, 2002). Alberghini et al. in turn emphasized the importance of spatial distribution for group behavior and thus proposed “positional sensing” or “cluster sensing” as the actual role of autoinducer-based systems (Alberghini et al., 2009), whereas Hense et al. suggested “efficiency sensing” as a unifying concept (Hense et al., 2007).

“Efficiency sensing” acknowledges the fact that autoinducer concentrations cannot possibly reflect cell density as such, but rather the combination of cell density, spatial distribution of cells, and loss of molecules by diffusion or flow (Hense et al., 2007). This idea of information integration was further elaborated in a “hybrid push-pull” concept (Hense et al., 2012): Here, cell density, spatial clustering and mass transfer aspects like diffusion were classified as “push” factors determining the potential efficiency of target behaviors, whereas starvation, other stress factors or host signals affecting autoinducer production were classified as “pull” factors reflecting the demand of the cells for the target behavior. All of these factors are integrated into the information conveyed by the final autoinducer concentration (Hense et al., 2012). Of note, however, Fuqua et al. had likewise discussed the influence of CRP-cAMP and other physiological factors when first introducing the term “quorum sensing”, suggesting that “two conditions [...] must be met for target genes to be induced: first, some external environmental signal other than an autoinducer must be perceived, and second, the bacteria must be at sufficiently high cell density for the autoinducer to accumulate to a threshold concentration” (Fuqua et al., 1994). And, much later, Platt and Fuqua acknowledged that the term “quorum sensing” does have shortcomings, since the emphasis “on the importance of local population density leads to oversimplification and neglect of other factors that can influence the concentration of the cues” (Platt & Fuqua, 2010).

1.4 An unexpected discovery: phenotypic heterogeneity in quorum sensing

Despite the ample data on physiological factors and the associated debates, the prevalent image of quorum sensing is primarily that of a means to determine when a certain cell density is reached, and to then coordinate or even synchronize the behavior of the group (Eickhoff & Bassler, 2018; Mukherjee & Bassler, 2019; Papenfort & Bassler, 2016; Schauder & Bassler, 2001; Uden, 2014). This image implies homogeneity both in autoinducer production and in target gene activation: Homogeneity in autoinducer production, since “in order for quorum sensing to operate correctly, as bacteria grow, they must continuously produce the autoinducer signal so that their concentration will reflect the population density” (Schauder & Bassler, 2001); and homogeneity in target gene activation, since “these processes are futile when undertaken by a single bacterium acting alone. Rather, success requires population-wide coordination of the individual cells” (Mukherjee & Bassler, 2019).

However, over the last two decades, more than two dozen reports of phenotypic heterogeneity – i.e., of nongenetic cell-to-cell variation – in quorum sensing-related gene expression have been published: For instance, in autoinducer precursor gene expression in the Gram-positive pathogen *Listeria monocytogenes* (Garmyn et al., 2011); in AHL synthase gene expression in the Gram-negative plant pathogen *Pseudomonas syringae* (Pradhan & Chatterjee, 2014) and in the Gram-negative plant symbionts *Sinorhizobium fredii* and *Sinorhizobium meliloti* (Fig. 4) (Grote et al., 2014; Schlüter et al., 2015); furthermore, regarding quorum sensing-regulated traits, in exopolysaccharide (EPS) production in *S. meliloti* (Schlüter et al., 2015); in endoglucanase gene expression in the Gram-negative plant pathogen *Xanthomonas campestris* (Pradhan & Chatterjee, 2014); in biosurfactant production in the Gram-negative saprotrophic

P. putida (Cárcamo-Oyarce et al., 2015); in biofilm formation and toxin production in the Gram-positive opportunistic pathogen *Staphylococcus aureus* (García-Betancur et al., 2017); in biosurfactant production, competence development or sporulation and related gene expression in the Gram-positive soil bacterium and commensal *Bacillus subtilis* (Bischofs et al., 2009; Maamar & Dubnau, 2005; Mutlu et al., 2018; Smits et al., 2005; Veening et al., 2005); and several more (Bettenworth et al., 2019; Grote et al., 2015).

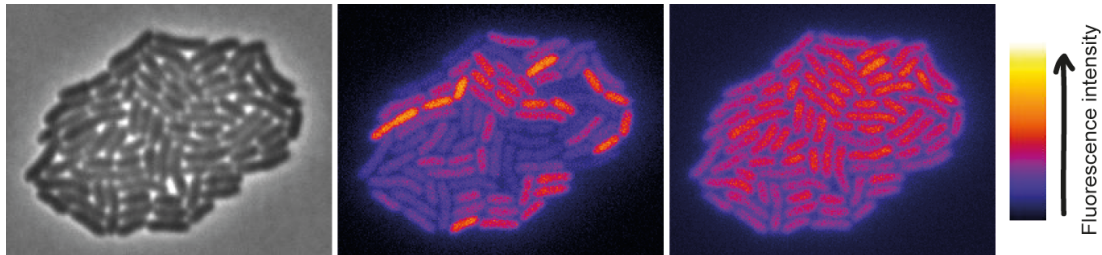


Figure 4. Heterogeneity in quorum sensing-related gene expression. Phase contrast (left) and fluorescence microscopy (middle & right) images of a *Sinorhizobium melliloti* microcolony displaying heterogeneous expression of an AHL synthase gene promoter-*mVenus* fusion (middle), and homogeneous *mCherry* expression from a constitutive promoter (right). Fluorescence microscopy images, Fiji “fire” lookup table.

Genome-wide analyses in the budding yeast *Saccharomyces cerevisiae* (Newman et al., 2006) and in *E. coli* (Silander et al., 2012; Taniguchi et al., 2010) have shown that the degree of cell-to-cell variation in gene expression varies from gene to gene, and that the extent to which a certain gene’s expression varies is linked to its function: Housekeeping genes, for instance, exhibit low levels of heterogeneity, stress response genes and genes encoding functions in carbon metabolism in contrast exhibit the highest levels. This finding first of all indicates that heterogeneity in gene expression is not inevitable, but can be controlled by network architecture, e.g., by uneven numbers of negative feedback loops (Raj & van Oudenaarden, 2008; Raser & O’Shea, 2005; Smits et al., 2006; Veening et al., 2008). Furthermore, it is generally interpreted as an indication for a function in the respective organism’s fitness. According to this rationale, natural selection would have minimized heterogeneity in expression of a given gene if it was harmful; its occurrence thus is generally taken to indicate that it must be favorable, or at least neutral (Lehner, 2008; Wang & Zhang, 2011).

The most prominent potential functions of phenotypic heterogeneity, and the ones usually proposed, are bet hedging and division of labor: Bet hedging is a risk-spreading strategy producing diverse phenotypes as a pre-adaptation to future changes in the environment; since the nature of these changes is unpredictable, phenotypic diversity will increase chances that at least some individuals, and consequently the corresponding genotype, will survive the changes (Ackermann, 2015; Bettenworth et al., 2019; Cohen, 1966; Veening et al., 2008). Division of labor in turn represents a more cost-effective way of fulfilling tasks of public interest in a community and thus likewise increases the fitness of the genotype (Ackermann, 2015; Bettenworth et al., 2019; West & Cooper, 2016; Z. Zhang et al., 2016). Both have been suggested with regard to the above-listed cases of heterogeneity in quorum sensing-related gene expression: Bet hedging for, e.g., heterogeneous expression of the AHL synthase gene *ahlI* in

P. syringae (Pradhan & Chatterjee, 2014), for heterogeneity in *agr* operon expression in *L. monocytogenes* (Garmyn et al., 2011), for the bimodal switch in the *S. aureus agr* quorum sensing system (García-Betancur et al., 2017), and for cell-to-cell variation in sporulation onset in *B. subtilis* and the resulting tradeoff between spore quantity and quality (Mutlu et al., 2018); division of labor for heterogeneous activation of quorum sensing-regulated bioluminescence and protease production in *V. harveyi* (Anetzberger et al., 2009, 2012), and for motility driven by surfactin and matrix producers in *B. subtilis* (van Gestel et al., 2015) (Fig. 5).

In addition to bet hedging and division of labor, “cheat protection” and “output modulation” were proposed as further potential benefits of quorum sensing-related heterogeneity (Bettenworth et al., 2019): According to evolutionary theory, cooperative traits like the quorum sensing-regulated production of public goods should be subject to exploitation by non-contributing mutants, so-called cheaters (West et al., 2006; West & Cooper, 2016); the cheat protection hypothesis suggests that phenotypic non-contributors in a heterogeneous population could protect the cooperative genotype against this exploitation since they – in contrast to the phenotypic contributors who pay the costs for the cooperative trait – can compete with the cheaters for reproductive success. According to the output modulation hypothesis, variation of the fraction of cells contributing to a given task would serve as a means to modulate the output of the population as a whole; in several of the above-listed cases of quorum sensing-related heterogeneity, environmental or physiological factors were indeed found to modulate the fraction of cells displaying a certain phenotype (Bettenworth et al., 2019).

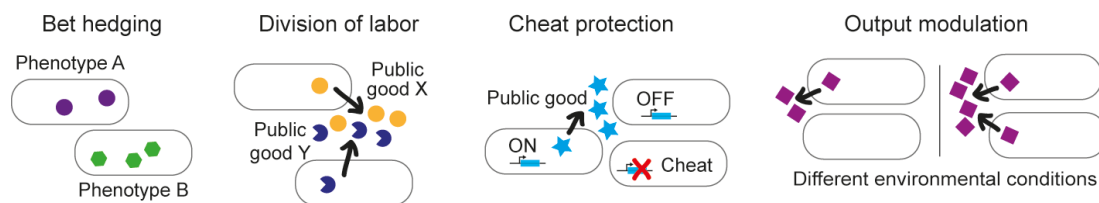


Figure 5. Potential functions of phenotypic heterogeneity in quorum sensing-related gene expression. Adapted from (Bettenworth et al., 2019).

Concerning the molecular mechanisms involved, e.g., the bistability in *B. subtilis* competence development (Maamar & Dubnau, 2005; Smits et al., 2005) or the bifurcation into biofilm-forming and toxin-producing subpopulations in *S. aureus* (García-Betancur et al., 2017) were linked to positive feedback mechanisms in the regulatory circuit. An even number of negative feedback loops in turn was suggested to contribute to the heterogeneity observed in sporulation onset in *B. subtilis* (Bettenworth et al., 2019; Bischofs et al., 2009). Both network architectures are known to promote bistability since they amplify pre-existing cell-to-cell variations (Raj & van Oudenaarden, 2008; Raser & O’Shea, 2005; Smits et al., 2006; Veening et al., 2008). At least in large colonies or biofilms, these initial cell-to-cell variations might be rooted in microenvironmental differences with respect to nutrient or oxygen supply or autoinducer concentrations, triggering different responses in cells located at different positions. However, many of the respective studies were conducted in well-shaken liquid cultures, and microenvironmental differences thus should not play a role. Here, and maybe even in the

biofilm-related cases, the most prominent explanation for phenotypic heterogeneity identified so far in quorum sensing-unrelated studies might apply: Stochasticity or “noise”, referring to statistical cell-to-cell variations, for instance, in the numbers of key molecules like transcription factors, or in biochemical processes like the binding and unbinding of these transcription factors to their target promoters that can cause qualitatively identical processes in different cells – e.g., the transcription of the same gene in two genetically identical cells – to produce quantitatively different results (Elowitz et al., 2002; Pedraza & Van Oudenaarden, 2005; Swain et al., 2002).

1.5 The model organism *S. meliloti* and its Sin quorum sensing system

S. meliloti (De Lajudie et al., 1994) (also *Ensifer meliloti* (Dangeard, 1926)) is a Gram-negative, rod-shaped and peritrichously flagellated bacterium. It belongs to the α -proteobacteria of the family of *Rhizobiaceae* and can either be found free-living in the soil, or in symbiosis with leguminous plants where it induces root nodule formation and differentiates into nitrogen-fixing bacteroids (Jones et al., 2007). Both the reference strain Sm1021 (Galibert et al., 2001) and the reference strain Sm2011 (Sallet et al., 2013) are spontaneous streptomycin-resistant derivatives of the wild-type isolate *S. meliloti* SU47, and all three strains possess the so-called Sin quorum sensing system that is a variation of the *A. fischeri* Lux system. However, other than the parental strain, both Sm1021 and Sm2011 carry an insertion sequence (*ISRm1*) in the AHL receptor gene (*SMc03899-SMc03896*) and are thus quorum sensing-unresponsive; the gene was restored in strains Rm8530 and Sm2B3001, respectively (Bahlawane et al., 2008; Pellock et al., 2002).

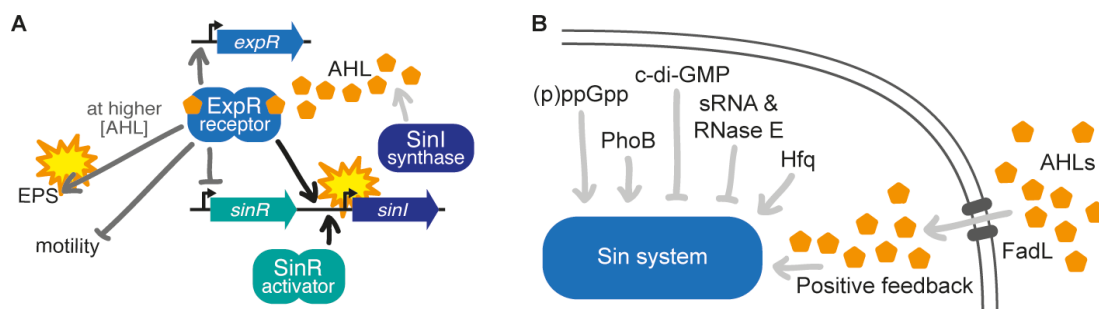


Figure 6. The *S. meliloti* Sin quorum sensing system and various factors influencing it. (A) Expression of the AHL synthase gene *sinI* is regulated by the two LuxR-type regulators SinR and ExpR, the latter in complex with AHLs. ExpR-AHL furthermore stimulates exopolysaccharide (EPS) production and inhibits motility. Bright asterisks mark components that have been shown to display phenotypic heterogeneity in gene expression. (B) Factors modulating activity of the Sin system. (A, B) Adapted from (Bettenworth et al., 2019).

In the Sin system (Fig. 6A), the autoinducer synthase SinI produces AHLs with remarkably long acyl chains of 14 to 18 carbons, of which 3-oxo-C16:1-HL and C16:1-HL are most prominent (Gao et al., 2005; Teplitski et al., 2003). Expression of the synthase gene strictly depends on the LuxR-type regulator SinR encoded immediately upstream of *sinI*; however, SinR is not the corresponding AHL receptor (Charoenpanich et al., 2013; McIntosh et al., 2008). Instead, AHLs are sensed by another LuxR-type regulator, ExpR, encoded at a different

location on the chromosome (Bartels et al., 2007; Marketon et al., 2002; McIntosh et al., 2008). Already at low AHL concentrations (5-10 nM when exogenously added to a *sinI* mutant), *sinI* transcription is enhanced via positive feedback by the ExpR-AHL complex (Charoenpanich et al., 2013; McIntosh et al., 2008); at intermediate autoinducer levels (>50 nM), transcription of *expR* is weakly stimulated (Charoenpanich et al., 2013); and at high autoinducer concentrations (>200 nM), *sinR* expression is downregulated by ExpR-AHL (Charoenpanich et al., 2013; McIntosh et al., 2009), preventing overshooting of the system.

In addition to the key promoters of the quorum sensing regulatory network, about 30 more promoters have been shown to be bound by ExpR-AHL, thus representing direct targets (Charoenpanich et al., 2013; Zatakia et al., 2014), and more than 500 genes were differentially expressed in *sinI* or *expR* mutants (Gao et al., 2005; Gurich & González, 2009; Hoang et al., 2004). Most prominently, ExpR-AHL represses transcription of motility genes and activates genes for EPS production (Charoenpanich et al., 2013; McIntosh et al., 2008; Pellock et al., 2002). The ExpR-AHL-induced production of galactoglucan (also termed EPS II) results in a mucoid colony phenotype that enhances survival during desiccation (Charoenpanich, 2015), is important for surface spreading (Dilanji et al., 2014; Gao et al., 2012), and furthermore makes *S. meliloti* cells more resistant to predation by *Myxococcus xanthus* (Pérez et al., 2014).

Like many other quorum sensing systems, the Sin system has been shown to be affected by various other factors than AHLs (Fig. 6B): For instance, expression of *sinR* is stimulated in response to nitrogen downshifts in presence of the *relA* gene encoding a functional (p)ppGpp synthetase (Krol & Becker, 2011). Expression of both *sinR* and *sinI* is upregulated under phosphate starvation, an increase that has been linked to the phosphate starvation response regulator PhoB (Krol & Becker, 2004; McIntosh et al., 2009). The lifestyle-switch second messenger c-di-GMP, on the other hand, reduces *sinI* expression, and this inhibition is most prominent during exponential growth as intracellular c-di-GMP concentrations in *S. meliloti* are 10- to 30-fold higher in exponential than in stationary growth phase (Schäper et al., 2016). Moreover, *sinI* mRNA can be bound by a small RNA and subsequently cleaved by RNaseE (Baumgardt et al., 2014, 2016), and *expR* mRNA levels are modulated by the RNA binding protein Hfq (Gao et al., 2015). Last but not least, the outer membrane protein FadL, a homolog of an *E. coli* fatty acid transporter, has been shown to facilitate uptake of long-chain AHLs and thus increase sensitivity to externally added autoinducers up to 100-fold; expression of *fadL* itself was not regulated by the ExpR-AHL complex (Krol & Becker, 2014).

As mentioned above, heterogeneity in quorum sensing-related gene expression was demonstrated in *S. meliloti*, specifically in a wild-type (Sm2B3001) background, for both the AHL synthase gene *sinI*, monitored via a promoter-*mVenus* fusion, and for a direct target of ExpR-AHL, the *wgeA* gene whose product is involved in production of the EPS galactoglucan, monitored via a promoter-*mCerulean* fusion (Schlüter et al., 2015). The molecular mechanisms of these heterogeneities were not investigated, but the fraction of cells activating *sinI* increased considerably over time, or with increasing colony sizes (Schlüter et al., 2015).

2 Aim of this work: a better understanding of quorum sensing dynamics

The overall aim of this work was to provide a better understanding of quorum sensing dynamics in the model organism *S. meliloti*.

In (Bettenworth et al., 2018), this objective was pursued on a larger scale, namely with respect to quorum sensing over larger distances on a two-dimensional plane, a proxy for the environment. Here, diffusion is regarded as the most important mechanism of autoinducer dispersal, and we used *S. meliloti* sender and receiver colonies located at varying distances to investigate key parameters of inter-colony communication: the changes in the concentration profile that might occur with increasing distance from the source; the speed with which a certain concentration level – the level necessary to trigger a response in the receiver colonies – travels over the plane; and the reach of the autoinducers, i.e., the maximal distance over which a response in receiver cells can be elicited.

In (Bettenworth et al., n.d.), quorum sensing dynamics were investigated on a smaller scale, namely with respect to autoinducer synthase gene expression in single cells and the ensuing quorum sensing response during development of the respective colonies. The above-mentioned cell-to-cell heterogeneity in autoinducer synthase gene expression observed by (Schlüter et al., 2015) was scrutinized with respect to where and how exactly it originated, i.e., which molecular mechanisms generate heterogeneity; whether and, if so, how it is affected by environmental or physiological factors; and whether and, if so, how this mode of gene expression affects *S. meliloti* quorum sensing response dynamics and colony behavior.

3 Results

The research presented in this thesis has been performed in collaboration with other scientists and published in or submitted to scientific journals. The following subchapters therefore cite the respective manuscript and co-authors, give a summary of the obtained results, and specifically list my contributions. Subsequently, the articles are reproduced in full.

3.1 Front-propagation in bacterial inter-colony communication

V. Bettenworth, M. McIntosh, A. Becker, B. Eckhardt. *Chaos: An Interdisciplinary Journal of Nonlinear Science* 28, 106316 (2018).

In this work, we investigated a large-scale aspect of quorum sensing dynamics, namely the spreading of autoinducer molecules by diffusion over large cell-free distances on a two-dimensional plane – a proxy for the environment. At first sight, diffusion over a plane should act to dilute the molecules (Alberghini et al., 2009; Carslaw & Jaeger, 1959) and thus, with increasing distance from the source, slow down progression of the threshold concentration capable of inducing a response in distantly-located bacteria of the respective species.

To thoroughly investigate the process, first modeling of diffusion for different types of sources is discussed: For a single autoinducer pulse, the concentration of molecules that are initially all localized at the source will spread over the plane with a Gaussian shape, and the gradient will decrease with time, so that the localization of a particular concentration level – e.g., the threshold concentration – becomes less well-defined. In contrast, a continuous autoinducer source constantly contributes new molecules that have to be added up, but the progression of a particular concentration level nevertheless decreases with time. However, for exponentially growing sources – like an exponentially growing population of autoinducer-synthesizing bacteria – the model predicts that concentration levels will spread over the plane with constant speed, and that the gradient in autoinducer concentrations will be preserved over time; diffusion from an exponentially growing source would thus be comparable to front propagation in pattern-forming systems (Fig. 1 & 2 in (Bettenworth et al., 2018)).

We furthermore analyzed the spreading of autoinducer molecules experimentally by time-lapse fluorescence microscopy, employing different *S. meliloti* strains as senders and receivers in an inter-colony communication setting (Fig. 3 & 4). Both sender and receiver strains carried a fluorescent reporter gene fused to the promoter of the AHL synthase gene *sinI* and thus showed an increase in fluorescence when experiencing autoinducer concentrations above the threshold level necessary to trigger the positive feedback on *sinI* expression by receptor-bound AHLs (McIntosh et al., 2009). However, while the sender strain had a wild-type genetic background and could thus produce and respond to the autoinducer molecules, receiver strains could not synthesize autoinducers due to a partial *sinI* deletion, but could still react to them with enhanced transcription from the *sinI* promoter. During the experiments, growing sender colonies (Fig. 5) served as sources of autoinducers on an agarose pad, generating a spatial gradient over this

essentially two-dimensional plane; growing receiver colonies localized at various distances to the source(s) served as indicators for the progression of the threshold autoinducer concentration. Of note, the above-described increase in fluorescence from the receiver colonies only occurred when sender cells were included on the agarose pad; if this was the case, the timing of the increase correlated – as expected – with the distance of the respective receiver colony from the sender colony or colonies.

To not only draw qualitative conclusions – that the timing of the receivers' reactions is indeed distance-dependent –, but to further characterize this dependence, we then analyzed the data as follows (Fig. 6): Two fits were made to the fluorescence intensities of the receiver colonies that showed an AHL-dependent increase in fluorescence, one to the intensities determined before the onset of the feedback, the other to the intensities determined afterwards; the intersection of the two fits thus marks the arrival of the autoinducer threshold concentration at the position of the respective receiver colony. These transition times containing the temporal information were then plotted against a spatial value – either the absolute distance of the respective receiver colony from the sender colony, or its relative position on a universal x-axis; the respective plots clearly indicated that the distance-dependence is of a linear form as proposed by our model (Fig. 7 & 8). Hence, our experimental data likewise supports the conclusion that autoinducers spread over a plane in propagating fronts. Moreover, the linear least square fit to the data yields a front speed of approximately 1100 $\mu\text{m}/\text{h}$, and, consequently, a diffusion constant of about 1120 $\mu\text{m}^2/\text{s}$ for the long-chain AHLs produced by *S. meliloti* (Fig. 9).

Personal contributions

I conceived the study together with Bruno Eckhardt. Furthermore, I constructed the sender strain and one of the two receiver strains used (the other had been built earlier by Matthew McIntosh), performed all experiments and corresponding image segmentation, and determined areas and mean fluorescence intensities of the colonies over time. I also wrote the parts of the manuscript concerning the biological system and experiments and composed the corresponding figures, and together with B. Eckhardt wrote introduction, results and discussion, and concluding remarks.



Front-propagation in bacterial inter-colony communication

Vera Bettenworth, Matthew McIntosh, Anke Becker, and Bruno Eckhardt

LOEWE-Zentrum für Synthetische Mikrobiologie (SYNMIKRO), Philipps-Universität Marburg

(Received 14 May 2018; accepted 9 September 2018; published online 12 October 2018)

Many bacterial species exchange signaling molecules to coordinate population-wide responses. For this process, known as quorum sensing, the concentration of the respective molecules is crucial. Here, we consider the interaction between spatially distributed bacterial colonies so that the spreading of the signaling molecules in space becomes important. The exponential growth of the signal-producing populations and the corresponding increase in signaling molecule production result in an exponential concentration profile that spreads with uniform speed. The theoretical predictions are supported by experiments with different strains of the soil bacterium *Sinorhizobium meliloti* that display fluorescence when either producing or responding to the signaling molecules. *Published by AIP Publishing.* <https://doi.org/10.1063/1.5040068>

In a process called quorum sensing, bacteria exchange signaling molecules to collect feedback on the size of their community and to initiate a population-wide change in behavior once a certain *quorum* has been reached. A variety of signaling molecules and different pathways for the production and detection of these molecules have been described for different species, but these studies have also shown that there are common features underlying many quorum sensing systems. Here, we focus on general spatiotemporal aspects of this communication, the transmission of information between far-scattered bacterial colonies over large cell-free distances where the main mode of signal propagation is diffusion. As we describe, the exponential growth of the colonies producing the signaling molecules has a profound effect on the way the signal spreads in space: While a constant source results in a distribution where the signaling molecules become more and more dilute with increasing distance from the source, the continuous boost in production by an exponentially growing colony conspires with diffusion to produce a front that travels from the source with constant speed. Experiments with the model bacterium *Sinorhizobium meliloti* with localized sources and spatially distributed receiver colonies show a position-dependent response that is in agreement with the main predictions from the theory.

I. INTRODUCTION

Living organisms employ a large variety of chemical, electrical, optical, or mechanical processes to sense their abiotic and biotic environment and to respond to this manifold of cues. In Braun's work, the focus has been on electrical signals, how they are generated by ion channels in neuronal membranes, and how they vary in response to external stimuli.^{1–4} Braun and his co-workers developed Hodgkin-Huxley-based mathematical models that show rich dynamics^{5,6} and are in sufficiently good agreement with observations that they have been implemented in a suite of simulation software for physiological experiments, available at <http://www.virtual-physiology.com/>. However, organisms

use such processes not only for sensing but also to communicate and interact—they set up chemical or electrical waves to transport signals coherently over large distances. As in the case of the sensory systems, the response and shape of the signals is a consequence of nonlinear excitatory dynamics.⁷ In this context, it is interesting to note that ion channels and potassium waves have been reported for bacterial biofilms as well, apparently providing a kind of neuron-like electrical signaling.^{8–10}

The bacterial communication system we explore is of purely chemical nature and generally seen as the means for bacteria to determine the size or density of their population and to regulate their behavior accordingly: Individual bacterial cells produce signaling molecules, so-called autoinducers, that spread in their environment where the molecules can be detected by other bacterial cells. If the concentration of the signaling molecules is high enough,¹¹ they induce a more or less population-wide change in behavior, e.g., the production of virulence factors in pathogenic bacteria or of extracellular matrix in the course of biofilm formation. Since the signal concentration, and thus the onset of the response, is related to the number of cells producing the signaling molecules, the term “quorum sensing” has been coined for this process.¹²

Quorum sensing systems have turned out to be so ubiquitous that by now they are thought of as *not the exception but, rather, the norm in the bacterial world*.¹³ The chemical nature of the signaling molecules as well as the number of signaling pathways employed differs from species to species, but many quorum sensing systems share a common set of elements. For instance, the regulatory circuits usually include a positive feedback loop of the signaling molecule on its own production, bringing about a rather defined transition into the quorum-sensing state.^{14,15} Note that while the response of the organisms to the signaling molecules thus has nonlinear elements, the diffusive spreading of the signal in the organisms' environment is of an essentially linear nature, in contrast to the nonlinear signal propagation in neuronal or chemical waves.

Research on the processes involved in quorum sensing has long been reinforced by theoretical studies, taking into account factors like flow, diffusion, adhesion, decay, or

degradation of the signaling molecules or growth of the signal-producing population (reviewed in Ref. 16). However, these studies often focus on processes in single cells or cells in well-mixed liquid systems. Only a few studies include or specifically investigate spatiotemporal signal propagation within single colonies or populations.^{17–21} Of particular relevance to our study of inter-colony communication is the description of diffusive spreading of signaling molecules beyond individual colonies in Ref. 22, where the spatial variation of the concentration and its dependence on the number of cells producing the signal are analyzed.

Diffusion will typically act to dilute the molecules and hence to attenuate the signal. For instance, for a constant source, the distance of a given concentration level from the source will increase with the square root of time. This is very different from the signals along nerve fibers or in chemical waves, where the propagation occurs at a constant speed. However, as we will deduce in the subsequent theoretical analysis, the interplay between diffusion and the exponentially increasing activity of a growing bacterial colony will set up a propagating front as well. This conclusion is supported by time-lapse experiments with sender and receiver colonies of the model bacterium *Sinorhizobium meliloti* that display an increase in fluorescence when entering the quorum-sensing state: The spatiotemporal pattern of the response of the receiver colonies to the signaling molecules produced by the sender colonies likewise suggests that the threshold signal concentration necessary to trigger the quorum sensing response spreads in the environment with uniform speed.

The outline of the paper is as follows: In Sec. II, we discuss the modeling of the diffusion process and describe the spatiotemporal variation of concentrations for different sources, including the formation of fronts by exponentially growing sources. In Sec. III, we describe our model system *S. meliloti* and the experimental setup. Results from the observations and the modeling are combined and discussed in Sec. IV. We conclude with a few general observations in Sec. V. Details of the experimental materials and methods are given in Sec. VI.

II. MODELLING DIFFUSIVE SPREADING FROM SOURCE COLONIES

As stated above, quorum sensing signaling molecules produced and released from bacterial cells spread diffusively in the environment. By Fick’s law, the concentration $c(\mathbf{x}, t)$ of molecules at spatial position \mathbf{x} and time t obeys the diffusion equation

$$\partial_t c = D\Delta c + \tilde{q}(\mathbf{x}, t), \quad (1)$$

with diffusion constant D and a term $\tilde{q}(\mathbf{x}, t)$ that contains the temporal variations and the spatial distribution of one or more sources.

Many examples of such diffusive processes in different geometries and dimensions are discussed in the classic text of Carslow and Jaeger.²³ Since the experimental setup we employ here mainly involves diffusion in the plane, we will subsequently focus on two-dimensional cases.

As a first situation, we consider a single signal pulse, in which the concentration of molecules that are initially localized will spread with a Gaussian shape. In two dimensions, the concentration is given by

$$c(r, t) = \frac{1}{4\pi Dt} e^{-\frac{r^2}{4Dt}}, \quad (2)$$

with r being the distance from the source. Levels of constant concentration $c(r, t) = c_0$ are circular and move in time according to

$$r_0^2 = 4Dt [\ln(1/c_0) - \ln 4\pi Dt]. \quad (3)$$

Leaving aside the second term, which is only important for very short and very long times, we find that $r_0(t) \propto \sqrt{t}$. Moreover, the gradient at that position and time, which relates uncertainties in concentration to variations in space according to $\delta r = \delta c / |\partial c / \partial r|$, is given by

$$\left. \frac{\partial c}{\partial r} \right|_{r_0} = -\frac{1}{\sqrt{Dt}} \quad (4)$$

and decreases with time so that the concentration level becomes less well defined.

In contrast to a single signal pulse, a time-dependent source $q(t)$ at the origin contributes new molecules at every time step, and their contributions have to be added up: If the source is turned on at time t_0 , the concentration profile is given by

$$c(r, t) = \int_{t_0}^t \frac{1}{4\pi D(t-t')} e^{-\frac{r^2}{4D(t-t')}} q(t') dt'. \quad (5)$$

For most sources, this has to be evaluated numerically (see below). An analytical solution is possible for our case where the sources of the signal are exponentially growing colonies of bacteria that release—if we assume a constant mean production rate once the cells have entered the quorum-sensing state—an exponentially growing number of signaling molecules. Such a source is described by an exponentially growing strength $q(t) = q_0 \exp \lambda t$. If we assume that it has been active forever ($t_0 \rightarrow -\infty$), the concentration becomes

$$c(r, t) = q_0 e^{\lambda t} \int_0^\infty \frac{1}{4\pi D\tau} e^{-\frac{r^2}{4D\tau}} e^{-\lambda\tau} d\tau, \quad (6)$$

which can be integrated exactly

$$c(r, t) = \frac{2q_0}{4\pi D} e^{\lambda t} K_0(r/\ell) \approx \frac{2q_0}{4\pi D} \sqrt{\frac{\pi\ell}{2r}} e^{\lambda t - r/\ell}, \quad (7)$$

where $K_0(\xi)$ is the modified Bessel function of index 0 and $\ell = \sqrt{D/\lambda}$ is the characteristic length. Note that space and time separate: There is an overall exponential increase in time with the same rate λ as for the source. The shape of the profile in space for fixed time is given by the Bessel function, which for large distances has an exponential decay (modulo a weaker $1/\sqrt{r}$ factor). Levels of constant concentration are circular and spread outwards like $r_0 = \sqrt{D\lambda}t$, with a constant speed

$$v = \sqrt{D\lambda}. \quad (8)$$

Moreover, the gradient at the position of the isocontour is essentially constant, $\partial c / \partial r \approx 1/\ell$. A constant speed of propagation and a preserved gradient link this process to front

propagation in pattern forming systems which shares the same properties.

The analysis given here is reminiscent of the front propagation described by Kendall,²⁴ which has also been discussed in the context of quorum sensing:²⁵ in a diffusion equation where the signal is amplified everywhere so that the source $\tilde{q} = \lambda c$ is proportional to the concentration with an amplification factor a , Kendall describes that there are propagating solutions $c(x, t) = f(x - vt)$. They exist for a range of velocities and the one that dominates in the long run has the smallest velocity, $v_c = 2\sqrt{D\lambda}$. The front speed has the same dependence on diffusion and growth rate as (8), but it is twice as large, which is due to the difference in the amplification process: In the Kendall problem, the concentration is amplified not only at the localized source but everywhere in space, and this gives the larger spreading speed.

To illustrate the effect of exponential growth on the spreading of the signal over time, we compare the propagation of a particular concentration level originating from an exponentially growing source to the spreading of the same concentration level produced by a constant source in Fig. 1. The profiles are obtained by numerical integration of (5). Since we do not have absolute values for the concentrations of the signaling molecules, we have to work with arbitrary units in the concentration. As diffusion constant, we use $D = 490 \mu\text{m}^2/\text{s}$ as estimated by Ref. 26 and also used by Ref. 22, as doubling time we work with $T_2 = 2.4 \text{ h}$, a representative value for our model system. The distances from the source are given in μm and can be compared directly with the experimental setup below. The arrows indicate the radial displacement of the particular concentration level over a time interval that corresponds to the doubling time for the exponentially growing source: They are of constant lengths for the exponential source and decrease with time for the constant source.

The preceding discussion focuses on diffusion in unbounded space. The full solution to the problem has to take into account the finite size of the domain with appropriate conditions near the boundaries. We assume that molecules are reflected at the walls so that there are no losses across the boundaries. For such Neumann boundary conditions, the normal derivative of the concentration vanishes. Moreover, we do not allow for degradation of the molecules or an absorption in the agarose so that all signaling molecules are conserved, and the overall concentration will increase as long as the source is active.

For the case of several sources that grow at the same rate, one can determine the spatial variation of the profile by splitting off the exponential growth, viz.,

$$c(\mathbf{x}, t) = \tilde{c}(\mathbf{x}) \exp(\lambda t). \quad (9)$$

Then, \tilde{c} satisfies the time-independent diffusion equation

$$\lambda \tilde{c} = D \Delta \tilde{c} + \tilde{q}_0(\mathbf{x}), \quad (10)$$

which can be solved numerically, for instance, by discretizing on a square lattice. As an example, we show in Fig. 2 the concentration for an isolated source in the center of a rectangular domain and with reflecting boundary conditions at the walls. The deviations from a radially symmetric concentration

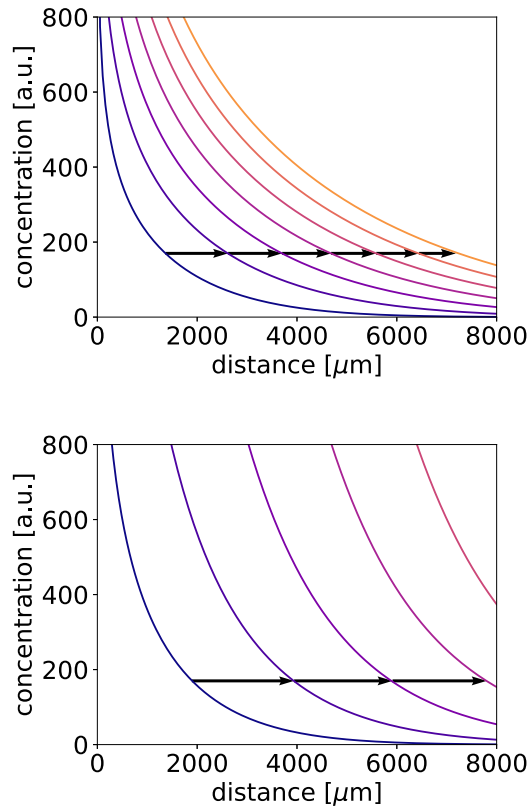


FIG. 1. Comparison between diffusive spreading for a colony with constant production (top) and frontal spreading for a colony with exponentially growing production (bottom). The time increases inwards to outwards (dark to light) in steps of the doubling time of the colonies. The arrows indicate the distance that a particular concentration level covers during one doubling time: in the case of the steady source, the length of the arrows decreases with time, whereas it is constant for the exponentially increasing source. Furthermore, the gradients decrease with time for the steady source but vary little for the exponentially growing source. The absolute concentrations for the exponentially growing source quickly outrun those for the constant source. The diffusion constant in these figures is $490 \mu\text{m}^2/\text{s}$, and the time between two profiles is 2.4 h.

profile are due to the influence from the boundaries, which is larger in the vertical direction than in the horizontal one because of the choice of a rectangular domain: it is 12 mm long and 6 mm wide, somewhat smaller than the agarose pads used in the experiment. The other parameters are a diffusion constant of $490 \mu\text{m}^2/\text{s}$ and a growth rate $\lambda = \ln 2/144 \text{ min}^{-1}$. Concentration profiles for several sources can be obtained by superimposing the profiles for individual sources. An example will be given below.

The response of the receiver colonies to this signal, which has been described by Refs. 27 and 28 for *S. meliloti*, can be used to detect the spreading of the front across the pad, as will be discussed in Sec. IV.

III. THE SOIL BACTERIUM *SINORHIZOBIUM MELILOTI* AS A MODEL SYSTEM

S. meliloti is a Gram-negative α -proteobacterium that engages in nitrogen fixation when living in symbiosis with

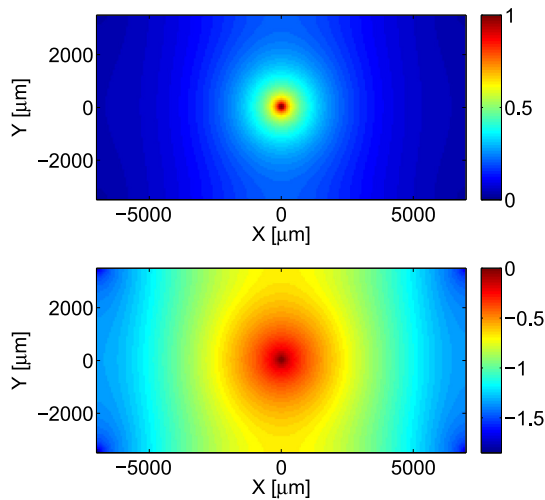


FIG. 2. Spatial concentration profile from a single source in the center of a rectangular pad with reflecting boundary conditions. The concentration profiles are shown in linear (top) and logarithmic scaling (bottom). The equidistant spacing between steps in color reflects the exponential decay. Deviations from the circular symmetry are due to the rectangular domain and boundary conditions.

leguminous plants.²⁹ However, it is not an obligate symbiont but can also be found free-living in the rhizosphere.³⁰ Quorum sensing plays an important role for both these lifestyles as it contributes to the establishment of symbiosis,³¹ and strongly stimulates extracellular matrix production, a key feature of biofilm formation.³²

The *S. meliloti* quorum sensing system (Fig. 3) is based on long-chained (C14-C18) acyl-homoserine lactones (AHLs) as signaling molecules.³³ These are produced by the AHL synthase SinI and sensed by the AHL receptor ExpR, a transcriptional regulator. Upon AHL binding, ExpR stimulates expression of a large number of quorum sensing target genes, some of which are associated with the above-mentioned changes in lifestyle. Furthermore, in a positive feedback loop, the ExpR-AHL complex stimulates expression of *sinI*, the gene encoding the AHL synthase SinI, and thus upregulates signal production. However, *sinI* expression can only take place in the presence of a second transcriptional activator, SinR. In the absence of AHLs or at low AHL concentrations, SinR is responsible for basal rate *sinI* expression and, consequently, basal rate signal production. At very high AHL concentrations, expression of the *sinR* gene is repressed by the ExpR-AHL complex, a negative feedback loop ultimately leading to a down-regulation of the whole quorum sensing system.^{27,34,35}

The experimental setup we used to explore the dynamics of the quorum sensing process between spatially separated bacterial colonies is sketched in Fig. 4 (for details, see materials and methods in Sec. VI). Essentially, we created a setting with only one-way signal transmission based on two genetically different *S. meliloti* strains: A sender strain that can both produce and sense the signal and can thus enter the above described state of positive-feedback-related increased signal production; and a receiver strain that cannot synthesize the

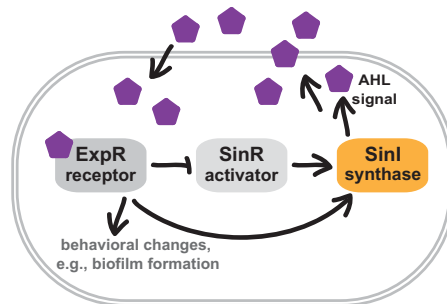


FIG. 3. Simplified illustration of the *S. meliloti* quorum sensing network. The AHL signaling molecules are produced by the AHL synthase SinI, spread in the environment, and are sensed by the AHL receptor ExpR. The ExpR-AHL complex (i) induces behavioral changes like biofilm formation and (ii) enhances expression of the synthase gene *sinI* in a positive feedback loop. At very high AHL concentrations, expression of *sinR*, the gene encoding the transcriptional activator of *sinI*, is repressed in a negative feedback loop. As SinR is essential for *sinI* expression, this results in a down-regulation of the whole quorum sensing system.

signaling molecules due to a partial deletion of the *sinI* promoter and *sinI* gene but can still react to them. Colonies of the sender strain serve as localized sources of signaling molecules on an agarose pad prepared with defined medium, generating a spatial gradient over this essentially two-dimensional experimental field. The timing of the response observed in receiver colonies located at varying distances to the sender colonies then enables us to extract information about the dynamics with which the signaling molecules spread.

In order to make this response traceable, both strains carry a gene encoding a fluorescent protein fused to the promoter of the AHL synthase gene *sinI*, i.e., the genomic region that ultimately regulates the production of the signaling molecules. Therefore, both strains show basal rate fluorescence—the sender strain as it engages in basal rate signal production, and the receiver strain as it tries to generate this basal signal level, albeit it is incapable of doing so. Furthermore, both strains can show an increase in fluorescence: the

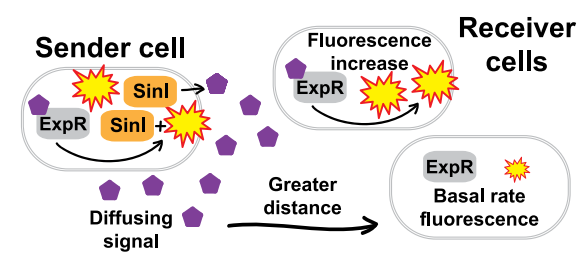


FIG. 4. Sketch of the experimental setup based on *S. meliloti* strains carrying a fluorescent reporter gene fused to the *sinI* promoter, thus serving as a proxy for the activity of the quorum sensing system. Sender cells (left) produce and release signaling molecules (purple pentagons) and display increased fluorescence due to the positive feedback characteristic of the quorum-sensing state. The signaling molecules diffuse across the agarose pad with receiver cells located at varying distances to the senders. When the receiver cells detect the signaling molecules, their fluorescence increases due to the same positive feedback loop (middle). Since the signal concentration strongly decreases with the distance from the senders, receiver cells at a greater distance will not experience this positive feedback and only show basal rate fluorescence (right).

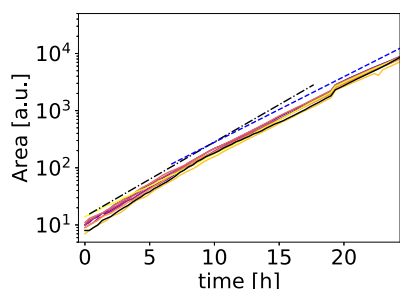


FIG. 5. Colony areas over time for one sender (black line) and eight receiver colonies; the respective experiment will be described in detail in Sec. IV. Initially, all areas increase exponentially with a doubling time of about 2.4 h, indicated by the black dash-dotted line. After about 10 h, cells push on top of each other and colonies grow in height as well so that the slope in area decreases slightly, as indicated by the blue dashed line. The kink in the growth curves near 20 h is due to a change in the microscope setting: As the colonies were about to grow larger than the field of view, their area and total fluorescence had to be determined by stitching 2×2 images per time frame.

sender when engaging in increased signal production after entering the quorum-sensing state, and the receiver when responding to an incoming signal.

Of these two strains, cell suspensions with very low optical density were spotted on the agarose pad: a single spot of the sender cell suspension, followed by five equidistant spots of the receiver cell suspension, yielding between about one dozen and eight dozen single cells on the whole pad, depending on the particular experiment. Through iterative growth and cell division, these single cells subsequently developed into large three-dimensional colonies. Colony growth and activity of the quorum sensing system in these colonies were followed via time-lapse fluorescence microscopy for approximately 24 h. During this period, colony areas grew exponentially with a mean doubling rate of 2.4 h for about 10 h (Fig. 5), which roughly corresponds to *S. meliloti* generation times reported by Ref. 36. Subsequently, colonies became three-dimensional, and the increase in area was slightly reduced. However, no difference was observed in the growth behavior of sender and receiver strains.

Activity from the AHL synthase promoter-fluorophore gene fusions was determined as mean fluorescence values, i.e., the total fluorescence intensity was collected over the whole colony area and then divided by the area. Based on this read-out, we observed different phenomena (Fig. 6). At early time points, there is considerable variation in fluorescence levels both in sender and in receiver colonies. This variation is probably due to inaccuracies in image segmentation, and/or to fluctuations in the fraction of cells in each colony activating their AHL synthase gene promoter, as this promoter is activated heterogeneously.³⁶ Both causes would weigh heavier the smaller the colonies and the lower the cell numbers. However, as this variation is limited to earlier time points, we did not explore it further.

Once inter-colony variation in fluorescence becomes negligible, fluorescence from the sender colonies is always significantly higher than that from receiver colonies. Thus, we conclude that sender colonies enter the quorum-sensing state already during the first few hours of colony development and

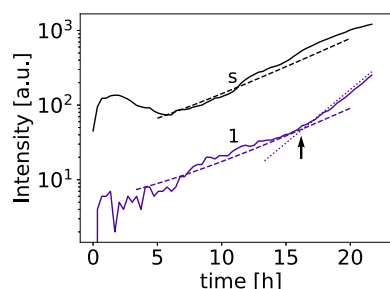


FIG. 6. Fluorescence intensities for a receiver colony (numbered 1) and a sender colony labelled “s.” The dashed lines and the dotted line are obtained from fits of the form $I(t) = a + b \exp(\lambda t)$ and are displayed after subtraction of a constant background intensity. During the initial phase, the signal intensity of the receiver colony shows the same increase as that of the sender colony (dashed lines). For later times, the signal from colony 1 shows a transition to a steeper slope (dotted line), with the transition point identified by the crossing of the two fits, as indicated by the arrow. The increase is caused by the response of the receiver colony to the AHL signal and marks the time when the respective threshold concentration reaches the position of the receiver colony.

then constantly produce signaling molecules at this elevated rate for most, if not all, of our observation time.

Next, we see a low but exponential increase in fluorescence from the AHL synthase gene expression reporter. This first increase is identical both in sender and in receiver colonies (even though absolute values are higher for sender than for receiver colonies, see preceding paragraph). This suggests that this first increase is unspecific, possibly originating from the accumulation of the fluorophores, scattered fluorescence, and fluorescence from cells within the three-dimensional colonies that are not in the focus plane of the microscope, but whose fluorescence signal is nevertheless detected by our camera. As this first increase reproducibly occurs in all colonies, we take it as the baseline for our observations.

The feature that is correlated with the spatiotemporal spreading of signaling molecules is limited to receiver cells only: they can show a second, more pronounced increase in fluorescence that rises well above the baseline. Whether or not this increase occurs at all depends on the presence of the sender strain—we did not observe it in a control experiment with receiver colonies growing on an agarose pad without any sender colonies. And if it occurs in experiments with both senders and receivers, the timing correlates with the distance of the respective receiver colony from the sender colony or colonies. Therefore, we interpret this second increase as the specific response of receiver colonies to incoming quorum sensing signaling molecules, namely, the activation of the above-described positive feedback loop on AHL synthase gene expression by receptor-bound AHLs, and, thus, the inter-colony communication we set out to study.

IV. RESULTS AND DISCUSSION

To be able to draw not only qualitative conclusions—but the timing of the receivers’ reactions is indeed distance-dependent—but to further characterise this dependence, we analyzed the data as described in Fig. 6: Two fits were made

to the fluorescence intensities of those receiver colonies that showed an AHL-dependent increase in fluorescence, one for earlier times, and the second for the part with the steeper increase. The crossing of the two fits marks the onset of the receivers' quorum sensing response and thus the arrival of the signal threshold concentration at the position of the receiver colony. These transition times containing the temporal information were then plotted against the spatial value, either the distance of the respective colony from the sender colony or its position on the x -axis (see below).

This is illustrated for the experiment with the single sender colony and eight receiver colonies in Fig. 7: In the top frame, the positions of the respective colonies on the agarose pad are shown. The middle frame gives the fluorescence intensities for all colonies, which already indicates the distance-dependence of the receivers' reactions, albeit only qualitatively (the curves of the receiver colonies are color-coded according to the distance from the source). The plot of the transition times against the distance from the sender colony in the bottom frame then clearly demonstrates that this dependence is of a linear form, as follows from the spreading of the quorum sensing signal in propagating fronts proposed by our model in Sec. II.

A further experiment with seven sources is analyzed in Fig. 8. Each of these sender colonies will contribute a radial signal profile like the one shown for a single source in Fig. 2. The combined signal concentration can be computed numerically, and the logarithmic presentation in the second frame demonstrates that the superposition of the contributions from the seven sources gives rise to a profile that hardly varies along the y -axis of the agarose pad, but falls off exponentially along the x -axis, as indicated by the equidistant spacing between the color regions. Effectively, over the distances analyzed here, the seven sources represent a line source in the vertical direction. It is thus possible to switch to a 1-d representation of the diffusion process and, for the spatial information, to replace the distance of the receiver colonies from the sender colonies by their horizontal position. Extracting the transition points in time for the different colonies from the fluorescence signals in the third frame and correlating them with the respective x -positions then gives the plot in the bottom frame: The data show a larger scatter than the ones from the experiment with the single source but the same linear spatiotemporal relationship.

Note that the response of the receivers in the present case with seven sources occurs at earlier times compared to that of the case of the single source. We interpret this as a consequence of the difference in sender cell numbers in the two experiments: To produce the same AHL threshold level at a particular distance—e.g., the position of the nearest receiver colony—the single sender colony needs to double about 2.8 times more often, for which it needs about 6.7 h, and this is roughly the shift between the response times in Figs. 7 and 8.

Thus, in each experiment, the absolute transition times of the receiver colonies depend on the number of sender colonies producing the signal. The absolute distances on the other hand depend on the location of the source. In order to combine data from different experiments, this dependence can be eliminated by shifting positions and times such that the mean values

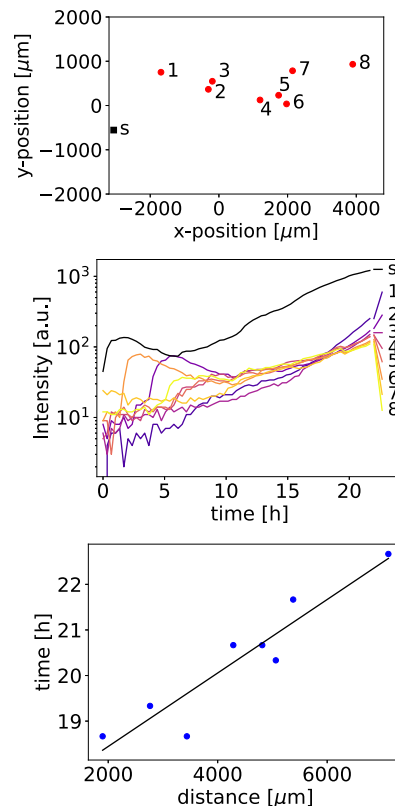


FIG. 7. The experiment with the single sender colony and eight receiver colonies. The top frame shows the locations of the sender colony (black square, label "s") and the receiver colonies, numbered 1 to 8. In the middle frame, the fluorescence signals from all colonies are shown. In the bottom frame, the times at which each fluorescence signal shows the AHL-induced increase is plotted vs. the distance of the respective receiver colony from the sender colony. The black line represents the linear regression.

vanish, i.e., with t_i being the response time at distance r_i , we compute the averages \bar{t} and \bar{r} and determine the relative times and positions $\tilde{t}_i = t_i - \bar{t}$ and $\tilde{r}_i = r_i - \bar{r}$, respectively. These numbers are independent of the actual number of sender cells and of the actual location of these cells, and they only give information about the dynamics of the signal propagation over the receiver-covered distance.

By applying such normalizations, we merged the data for the two experiments shown in Figs. 7 and 8, as well as additional data from two further experiments with 3 and 68 sender colonies, respectively. The fact that some of the data in the resulting Fig. 9 is rather scattered might be explained as follows: For the temporal axis, the determination of exact transition points is sometimes hindered by, e.g., fluctuations in the fluorescence signal, as these can impede the calculation of the fits, or by the time-lapse character of our data acquisition where imaging might have taken place right after or right before the onset of a given transition. For the spatial axis, at least in the experiments with more than one source, the x -positions of the receiver colonies are only an approximation and very likely not as precise as the absolute distances given for the case with the single source—the least-scattered

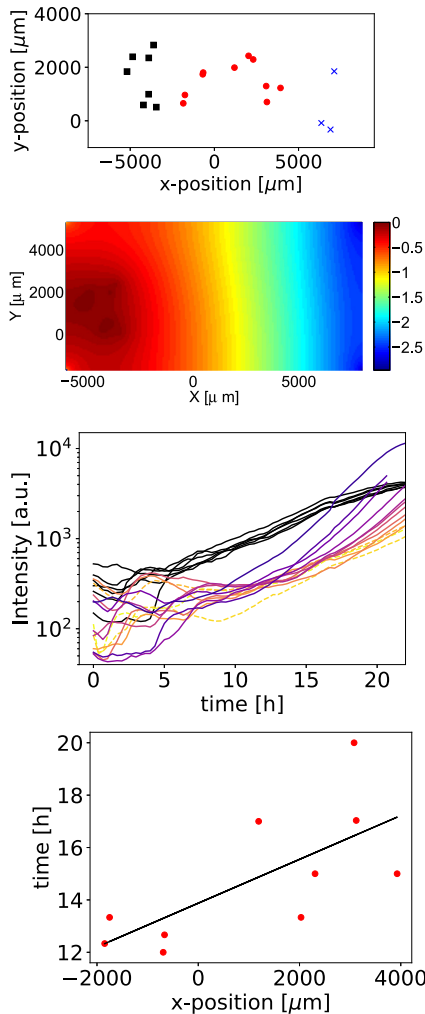


FIG 8. An experiment with seven sender colonies. The top frame again shows the location of the sender colonies (black squares), 10 receiver colonies that do show a response to the AHL signal (red dots), and 3 further receiver colonies that do not (blue crosses). Second frame: The solution of the diffusion equation for the spatial profile in the logarithmic scale shows that to a reasonable approximation the concentration profile falls off exponentially along the x-axis and is constant along the y-axis. Third frame: The fluorescence signals collected from all sender colonies (black) and the responding receiver colonies (color-coded from dark to light depicting increasing distance from the source). The dashed curves show the fluorescence from the three colonies that do not respond to the AHL signal. The bottom frame shows the relation between times of transition and position of the receiver colonies, including a linear regression.

of our data sets. Nevertheless, the data of the four independent experiments are all distributed in a similar fashion, are all compatible with a linear increase in time with increasing distance from the source, and thus all support spreading of the quorum sensing signal in propagating fronts.

For the velocity of the front, we can determine the slopes in linear least square fits. Both the experiments with the single sender and the seven senders—i.e., Figs. 7 and 8, respectively—give a front velocity of $v = 1200 \mu\text{m}/\text{h}$. A linear regression to the collected data in Fig. 9 gives a slightly

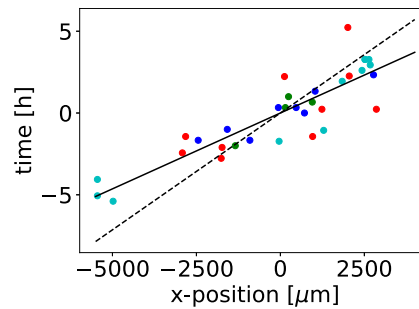


FIG 9. Transition time vs. position for four data sets, the two shown in Figs. 7 (blue) and 8 (red), as well as one case with three sender colonies (dark green) and one with 68 sender colonies (cyan). In order to be able to compare the data in one figure, all sets have been balanced in position and time so that the averages are zero. The slope of a linear regression then still gives the velocities: the continuous line is the result from a linear regression of all data points, with $c = 1080 \mu\text{m}/\text{h}$, the dashed line indicates a relation with a front speed of $v = 700 \mu\text{m}/\text{h}$ that follows from a diffusion constant of $D = 490 \mu\text{m}^2/\text{s}$ as estimated by Ref. 26.

smaller front propagation speed of about $v = 1080 \mu\text{m}/\text{h}$. In order to connect to other data in the literature, we use the relation between velocity, diffusion constant, and growth rate given by Eq. (8) so that $D = v^2/\lambda$. With a doubling time of 2.4 h, the growth rate λ becomes $\lambda = 0.29 \text{ h}^{-1}$, which together with the front speed of $v = 1080 \mu\text{m}/\text{h}$ gives a diffusion constant of about $1120 \mu\text{m}^2/\text{s}$.

This value is much larger than that used by Ref. 17 in their simulations ($D = 17 \mu\text{m}^2/\text{s}$) and also larger than the value given in Ref. 37 ($D = 71 \mu\text{m}^2/\text{s}$). However, Stewart²⁶ gives estimates for diffusion constants of 490 and $720 \mu\text{m}^2/\text{s}$ for AHLs with chains of 12 and 4 carbon atoms, respectively, Ref. 22 uses the value of $490 \mu\text{m}^2/\text{s}$ for their calculations, and Ref. 19 uses $720 \mu\text{m}^2/\text{s}$. Furthermore, as discussed by Ref. 19, diffusion of AHLs is influenced by, e.g., the length of the acyl side chains, and the stability of the molecules is strongly affected by the pH.

The relation we use to deduce the diffusion constant contains the square of the front velocity so that uncertainties in the front velocity are amplified considerably. On the other hand, assuming the same growth rate, but a diffusion constant that is 16 times smaller (i.e., going down from $1600 \mu\text{m}^2/\text{s}$ to $100 \mu\text{m}^2/\text{s}$) would reduce the front speed by a factor of 4, down to $320 \mu\text{m}/\text{h}$. Accordingly, the time to cover the distance over which the responding receiver colonies are spread in our experiments (about $6000 \mu\text{m}$) would increase from the observed interval of about 5 h to 20 h, close to the total run time of our experiment. Alternatively, in order to obtain the front velocity deduced from Fig. 9 with such a small diffusion constant would require a growth rate that would have to be 16 times faster than the one we used for our calculations, which is well outside the range of uncertainty of our experiments. On the other hand, a diffusion constant of $490 \mu\text{m}^2/\text{s}$ as estimated by Ref. 26 gives a front speed of $700 \mu\text{m}/\text{h}$, corresponding to the dotted line in Fig. 9: It has a steeper slope but still runs through most of the data, and it would also be compatible with the time interval of about 5 h over which the receiver colonies respond to the signal. Thus, while the

origin of the variations between the different experiments and estimates remains unclear, we conclude that front speeds in the range of 700–1100 μ /h, with diffusion constants in the range of 500–1150 μm^2 /s are compatible with the present observations.

V. CONCLUDING REMARKS

Without nonlinear effects, diffusion gives rise to concentration profiles with poorly defined gradients so that receiver cells that react to a certain signal concentration will have a large variability in their response in space and time. However, as we have shown here, the combination of exponentially growing sender colonies that release an exponentially increasing number of signaling molecules together with the diffusive spreading of the molecules creates a concentration profile where levels of constant concentration spread in a front-like fashion: The speed and the slopes of the profiles are constant as in many other examples of propagating fronts. The front speed $v = \sqrt{D\lambda}$ is given by a combination of diffusion constant D and growth rate λ . For a fixed time, the concentration profile varies exponentially in space, with a characteristic length $\ell = \sqrt{D/\lambda}$.

Observations on *S. meliloti* are used to test the theoretical predictions. Exponentially growing sender colonies release signaling molecules that spread over the agarose pad and trigger responses in receiver colonies that themselves cannot produce AHLs. The response is detected by an increase of fluorescence signal, and the time of response correlates linearly with the distance from the source.

The exponential variation of the signal concentration in space could not be verified directly; this would require either a direct measurement of AHL concentrations in agarose pads or receiver colonies with different thresholds for the AHL response. But even with the single signal threshold level displayed by our receiver strain, the quorum sensing response of *S. meliloti* to AHLs offers interesting possibilities: It sets in at low concentrations in the nanomolar range but is blocked again at higher concentrations by a negative feedback loop.^{27,28} Combined with the homogeneously decaying profile proposed by our model, this regulatory network architecture should create an outwards-moving ring around producer colonies where receiver colonies will respond. This feature could be a mechanism for the creation of ringlike spatial patterns, similar to the ones discussed by Ref. 17.

Another interesting consideration resulting from the work presented here is the following: The expression for the front speed $v = \sqrt{D\lambda}$ contains the growth rate as one of the factors. One can therefore expect that systems that grow more rapidly will also spread their signals more rapidly, and conversely if the growth rate is lower. For colonies producing and responding to the same signaling molecules, this dependence on the growth rate carries an additional means of sensing and reacting to local environmental conditions: Since regions with higher growth rates presumably have better nutrient supply and growth conditions, colonies growing here might dominate the local signal landscape, and if bacteria in the vicinity can follow the signal gradient, they might thus be attracted to more favorable environments. The linear spreading and the

well defined gradients would make this signal much easier to follow than nutrient gradients that only spread diffusively.

VI. MATERIALS AND METHODS

A. Bacterial strains and growth conditions

The strains used in this study were generated using standard genetic techniques and grown applying standard laboratory practice.^{35,38} After cloning in *Escherichia coli* DH5 α , final constructs were verified by DNA sequencing, and if subsequent homologous recombination in *S. meliloti* was involved, the resulting strains were again verified by DNA sequencing.

For the sender strain, the AHL synthase gene promoter including the downstream native ribosome binding site and the first 27 base pairs of the *sinI* gene, the *mVenus* gene³⁹ including stop codon, and the AHL synthase gene *sinI* with its native ribosome binding site were inserted into the plasmid pK18mobsacB⁴⁰ in *E. coli* DH5 α . This construct was transferred to *S. meliloti* strain Sm2B3001⁴¹ by *E. coli* S17-1-mediated conjugation.²⁸ Double recombinants carrying the transcriptional fusion at the chromosomal *sinI* locus were selected on Lysogeny broth (LB)²⁸ agar containing 10% sucrose.

Receiver constructs were based on the same AHL synthase promoter sequence as the sender strain. For the experiment with seven sender colonies, this promoter sequence was fused to the *mCherry* gene⁴² on the low copy plasmid pPHU231;⁴³ the plasmid also carried a second copy of the same promoter fused to *cerulean*⁴⁴ and the promoter of *S. meliloti* gene *SMc00877* fused to *mVenus*, both of which were not analyzed for this study. By *E. coli* S17-1-mediated conjugation, the final construct was transferred to *S. meliloti* Sm2B4001³⁵ carrying a deletion starting 102 base pairs upstream of the *sinI* ATG and including the first 66 base pairs of the *sinI* gene. For all other experiments including the receiver-only control, the AHL synthase promoter sequence followed by the *mVenus* gene was inserted into the suicide plasmid pK18mob2_Km.⁴⁰ The final construct was transferred to *S. meliloti* Sm2B4001 via *E. coli* S17-1-mediated conjugation. Recombinants carried the plasmid integrated at the chromosomal *sinI* promoter locus.

For most experiments, the *sinI* promoter-*mVenus* strains also carried a synthetic version of the *trp* promoter regulating expression of the *mCherry* gene as a constitutive reporter. For the sender, this construct was cloned into the suicide plasmid pK18mob2_Km also carrying a *wgeA* promoter-*cerulean* fusion—the *wgeA* promoter drives expression of genes essential for exopolysaccharide production and served as the integration site for the plasmid. The receiver strain with the *sinI* promoter-*mVenus* fusion carried only the synthetic *trp* promoter-*mCherry* fusion cloned into the single copy plasmid pABC1mob.³⁸

Starter cultures for time-lapse microscopy were grown in tryptone-yeast extract (TY) medium²⁸ to an optical density measured at a wavelength of 600 nm (OD_{600}) of around 0.8. After harvest, cells were washed three times in an equal volume of morpholinepropanesulfonic acid (MOPS)-buffered medium.⁴⁵ Cell density was then adjusted to an OD_{600} of

0.000005, 0.00001, 0.000025, or 0.00025, depending on the particular experiment. Agarose pads were prepared in 17 × 28 mm Frame Seal *in situ* polymerase chain reaction (PCR) and Hybridization slide chambers (Biorad) with MOPS-buffered medium containing 2 mM phosphate and 1.2 % agarose. Corners were cut off to create air reservoirs. Slightly off the middle of the agarose pads, 0.3 μ l of the sender cell suspension were spotted, followed by five spots of the same volume of receiver cell suspensions at 2, 4, 6, 8, and 10 mm distance to the sender spot along a horizontal line. For the control experiment, only receiver cell suspension was spotted mimicking the original experimental setup.

B. Time-lapse fluorescence microscopy

Time-lapse fluorescence microscopy was performed with an Eclipse Ti-E inverse research microscope (Nikon) equipped with a Plan Apo λ 100x/1.45 oil objective (Nikon) in an incubation chamber set to 30 °C. Individual *S. meliloti* cells on the agarose pad were searched for using the live imaging mode of the NIS Elements Advanced Research software version 4.13 (Nikon). x, y, and z coordinates of the cells were recorded in the ND Acquisition module of the same software, and phase contrast and fluorescence images of the respective colonies were automatically taken every 20 minutes using an IXON X3885 camera (Andor, Oxford Instruments) over a period of at least 24 h. When colonies were about to leave the field of vision of the camera after about 17 h, the 2×2 Large Image function of the ND Acquisition module was used to further follow colony expansion. After the time lapse was stopped, an overview of the agarose pad was produced with the Scan Large Image function and a Plan Fluor 4×/0.13 objective (Nikon).

Fluorophore excitation was carried out with an Intensilight Hg Precentered Fiber Illuminator (Nikon). Specific interference and absorption filter sets were applied for mCherry and mVenus fluorescent proteins.³⁶ 2×2 binning was used to reduce excitation intensity and exposure time, and, thus, phototoxicity. Electron-Multiplying (EM) gain was set to 30 for mVenus and 10 for mCherry; conversion gain was always set to 1. For each channel, excitation intensity and exposure time were then selected to assure optimal illumination.

C. Image analysis

Image analysis was performed using the General Analysis module of the NIS Elements Advanced Research software version 4.5. Binary layer construction, i.e., determination of colony perimeters, was performed on phase contrast images, whenever possible combined with quorum-sensing-unrelated fluorescence images from the *trp* promoter-*mCherry* fusion. Based on these colony perimeters, colony area and mean fluorescence values, i.e., the ratio of total fluorescence intensity per area, were determined. From these mean fluorescence values, background fluorescence was subtracted.

ACKNOWLEDGMENTS

We thank Gabriele Malengo for discussing imaging conditions, Stephan Ringshandl for initial help with image

analysis, Yasmin Hengster for the preparation of some of the parameter fits and figures, and Peter Lenz, Knut Drescher, and Moritz Linkmann for helpful comments on the problem and the manuscript. This work was supported by the priority program SPP 1617 (German Research Foundation) and the LOEWE Program of the State of Hesse (SYNMIKRO). This work was dedicated to Hans Braun on occasion of his seventieth birthday.

¹H. A. Braun, K. Wissing, K. Schäfer, and M. C. Hirsch, “Oscillation and noise determine signal transduction in shark multimodal sensory cells,” *Nature* **367**, 270–273 (1994).

²A. Neiman, X. Pei, D. Russell, W. Wojtenek, L. Wilkens, F. Moss, H. A. Braun, M. T. Huber, and K. Voigt, “Synchronization of the noisy electrosensitive cells in the paddlefish,” *Phys. Rev. Lett.* **82**, 660–663 (1999).

³H. A. Braun, K. Schäfer, K. Voigt, B. Peters, F. Bretschneider, X. Pei, L. Wilkens, and F. Moss, “Low-dimensional dynamics in sensory biology 1: Thermally sensitive electroreceptors of the catfish,” *J. Comput. Neurosci.* **4**, 335–347 (1997).

⁴H. A. Braun, M. Dewald, M. Schäfer, K. Voigt, X. Pei, K. Dolan, and F. Moss, “Low-dimensional dynamics in sensory biology 2: Facial cold receptors of the rat,” *J. Comput. Neurosci.* **7**, 17–32 (1999).

⁵W. Braun, B. Eckhardt, H. A. Braun, and M. Huber, “Phase-space structure of a thermoreceptor,” *Phys. Rev. E* **62**, 6352–6360 (2000).

⁶U. Feudel, A. Neiman, X. Pei, W. Wojtenek, H. Braun, M. Huber, and F. Moss, “Homoclinic bifurcation in a Hodgkin–Huxley model of thermally sensitive neurons,” *Chaos* **10**, 231–239 (2000).

⁷J. Keener and J. Sneyd, *Mathematical Physiology I: Cellular Physiology* (Springer, 2008).

⁸A. Prindle, J. Liu, M. Asally, S. Ly, J. Garcia-Ojalvo, and G. M. Stiel, “Ion channels enable electrical communication in bacterial communities,” *Nature* **527**, 59–63 (2015).

⁹J. Liu, A. Prindle, J. Humphries, Marçal. Gabalda-Sagarra, M. Asally, D. D. Lee, S. Ly, J. Garcia-Ojalvo, and G. M. Stiel, “Metabolic co-dependence gives rise to collective oscillations within biofilms,” *Nature* **523**, 550–554 (2015).

¹⁰J. Humphries, L. Xiong, J. Liu, A. Prindle, F. Yuan, H. A. Arjes, L. Tsimring, and G. M. Stiel, “Species-independent attraction to biofilms through electrical signaling,” *Cell* **168**, 200–209.e12 (2017).

¹¹H. B. Kaplan and E. P. Greenberg, “Diffusion of autoinducer is involved in regulation of the *Vibrio fischeri* luminescence system,” *J. Bacteriol.* **163**, 1210–1214 (1985), available at <https://jb.asm.org/content/163/3/1210.short>.

¹²C. W. Fuqua, S. C. Winans, and E. P. Greenberg, “Quorum sensing in bacteria: The LuxR-LuxI family of cell density-responsive transcriptional regulators,” *J. Bacteriol.* **176**, 269–275 (1994).

¹³B. L. Bassler and R. Losick, “Bacterially speaking,” *Cell* **125**, 237–246 (2006).

¹⁴M. B. Miller and B. L. Bassler, “Quorum sensing in bacteria,” *Ann. Rev. Microbiol.* **55**, 165–199 (2001).

¹⁵T. Long, K. C. Tu, Y. Wang, P. Mehta, N. P. Ong, B. L. Bassler, and N. S. Wingreen, “Quantifying the integration of quorum-sensing signals with single-cell resolution,” *PLoS Biol.* **7**, e1000068 (2009).

¹⁶J. Pérez-Velázquez, M. Gölgeli, and R. García-Contreras, “Mathematical modelling of bacterial quorum sensing: A review,” *Bull. Math. Biol.* **78**, 1585–1639 (2016).

¹⁷S. Basu, Y. Gerchman, C. H. Collins, F. H. Arnold, and R. Weiss, “A synthetic multicellular system for programmed pattern formation,” *Nature* **434**, 1130–1134 (2005).

¹⁸T. Danino, O. Mondragón-Palomino, L. Tsimring, and J. Hasty, “A synchronized quorum of genetic clocks,” *Nature* **463**, 326–330 (2010).

¹⁹G. E. Dilanji, J. B. Langebrake, P. De Leenheer, and S. J. Hagen, “Quorum activation at a distance: Spatiotemporal patterns of gene regulation from diffusion of an autoinducer signal,” *J. Am. Chem. Soc.* **134**, 5618–5626 (2012).

²⁰J. B. Langebrake, G. E. Dilanji, S. J. Hagen, and P. De Leenheer, “Traveling waves in response to a diffusing quorum sensing signal in spatially-extended bacterial colonies,” *J. Theor. Biol.* **363**, 53–61 (2014).

²¹T. Ramalho, A. Meyer, A. Mückl, K. Kapsner, U. Gerland, and F. C. Simmel, “Single cell analysis of a bacterial sender–receiver system,” *PLoS ONE* **11**, e0145829 (2016).

- ²²S. Alberghini, E. Polone, V. Corich, M. Carlot, F. Seno, A. Trovato, and A. Squartini, “Consequences of relative cellular positioning on quorum sensing and bacterial cell-to-cell communication,” *FEMS. Microbiol. Lett.* **292**, 149–161 (2009).
- ²³H. S. Carslow and J. C. Jaeger, *Conduction of Heat in Solids* (Oxford Clarendon Press, 1959).
- ²⁴D. G. Kendall, “A form of wave propagation associated with the equation of heat conduction,” *Mathematical Proceedings of the Cambridge Philosophical Society* **44**(4), 591–594 (1948).
- ²⁵X. Fu, L.-H. Tang, C. Liu, J.-D. Huang, T. Hwa, and P. Lenz, “Stripe formation in bacterial systems with density-suppressed motility,” *Phys. Rev. Lett.* **108**, 198102 (2012).
- ²⁶P. Stewart, “Diffusion in biofilms,” *J. Bacteriol.* **185**, 1485–1491 (2003).
- ²⁷P. Charoenpanich, S. Meyer, A. Becker, and M. McIntosh, “Temporal expression program of quorum sensing-based transcription regulation in *Sinorhizobium meliloti*,” *J. Bacteriol.* **195**, 3224–3236 (2013).
- ²⁸E. Krol and A. Becker, “Rhizobial homologs of the fatty acid transporter FadL facilitate perception of long-chain acyl-homoserine lactone signals,” *Proc. Nat. Acad. Sci. U.S.A.* **111**, 10702–10707 (2014).
- ²⁹K. M. Jones, H. Kobayashi, B. W. Davies, M. E. Taga, and G. C. Walker, “How rhizobial symbionts invade plants: *The Sinorhizobium–Medicago model*,” *Nat. Rev. Microbiol.* **5**, 619–633 (2007).
- ³⁰L. V. Rinaudi and W. Giordano, “An integrated view of biofilm formation in rhizobia,” *FEMS. Microbiol. Lett.* **304**, 1–11 (2010).
- ³¹N. Gurich and J. E. Gonzalez, “Role of quorum sensing in *Sinorhizobium meliloti*-Alfalfa symbiosis,” *J. Bacteriol.* **191**, 4372–4382 (2009).
- ³²M. McIntosh, E. Krol, and A. Becker, “Competitive and cooperative effects in quorum-sensing-regulated galactoglucan biosynthesis in *Sinorhizobium meliloti*,” *J. Bacteriol.* **190**, 5308–5317 (2008).
- ³³M. M. Marketon, M. R. Gronquist, A. Eberhard, and J. E. Gonzalez, “Characterization of the *Sinorhizobium meliloti sinR/sinI* locus and the production of novel N-acyl homoserine lactones,” *J. Bacteriol.* **184**, 5686–5695 (2002).
- ³⁴M. Gao, H. Chen, A. Eberhard, M. R. Gronquist, J. B. Robinson, B. G. Rolfe, and W. D. Bauer, “*sinI*- and *expR*-dependent quorum sensing in *Sinorhizobium meliloti*,” *J. Bacteriol.* **187**, 7931–7944 (2005).
- ³⁵M. McIntosh, Stefan Meyer, and A. Becker, “Novel *Sinorhizobium meliloti* quorum sensing positive and negative regulatory feedback mechanisms respond to phosphate availability,” *Mol. Microbiol.* **74**, 1238–1256 (2009).
- ³⁶J. P. Schlüter, P. Czuppon, O. Schauer, P. Pfaffelhuber, M. McIntosh, and A. Becker, “Classification of phenotypic subpopulations in isogenic bacterial cultures by triple promoter probing at single cell level,” *J. Biotechnol.* **198**, 3–14 (2015).
- ³⁷M. E. Ortiz and D. Endy, “Engineered cell-cell communication via DNA messaging,” *J. Biol. Eng.* **6**, 1–10 (2012).
- ³⁸J. Döhlemann, M. Wagner, C. Happel, M. M. Carrillo, P. Sobetzko, T. J. Erb, M. Thanbichler, and A. Becker, “A family of single copy *repABC*-type shuttle vectors stably maintained in the alpha-Proteobacterium *Sinorhizobium meliloti*,” *ACS Synth. Biol.* **6**, 968–984 (2017). pMID:28264559
- ³⁹T. Nagai, K. Ibata, E. S. Park, M. Kubota, K. Mikoshiba, and A. Miyawaki, “A variant of yellow fluorescent protein with fast and efficient maturation for cell-biological applications,” *Nat. Biotechnol.* **20**, 87–90 (2002).
- ⁴⁰A. Schäfer, A. Tauch, W. Jäger, J. Kalinowski, G. Thierbach, and A. Pühler, “Small mobilizable multi-purpose cloning vectors derived from the *Escherichia coli* plasmids pK18 and pK19: Selection of defined deletions in the chromosome of *Corynebacterium glutamicum*,” *Gene* **145**, 69–73 (1994).
- ⁴¹C. Bahlawane, M. McIntosh, E. Krol, and A. Becker, “*Sinorhizobium meliloti* regulator MucR couples exopolysaccharide synthesis and motility,” *Mol. Plant Microbe Interact.* **21**, 1498–1509 (2008).
- ⁴²N. C. Shaner, R. E. Campbell, P. A. Steinbach, B. N. G. Giepmans, A. E. Palmer, and R. Tsien, “Improved monomeric red, orange and yellow fluorescent proteins derived from *Discosoma* sp. red fluorescent protein,” *Nat. Biotechnol.* **22**, 1567–1572 (2004).
- ⁴³P. Hübner, J. C. Willison, P. M. Vignais, and T. A. Bickle, “Expression of regulatory *nif* genes in *Rhodobacter capsulatus*,” *J. Bacteriol.* **173**, 2993–2999 (1991).
- ⁴⁴M. A. Rizzo, G. H. Springer, B. Granada, and D. W. Piston, “An improved cyan fluorescent protein variant useful for FRET,” *Nat. Biotechnol.* **22**, 445–449 (2004).
- ⁴⁵H. Zhan, C. C. Lee, and J. A. Leigh, “Induction of the second exopolysaccharide (EPSb) in *Rhizobium meliloti* SU47 by low phosphate concentrations,” *J. Bacteriol.* **173**, 7391–7394 (1991).

3.2 Frequency modulation of a bacterial quorum sensing response

V. Bettenworth, S. van Vliet, B. Turkowyd, A. Bamberger, H. Wendt, M. McIntosh, W. Steinchen, U. Endesfelder, A. Becker. *Under review at Nature Communications*.

In this work, we scrutinized open questions concerning AHL synthase gene expression and quorum sensing response dynamics in *S. meliloti*, thereby focusing on the cell-to-cell heterogeneity reported by (Schlüter et al., 2015): Although this work – like that of others on heterogeneous autoinducer synthase or precursor gene expression in other organisms (Garmyn et al., 2011; Grote et al., 2014; Pradhan & Chatterjee, 2014) – had indicated that the homogeneous autoinducer production implied in the textbook quorum sensing model (Dunn & Stabb, 2006; Schauder & Bassler, 2001; Uden, 2014) is not universally valid, the phenomenon had not been characterized in detail, and neither its molecular origins nor potential roles in group behavior had been addressed experimentally.

Regarding the exact nature of the phenomenon, we investigated (i) whether the observed heterogeneity originates upstream in the regulatory network or results from stochastic events inherent to *sinI* expression, and (ii) whether it represents stable subpopulations with distinct expression levels or rather variations over time. To address the first question, we examined strains carrying two identical copies of the *sinI* promoter fused to two different fluorophore genes; in such strains, heterogeneity already present upstream in the regulatory network should affect both reporters to a similar degree within individual cells, whereas stochastic events during *sinI* expression should affect the two fluorophores independently and thus lead to uncorrelated variations in a given cell (Elowitz et al., 2002; Raj & van Oudenaarden, 2008). Analysis of strains carrying such constructs by microscopy snapshots and flow cytometry measurements revealed a low degree of correlation between the two fusions, thus indicating that heterogeneity mainly stems from stochasticity (Fig. 1b & Supplementary Fig. 2 in (Bettenworth et al., n.d.)). To address the second question, we tracked cell lineages over time with fluorescence microscopy and ensuing computational analysis, revealing that the observed heterogeneity stems from *sinI* expression in asynchronous pulses (Fig. 1c & Supplementary Fig. 3).

Regarding the molecular origins of the phenomenon, we could demonstrate by protein stability assays and ensuing Western blot analysis that SinR, the LuxR-type regulator essential for *sinI* expression, has a half-life of about 3 minutes (Fig. 2b & Supplementary Fig. 4a, b). We furthermore showed by single molecule microscopy that SinR is a scarce protein and, under rich growth conditions, present in only 10% or less of the cells (Fig. 2c & Supplementary Fig. 4c); moreover, SinR presumably has a very low binding affinity to the *sinI* promoter, as we could not detect binding of SinR alone by electrophoretic mobility shift assay (EMSA) (Fig. 3c). As these characteristics might well form the molecular basis for the stochasticity observed in *sinI* expression, we then generated two strains with slightly decreased and slightly increased *sinR* expression levels, respectively. These modifications not only altered SinR levels in single molecule microscopy as expected, but also resulted in correspondingly decreased and increased

sinI expression pulse frequencies in time-lapse microscopy (Fig. 2d & Supplementary Fig. 6), and in correspondingly decreased and increased fractions of fluorescent cells in flow cytometry (Supplementary Fig. 5), a proxy for pulse frequency. Taken together, this data indicates that SinR scarcity is indeed a determining factor in *sinI* expression pulsing.

Concerning potential roles of *sinI* expression heterogeneity, we explored whether pulse modulation – as achieved artificially by altering *sinR* expression levels – also occurs physiologically. Various environmental and physiological cues are known to affect quorum sensing (Boyer & Wisniewski-Dyé, 2009; Dunn & Stabb, 2006; Hense et al., 2012), and in *S. meliloti* population-level studies had shown *sinI* expression to be enhanced by phosphate starvation (McIntosh et al., 2009), to be decreased by elevated levels of the mobile-to-sessile lifestyle-switch second messenger c-di-GMP (Schäper et al., 2016), and to be enhanced by the AHL receptor ExpR in complex with its autoinducer (McIntosh et al., 2009). When we examined the effects of the respective growth conditions and genetic backgrounds at the single-cell level by time-lapse microscopy and flow cytometry, we found that all of these factors indeed modulate *sinI* expression pulse frequency (Fig. 3 & Supplementary Fig. 7). Furthermore, single molecule microscopy and Western blot analysis indicated that both phosphate starvation and c-di-GMP levels produce this effect by altering SinR abundance, while EMSAs indicated that ExpR-AHL does so by increasing SinR binding affinity to the *sinI* promoter (Fig. 3 & Supplementary Fig. 7). Last but not least, we could show by time-lapse microscopy and plate reader measurements that – as a consequence of the common pool of autoinducers in the environment – higher or lower pulse frequencies in *sinI* expression trigger the onset of the *S. meliloti* quorum sensing response at lower or higher cell numbers, respectively (Fig. 4 & Supplementary Fig. 12). Thus, physiological cues modulate autoinducer synthase gene expression pulse frequency at the single-cell level and, consequently, the timing of the quorum sensing behavioral switch at the level of the group.

Personal contributions

I designed the study and experiments, constructed all strains except precursor strains, performed all experiments except single molecule microscopy and EMSAs, and analyzed all data except single molecule microscopy data. Furthermore, I wrote the manuscript except for the Materials & Methods section on segmentation, tracking and single-cell analysis of early (2D) time-lapse microscopy data (written by Simon van Vliet who had developed pulse analysis procedure and software), the Materials & Methods section on single molecule microscopy, image processing and analysis (written by Bartosz Turkowyd who had performed single molecule microscopy and analyzed the corresponding data), and the Materials & Methods section on protein production and purification (written by Wieland Steinchen who had purified proteins together with Annika Bamberger), and composed all figures except Supplementary Figures 1 (by W. Steinchen, including the corresponding caption) and 4c & 10 (by B. Turkowyd and Ulrike Endesfelder, including the corresponding captions). The *pde0* precursor strain had been constructed and characterized by Heiko Wendt.

Frequency modulation of a bacterial quorum sensing response

Vera Bettenworth^{1*}, Simon van Vliet^{2†}, Bartosz Turkowyd^{3,4†‡}, Annika Bamberger¹, Heiko Wendt¹, Matthew McIntosh^{1§}, Wieland Steinchen¹, Ulrike Endesfelder^{3,4‡}, Anke Becker^{1*}

¹Center for Synthetic Microbiology (SYNMIKRO), Philipps-Universität Marburg, Marburg, Germany.

²Biozentrum, University of Basel, Basel, Switzerland.

³Max Planck Institute for Terrestrial Microbiology, Marburg, Germany.

⁴Department of Physics, Carnegie Mellon University, Pittsburgh, Pennsylvania, USA.

‡Current address: Institut für Mikrobiologie und Biotechnologie, Rheinische Friedrich-Wilhelms-Universität Bonn, Bonn, Germany.

§Current address: Institut für Mikrobiologie und Molekularbiologie, Justus-Liebig-Universität Gießen, Gießen, Germany.

†These authors contributed equally to this work.

*Corresponding authors. Email: vera.bettenworth@gmx.de, anke.becker@synmikro.uni-marburg.de

In quorum sensing, bacteria secrete or release small molecules into the environment that, once they reach a certain threshold, trigger a behavioural change in the population. As the number of these so-called autoinducers is supposed to reflect population density, they were originally assumed to be continuously produced by all cells in a population. However, here we show that in the α -proteobacterium *Sinorhizobium meliloti* expression of the autoinducer synthase gene is realized in asynchronous stochastic pulses that result from scarcity and, presumably, low binding affinity of the key activator. Physiological cues modulate pulse frequency, and pulse frequency in turn modulates the velocity with which autoinducer levels in the environment reach the threshold to trigger the quorum sensing response. We therefore propose that frequency-modulated pulsing in *S. meliloti* represents the molecular mechanism for a collective decision-making process in which each cell's physiological state and need for behavioural adaptation is encoded in the pulse frequency with which it expresses the autoinducer synthase gene; the pulse frequencies of all members of the population are then integrated in the common pool of autoinducers, and only once this vote crosses the threshold, the response behaviour is initiated.

Far-reaching behavioural changes in bacterial populations are often initiated as a reaction to small molecules that the cells themselves produce and release into their environment. These molecules accumulate while the population grows and, once they reach a certain threshold, trigger changes in gene expression leading to, e.g., bioluminescence, virulence or biofilm formation. As the respective molecules are self-produced, they were termed autoinducers, and the phenomenon was initially referred to as autoinduction¹; as the triggered behaviours were assessed to be effective only when performed by a large enough group and the autoinducer concentration to indicate when this sufficient population size – the quorum – is reached, the far more popular term for the process now is ‘quorum sensing’².

Based on their ascribed role as indicators of population density, autoinducers were originally assumed to be continuously produced by all cells in a population^{3,4}. However, over the past decade several cases of cell-to-cell heterogeneity in autoinducer synthase or precursor gene expression have been reported: e.g., in expression of the *Listeria monocytogenes agr* operon

encoding the autoinducer precursor AgrD⁵, and in expression of the autoinducer synthase genes *ahII* in *Pseudomonas syringae*⁶, *traI* and *ngrI* in *Sinorhizobium fredii*⁷, and *sinI* in *Sinorhizobium meliloti*⁸. Both the precise nature of these heterogeneities – whether they represented stable subpopulations with distinct expression levels, or rather variations over time – and their molecular origins remained unclear, but their observation nevertheless indicated that the model of constitutive autoinducer production is not universally valid^{9,10}.

Moreover, both biotic factors like nutrient availability or stress and abiotic factors like diffusion or flow have long been known to affect autoinducer-mediated regulation^{3,11–14}. For instance, luciferase production and bioluminescence in *Aliivibrio fischeri* is delayed via catabolite repression of the autoinducer receptor gene in presence of glucose^{15–19}. Similarly, autoinducer production and target gene expression in *Erwinia carotovora* are altered by the type of carbon source provided²⁰, and activation of the *Pseudomonas aeruginosa las* and *rhl* quorum sensing systems likewise varies depending on growth conditions²¹. It has therefore been repeatedly acknowledged that the term ‘quorum sensing’ represents an oversimplification^{3,11–13} and should be used with full appreciation of the many environmental factors influencing it^{14,22}. Even functions alternative or complementary to cell-density sensing were proposed, ranging from simple sensing of diffusion rates²³ to the integration of different cues like cell density, clustering and diffusion²⁴, or nutritional status and stress²⁵. Here we show how in the α -proteobacterium *S. meliloti* phenotypic heterogeneity in autoinducer synthase gene expression and physiological influences on quorum sensing are linked in a collective decision-making process in which the first represents the key for integration of the latter.

Results

Stochastic pulsing in a canonical LuxR-LuxI-type quorum sensing system. *S. meliloti* is a widely-studied model organism for symbiosis with leguminous plants, but like other rhizobia it can also be found free-living in the soil. It has a canonical Gram-negative quorum sensing system homologous to the *A. fischeri* LuxR-LuxI system where LuxI is the synthase producing *N*-acyl homoserine lactones (AHLs) as autoinducers and LuxR is the cognate receptor, triggering the response upon AHL binding^{2,4}. In the Sin system²⁶ (Fig. 1a), the LuxI-type synthase SinI produces long-chain AHLs that are sensed by the LuxR-type regulator ExpR. However, the Sin system has an additional player: SinR, a LuxR-type regulator that, according to our analysis, has a degenerated AHL binding motif (Supplementary Fig. 1) and whose activity is not affected by AHLs²⁷. Transcription of *sinI* strictly depends on SinR and is enhanced by binding of ExpR-AHL to the *sinI* promoter, giving rise to a positive feedback loop; at very high AHL concentrations, ExpR-AHL represses *sinR* transcription²⁸.

As indicated above, expression of *sinI* in wild-type *S. meliloti* has been found to show strong cell-to-cell variation in fluorescence levels from a *sinI* promoter-fluorophore gene fusion⁸. To examine whether this variation reflects heterogeneity already present upstream in the regulatory network or rather stochastic processes inherent to *sinI* expression, we first generated strains carrying two identical copies of the *sinI* promoter fused to two different fluorophore genes. In these strains, upstream heterogeneity should affect both reporters to a similar degree within individual cells, whereas stochastic events during *sinI* expression should affect the two fusions independently and thus lead to uncorrelated variations^{29,30}. Analysis of wild-type and *expR*⁻ strains carrying such constructs by microscopy snapshots (Fig. 1b & Supplementary Fig. 2a) and flow cytometry (Supplementary Fig. 2b) showed a considerable fraction of non-fluorescing cells in both backgrounds. Furthermore, in some wild-type cells variation in fluorescence affected both reporters to a similar extent, whereas other wild-type cells displayed highly diverging intensities from the two reporters. In *expR*⁻ cells, activation of the two promoter-fluorophore gene fusions was almost entirely uncorrelated, with most of the fluorescing cells showing fluorescence from either one or

the other reporter. The overall low degree of correlation indicates that heterogeneity mainly stems from stochasticity inherent to *sinI* expression.

To further explore this stochasticity, we next followed *expR*⁻ microcolonies carrying a single *sinI* promoter-*mVenus* fusion via time-lapse microscopy (Fig. 1c, Supplementary Movie 1). Here, cells were usually dark, and when fluorescence appeared, it did so not in a coordinated fashion comprising the whole colony, but only in individual cells, and only temporarily. However, fluorescent reporters are stable proteins, and their levels thus reflect both current and past expression; to more accurately examine changes in *sinI* expression over time, we therefore calculated its expression rate adapted from Locke *et al.*³¹ (Fig. 1c, Supplementary Fig. 3a). This computational approach revealed unsynchronized sporadic pulses of *sinI* expression with a mean frequency of about 0.028 events per hour and cell (Supplementary Fig. 3b).

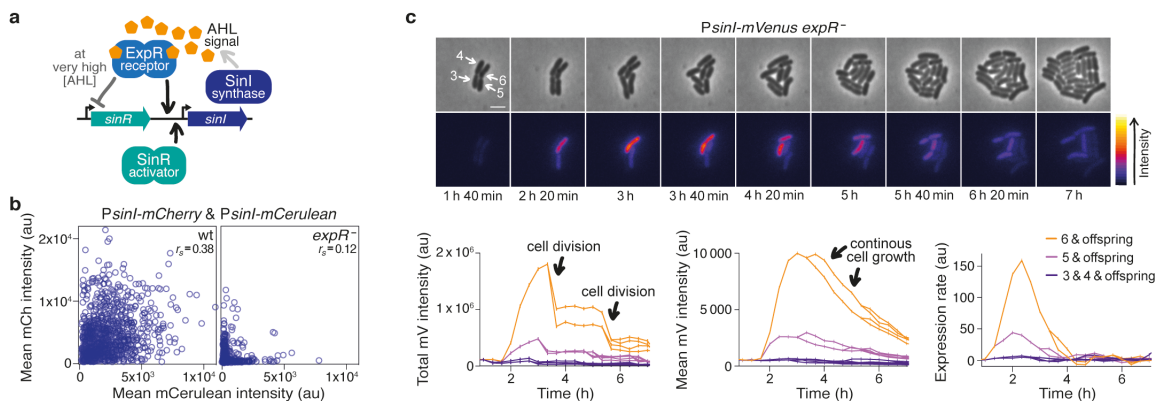


Fig. 1. *sinI* expression is realized in stochastic pulses. **a** Simplified sketch of the regulatory network controlling AHL synthase gene expression in *S. meliloti*. **b** Fluorescence intensities from two *sinI* promoter-reporter gene fusions within individual cells determined by microscopy. Pooled data from 3 biological replicates; $N = 1,190$ (wt), 1,287 (*expR*⁻); au, arbitrary units; r_s , Spearman's correlation coefficient; $P < 0.0001$ for both data sets. See Supplementary Fig. 2a for raw images and details on the construct, Supplementary Fig. 2b for confirmation from an alternative construct. **c** (Top) Phase contrast and fluorescence images from a microscopy time lapse of an *expR*⁻ microcolony carrying a *PsinI-mVenus* fusion, and the 'red fire' lookup table applied to the fluorescence images. Scale bar, 2 μ m. (Bottom) For cells #5 and #6, both total and mean fluorescence intensities first increase. Total fluorescence then drops with cell divisions and stays almost constant in between, while mean fluorescence constantly decreases with cell growth. Gene expression rate is calculated as the change in mean fluorescence intensity over time; peaks in gene expression rate are broadened by the regression involved in the calculation. See Methods and Supplementary Fig. 3a for details and further examples.

A regulatory system based on very low odds. As intrinsic stochasticity was manifest both in the wild type and the *expR*⁻ strain, and was even more pronounced in the latter, we next investigated its most likely source – the essential transcription activator SinR – in the *expR*⁻ background. Expression of *sinR*, when assayed with a *sinR* promoter-*mCherry* fusion via microscopy, appeared rather weak and homogeneous (Fig. 2a), consistent with the above-drawn conclusion that heterogeneity in *sinI* expression does not originate upstream in the regulatory network. However, *in vivo* protein stability assays yielded a half-life of only about 3 minutes for a Flag-tagged SinR fusion protein when produced from the chromosomal *sinR* promoter (Fig. 2b, Supplementary Fig. 4a, b); and single molecule microscopy of fixed cells carrying an *mScarlet-I-sinR* translational fusion at the chromosomal locus indicated that – after background subtraction – only about 10% of cells in a population, at a given time, have mScarlet-I-SinR spots (Fig. 2c; Supplementary Fig. 4c). Furthermore, when examining the effects of Flag-tagged SinR and

mScarlet-I-SinR on the *PsinI-mVenus* reporter construct, the fusion proteins produced much higher fractions of fluorescing cells in flow cytometry measurements than native SinR (Supplementary Fig. 4d), suggesting that the latter is even less stable and/or abundant than its tagged versions. Such low protein abundance might seem unusual; however, a half-life of only 2 minutes has been reported for the *Agrobacterium tumefaciens* LuxR-type regulator TraR in absence of autoinducer³², and when Taniguchi *et al.*³³ quantified the *Escherichia coli* proteome with a fusion protein library, about 40 of the 1,018 proteins assayed could likewise only be detected in 10% or less of the cells.

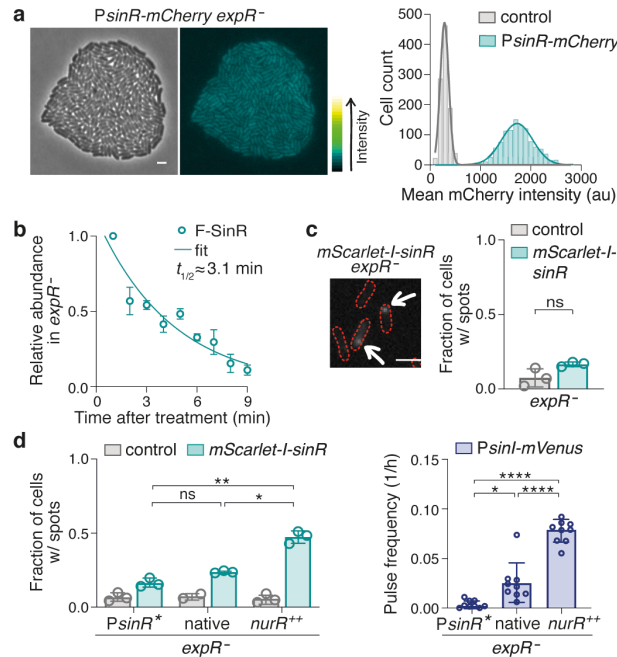


Fig. 2. SinR scarcity is a key factor in *sinI* expression pulsing. **a** (Left) Raw phase contrast and fluorescence microscopy images of a strain carrying a *sinR* promoter-*mCherry* fusion, and the 'green fire' lookup table applied to the fluorescence image. Scale bar, 2 μ m. (Right) Frequency distributions of mean mCherry intensities per cell and corresponding Gaussian fits suggest homogeneous *sinR* expression in the *expR⁻* strain. Pooled data from snapshots of 7 and 6 colonies, respectively, imaged on 2 different days. $N = 1,077$ cells (*PsinR-mCherry*), 1,004 (promoterless control). **b** Relative abundance of Flag-tagged SinR (F-SinR) after chloramphenicol treatment in 1-minute intervals determined by Western blot analysis and a one phase exponential decay fit to the data. Error bars, standard deviation (SD) of three biological replicates. **c** (Left) Cut-out from a single molecule microscopy snapshot of an *expR⁻* strain expressing an *mScarlet-I-sinR* fusion from the chromosomal *sinR* promoter. Arrows mark fluorescing spots. (Right) Bar plots indicating the fraction of cells with fluorescing spots in this strain and the corresponding control strain lacking the fluorophore gene in three biological replicates; bars represent means, error bars represent standard deviations, open circles represent individual data. $N = 2,293$ (*mScarlet-I-sinR*), 1,670 (control). **d** Manipulation of (*mScarlet-I-sinR*) transcription levels yields corresponding patterns of (left) the fraction of cells displaying mScarlet-I-SinR spots in single molecule microscopy and (right) *PsinI-mVenus* expression pulse frequencies in time-lapse fluorescence microscopy. *PsinR^{*}*, promoter mutation resulting in reduced transcription; native, native promoter; *nurR⁺⁺*, native promoter while overproducing its transcription activator NurR. Bar plots indicate means, standard deviations and individual data from (turquoise) single molecule microscopy performed in 3 biological replicates and (blue) time-lapse fluorescence microscopy of 9 colonies imaged on 3 different days. ns, $P \geq 0.05$; *, $P < 0.05$; **, $P < 0.01$; ****, $P < 0.0001$; for exact P values see Supplementary Table 2, for N see Supplementary Table 3.

To test whether SinR scarcity is a determinant in *sinI* expression pulsing, we then generated two strains with slightly reduced and slightly increased *sinR* expression levels, respectively; the former by introducing a mutation into the *sinR* promoter interfering with binding of its transcription activator NurR³⁴, the latter by overexpressing *nurR* from a plasmid. Single molecule microscopy confirmed that the fraction of cells displaying mScarlet-I-SinR spots in the two strains was altered by the manipulations as intended, and time-lapse microscopy indeed yielded about 7-fold reduced and 3-fold increased *sinI* expression pulse frequencies, respectively (Fig. 2d & Supplementary Fig. 5a). When we repeated the analysis with different thresholds for what is considered a pulse, absolute pulse frequencies of course changed, but the relative differences between the strains remained (Supplementary Fig. 6). Furthermore, the fraction of fluorescent cells in flow cytometry measurements – a proxy for pulse frequency, as, e.g., a higher frequency over time in individual cells should produce a higher fraction of fluorescent cells in a population at a given time – was altered in a corresponding fashion (Supplementary Fig. 5b); *nurR* overexpression in a *sinR*⁻ or *sinR* promoter mutation background in turn did not affect this fraction (Supplementary Fig. 5c). In contrast, direct overproduction of (mScarlet-I-)SinR from a plasmid not only abolished heterogeneity in fluorescence both from the mScarlet-I-SinR and the *PsinI-mVenus* fusion, but also greatly increased fluorescence intensities (Supplementary Fig. 5d), disrupting the otherwise stochastic regulatory system. Thus, scarcity of SinR is indeed a determining factor for *sinI* expression in a pulsatile rather than a continuous fashion.

Pulse frequency fine-tuned by physiological factors. As we were able to modify *PsinI-mVenus* pulse frequencies artificially, we next explored whether pulse modulation also occurs physiologically. As mentioned above, effects of various biotic and abiotic cues on quorum sensing are well-established^{3,11–13,25}, and pulse modulation might well represent a mechanism for integrating physiological information on the dynamic scale. Population-level studies in *S. meliloti* had shown *sinI* expression to be enhanced by phosphate starvation²⁸, to be decreased by elevated levels of the mobile-to-sessile lifestyle-switch second messenger cyclic di-GMP (c-di-GMP)³⁵, and, as mentioned above, to be enhanced by ExpR-AHL-mediated positive feedback in the wild type²⁸. When we examined the effects of the respective growth conditions and genetic backgrounds at the single-cell level, phosphate starvation indeed increased *sinI* expression pulse frequency, the fraction of *PsinI-mVenus* fluorescing cells, and the fraction of cells with mScarlet-I-SinR spots in the *expR*⁻ background compared to rich growth conditions (Fig. 3a, Supplementary Fig. 7a, b); and an *expR*⁻ strain incapable of producing detectable amounts of c-di-GMP (*dgc0*)³⁵ likewise showed increased *sinI* pulse frequency, fraction of fluorescing cells, and cells with mScarlet-I-SinR spots, while an *expR*⁻ strain producing elevated levels of c-di-GMP (*pde0*) (Supplementary Fig. 8) showed the reverse phenotype, namely reduced pulse frequency, a smaller fraction of fluorescing cells, and fewer cells with mScarlet-I-SinR spots (Fig. 3b, Supplementary Fig. 7c, d).

In the wild type capable of ExpR-AHL-mediated positive feedback, pulse frequency and flow cytometry fraction were even raised approximately 10-fold compared to the *expR*⁻ strain, to about 0.28 pulses per hour and cell (Fig. 3c, Supplementary Fig. 7e, f, Supplementary Movie 2). However, presence of *expR* did not increase the fraction of cells with mScarlet-I-SinR spots correspondingly (Supplementary Fig. 7g). Instead, we could detect a His-GB1-SinR-dependent supershift of the *sinI* promoter in electrophoretic mobility shift assays (EMSAs) in the presence of His-ExpR-AHL, but no shift by purified His-GB1-SinR alone even at high concentrations (Fig. 3c). First, this observation suggests a very low binding affinity for SinR alone – too low to be detectable by our assay, and a feature that very likely adds to the stochasticity of the system (see Supplementary Fig. 7h for in vivo functionality of His-GB1-SinR in *expR*⁻). Second, ExpR-AHL seems to achieve its positive feedback by facilitating binding of SinR to the *sinI* promoter, while both phosphate starvation and c-di-GMP levels modulate SinR abundance (see Supplementary Fig. 7i for confirmation of relative differences by western blot analysis), thus all fine-tuning the probability for a *sinI* expression pulse. Consequently, the frequency modulation by phosphate

starvation and c-di-GMP levels observed in *expR*⁻ strains also occurred in the wild-type background, only at elevated levels (Fig. 3d).

Since large cell aggregates like biofilms are known to exhibit concentration gradients of oxygen, nutrients, and autoinducers^{36,37}, we furthermore scrutinized two of our data sets (Fig. 2d & 3c) for a potential effect of a cell's position within the colony, and for potential changes over the course of colony development, i.e., over time. The data set with different *sinR* expression levels did show a significant increase in *sinI* expression from colony edge to colony centre; however, these differences were small compared to the differences between the respective strains (Supplementary Fig. 9a). Moreover, no such effect could be detected for the data set comparing the *expR*⁻ strain with the wild type (Supplementary Fig. 9b). When the same data sets were subdivided into three observation periods, no change in pulse frequency was observed between the temporal subsets (Supplementary Fig. 9c, d). Thus, while in view of our other data both temporal and positional effects on *sinI* expression pulse frequency would be expected in larger cell aggregates, the colonies we analysed at the single-cell level are very likely too small to already comprise the necessary chemical gradients.

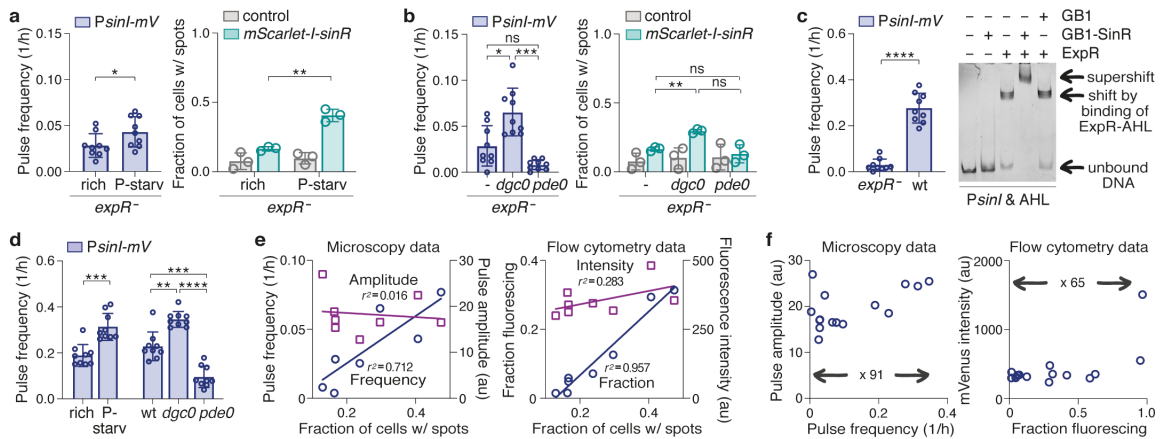


Fig. 3. Physiological factors modulate pulse frequency by changing SinR abundance and DNA binding affinity. **a, b** Phosphate starvation (**a**) and cyclic-di-GMP levels (**b**) modulate both the frequency of *sinI* expression pulses (left, respectively) and the fraction of cells displaying mScarlet-I-SinR spots (right, respectively) in corresponding patterns. Here and in (**c, d**): Bar plots show means, standard deviations and individual data from (turquoise) single molecule microscopy performed in 3 biological replicates and (blue) time-lapse fluorescence microscopy of 9 colonies imaged on 3 different days. ns, $P \geq 0.05$; *, $P < 0.05$; **, $P < 0.01$; ***, $P < 0.001$; ****, $P < 0.0001$. **c** The wild type with AHL-induced positive feedback likewise displays elevated *sinI* expression pulse frequency compared to the *expR*⁻ strain (left). EMSA indicating that the AHL receptor increases SinR binding affinity to the *sinI* promoter: His-GB1-SinR does not induce a shift of *sinI* promoter DNA, but causes a supershift in the presence of His-ExpR-AHL. His-GB1-SinR, 70 μ M; His-GB1, 70 μ M; His-ExpR, 1 μ M; AHL, 10 μ M (right). **d** Modulation of *sinI* expression pulse frequency by phosphate starvation (left) and c-di-GMP levels (right) in the wild type. **e** Summary of pulse data determined by microscopy (left) and flow cytometry (right) indicating a linear correlation between the fraction of cells with mScarlet-I-SinR spots and pulse frequency. Circles represent pulse frequency (left) or fraction of cells fluorescing (right), squares represent median pulse amplitude (left) or median fluorescence intensity (right), both plotted against the respective fraction of cells with mScarlet-I-SinR spots; lines represent corresponding linear fits to the data. r^2 calculated from Pearson's correlation coefficient; $P = 0.0085$ for pulse frequencies, $P < 0.0001$ for fractions fluorescing, $P = 0.7625$ for pulse amplitude, $P = 0.1746$ for fluorescence intensity data. **f** Median pulse amplitude plotted over mean pulse frequency (left), and median fluorescence intensity plotted over mean fluorescing fraction (right), in both *expR*⁻ and wild-type backgrounds. The increase in flow cytometry intensities corresponding with very large fluorescing fractions are

not reflected in pulse data and possibly result from consecutive pulses that are still separated by time-lapse analysis, but add up in terms of total fluorescence intensities. See Supplementary Fig. 11 for raw data on pulse amplitudes and fluorescence intensities.

A linear correlation between key activator abundance and pulse frequency. Based on our hitherto cumulated data, we furthermore sought to analyse the relationship between mScarlet-I-SinR abundance and *sinI* expression more deeply. Both the high degree of stochasticity observed in *sinI* expression (Fig. 1b) and the homogeneity observed in *sinR* expression (Fig. 2a) had already indicated that heterogeneity in *sinI* promoter activity does not originate upstream in the regulatory network, i.e., from cell-to-cell differences in *sinR* expression. Closer examination of the single molecule microscopy data from all *mScarlet-I-sinR* strains (with exception of the overexpression strain) supports this conclusion, as it suggests that mScarlet-I-SinR spots do not contain higher-order multimers, but only one or two functional mScarlet-I molecules, and thus very likely only one or two SinR molecules (Supplementary Fig. 10). Moreover, all data gathered in the *expR* background indicates a linear correlation between the fraction of cells displaying mScarlet-I-SinR spots and frequency of *sinI* expression pulses (Fig. 3e; Supplementary Table 1). In contrast, pulse amplitude and fluorescence intensity as its corresponding property in flow cytometry data do not appear to correlate with SinR abundance. When plotting pulse amplitude against frequency for all *expR* and wild-type data, frequency increases about 91-fold over the whole data set, while amplitude varies only about 2-fold; flow cytometry data shows a similar trend, with a 65-fold change in the fraction of fluorescing cells, and a 6-fold change in intensity (Fig. 3f; Supplementary Table 1). Hence, regulation of *sinI* expression primarily happens through frequency modulation, and amplitude modulation plays a minor role at best.

Response dynamics determined by pulse frequency. The differences in *sinI* expression pulse frequency in single cells should in turn impact behaviour on the level of the group, as they will affect the overall AHL production rate of the population, and, consequently, the velocity with which autoinducer concentrations in the environment reach the threshold to trigger the quorum sensing response. To test this rationale, we followed the wild-type colonies that had shown frequency-modulated pulsing in *sinI* expression due to growth conditions or c-di-GMP levels (Fig. 3d) for 10 or more hours after they became three-dimensional. At this stage we assessed fluorescence no longer at the single-cell level, but as mean fluorescence intensities of the whole colony from a *wgeA* promoter-*mCerulean* fusion – the *wgeA* promoter regulates expression of a gene cluster involved in production of galactoglucan, an exopolysaccharide (EPS) that plays an important role in *S. meliloti* colony expansion and sliding motility^{38–40} and that is a central part of the organism's quorum sensing response^{27,41}. As expected, response onset in strains displaying higher *sinI* expression pulse frequencies could be observed several hours earlier and at smaller colony sizes (Fig. 4a, Supplementary Fig. 12a-f) than in colonies with lower pulse frequencies.

However, as phosphate starvation and c-di-GMP levels might impact EPS production not only via quorum sensing (e.g., Supplementary Fig. 12c), we furthermore sought to isolate AHL production-response-dynamics from other regulatory networks in the organism. To this end, we made use of the constructs with artificially altered *sinR* expression levels and *sinI* expression pulse frequencies (Fig. 2d, Supplementary Fig. 5), harvested their supernatants at various optical densities and added them to the growth medium of an *S. meliloti* AHL indicator strain, assuming that differences in the quorum sensing response of the latter should then solely result from differences in the amount of AHLs in the respective supernatants (Supplementary Fig. 12g, h). Even in this decoupled system, response curves staggered according to pulse frequencies of the donor strains (Fig. 4b). Thus, when adapting to changes in environment or lifestyle, *S. meliloti* cells adjust AHL synthase gene expression pulse frequency, resulting in response onset at larger or smaller cell numbers (Fig. 4c).

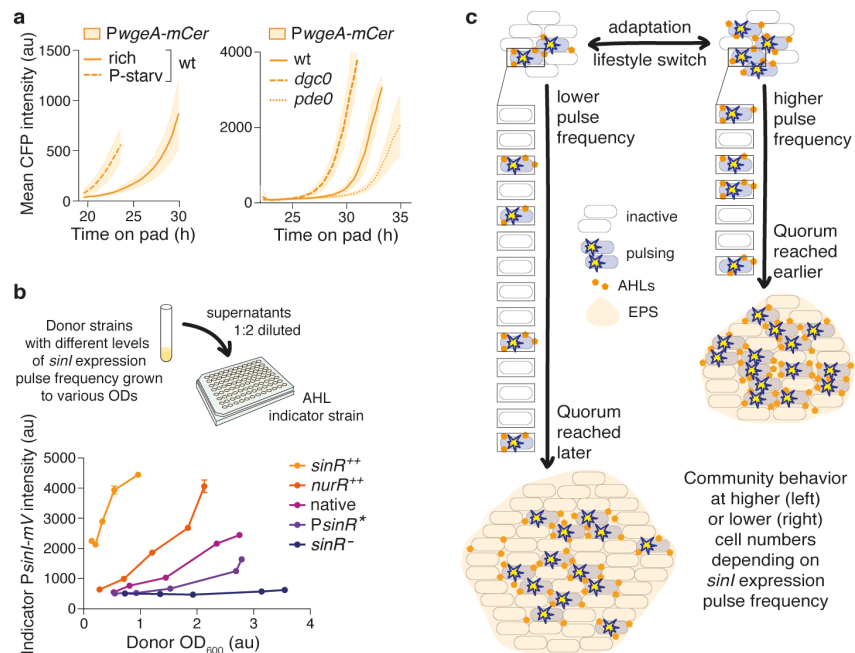


Fig. 4. *sinI* expression pulse frequency determines quorum sensing response dynamics. **a** Different *sinI* expression pulse frequencies correlate with different quorum sensing response dynamics, i.e., earlier or later activation of the EPS promoter *PwgeA*. Curves show means and standard deviations of the same 9 colonies as in Fig. 3d followed for approx. 10 more hours (left), and of 6 colonies from 2 biological replicates in Fig. 3d followed for approx. 12 more hours (right); the 3 colonies from the third biological replicate show similar relative differences, but different absolute timing (Supplementary Fig. 12f) that could be due to, e.g., differences in AHL stability on the pad. **b** Experimental setup applied to test the effect of different *sinR* expression levels – and corresponding different *sinI* expression pulse frequencies – on quorum sensing response dynamics of an *S. meliloti* AHL indicator strain (top). The different donor strains need to grow to different optical densities (OD_{600}) till their culture supernatants induce the positive feedback on the *PsinI-mVenus* fusion in the indicator strain, confirming differences in the amount of secreted AHLs as the origin of distinct quorum sensing response dynamics (bottom). We could not observe an effect on *PwgeA*, probably due to substantial loss of AHLs during harvest and sterile filtration of the supernatants. **c** Model illustrating frequency modulation of the *S. meliloti* quorum sensing response.

Discussion

The stochastic pulsing in *sinI* expression reported here resembles the pulsatile activity of several stress-responsive transcription factors in *Saccharomyces cerevisiae*^{42–44}, σ^B and other alternative sigma factors in *Bacillus subtilis*^{31,45}, and the short gene expression bursts from the uninduced *lac* promoter in *E. coli*^{46,47}. Similar activity profiles have been furthermore described for higher eukaryotes including mammals, and the terms ‘transcription pulse’ and ‘transcriptional burst’ are sometimes used synonymously to describe such phenomena^{48,49}. In contrast, Levine et al. define pulsing as a phenomenon “generated by genetic circuits that activate and deactivate key regulators and modulate pulse characteristics, such as frequencies and amplitudes”, whereas “transcriptional bursting [...] results from the stochastic nature of gene expression”⁵⁰. However, judging from our findings on *sinI* expression, the genetic circuit and the stochastic nature of gene expression are not always clearly distinguishable; rather, stochasticity is an integral part of the *S. meliloti* Sin system.

For instance, when comparing *sinI* expression pulsing and the pulsatile activity of the *B. subtilis* stress response sigma factor σ^{B31} , both are asynchronous and share features like

variability in amplitude and frequency modulation by physiological factors. On the other hand, they differ fundamentally with respect to the stochasticity involved, indicative of the disparate mechanisms underlying the two phenomena: Whereas *S. meliloti* cells carrying two different *sinI* promoter-fluorophore gene fusions displayed highly diverging intensities from the two reporters both from cell to cell and within individual cells (Fig. 1b, Supplementary Fig. 2), fluorescence intensities of analogous *sigB* promoter-fluorophore fusions in *B. subtilis* only varied from cell to cell, but were highly correlated within cells³¹. Moreover, activity of the *sigB* promoter was also highly correlated with activities of other σ^B -regulated promoters in the respective cells³¹. Stochasticity in σ^B activity is thus restricted to whether or not, in a given cell at a given time, a pulse is initiated. This decision is triggered by a phosphoswitch, i.e., fluctuations in the ratio of phosphatases and kinases acting on the σ^B anti-anti-sigma factor that set off time-delayed positive and negative feedback loops, with the positive feedback first turning stochastic *sigB* promoter activation into a cell-wide pulse, and the negative feedback subsequently terminating it³¹.

In contrast, *sinI* expression pulses begin and end without feedback loops. Instead, they very simply stem from instability and scarcity of the key activator SinR (Fig. 2, Fig. 3e), and very likely also from low binding affinity of SinR to the *sinI* promoter (Fig. 3c). Together, these biochemical properties of SinR yield a very low probability for a *sinI* transcription event, and a short duration of such an event if it does occur. With respect to the underlying mechanism, pulsing in *sinI* expression thus is a reversed image of stochastic gene expression from uninduced *lac* promoters in *E. coli*: For a reduced version of the promoter comprising only the O_1 and O_3 operators, Yu *et al.* reported short transcriptional bursts with a mean frequency of 1.2 events per cell cycle⁴⁶, and Cai *et al.* reported similarly brief bursts with a mean frequency of 0.11 events per cell cycle for the wild-type *lac* promoter comprising all three operators O_1 , O_2 and O_3 ⁴⁷. In both cases, the transcriptional bursts were attributed to stochastic and brief dissociation of the *lac* repressor LacI from the respective promoters. Furthermore, both cell-to-cell and within-cell heterogeneity was observed in a seminal study by Elowitz *et al.* from two promoter-fluorophore gene fusions in which the identical synthetic promoters contained the O_1 operator²⁹. However, stochasticity in this case was much less prominent than observed for the two analogous *sinI* promoter-fluorophore gene fusions (Fig. 1b, Supplementary Fig. 2), probably because the synthetic promoter⁵¹ does not enable the DNA loop formation crucial for enhanced repression by LacI⁵², thus making dissociation events much more likely. Based on differences in repression of the *lac* promoter versions⁵², and on differences in burst frequencies^{46,47}, one would therefore expect stochasticity to be more prominent for the O_1 & O_3 *lac* promoter version used by Yu *et al.*, and even more so for the wild-type version comprising all three operators studied by Cai *et al.*.

Due to the very low probability for SinR binding to the *sinI* promoter, it is impossible to predict whether or not a given cell at a given time will experience a *sinI* expression pulse. Nevertheless, *sinI* expression is by no means random or arbitrary in the sense of ‘happening without cause or reason’ – over a large enough population, the fraction of cells with a SinR-*sinI* promoter complex and ensuing *sinI* expression is clearly defined by abundance of SinR, and by abundance of ExpR and AHLs affecting SinR binding affinity (Fig. 3). Similarly, the term ‘noise’, albeit widely used as a synonym for stochasticity^{30,53,54}, does not seem appropriate in this context, since it has connotations of mere statistical fluctuations. In contrast, the Sin system is based on low probabilities, and without them, regulation of *S. meliloti* quorum sensing would be entirely different: A higher binding affinity of SinR to its promoter, for instance, with everything else unchanged, would considerably increase *sinI* expression rate, and the same is of course true for higher SinR abundance (Supplementary Fig. 5d); both would thus strongly increase AHL production in the population and accelerate quorum sensing dynamics (Fig. 4b). If, on the contrary, the dynamics were to be preserved, a steady *sinI* transcription would have to be compensated for by, e.g., a reduced *sinI* translation rate, a reduced AHL production rate, and/or a reduced sensitivity of the AHL receptor to autoinducers. The Sin system thus represents a probabilistic switch operating at low odds, and the setup of this switch furthermore allows for the integration of

physiological factors, as these either fine-tune abundance of SinR (Fig. 3a, b), or its binding affinity (Fig. 3c), and thereby modulate *sinI* expression pulse frequency.

The connection between environmental cues and quorum sensing dynamics per se is not novel: Population-level studies in *S. meliloti* had already shown *sinI* expression to be affected by the respective cues^{28,35}, just as – for instance – population-level studies in *A. fischeri* had shown luciferase production and bioluminescence to be delayed via catabolite repression^{15–19}. Indeed, Fuqua *et al.* emphasized the role of physiological factors when first proposing the term ‘quorum sensing’, stating that, in addition to the sufficiently high cell density for autoinducers to accumulate to a threshold concentration, “first, some external environmental signal other than an autoinducer must be perceived”². Dunn and Stabb reasoned that “by embedding quorum signalling with [...] regulatory systems [like catabolite repression], bacteria are able to modulate the production of autoinducers such that their concentration reflects not only cell density but also specific parameters of their environment”, and that target genes are thus regulated “not always with direct correlation to population numbers”³. And after examining the activity of *P. aeruginosa las* and *rhl* quorum sensing systems under 46 growth conditions, Duan and Surette even concluded that “no correlation could be established between cell densities and the activation of quorum sensing expression [...], indicating the absence of a specific cell density as a prerequisite for quorum sensing activation”²¹.

Similarly, we found that the onset of the quorum sensing response in *S. meliloti* populations is triggered at smaller or larger cell numbers depending on the physiological state of the individual cells (Fig. 4a, Supplementary Fig. 12), implying that the process of autoinducer production and sensing in *S. meliloti* is likewise not a simple matter of counting cell numbers as suggested by the analogy of the quorum. Since we furthermore found that the physiological state of the individual cells is encoded in their *sinI* expression pulse frequency (Fig. 3), the process seems more comparable to a voting in a local community, or to the collective decision-making described for social insects, e.g., during selection of a new nest site by a swarm of honey bees^{55–59}: Whereas the length of a scout bee’s waggle dance is proportional to the quality of the potential nest site it has explored, convincing more bees to likewise visit that site and cast their votes, the pulse frequency with which an individual *S. meliloti* cell expresses the AHL synthase gene carries information about its physiological state and need for behavioural adaptation. Even a similar amplification process appears to be involved, as the AHLs produced by one bacterium facilitate *sinI* expression in its neighbours by increasing binding affinity of SinR to the *sinI* promoter, should the neighbours experience a similar need for action and, thus, a similar increase in SinR abundance. Due to the common pool of autoinducers – comparable to a ballot box – the pulse frequencies of all members of the population are then integrated into the total AHL concentration; only if this vote crosses the threshold, the response behaviour is initiated.

As mentioned above, phenotypic heterogeneity has been reported not only for AHL synthase gene expression in *S. meliloti*⁸, but also for expression of the homologous genes *ngrI* and *traI* in its close relative *S. fredii*⁷, the homologue *ahII* of *P. syringae*⁶, and for expression of the *agr* operon encoding the quorum sensing system of *L. monocytogenes*⁵; in these studies, the respective quorum sensing-‘ON’ and -‘OFF’ fractions determined by microscopy snapshots or flow cytometry were also affected by environmental factors^{5–7}. Furthermore, there is indication of inherent heterogeneity in AHL synthase gene expression in *Pseudomonas putida*⁶⁰. It would be curious to see whether these heterogeneities represent stable subpopulations, or likewise result from asynchronous stochastic pulsing, thus making frequency-modulation as described here a recurring mode for collective decision-making in bacterial quorum sensing.

Methods

Media and growth conditions. Rich media were used for strain construction and maintenance: lysogeny broth (LB) medium (10 g/l tryptone, 5 g/l yeast extract, 5 g/l NaCl) for *Escherichia coli*

strains, tryptone-yeast extract (TY) medium (5 g/l tryptone, 3 g/l yeast extract, 0.4 g/l CaCl₂ x 2 H₂O) for *Sinorhizobium meliloti* strains.

If required for selection during *E. coli* strain construction or for plasmid maintenance in *E. coli* strains, kanamycin was added at 50 mg/l, gentamicin at 8 mg/l and ampicillin at 150 mg/l to solid media. For selection during *S. meliloti* strain construction and for plasmid maintenance in *S. meliloti*, streptomycin was added at 600 mg/l to solid media, kanamycin at 200 mg/l, and gentamicin at 30 mg/l. For liquid cultures, antibiotic concentrations were generally reduced by half if not indicated otherwise. Selection for sucrose sensitivity of *S. meliloti* clones after double homologous recombination was carried out on LB agar containing 10% (w/v) sucrose⁶¹.

Starter cultures for (time-lapse) fluorescence microscopy were grown overnight in 3 ml TY medium to stationary phase; the rationale for beginning microscopy experiments with stationary phase cells was that – despite potentially different quorum sensing response dynamics – this way all wild-type (*expR*⁺) strains should have reached the same stage of the quorum sensing process, i.e., the ExpR-AHL-induced negative feedback on *sinR* expression at very high AHL concentrations^{27,28}.

Starter cultures for flow cytometry, microplate reader measurements, single molecule microscopy and western blot analysis of Flag-tagged SinR were grown in 3 ml modified morpholinopropane sulfonate (MOPS)-buffered medium slightly adapted from⁶² to exponential phase; the exact composition was 1x MOPS solution (10 g/l MOPS, 10 g/l mannitol, 3.93 g/l sodium glutamate, 0.246 g/l MgSO₄ x 7 H₂O, pH 7.2, autoclaved), with CaCl₂ (37 mg/ml, autoclaved), FeCl₃ x 6 H₂O (10 mg/ml, filter-sterilized and stored at 4 °C), oligo-elements (3 mg/ml H₃BO₃, 2.23 mg/ml MnSO₄ x 4 H₂O, 0.288 mg/ml ZnSO₄ x 7 H₂O, 0.125 mg/ml CuSO₄ x 5 H₂O, 0.065 mg/ml CoCl₂ x 6 H₂O, 0.12 mg/ml NaMoO₄ x 2 H₂O, filter-sterilized) and biotin (1 mg/ml, filter-sterilized and stored at 4 °C) all added in a 1:1,000 dilution, and KH₂PO₄ (174 mg/ml, autoclaved) added in a 1:500 dilution. For experiments involving titration of *sinR* expression levels, all starter cultures were grown in presence of gentamicin for plasmid maintenance. For main cultures, if not otherwise indicated, 3 ml fresh modified MOPS-buffered medium without antibiotics was inoculated from starter cultures to yield an OD₆₀₀ of about 0.1-0.3 at harvest the next morning; when involving titration of *sinR* expression levels, isopropyl-β-D-thiogalactopyranoside (IPTG) was added at 0.5 mM. For phosphate starvation, overnight cultures were harvested, washed three times in MOPS-buffered medium without phosphate, resuspended in MOPS-buffered medium without phosphate, and incubated for 5 more hours.

E. coli strains were grown at 37 °C, *S. meliloti* strains at 30 °C. Conjugations were incubated at 30 °C. Liquid cultures were grown in glass test tubes shaking at 200 rpm.

Strain construction. Cloning was performed in *E. coli* DH5α, and final constructs were verified by DNA sequencing. Plasmid transfer into *S. meliloti* was carried out by *E. coli* S17-1-mediated conjugation, and if integration into the *S. meliloti* genome via single or double homologous recombination was involved, the resulting strains were again verified by sequencing. Strains, plasmids and primers used are listed in Supplementary Tables 4-6. Details on strain constructions are given in the Supplementary Methods 1.

(Time-lapse) fluorescence microscopy. Starter cultures were prepared as described above. 1 ml of starter culture were harvested by centrifugation (4,000 x g, 5 min, RT), and cells were either immediately resuspended in modified MOPS-buffered medium to an OD₆₀₀ of 0.25, or first washed three times in 1 ml MOPS-buffered medium without phosphate (for phosphate starvation conditions, to remove residual phosphate) or in 1 ml MOPS-buffered medium containing 2 mM phosphate (for the corresponding rich growth condition; and for *expR*⁺ strains, to remove accumulated AHLs). Cell density was adjusted via serial dilutions to an OD₆₀₀ of 0.000025.

2-3 hours before harvest, agarose pads made from modified MOPS-buffered medium containing 1.5% (w/v) molecular biology grade agarose (Eurogentec) were cast either in 17 x 28 mm or 9 x 9

mm Frame Seal *in situ* polymerase chain reaction and hybridization slide chambers (Biorad); the smaller frame size was chosen for side-by-side comparison of phosphate starvation vs. rich growth conditions as these required different pad composition, and for comparison of wt, *dgc0* and *pde0* strains to avoid alteration of strain-specific quorum sensing response dynamics by diffusing AHLs. Prior to adding cells, pads were allowed to dry for 8-12 minutes depending on temperature and air flow; then, 0.3 μ l per cell suspension (OD₆₀₀ of 0.00025) were spotted on the pads, yielding approximately 3-4 dozen single cells per spot. For the phosphate starvation condition and the corresponding control condition, three additional 0.3 μ l spots of scavenger/indicator cells (OD₆₀₀ of 0.01) were added at the far side of the pads to speed up consumption of residual phosphate and onset of discernible phosphate starvation. To detect the latter, scavenger/indicator cells carried the *pstS* promoter-*mVenus* fusion; to exclude direct effects on the read-out, they also carried a *sinI* deletion and were thus incapable of producing AHLs.

Microscopy was performed with an Eclipse Ti-E inverse research microscope (Nikon) with automated stage and shutters and a Plan Apo λ 100x/1.45 oil objective (Nikon) in an incubation chamber set to 30 °C. For snapshots, pads were incubated 15-17 hours before imaging; for time-lapse fluorescence microscopy, pads were immediately searched for individual cells. Coordinates of the cells were recorded, and phase contrast and fluorescence images of the growing colonies were automatically taken every 20 minutes using the NIS Elements Advanced Research software version 4.13 (Nikon) and an iXon3 electron-multiplying charge-coupled device (EMCCD) camera (Andor, Oxford Instruments) over a period of at least 15 hours. Subsequently, *expR*⁺ strains were followed for at least 10 more hours using the 2x2 Large Image function of the NIS Elements ND Acquisition module, as colonies then grew larger than the field of vision of the camera. In this case, stitching of the image stacks was performed immediately on phase contrast images (15% overlap) using the NIS Elements software. Over the whole time-lapse experiment, focus was maintained using the Perfect Focus System (PFS). Furthermore, to facilitate focus maintenance, microscope and incubation chamber were preheated for at least 4-5 hours, preferably even overnight.

Fluorophores were excited with lasers: mCerulean with a 445 nm CUBE Laser (Coherent Inc., USA) [excitation band pass (ex bp) 445/30, beamsplitter (bs) 458, emission band pass (em bp) 483/32], mVenus with a 514 nm OBIS Laser (Coherent Inc., USA) (ex bp 500/24 nm, bs 520 nm, em bp 542/27 nm) and mCherry with a 561 nm Sapphire Laser (Coherent Inc., USA) (ex bp 562/40 nm, bs 593 nm, em bp 624/40 nm). Laser intensities, exposure times and EM gains were applied as follows: 3%, 600 ms, 100 for *PsinI-mVenus*; 5%, 600 ms, 100 for *Pptrp-mCherry*; 8%, 1 s, 100 for *PsinI-mCerulean*; 5%, 1 s, 100 for *PsinI-mCherry*; 4%, 1 s, 100 for *Plac-mVenus*; 25%, 1s, 100 for *PsinR-mCherry*. For the 2x2 images, settings were modified as follows: 0.5%, 2x2 binning, 1 s, 100 for *PsinI-mVenus*; 0.5% 2x2 binning, 600 ms, 150 for *PwgeA-mCerulean*. Conversion gain was always set to 1. Generally, excitation intensities and exposure times were chosen as low as possible to minimize phototoxicity.

Processing, segmentation, tracking and single-cell analysis of early (2D) time-lapse data. The NIS Elements software was used to crop image stacks to the maximum spatial extent of the colony and to the time period during which cells were growing in a single layer. Further processing was done with a combination of Schnitzcells version 1.1⁶³, Ilastik version 1.3.3post3⁶⁴, and a custom-built Matlab (MathWorks, Natick, Massachusetts) program⁶⁵. The workflow closely follows the pipeline developed by van Vliet *et al.*⁶⁵, with the exception that segmentation was performed using Ilastik instead of Schnitzcells.

Segmentation was done either on the RFP (for *Pptrp-mCherry*) or the YFP (for *Plac-mVenus*) channel using the Ilastik pixel classification workflow⁶⁴. Before import into Ilastik, fluorescent images were deconvolved applying the Lucy-Richardson method (as implemented in the Matlab ‘deconvlucy’ function) using the experimentally determined Point Spread Function (PSF) of the microscope. Pixels were then classified into two classes (‘background’ and ‘cells’), and the resulting probability images were imported into Matlab for post-processing. The cell class

probabilities were smoothed using a Gaussian kernel (with a size of 1 pixel) and thresholded using a fixed threshold value of 0.6 to obtain putative cell masks. Subsequently, a binary closure operation was performed to remove internal holes in the cell masks, and a morphological opening operation (erosion followed by dilation) to separate adjacent cells. The morphological opening was done in two passes: First, all cell masks were opened by 1 pixel; subsequently, any remaining objects that exceeded the expected cell width were automatically classified as potential cell clusters and a second opening by 2 pixels was applied to separate cells in these clusters. The resulting cell segmentation masks were then manually corrected using the Schnitzcells graphical user interface (GUI).

Cell tracking was performed with the automated tracking routine of Schnitzcells 1.1 (original version)⁶³. Subsequently, all tracking results were manually checked and corrected using the Schnitzcells GUI.

Cell features (length, growth rate, and mean fluorescence intensity as a proxy for gene expression level *etc.*) were extracted using a custom-written Matlab program which had been previously developed for *E. coli* microcolonies⁶⁵ and which was here adapted for *S. meliloti*. We summarize the most important details below.

Cell lengths were estimated using the method developed by Kiviet et al.⁶⁶. Here, a third-degree polynomial, $f(x)$, is fitted to the cell mask. This polynomial is extrapolated by 10 pixels in both directions and the locations of the cell poles are determined automatically by calculating the silhouette proximity (sum of the squared distances to closest 25 pixels in cell mask) along the centerline. This measure increases sharply at the cell poles, and the location of the poles can thus be taken as the points where the silhouette proximity reaches 110% of the average value in the cell centre. Subsequently, the cell length is calculated as $L = \int_{x_0}^{x_1} \sqrt{1 + f'(x)^2} dx$, where $f'(x)$ is the derivative of $f(x)$ and x_0 and x_1 are the positions of the cell pole (x is the coordinate along the cell-centerline). In addition, we estimated cell lengths using the length of the major axis of an ellipse fitted to the cell masks (calculated using the Matlab ‘regionprops’ function). Overall, the two methods agree well, however the first (based on polynomial fitting) is more robust to curved cells and it was therefore used for all data shown in the figures.

Cell growth rates, r , were calculated by fitting an exponential curve to time-trajectories of the measured cell length over time: $L(t) = L(0) \cdot e^{r \cdot t}$. To estimate the growth rate directly before and after cell division, we first extended cell length measurement across divisions by summing up the cell lengths of the two daughter cells (extension after cell divides) and by taking a fraction of $L_0 / (L_0 + L_{0,sister})$ of the mother cell length, where L_0 and $L_{0,sister}$ are the lengths of a cell and its sister at their birth (extension before cell is born)^{65,66}. We then performed a linear regression on the log-transformed cell lengths over a sliding window of 11 time points (200 min) to obtain an estimate of the growth rate.

To accurately estimate expression levels of genes of interest, the respective fluorescence images were corrected for imaging artefacts, following the procedure described in van Vliet et al.⁶⁵: First, we performed a shading correction to correct for inhomogeneities in the light field by dividing each pixel in the fluorescence images by the corresponding pixel in the shading images (an image obtained from a homogenous fluorescent sample, normalized to an average intensity of 1). Second, we corrected for diffraction artefacts by performing a deconvolution using the Lucy-Richardson method (as implemented in the Matlab ‘deconvlucy’ function) applying the experimentally determined PSF of the microscope. Third, we performed a background correction by subtracting the median intensity over all background pixels (i.e., all pixels that are not part of any segmented cell). Finally, we corrected for segmentation inaccuracies by only estimating the mean fluorescence intensity within the centre of the cell mask. To do so we first eroded the cell mask with 5% of the cell width; subsequently, we calculated the mean fluorescence intensity, M , over all pixels within this eroded cell mask.

The change in gene expression level over time – which we call ‘expression rate’ in short – was calculated like the promoter activity P in Locke et al.³¹. There the authors define this rate per unit length \tilde{P} as: $\tilde{P} = \frac{P}{L} = rM + \gamma M + \frac{dM}{dt}$. In this equation, L is the length, r the elongation rate, and M the mean fluorescence intensity of the cell, all calculated as described above. $\frac{dM}{dt}$ is the change in mean fluorescence intensity over time and was estimated as the coefficient of a linear regression calculated over a sliding window of 11 time points (200 min). Before performing the regression, we extended cell measurements across division events by adding the mean values of the intensity in the two daughter cells for time points after cell division and by adding the intensity in the mother cell for time points before cell birth. The final constant in the equation above, γ , is the degradation rate of the fluorescent protein. We estimated its value by manually selecting 51 cells in which there was no discernable gene expression rate (i.e., $P = \tilde{P} = 0$). From the equation above it follows that when $\tilde{P} = 0$ we can estimate the degradation rate as: $\gamma = -r - \frac{d[\log M]}{dt}$, where the elongation rate, r , is measured as described above, and where $\frac{d[\log M]}{dt}$ is estimated as the coefficient of a linear regression of $\log M$ vs. time; the regression was again calculated over a sliding window of 11 time points, and in doing so $\log M$ values were again extended across cell division using the respective values from mother and daughter cells. We thus obtained an estimated value of $\gamma = 0.0015$ 1/min.

We defined pulses as a transient increase in \tilde{P} . Since a pulse can last longer than a cell life time, or begin in a mother cell and continue in one or both of its daughters, we needed a method that is not affected by cell division events to detect them. To this end we first traced all cell lineages backward in time; for each cell present in the last frame of the image stack we thereby obtained an extended lineage that starts at frame 1 with a founder cell and ends at the last frame with the focal cell itself. It is important to note that these lineages are not statistically independent – cells that occur early in a colony are of course part of multiple lineages; however, we correct for this at a later stage by removing all multiple detections.

For each lineage we then used a peak finding algorithm (implemented in the Matlab function ‘peakfinder’) to find all candidate pulses. As this ‘peakfinder’ function considers symmetric prominence – i.e., both increase and decrease –, we subsequently calculated for each candidate pulse the prominence backward in time: This corresponds to an increase in the gene expression rate relative to the lowest value obtained since the last pulse, or since the beginning of the movie, whichever comes first. Only pulses with a prominence backward in time of more than 6 1/min were maintained; this threshold value had been determined based on visual inspection of a large number of trajectories of the strain with the lowest pulse frequency (the *sinR* promoter mutant), and the same threshold was used for all strains and conditions. Finally, we removed all duplicate detections and characterized each pulse by its prominence (backward in time, i.e., the increase), its absolute height, and the time since the last pulse.

The average pulsing frequency per unit time was calculated for each colony as: $f_{pulse} = \frac{N_{pulse}}{dt \cdot \sum_{i=1}^T n_i}$, where N_{pulse} is the total number of pulses that occurred in the colony, dt is the time interval between frames, n_i is the number of cells present at frame i , and the sum is over all T frames in the movie. The denominator measures the total observation time, taking into account that the number of cells increases over the duration of the movie.

Processing, segmentation and per-colony analysis of late (3D) time-lapse data. Image stacks were cropped using the above-mentioned NIS Elements software version 4.13. Image analysis was performed as previously described⁶⁷, using the General Analysis module of the NIS Elements Advanced Research software version 4.5: Binary layers were constructed along colony perimeters on phase contrast images. Based on binary layers, colony area and mean fluorescence intensity per colony were determined, i.e., the ratio of total fluorescence intensity per colony area. From these mean fluorescence values, background fluorescence intensities were subtracted.

Flow cytometry and flow cytometry data analysis. Starter cultures were prepared as described above. 1 ml of final cultures were harvested by centrifugation (4,000 x g, 5 min, 4 °C), resuspended in an equal volume of ice-cold phosphate-buffered saline (PBS; 8 g/l NaCl, 0.2 g/l KCl, 1.44 g/l Na₂HPO₄, 0.24 g/l KH₂PO₄, pH 7.2), diluted to a final OD₆₀₀ of 0.0125 in ice-cold PBS and kept on ice until analysis.

Fluorescence-activated cell analysis was carried out with a BD LSRFortessa SORP flow cytometer (BD Biosciences, Germany). mNeonGreen intensity was assessed employing a 488 nm laser [band pass filter (bp) 510/20 nm], mVenus intensity employing a 514 nm laser (bp 542/27 nm), and mScarlet-I intensity employing a 561 nm laser (bp 586/15 nm) lasers.

Flow cytometry data was collected in FCS 3.0 file format, and data analysis was carried out with FlowJo 10.6.0 software (BD). Gating (Supplementary Fig. 13) was first performed on forward and side scatters (FSC and SSC, respectively) to remove dead cells and debris (SSC-A over FSC-A) and to exclude doublets (SSC-W over SSC-H). Subsequently, using the FlowJo Exchange DownSample plugin, the number of events per sample was reduced to 15,000 to ensure equal sample size. Strains lacking the *sinI* promoter-fluorophore gene fusion(s) with otherwise identical genetic backgrounds served as negative controls. Cells in the read-out samples with higher fluorescence intensities than those of the respective control cells were assessed as ‘positive’. The fraction of cells per sample assessed as ‘positive’ and their corresponding median fluorescence values were likewise determined with FlowJo.

Microplate reader fluorescence and optical density measurements. To assess the effect of different *sinI* expression pulse frequencies on quorum sensing response dynamics, for each of the five strains with different *sinR* expression levels (analogous to the strains used for Fig. 2d, but without the fluorophore gene fusion) five test tubes with modified MOPS-buffered medium containing 0.5 mM IPTG were inoculated to five different OD₆₀₀ and grown overnight. The next morning, 2 ml of each culture were harvested and cells pelleted by centrifugation (4,000 x g, 5 min, RT). Supernatants were transferred to fresh tubes, sterile-filtered, and 500 µl of sterile supernatants mixed with 500 µl of indicator strain culture adjusted to an OD₆₀₀ of 0.375. Of each of the 25 supernatant-indicator strain suspensions, 3 x 100 µl were distributed in a 96-well microtiter plate as technical replicates. Further wells were filled with 3 x 100 µl of indicator strain mixed 1:2 with fresh medium, and with medium only as sterile/blank control. Plates were covered and incubated for 12 hours in an Infinite M Plex microplate reader (Tecan) set to 30 °C and shaking at 200 rpm. Every 30 minutes, mVenus intensity and OD₆₀₀ were measured.

To assess an effect of different *sinR* expression levels on growth, starter cultures of the respective strains were diluted to an OD₆₀₀ of 0.15 in modified MOPS-buffered medium containing 0.5 mM IPTG, and 6 x 100 µl per strain were distributed in a 96-well microtiter plate as technical replicates; further wells were filled with medium only as sterile/blank control. Plates were covered and incubated for 20 hours in the same Infinite M Plex microplate reader set to 30 °C and shaking at 200 rpm, and OD₆₀₀ was measured every 30 minutes.

Single molecule microscopy, image processing and analysis. Starter cultures were prepared as described above. Final cultures were harvested by centrifugation (4,000 x g, 5 min, RT) and washed twice with 1 ml modified MOPS-buffered medium. Formaldehyde was then added to a final concentration of 3.7% (v/v), mixed gently by inversion and incubated for 15-20 minutes. After fixation, cells were washed twice with 1 ml EZ rich defined medium (EZRDM; Teknova, USA) and finally resuspended in 1 ml EZRDM.

For agarose pads, 1% (w/v) low melting agarose (Merck/Sigma Aldrich, Germany) in EZRDM was incubated at 70 °C for 12 minutes to melt the agarose and then cooled down to 37 °C. The agarose solution at 37 °C was placed on indented microscope slides (Thermo Fisher, Germany), sealed with coverslips that had been cleaned overnight in 1 M KOH (Merck/Sigma Aldrich), and allowed to set for two hours.

Cells were then placed on the pads and imaged on a custom-built setup based on a Nikon Ti Eclipse microscope equipped with a set of dichroic mirrors and filters (ET dapi/Fitc/cy3 dichroic, ZT405/488/561rpc rejection filter, ET525/50 or ET610/75 bandpass, all AHF Analysentechnik, Germany), and a CFI Apo TIRF 100x/1.49 oil objective (Nikon). A 561 nm OBIS laser (Coherent Inc., USA) was controlled via an acousto-optical tunable filter (AOTF; Gooch and Housego, USA). Laser intensity was set to 100 W/cm² and each field of view was imaged for 6 seconds with 60 ms frame time (100 frames) to record a single-molecule movie. Furthermore, for each field of view a bright light snapshot was recorded to manually determine the number of cells.

For data analysis each single-molecule movie was flattened to a single frame where each pixel was averaged over the entire movie. The resulting image was post-processed with the ThunderSTORM ImageJ plugin (<https://github.com/zitmen/thunderstorm>) to count fluorescent spots. Here, an intensity threshold of 20 photons (based on the negative control strain lacking *mScarlet-1*) was used to avoid false-positive spots, and results were furthermore filtered in order to discard events outside of cells.

***In vivo* protein stability assay.** Starter cultures were prepared as described above. Prior to the experiment, 9 x 15 ml of 150 ml overnight culture were distributed in 100 ml Erlenmeyer flasks equilibrated to 30 °C and further incubated for 15 min at 30 °C shaking at 200 rpm. Chloramphenicol was added to the flasks at 20 µg/ml⁶⁸ in 1-minute intervals; after addition of chloramphenicol to the last flask, all flasks were shaken for another minute to ensure homogeneous distribution and uptake of the antibiotic even in the last sample. At harvest, all flasks were put on ice, 10 ml per sample transferred to pre-cooled centrifuge tubes, and cells pelleted by centrifugation (10,000 x g, 5 min, 4 °C). Most of the supernatant was decanted, cells resuspended in residual medium, transferred to pre-cooled 2 ml tubes and again pelleted by centrifugation (10,000 x g, 5 min, 4 °C). After removal of all supernatant cells were resuspended in 2 x Laemmli loading dye to a calculated OD₆₀₀ of 20 and lysed by incubation at 95 °C for 20 minutes and repeated vortexing. Samples were stored at -20 °C for western blot analysis.

Western blot analysis. For mere comparison of strain/growth condition effects via western blot analysis, cultures were prepared and harvested as above.

5 µl of samples were loaded on a 12.5% SDS-polyacrylamide gel, and after electrophoresis separated proteins were transferred to a polyvinylidene difluoride (PVDF) membrane (Thermo Scientific) equilibrated in transfer buffer (0.025 M Tris, 0.192 M glycine, 20% (v/v) methanol) using the semi-dry blotting procedure. The membrane was then incubated with 1 x phosphate-buffered saline supplemented with Tween-20 (PBST) (8 g/l NaCl, 1.44 g/l Na₂HPO₄ x 2 H₂O, 0.2 g/l KCl, 0.24 g/l KH₂PO₄, 1 ml/l Tween-20, pH 7.2) containing 2% (m/v) milk powder for 1 hour at room temperature to block unspecific binding of antibodies.

Subsequently, the membrane was cut horizontally immediately above the 55 kDa band of the molecular weight standard, and the two parts treated separately. The upper part was incubated in 15 ml PBST with an anti-DnaK antibody raised in rabbit (Biorbyt Ltd, Cambridge) in a 1:20,000 dilution at 4 °C overnight; the lower part was incubated in 15 ml PBST containing 2% (m/v) milk powder with anti-FLAG M2-Peroxidase (horseradish peroxidase, HRP) antibody produced in mouse (Sigma Aldrich) added in a 1:1,000 dilution, likewise at 4 °C overnight. The next morning, the upper part was washed 3 times for 10-15 minutes with 20 ml PBST at room temperature and incubated for 1 hour in 15 ml PBST with a mouse anti-rabbit IgG-HRP (Santa Cruz Biotechnology) in a 1:10,000 dilution at room temperature. Finally, both parts were washed 3 times for 10-15 minutes with 20 ml PBST at room temperature and developed with Pierce ECL Western Blotting Substrate (Thermo Scientific) according to manufacturer instructions. Images were taken with a ChemiDoc MP Imaging System (Biorad) and the ImageLab software version 5.2.1 set to Chemi hi sensitivity mode (4x4 binning and signal accumulation).

Blot images were analysed using the Gel Analysis method provided in the Fiji/ImageJ image processing software (<http://imagej.nih.gov/ij>). The one phase exponential decay fits to the data were performed with Graphpad Prism software (San Diego, California).

Protein production and purification. His₆-ExpR was produced from pET28a-*expR*, His₆-GB1-SinR from pEM-GB1-*sinR*, and His₆-GB1 from the empty pEM-GB1 vector. *E. coli* BL21 (DE3) cells carrying the respective plasmid were grown at 37 °C under rigorous shaking in LB medium supplemented with 50 mg/l kanamycin (for pET28a-*expR*) or 100 mg/l ampicillin (for pEM-GB1-*sinR* or pEM-GB1). At an OD₆₀₀ of approximately 0.6, the culture was shifted to 20 °C and protein production induced by addition of 1 mM IPTG. After further incubation for 20 h, cells were harvested by centrifugation (4,000 x g, 20 min, 4 °C), resuspended in lysis buffer (20 mM of HEPES-Na pH 8.0, 20 mM KCl, 20 mM MgCl₂, 250 mM NaCl and 40 mM imidazole) and lysed with an LM10 Microfluidizer (Microfluidics) at 12,000 psi pressure. Cell debris was removed by centrifugation (47,850 x g, 20 min, 4 °C), and purification was then continued at room temperature. The clear supernatant was loaded on a 1-ml HisTrap column (GE Healthcare) equilibrated with 10 column volumes (CV) lysis buffer. After washing with further 10 CV of lysis buffer, proteins were eluted with 5 CV elution buffer (lysis buffer containing 500 mM imidazole). Proteins were further purified by size-exclusion chromatography (SEC) on a HiLoad 26/600 Superdex 200 pg column (GE Healthcare) equilibrated with SEC buffer (20 mM of HEPES-Na pH 7.5, 20 mM KCl, 20 mM MgCl₂, 200 mM NaCl). Fractions containing the desired protein were pooled, concentrated [Amicon Ultra-0.5 Centrifugal Filter Unit, 10 kDa MWCO (Millipore)], deep-frozen in liquid nitrogen and stored at -80 °C. Protein concentration was determined using a spectrophotometer (NanoDrop Lite, Thermo Scientific).

Electrophoretic mobility shift assay (EMSA). A 177 bp Cy3-labeled fragment of the *sinI* promoter including the ExpR and SinR binding sites was generated via PCR with primers [Cy3]264f and 440r. DNA fragments were mixed at 2.75 nM with purified proteins in reaction buffer containing 20 mM of HEPES-Na pH 7.5, 200 mM NaCl, 50 mM KCl, 20 mM MgCl₂, 1 µg/µl bovine serum albumin (Sigma), 0.0025 U/µl sonicated sperm DNA (GE Healthcare), 10 µM 3-oxo-C16:1-HSL (N-3-oxo-hexadec-11(Z)-enoyl-L-homoserine lactone, Cayman Chemical), and 0.1% (v/v) DMSO in a final volume of 10 µl. If included, His₆-ExpR was added at 1 µM, His₆-GB1-SinR and His₆-GB1 at 70 µM. Reactions were shielded from light and incubated for 30 minutes at room temperature. Subsequently, 2.5 µl loading buffer [5 parts 5 x Tris/Borate/EDTA (TBE) buffer (Tris 54 g/l, boric acid 27.5 g/l, EDTA 10 mM, pH 8.3) mixed with 3 parts 87% glycerol] were added, and reactions were loaded on 8% polyacrylamide gels casted with 1 x TBE buffer. After electrophoresis (90 V, 2.5 h, covered from light), gels were scanned using a Typhoon imager (Typhoon Trio, Amersham Biosciences).

Statistical analysis, correlations and regressions. All statistical analysis, except for determination of means and medians of fluorescence intensities measured by flow cytometry (which were calculated by FlowJo), was performed with Graphpad Prism software (San Diego, California). To assess statistical significance of single molecule microscopy, time-lapse microscopy and flow cytometry data sets comparing two strains or growth conditions, two-tailed unpaired t-tests with Welch's correction were performed, *i.e.*, assuming that both groups of data were drawn from populations with a Gaussian distribution, but not assuming identical standard deviations for the two populations. To assess statistical significance when comparing three different strains, Welch's ANOVA tests with a post-hoc Dunnett's T3 multiple comparisons test was performed, again assuming that all groups of data were drawn from Gaussian populations with individual variances. Statistical differences between positional subsets of data (Supplementary Fig. 9a, b) were assessed using a Kruskal-Wallis test, since the data even after log transformation did not follow a Gaussian distribution. Results of significance tests are always indicated as follows: ns, $P \geq 0.05$; *, $P < 0.05$; **, $P < 0.01$; ***, $P < 0.001$; ****, $P < 0.0001$.

Correlation of *PsinI-mCerulean* & *PsinI-mCherry* data (Fig. 1b) was calculated as Spearman's correlation (i.e., not assuming a Gaussian distribution of the respective values); r^2 for pulse data vs. mScarlet-I-SinR spots (Fig. 3e) in turn was calculated from Pearson's correlation coefficient assuming that x and y values (i.e., means of the fraction of cells with mScarlet-I-SinR spots per strain/growth condition, means of pulse frequencies, and medians of pulse amplitudes) were sampled from populations that at least approximately follow a Gaussian distribution.

Data availability

Source data are provided in the Excel file 'Supplementary Data 1'; pulse data are available in combination with the code, see below.

Code availability

The custom code used for pulse analysis together with the respective data and instructions is available in the folder 'Supplementary Data 2'.

References

1. Neilson, K. H., Platt, T. & Hastings, J. W. Cellular control of the synthesis and activity of the bacterial luminescent system. *J. Bacteriol.* **104**, 313–322 (1970).
2. Fuqua, W. C., Winans, S. C. & Greenberg, E. P. Quorum sensing in bacteria: the LuxR-LuxI family of cell density-responsive transcriptional regulators. *J. Bacteriol.* **176**, 269–275 (1994).
3. Dunn, A. K. & Stabb, E. V. Beyond quorum sensing: the complexities of prokaryotic parliamentary procedures. *Anal. Bioanal. Chem.* **387**, 391–398 (2006).
4. Schauder, S. & Bassler, B. L. The languages of bacteria. *Genes Dev.* **15**, 1468–1480 (2001).
5. Garmyn, D. *et al.* Evidence of autoinduction heterogeneity via expression of the Agr system of *Listeria monocytogenes* at the single-cell level. *Appl. Environ. Microbiol.* **77**, 6286–6289 (2011).
6. Pradhan, B. B. & Chatterjee, S. Reversible non-genetic phenotypic heterogeneity in bacterial quorum sensing. *Mol. Microbiol.* **92**, 557–569 (2014).
7. Grote, J. *et al.* Evidence of autoinducer-dependent and -independent heterogeneous gene expression in *Sinorhizobium fredii* NGR234. *Appl. Environ. Microbiol.* **80**, 5572–5582 (2014).
8. Schlüter, J.-P. *et al.* Classification of phenotypic subpopulations in isogenic bacterial cultures by triple promoter probing at single cell level. *J. Biotechnol.* **198**, 3–14 (2015).
9. Grote, J., Krysciak, D. & Streit, W. R. Phenotypic heterogeneity, a phenomenon that may explain why quorum sensing does not always result in truly homogenous cell behavior. *Appl. Environ. Microbiol.* **81**, 5280–5289 (2015).
10. Bettenworth, V. *et al.* Phenotypic heterogeneity in bacterial quorum sensing systems. *J. Mol. Biol.* **431**, (2019).
11. Hense, B. A. & Schuster, M. Core principles of bacterial autoinducer systems. *Microbiol. Mol. Biol. Rev.* **79**, 153–169 (2015).
12. Popat, R., Cornforth, D. M., McNally, L. & Brown, S. P. Collective sensing and collective responses in quorum-sensing bacteria. *J. R. Soc. Interface* **12**, 20140882 (2014).

13. Boyer, M. & Wisniewski-Dyé, F. Cell-cell signalling in bacteria: not simply a matter of quorum. *FEMS Microbiol. Ecol.* **70**, 1–19 (2009).
14. Moreno-Gámez, S. *et al.* Quorum sensing integrates environmental cues, cell density and cell history to control bacterial competence. *Nat. Commun.* **8**, 1–12 (2017).
15. Dunlap, P. V. & Greenberg, E. P. Control of *Vibrio fischeri* luminescence gene expression in *Escherichia coli* by cyclic AMP and cyclic AMP receptor protein. *J. Bacteriol.* **164**, 45–50 (1985).
16. Dunlap, P. V. & Greenberg, E. P. Control of *Vibrio fischeri lux* gene transcription by a cyclic AMP receptor protein-LuxR protein regulatory circuit. *J. Bacteriol.* **170**, 4040–4046 (1988).
17. Friedrich, W. F. & Greenberg, E. P. Glucose repression of luminescence and luciferase in *vibrio fischeri*. *Arch. Microbiol.* **134**, 87–91 (1983).
18. Nealson, K. H., Eberhard, A. & Hastings, J. W. Catabolite repression of bacterial bioluminescence: functional implications. *Proc. Natl. Acad. Sci.* **69**, 1073–1076 (1972).
19. Lyell, N. L. *et al.* Cyclic AMP receptor protein regulates pheromone-mediated bioluminescence at multiple levels in *Vibrio fischeri* ES114. *J. Bacteriol.* **195**, 5051–5063 (2013).
20. McGowan, S. J. *et al.* Carbapenem antibiotic biosynthesis in *Erwinia carotovora* is regulated by physiological and genetic factors modulating the quorum sensing-dependent control pathway. *Mol. Microbiol.* **55**, 526–545 (2005).
21. Duan, K. & Surette, M. G. Environmental regulation of *Pseudomonas aeruginosa* PAO1 Las and Rhl quorum-sensing systems. *J. Bacteriol.* **189**, 4827–4836 (2007).
22. Platt, T. G. & Fuqua, W. C. What’s in a name? The semantics of quorum sensing. *Trends Microbiol.* **18**, 383–387 (2010).
23. Redfield, R. J. Is quorum sensing a side effect of diffusion sensing? *Trends Microbiol.* **10**, 365–370 (2002).
24. Hense, B. A. *et al.* Does efficiency sensing unify diffusion and quorum sensing? *Nat. Rev. Microbiol.* **5**, 230–239 (2007).
25. Hense, B. A., Müller, J., Kuttler, C. & Hartmann, A. Spatial heterogeneity of autoinducer regulation systems. *Sensors* **12**, 4156–4171 (2012).
26. Calatrava-Morales, N., McIntosh, M. & Soto, M. J. Regulation mediated by N-acyl homoserine lactone quorum sensing signals in the *Rhizobium*-legume symbiosis. *Genes* vol. 9 263 (2018).
27. Charoenpanich, P., Meyer, S., Becker, A. & McIntosh, M. Temporal expression program of quorum sensing-based transcription regulation in *Sinorhizobium meliloti*. *J. Bacteriol.* **195**, 3224–3236 (2013).
28. McIntosh, M., Meyer, S. & Becker, A. Novel *Sinorhizobium meliloti* quorum sensing positive and negative regulatory feedback mechanisms respond to phosphate availability. *Mol. Microbiol.* **74**, 1238–1256 (2009).
29. Elowitz, M. B., Levine, A. J., Siggia, E. D. & Swain, P. S. Stochastic gene expression in a single cell. *Science (80-.)*. **297**, 1183–1186 (2002).
30. Raj, A. & van Oudenaarden, A. Nature, nurture, or chance: stochastic gene expression and its consequences. *Cell* **135**, 216–226 (2008).
31. Locke, J. C. W., Young, J. W., Fontes, M., Jimenez, M. J. H. & Elowitz, M. B. Stochastic

- pulse regulation in bacterial stress response. *Science (80-.)*. **334**, 366–369 (2011).
32. Zhu, J. & Winans, S. C. Autoinducer binding by the quorum-sensing regulator TraR increases affinity for target promoters *in vitro* and decreases TraR turnover rates in whole cells. *Proc. Natl. Acad. Sci.* **96**, 4832–4837 (1999).
 33. Taniguchi, Y. *et al.* Quantifying *E. coli* proteome and transcriptome with single-molecule sensitivity in single cells. *Science (80-.)*. **329**, 533–538 (2010).
 34. McIntosh, M., Serrania, J. & Lacanna, E. A novel LuxR-type solo of *Sinorhizobium meliloti*, NurR, is regulated by the chromosome replication coordinator, DnaA and activates quorum sensing. *Mol. Microbiol.* **112**, 678–698 (2019).
 35. Schäper, S. *et al.* Cyclic di-GMP regulates multiple cellular functions in the symbiotic alphaproteobacterium *Sinorhizobium meliloti*. *J. Bacteriol.* **198**, 521–535 (2016).
 36. Flemming, H.-C. *et al.* Biofilms: an emergent form of bacterial life. *Nat. Rev. Microbiol.* **14**, 563–575 (2016).
 37. Stewart, P. S. & Franklin, M. J. Physiological heterogeneity in biofilms. *Nat. Rev. Microbiol.* **6**, 199–210 (2008).
 38. Dilanji, G. E., Teplitski, M. & Hagen, S. J. Entropy-driven motility of *Sinorhizobium meliloti* on a semi-solid surface. *Proc. R. Soc. B Biol. Sci.* **281**, 20132575 (2014).
 39. Gao, M., Coggin, A., Yagnik, K. & Teplitski, M. Role of specific quorum-sensing signals in the regulation of exopolysaccharide II production within *Sinorhizobium meliloti* spreading colonies. *PLoS One* **7**, e42611-13 (2012).
 40. Nogales, J., Bernabéu-Roda, L., Cuéllar, V. & Soto, M. J. ExpR is not required for swarming but promotes sliding in *Sinorhizobium meliloti*. *J. Bacteriol.* **194**, 2027–2035 (2012).
 41. Pellock, B. J., Teplitski, M., Boinay, R. P., Bauer, W. D. & Walker, G. C. A LuxR homolog controls production of symbiotically active extracellular polysaccharide II by *Sinorhizobium meliloti*. *J. Bacteriol.* **184**, 5067–5076 (2002).
 42. Cai, L., Dalal, C. K. & Elowitz, M. B. Frequency-modulated nuclear localization bursts coordinate gene regulation. *Nature* **455**, 485–490 (2008).
 43. Hao, N. & O’Shea, E. K. Signal-dependent dynamics of transcription factor translocation controls gene expression. *Nat. Struct. Mol. Biol.* **19**, 31–39 (2012).
 44. Dalal, C. K., Cai, L., Lin, Y., Rahbar, K. & Elowitz, M. B. Pulsatile dynamics in the yeast proteome. *Curr. Biol.* **24**, 2189–2194 (2014).
 45. Park, J. *et al.* Molecular time sharing through dynamic pulsing in single cells. *Cell Syst.* **6**, 216-229.e15 (2018).
 46. Yu, J., Xiao, J., Ren, X., Lao, K. & Xie, X. S. Probing gene expression in live cells, one protein molecule at a time. *Science (80-.)*. **311**, 1600–1603 (2006).
 47. Cai, L., Friedman, N. & Xie, X. S. Stochastic protein expression in individual cells at the single molecule level. *Nature* **440**, 358–362 (2006).
 48. Smirnov, E., Hornáček, M., Vacík, T., Cmarko, D. & Raška, I. Discontinuous transcription. *Nucleus* **9**, 149–160 (2018).
 49. Tunnacliffe, E. & Chubb, J. R. What is a transcriptional burst? *Trends Genet.* **36**, 288–297 (2020).
 50. Levine, J. H., Lin, Y. & Elowitz, M. B. Functional roles of pulsing in genetic circuits. *Science (80-.)*. **342**, 1193–1200 (2013).

51. Lutz, R. & Bujard, H. Independent and tight regulation of transcriptional units in *Escherichia coli* via the LacR/O, the TetR/O and AraC/I1-I2 regulatory elements. *Nucleic Acids Res.* **25**, 1203–1210 (1997).
52. Oehler, S., Eismann, E. R., Krämer, H. & Müller-Hill, B. The three operators of the *lac* operon cooperate in repression. *EMBO J.* **9**, 973–979 (1990).
53. Eldar, A. & Elowitz, M. B. Functional roles for noise in genetic circuits. *Nature* **467**, 167–173 (2010).
54. Li, G.-W. & Xie, X. S. Central dogma at the single-molecule level in living cells. *Nature* **475**, 308–315 (2011).
55. Seeley, T. D. & Visscher, P. K. Group decision making in nest-site selection by honey bees. *Apidologie* **35**, 101–116 (2004).
56. Couzin, I. D. Collective cognition in animal groups. *Trends Cogn. Sci.* **13**, 36–43 (2009).
57. Seeley, T. D. Honeybee Democracy. (Princeton University Press, Princeton and Oxford, 2010).
58. Seeley, T. D. & Visscher, P. K. Sensory coding of nest-site value in honeybee swarms. *J. Exp. Biol.* **211**, 3691–3697 (2008).
59. Seeley, T. D. & Buhrman, S. C. Nest-site selection in honey bees: how well do swarms implement the "best-of- N " decision rule? *Behav. Ecol. Sociobiol.* **49**, 416–427 (2001).
60. Cárcamo-Oyarce, G., Lumjiaktase, P., Kümmerli, R. & Eberl, L. Quorum sensing triggers the stochastic escape of individual cells from *Pseudomonas putida* biofilms. *Nat. Commun.* **6**, 5945 (2015).
61. Gay, P., Le Coq, D., Steinmetz, M., Berkelman, T. & Kado, C. I. Positive selection procedure for entrapment of insertion sequence elements in Gram-negative bacteria. *J. Bacteriol.* **164**, 918–921 (1985).
62. Zhan, H. J., Lee, C. C. & Leigh, J. A. Induction of the second exopolysaccharide (EPSb) in *Rhizobium meliloti* SU47 by low phosphate concentrations. *J. Bacteriol.* **173**, 7391–7394 (1991).
63. Young, J. W. *et al.* Measuring single-cell gene expression dynamics in bacteria using fluorescence time-lapse microscopy. *Nat. Protoc.* **7**, 80–88 (2011).
64. Berg, S. *et al.* ilastik: interactive machine learning for (bio)image analysis. *Nat. Methods* **16**, 1226–1232 (2019).
65. van Vliet, S. *et al.* Spatially correlated gene expression in bacterial groups: The role of lineage history, spatial gradients, and cell-cell interactions. *Cell Syst.* **6**, 496-507.e6 (2018).
66. Kiviet, D. J. *et al.* Stochasticity of metabolism and growth at the single-cell level. *Nature* **514**, 376–379 (2014).
67. Bettenworth, V., McIntosh, M., Becker, A. & Eckhardt, B. Front-propagation in bacterial inter-colony communication. *Chaos An Interdiscip. J. Nonlinear Sci.* **28**, 106316 (2018).
68. Schallies, K. B., Sadowski, C., Meng, J., Chien, P. & Gibson, K. E. *Sinorhizobium meliloti* CtrA stability is regulated in a CbrA-dependent manner that is influenced by CpdR1. *J. Bacteriol.* **197**, 2139–2149 (2015).

Acknowledgements

We are grateful to A. Dal Co, S. González Sierra, R. Hartmann, R. Hernandez Tamayo, E. Krol and G. Malengo for technical advice, E. Krol for sharing strains and plasmids, M. Wagner for sharing pK18*mob3*, F. Altegoer for sharing pEM-GB1, B. Waidner, K. Neuhaus and L. Søgaard-Andersen for sharing equipment, M. Ackermann, G. Bange, B. Eckhardt, P. L. Graumann and P. Lenz for fruitful discussions, and M. Ackermann and V. Sourjik for critical comments on the manuscript and/or figures. This work is dedicated to B. Eckhardt. It was supported by German Research Foundation Priority Program SPP 1617 grant BE2121/6-2 and the State of Hesse (Germany) LOEWE program-SYNNMIKRO to A. Be., and Max Planck Society group funds, Carnegie Mellon University start-up funds and National Science Foundation grant PHY-2020295 to U. E..

Competing interests

Authors declare that they have no competing interests.

Additional information

Supplementary information, movies and data are available.

Correspondence and material requests should be addressed to V. B. or A. Be.

Supplementary Information

Frequency modulation of a bacterial quorum sensing response

Vera Bettenworth^{1*}, Simon van Vliet^{2†}, Bartosz Turkowyd^{3,4†‡}, Annika Bamberger¹, Heiko Wendt¹, Matthew McIntosh^{1§}, Wieland Steinchen¹, Ulrike Endesfelder^{3,4‡}, Anke Becker^{1*}

Contents

Supplementary Figure 1. SinR has a degenerated AHL binding site.

Supplementary Figure 2. Stochasticity in *sinI* expression.

Supplementary Figure 3. *sinI* expression rate.

Supplementary Figure 4. SinR is very unstable and scarce.

Supplementary Figure 5. SinR as a key factor.

Supplementary Figure 6. Quantification of pulse data is robust to changes in peak prominence threshold.

Supplementary Figure 7. Phosphate starvation, c-di-GMP and *expR* effects.

Supplementary Figure 8. The *pde0 expR*⁻ strain displays elevated c-di-GMP levels.

Supplementary Figure 9. Potential positional and temporal effects.

Supplementary Figure 10. mScarlet-I-SinR spots are homogeneous.

Supplementary Figure 11. Pulse amplitudes and fluorescence intensities.

Supplementary Figure 12. Effects on the quorum sensing response.

Supplementary Figure 13. Gating and quantification of flow cytometry data.

Supplementary Table 1. Data summary.

Supplementary Table 2. *P* values for comparisons of pulse frequencies and ‘positive’ fractions in flow cytometry and single molecule microscopy data.

Supplementary Table 3. Sample sizes of pulse frequency and single molecule microscopy data.

Supplementary Table 4. Strains.

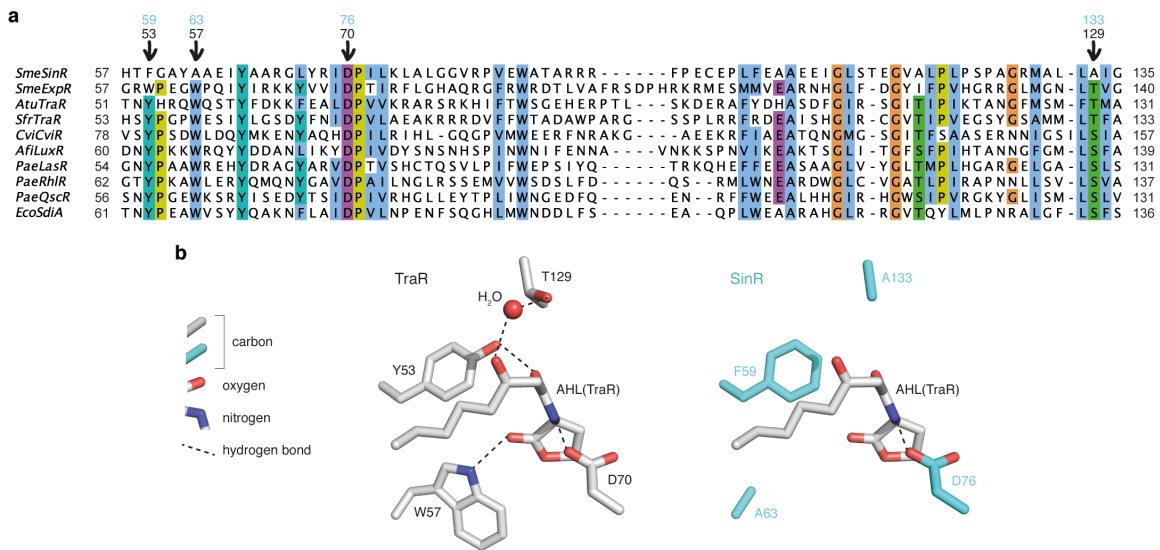
Supplementary Table 5. Plasmids.

Supplementary Table 6. Oligonucleotides and synthetic genes.

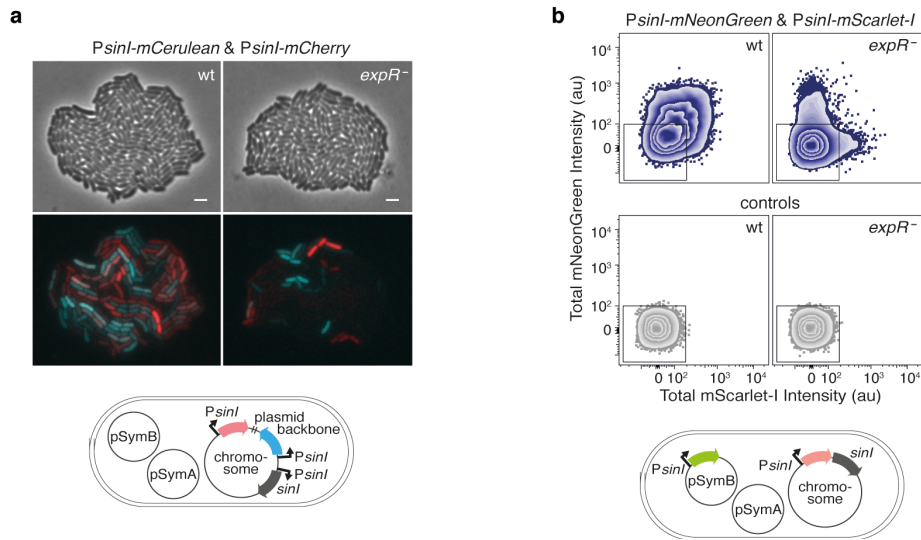
Supplementary Methods 1. Details on strain constructions.

Supplementary Methods 2. Construction and characterization of the *pde0* strain.

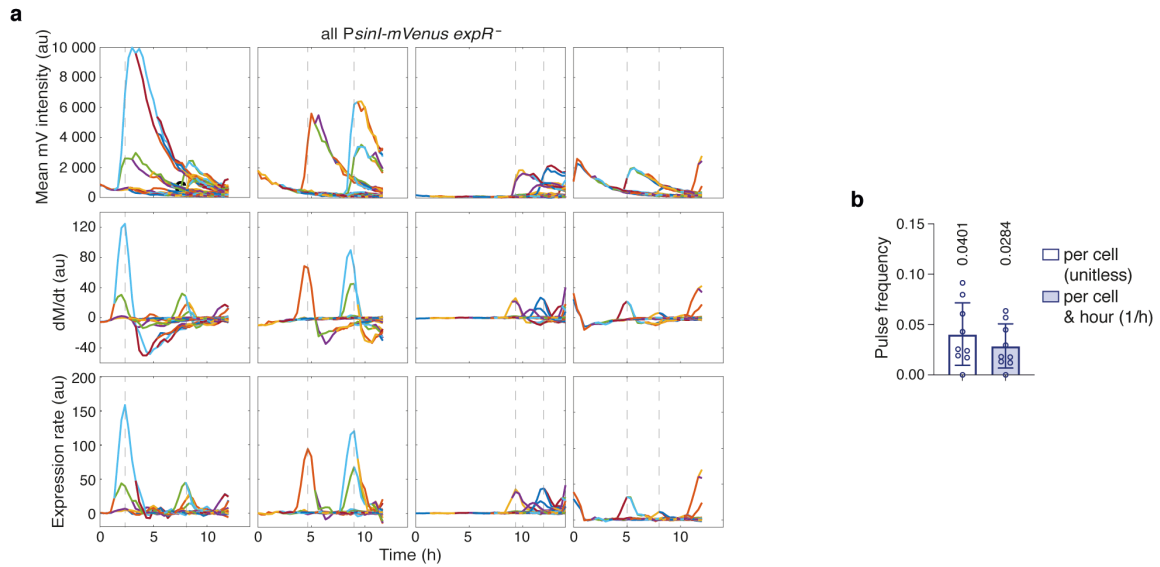
References



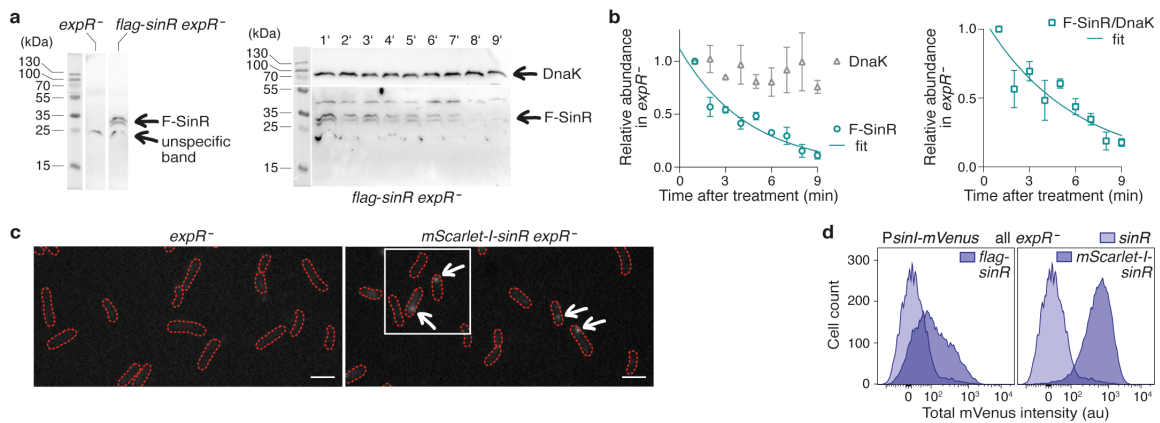
Supplementary Figure 1. SinR has a degenerated AHL binding site. a Amino acid sequence alignment of the AHL binding domains of 10 LuxR-type regulators illustrating changes of SinR in residues crucial for AHL coordination. *SmeSinR*, *Sinorhizobium meliloti* SinR (Uniprot accession number Q92PD1); *SmeExpR*, *S. meliloti* ExpR (Q2HY11); *AtuTraR*, *Agrobacterium tumefaciens* TraR (P33905); *SfrTraR*, *Sinorhizobium fredii* NGR234 TraR (P55407); *CviCviR*, *Chromobacterium violaceum* CviR (D3W065); *AfiLuxR*, *A. fischeri* LuxR (P12746); *PaeLasR*, *Pseudomonas aeruginosa* LasR (P25084); *PaeRhIR*, *P. aeruginosa* RhIR (P54292); *PaeQscR*, *P. aeruginosa* QscR (Q9RMS5); *EcoSdiA*, *Escherichia coli* SdiA (P07026). Arrows mark residues involved in coordination of the lactone ring and the 3-oxo moiety of the AHL in the crystal structure of *A. tumefaciens* TraR¹ (see **b**), numbers above indicate positions in TraR (black) and SinR (turquoise) amino acid sequences. Numbers on the left and right denote the first and last residues shown in the alignment. Residues with 60% or higher conservation are indicated by boxes according to the Clustal X Colour Scheme². **b** 3D structure of *A. tumefaciens* TraR (PDB entry 1L3L)¹ (left). The AHL is coordinated by hydrogen bond interactions provided by tyrosine (Y53), tryptophan (W57) and aspartate (D70). Threonine (T129) coordinates a water molecule which in turn establishes a hydrogen bond to the 3-oxo moiety of the AHL. The SinR AHL binding site (right) is modelled based on *A. tumefaciens* TraR (PDB entry 1L3L). Three of the four residues coordinating the AHL in TraR are exchanged in SinR for residues lacking the potential to establish hydrogen bonds with an AHL molecule, providing a structural basis for SinR being irresponsive to AHLs³.



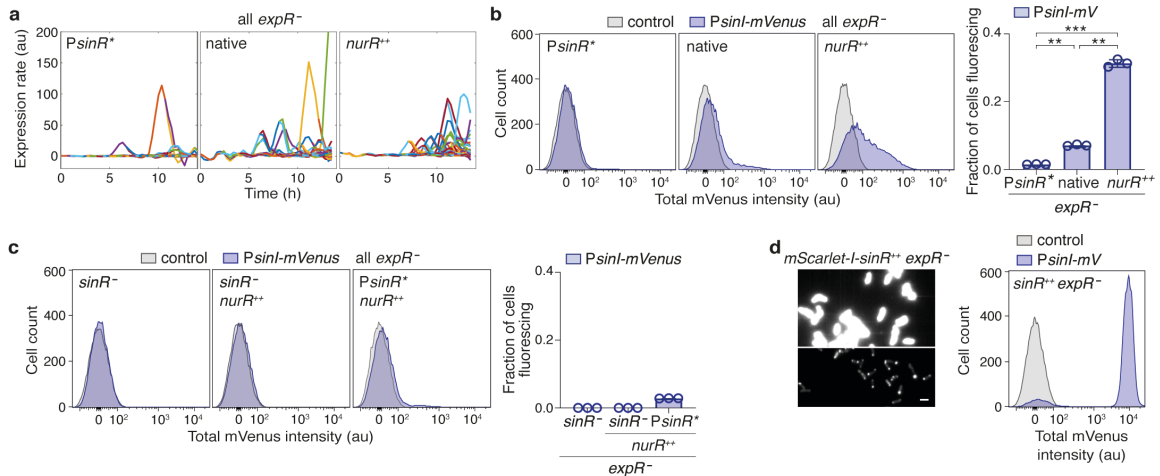
Supplementary Figure 2. Stochasticity in *sinI* expression. **a** Phase contrast and fluorescence microscopy snapshots (top) of wild-type (wt) and *expR*⁻ colonies carrying two copies of the *sinI* promoter fused to *mCerulean* and *mCherry* fluorophore genes, respectively, representing raw data for Fig. 1b. Scale bars, 2 μ m. Simplified sketch (bottom) of the respective promoter-fluorophore gene fusions. Both the *sinI* promoter-*mCerulean* and the *sinI* promoter-*mCherry* fusion are located on the same suicide plasmid integrated into the *S. meliloti* chromosome at the native *sinI* locus. The two promoter-fluorophore fusions are separated by approx. 4 kb of plasmid DNA. The plasmid also comprises a constitutive promoter-*mVenus* fusion for segmentation of microscopy images; the strains furthermore possess a third, dark copy of the *sinI* promoter regulating expression of *sinI*. **b** Flow cytometry analysis (top) of wt and *expR*⁻ cells likewise carrying two *sinI* promoter-fluorophore gene fusions during exponential growth confirm strong stochasticity of *sinI* expression. Each plot indicates fluorescence intensities of 15,000 cells measured in one experiment. Blue, cells carrying the fluorophore gene fusions; grey, respective background controls. Rectangles indicate the ‘negative’ gate comprising at least 99.9% of background controls. Data is representative of 3 independent experiments. Simplified sketch (bottom) of the constructs employed for flow cytometry: A *sinI* promoter-*mScarlet-I* fusion is integrated into the chromosome in between the native *sinI* promoter and the *sinI* coding sequence (i.e., at the native *sinI* locus) by double homologous recombination, and a *sinI* promoter-*mNeonGreen* fusion is located on a suicide plasmid integrated into the single-copy megaplasmid pSymB in the intergenic region between the *exoP* and the *thiD* gene; pSymB is essential for *S. meliloti* viability unless crucial elements are first transferred onto the chromosome⁴. The control strains lack the fluorophore on the chromosome and carry a promoterless *mNeonGreen* on an otherwise identical suicide plasmid likewise integrated in the *exoP*-*thiD* intergenic region.



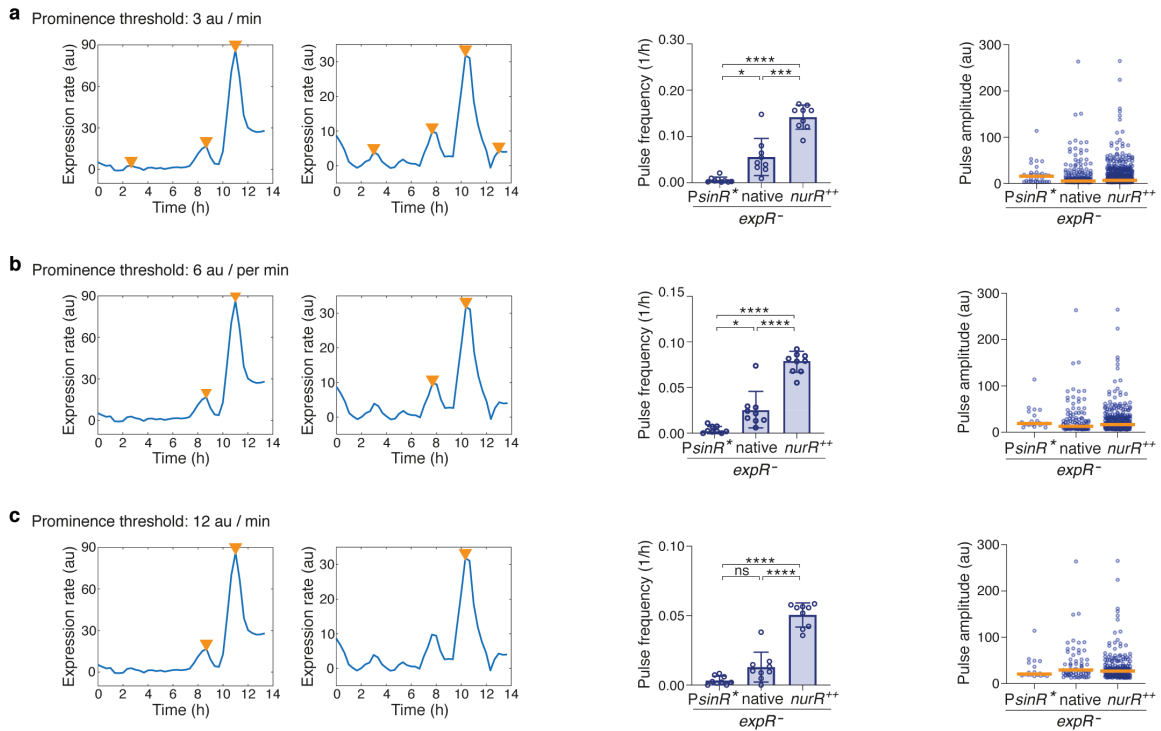
Supplementary Figure 3. *sinI* expression rate. **a** Plots of mean fluorescence intensities from the *PsinI-mVenus* fusion (top), the time derivatives of these mean fluorescence intensities (middle), and the corresponding *sinI* expression rates (bottom) of the *expR⁻* microcolony from Fig. 1c over the whole experiment run time (first column) and three more *expR⁻* microcolonies (columns two to four). Once a pulse has ended, no more fluorophores are produced, and mean fluorescence intensities slowly decline due to dilution by cell growth and/or degradation. Since the time derivatives represent the change in mean fluorescence intensities over time they decrease as soon as fluorophore production has passed its maximum; they become negative once it completely petered out, as they then only represent the effects of fluorophore dilution and/or degradation. To deduce the actual expression rate, the time derivative is set off against a term for the dilution of fluorophores by cell growth, and a term for their – albeit small – degradation rate. In principle, the expression rate should be either 0 or above, but small negative values are possible due to inaccuracies, e.g., in single fluorescence measurements, determination of cell elongation rates (feeding into the term for fluorophore dilution), or fluorophore degradation rate. Both the time derivative and the expression rate represent fits to the data calculated over a sliding window of 11 time points; see Methods for details. In every plot, the maxima of two *sinI* expression pulses – i.e., the measurements ensuing the highest fluorophore production rate – are marked with broken lines. **b** Compilation of pulse frequencies per cell life time, and per cell life time and hour from nine *expR⁻* colonies imaged in three different experiments. Respective means are given and indicated by the bars, error bars indicate standard deviations. $N = 2,293$ cells.



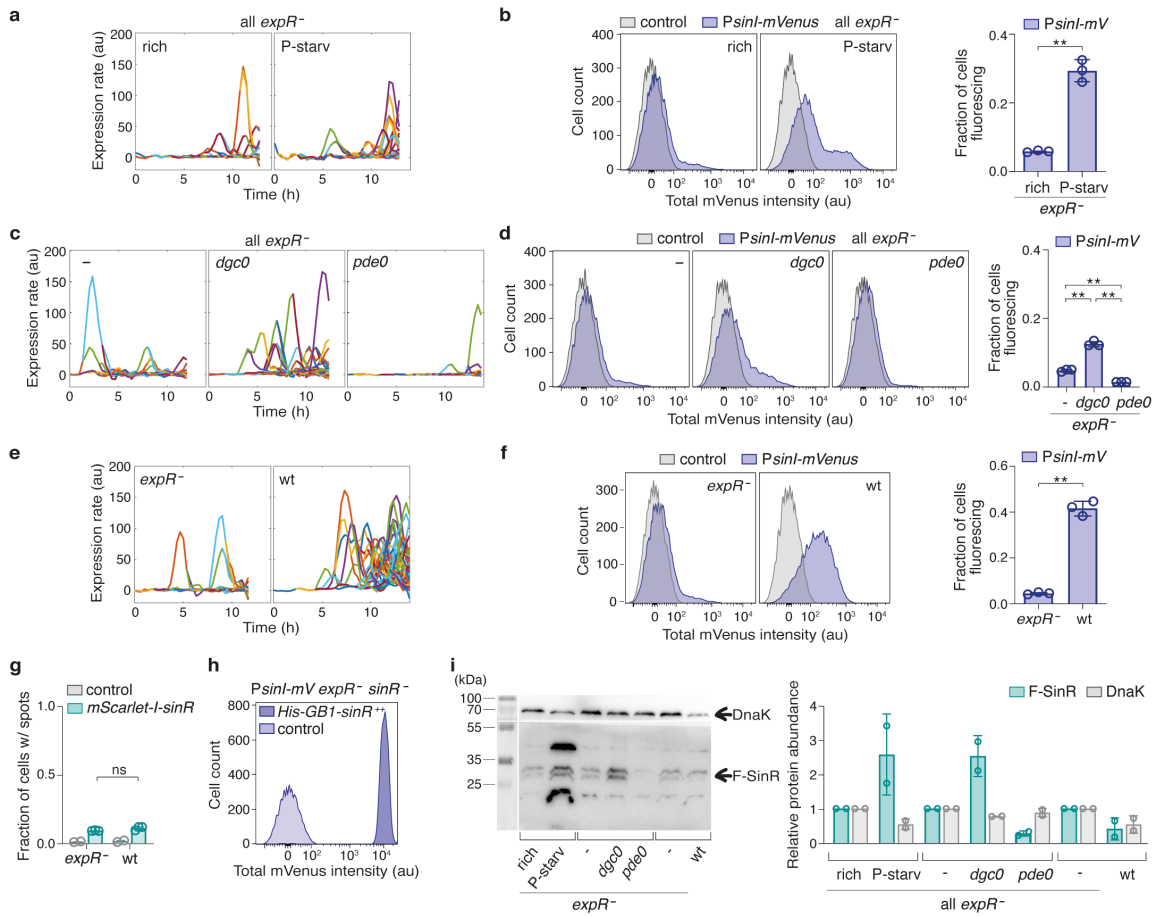
Supplementary Figure 4. SinR is very unstable and scarce. **a** Western blots of cell lysates identifying the Flag-tagged SinR (F-SinR) band (left) and indicating rapid F-SinR degradation after chloramphenicol treatment at 1-minute intervals (right). Numbers on the left indicate molecular weight standards. **b** Plots of relative abundance of F-SinR and DnaK (left) and F-SinR normalized to DnaK (right), each fitted with a model of one phase exponential decay. The fits were constrained with $K > 0$ (i.e., a degradation over time) and plateau = 0 and yield a half-life of 3.1 minutes for F-SinR [$Y(0) = 1.12$, $R^2 = 0.87$] and of 4.0 minutes for F-SinR/DnaK [$Y(0) = 1.08$, $R^2 = 0.78$]. Data for F-SinR alone is given in main text and figure since standard deviation in DnaK data – and thus F-SinR/DnaK data – is larger than for F-SinR data alone. Degradation of DnaK could not be fitted. **c** Fluorescence microscopy images of cells of an *expR⁻* control strain (left) and an *expR⁻* strain carrying the *mScarlet-I-sinR* fusion (right). White square, area displayed in Fig. 2b. Scale bar, 2 μ m. **d** Histograms of fluorescence intensities from the *sinI* promoter-*mVenus* fusion either with native *sinR* (light blue), or *flag-sinR* or *mScarlet-I-sinR* (dark blue), expressed from the native *sinR* promoter suggest that native, i.e., untagged SinR is even less stable and/or less abundant than suggested by western blot analysis and single molecule microscopy. Each histogram indicates fluorescence intensities of 15,000 cells measured in one experiment and is representative of three independent measurements.



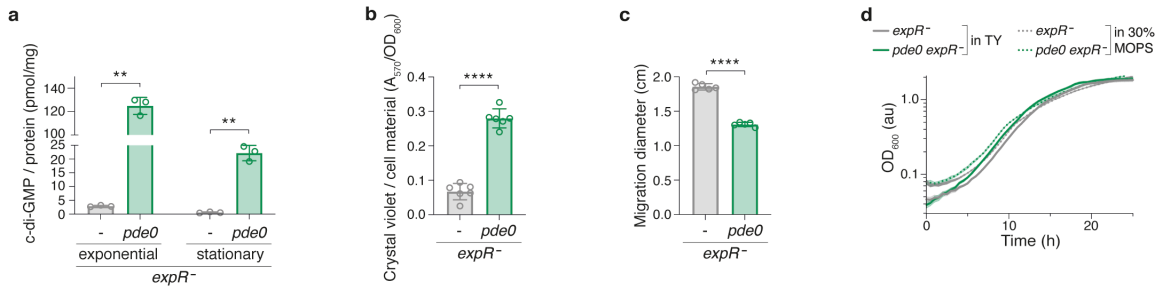
Supplementary Figure 5. SinR as a key factor. **a** Trajectories showing *sinI* expression pulses in colonies with different levels of *sinR* transcription, related to Fig. 2d. **b** Representative flow cytometry data (left) confirming relative differences in *sinI* expression pulse frequency: Histograms of fluorescence intensities from 15,000 cells carrying the *sinI* promoter-*mVenus* fusion (blue) with the same genetic modifications as in (a) and Fig. 2d, and 15,000 cells of the respective control strains without a fluorophore gene fusion (grey); the latter were used as donor strains for the experiment in Fig. 4b. Bar plots (right) indicate the fraction of cells in the samples displaying fluorescence intensities higher than those of the control strains in three biological replicates and their means and standard deviations. **c** Representative flow cytometry data (left) verifying that *nurR* exerts its effect on *sinI* expression via increasing SinR levels and not directly: *nurR* overexpression has no effect on fluorescence intensities from the *sinI* promoter-*mVenus* fusion in the *sinR*⁻ strain, and hardly any on the strain carrying the *sinR* promoter mutation. Histograms of 15,000 cells carrying the *sinI* promoter-*mVenus* fusion (blue) and 15,000 cells of the respective control strains (grey) per genetic background. Bar plots (right) indicate the fraction of cells in the samples displaying fluorescence intensities higher than those of the control strains in three biological replicates and their means and standard deviations. **d** Representative fluorescence microscopy image (left) and flow cytometry data (right) illustrating that direct overexpression of (*mScarlet-I*-)*sinR* disrupts the otherwise stochastic regulatory system: It not only abolishes heterogeneity in fluorescence, but also greatly augments fluorescence intensities. Fluorescence image acquired with identical settings as in Supplementary Fig. 4c, upper part reproduced with identical dynamic range as in Supplementary Fig. 4c, lower part with a 10-fold wider dynamic range. Scale bar, 2 μ m. Flow cytometry data acquired with identical settings as in (b); blue, 15,000 cells carrying the *sinI* promoter-*mVenus* fusion; grey, 15,000 cells of the respective control strain.



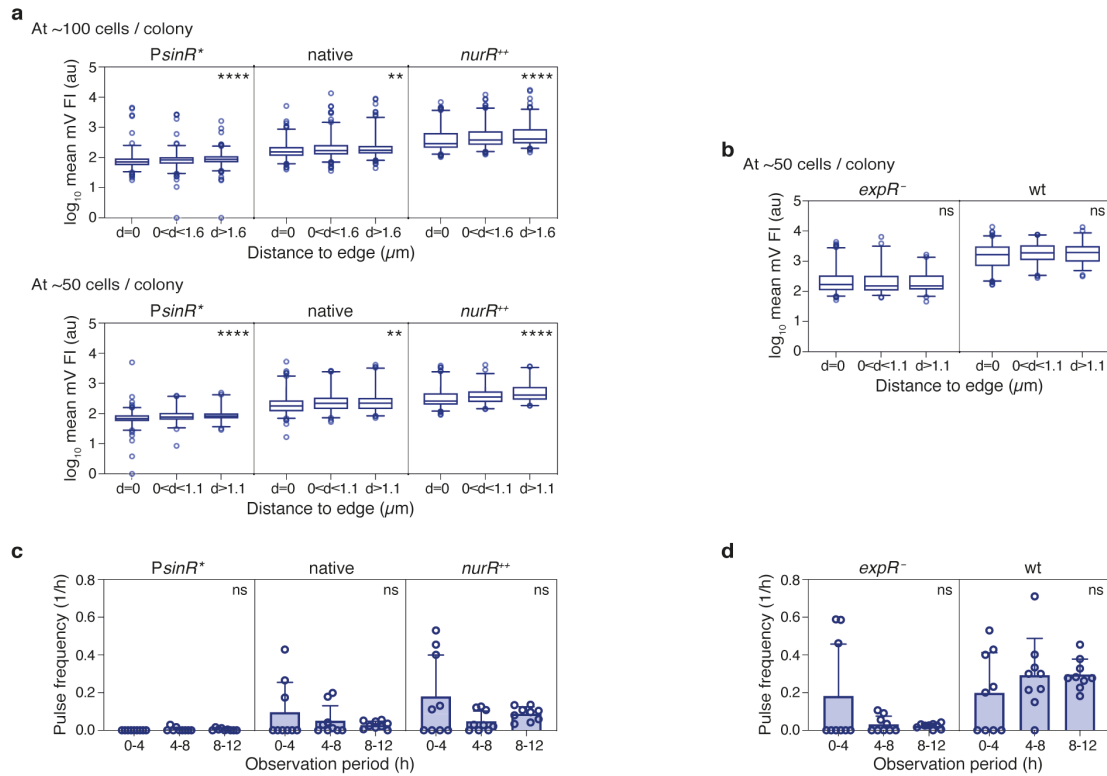
Supplementary Figure 6. Quantification of pulse data is robust to changes in peak prominence threshold. To test whether our results might have been falsified by our choice of threshold for what is considered a pulse, the data set with different *sinR* expression levels (Fig. 2d) was analysed with different threshold values, namely a minimal prominence backward in time of **a** 3 arbitrary units per minute, **b** 6 arbitrary units per minute as in the main analysis, and **c** 12 arbitrary units per minute. The histograms (left) always show *PsinI-mVenus* expression rates of the same two representative cell lineages of the *nurR* overexpression strain (i.e., with elevated *sinR* expression levels); orange triangles mark what is considered a pulse with the respective threshold. Bar plots (middle) show mean *PsinI-mVenus* expression pulse frequencies for the whole data set determined with the respective threshold and corresponding standard deviations; different thresholds yield different absolute pulse frequencies, but do not change relative differences between different genetic backgrounds. Scatter dot plots showing amplitudes of individual pulses (right) are identical above the highest threshold (**c**); median values indicated by orange bars are only slightly affected by the choice of threshold.



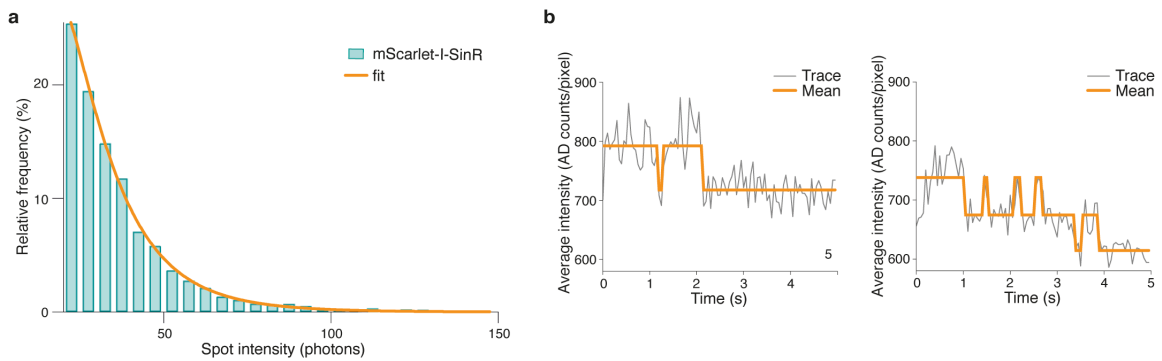
Supplementary Figure 7. Phosphate starvation, c-di-GMP and *expR* effects. **a, c, e** Representative trajectories of *sinI* expression (**a**) under rich growth conditions vs. phosphate starvation in *expR*⁻ background, (**c**) in *expR*⁻, *dgc0 expR*⁻ and *pde0 expR*⁻ strains, and (**e**) in *expR*⁻ and wild-type strains. **b, d, f** Representative histograms (left) of 15,000 cells carrying the *sinI* promoter-*mVenus* fusion (blue) and 15,000 cells of the respective control strains (grey) per condition or genetic background, respectively, as in (**a, c, e**) determined by flow cytometry. Bar plots (right) indicate the fraction of cells in the samples displaying fluorescence intensities higher than those of the control strains in three biological replicates and their means and standard deviations. **g** Bar plots of single molecule microscopy data indicate that *expR* does not affect mScarlet-I-SinR levels. Open circles represent data from three biological replicates, bars represent their means and standard deviations. **h** Histograms of fluorescence intensities from the *PsinI-mVenus* fusion in a *sinR*⁻ *expR*⁻ strain (light blue) and the same strain overproducing His-GB1-SinR (dark blue) indicate *in vivo* activity of the fusion protein. **i** Representative western blot of Flag-tagged SinR (left) and quantification of relative protein abundances in two biological replicates (right) confirm relative differences in SinR abundance under rich growth conditions vs. phosphate starvation in *expR*⁻ background and *expR*⁻, *dgc0 expR*⁻ and *pde0 expR*⁻ strains determined by single molecule microscopy; likewise, western blot data confirms that presence of *expR* in the wild-type background does not increase of F-SinR levels.



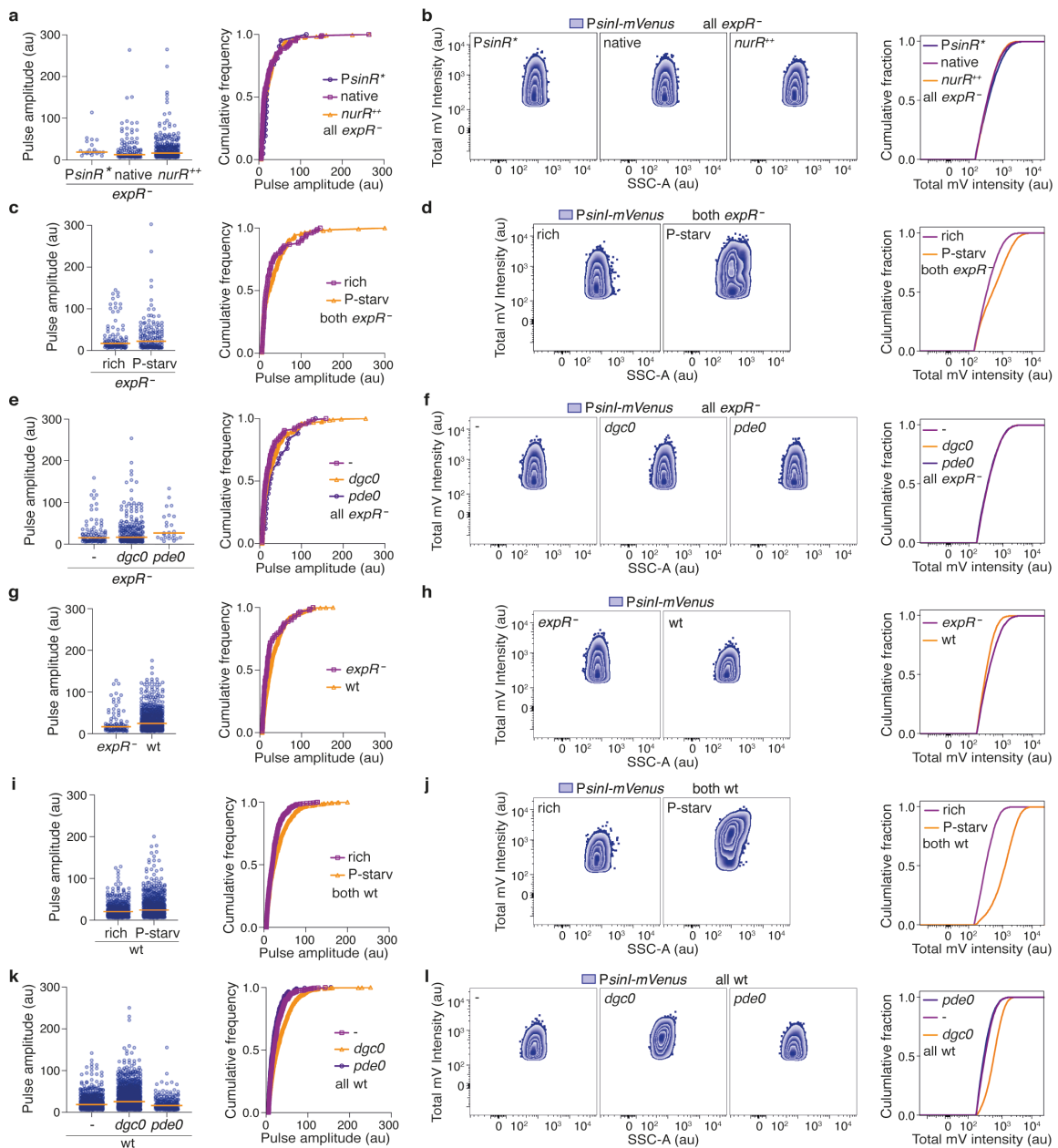
Supplementary Figure 8. The *pde0 expR*⁻ strain displays elevated c-di-GMP levels. **a, b, c** Bar graphs indicating elevated c-di-GMP levels (**a**), increased attachment detected by crystal violet staining (**b**), and decreased motility on soft agar plates (**c**) of the *pde0 expR*⁻ strain compared to the *expR*⁻ parental strain. Bars represent means, error bars represent standard deviations, and open circles represent data from 3, 6 and 5 underlying biological replicates, respectively. Statistical analysis, two-tailed unpaired t-tests with Welch's correction. **a** Whereas 2.9 ± 0.27 pmol c-di-GMP per mg protein were detected in exponential phase samples of the *expR*⁻ parental strain, and 0.5 ± 0.21 pmol c-di-GMP per mg protein in *expR*⁻ stationary phase samples, 124.8 ± 7.27 pmol c-di-GMP per mg protein were detected in exponential phase samples of the *pde0 expR*⁻ strain, and 22.1 ± 2.93 pmol c-di-GMP per mg protein in *pde0 expR*⁻ stationary phase samples. $OD_{600} \approx 0.45$, $P = 0.0012$ for exponential phase; $OD_{600} > 2$, $P = 0.0053$ for stationary phase. **b** Surface attachment in the *pde0 expR*⁻ strain is elevated approximately 4-fold compared to the parental strain ($P < 0.0001$), consistent with prior findings that c-di-GMP stimulates production of, e.g., arabinose-containing polysaccharide and other polysaccharides important for attachment in rhizobia⁵⁻⁷. Of note, these attachment-related polysaccharides are regulated differently than the exopolysaccharide galactoglucan which plays an important role in *S. meliloti* colony expansion and sliding motility⁸⁻¹⁰ and is part of the organism's quorum sensing response^{3,11}. **c** Motility of the *pde0 expR*⁻ strain is reduced by approximately 30% compared to the parental strain ($P < 0.0001$), consistent with prior findings that elevated c-di-GMP levels repress swimming motility in *S. meliloti*^{5,6}. **d** Measurements of optical densities every 30 minutes for 25 hours indicate no difference in growth of the *pde0 expR*⁻ strain compared to the *expR*⁻ parental strain. For details on construction and characterization of the *pde0 expR*⁻ strain see Supplementary Methods 2.



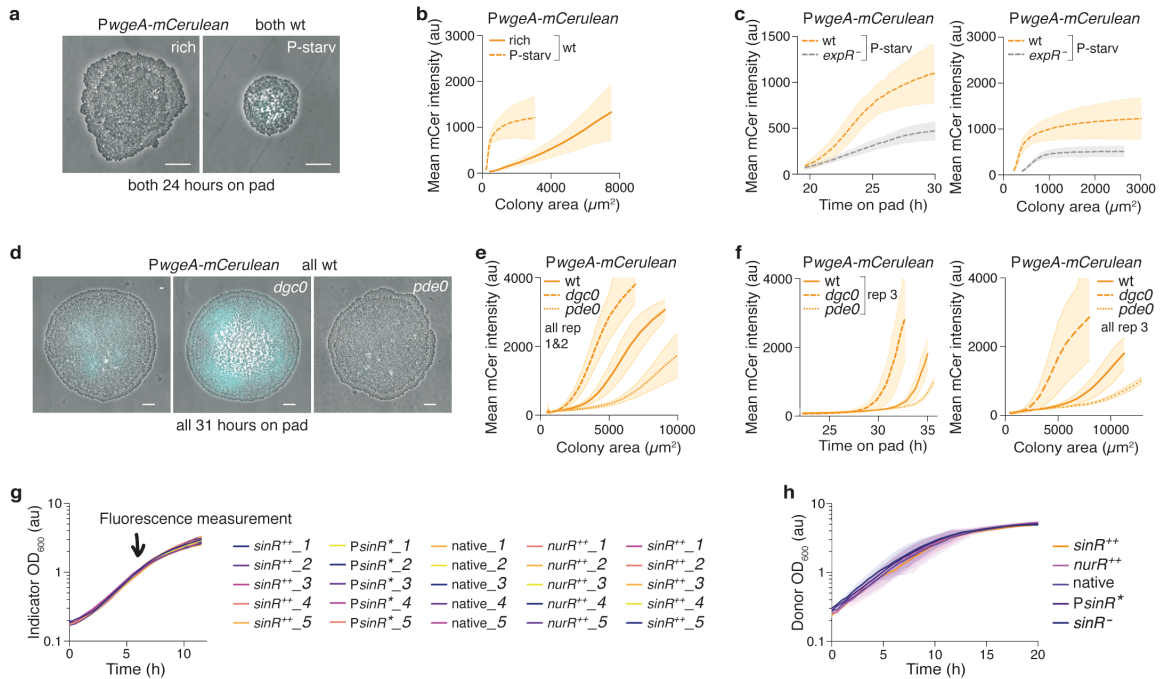
Supplementary Figure 9. Potential positional and temporal effects. **a, b** Analysis of two data sets, each consisting of 9 colonies per strain, with respect to potential positional effects on *sinI* expression pulse frequency. Cells were grouped in three bins according to their distance from the colony edge: the colony boundary ($d = 0 \mu\text{m}$), followed by a ring of intermediate distance (e.g., $0 < d < 1.6 \mu\text{m}$), and the colony centre (e.g., $d > 1.6 \mu\text{m}$); the boundary between the last two bins was chosen to yield equal-sized groups. The boxes in the plots indicate median, 25th and 75th percentile of mean mVenus fluorescence intensities of individual cells from the *PsinI-mVenus* fusion (log-transformed to account for high skew in distribution), the whiskers indicate 2.5th and 97.5th percentiles, individual points indicate outliers. Comparison of the three positional subgroups for each strain yielded small but significant effects for **(a)** the data set with different *sinR* expression levels (Fig. 2d) (medians 1.8523, 1.9175 and 1.9380 for *PsinR**, 2.1874, 2.2272 and 2.2391 for native, 2.4597, 2.5829 and 2.6148 for *nurR⁺⁺* at ~100 cells; 1.8293, 1.8825 and 1.9156 for *PsinR**, 2.2525, 2.3378 and 2.3424 for native, 2.4133, 2.5478 and 2.6130 for *nurR⁺⁺* at ~50 cells) and no significant differences for **(b)** the data set comparing receptor mutant (*expR⁻*) and wild type (Fig. 3c) (medians 2.2287, 2.1817 and 2.1822 for *expR⁻*, 3.2196, 3.2773, 3.2875 for wt). Mean fluorescence intensities were used as a proxy for pulses since pulse frequency must be determined over time, but cell position within the colony is bound to change over time. **c, d** Similarly, developing microcolonies were analysed separately for the first, second and third four-hour period of the experiment. Plots show pulse frequencies for 9 colonies per strain and respective means and standard deviations for each observation period. Comparison of the temporal subgroups for each strain did not yield significant differences neither for **(c)** the data set with different *sinR* expression levels, nor for **(d)** the data set comparing receptor mutant (*expR⁻*) and wild type. ns, $P \geq 0.05$; **, $P < 0.01$; ***, $P < 0.001$; ****, $P < 0.0001$.



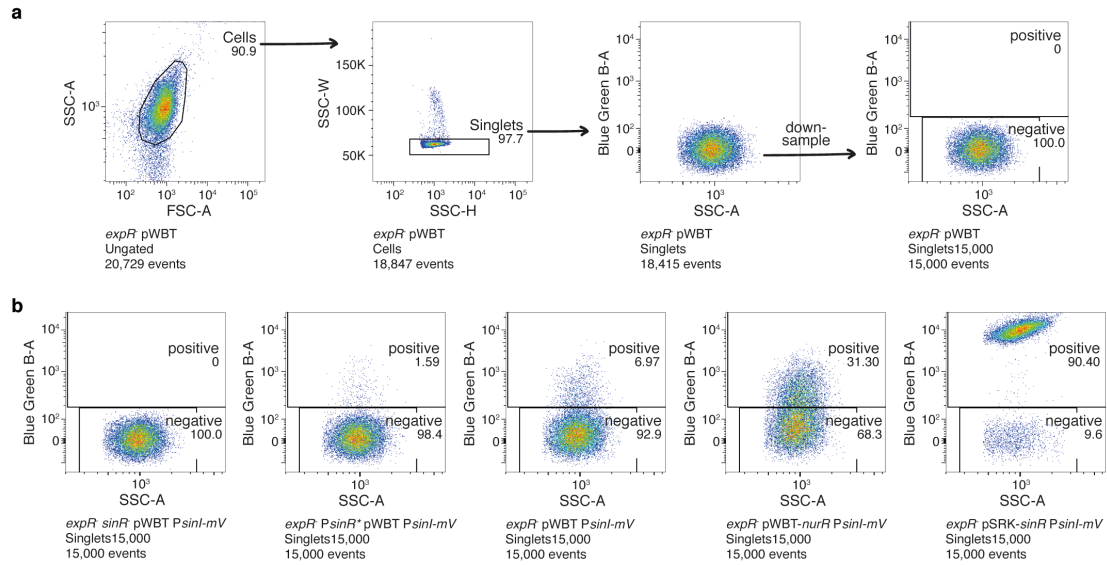
Supplementary Figure 10. mScarlet-I-SinR spots are homogeneous. Single molecule movies had been recorded with the aim to establish the frequency of mScarlet-I-SinR spots in *S. meliloti* populations; nevertheless, we can draw some conclusions on the nature of the observed spots with respect to the number of fluorophores they contain. **a** Histogram of fluorescence intensities of all spots detected in *mScarlet-I-sinR* strains in this work (Fig. 2c, 3a, b, Supplementary Fig. 7g) ($N = 3,277$) except for the *mScarlet-I-sinR* overexpression strain (Supplementary Fig. 5d). The frequency distribution of spot intensities can be fitted with a log-normal distribution (orange line), indicating a single, homogeneous population. Fitting models with multiple populations reduce to a single population and do not take the small increase between 70-100 photons into account that might be indicative of a second population. Taken together, this suggests that the mScarlet-I-SinR spots represent a largely homogeneous SinR population rather than a mixture of higher-order multimers¹². Furthermore, the low intensities per spot, i.e., the very low number of emitted photons, indicates that the fluorescent spots are low copy number mScarlet-I-SinR spots, i.e. either SinR monomers or dimers. **b** Representative fluorescence intensity traces for selected spots, showing clear bleaching events of single fluorophores. The large majority of traces with bleaching events only have a single bleaching event until the background level is reached (left), but we also find some traces with two bleaching events (right). The step heights of bleaching events are the same for all traces (~ 70 -90 AD counts). In addition, short fluorescence fluctuations are present in all traces, caused by brief ON- and OFF-blinking events of single mScarlet-I fluorophores. Taken together, this suggests a large population of mScarlet-I-SinR monomers and a small population of dimeric spots. Because our samples were chemically fixed, we cannot distinguish which of them are target-bound and which of them are part of a free, cytosolic population. Importantly, however, we find no evidence of higher-order multimers in both spot intensity and photobleaching trace analyses. Thus, this data adds strong evidence to the central finding of this work that heterogeneity in *sinI* expression is not caused by different expression levels of *sinR* but by the presence or absence of individual SinR molecules in each cell.



Supplementary Figure 11. Pulse amplitudes and fluorescence intensities. Comparison of *sinI* expression pulses (analysed with respect to pulse frequency/fraction fluorescing in Fig. 2 & 3 and Supplementary Fig. 5 & 7) with respect to (a, c, e, g, i, k) pulse amplitude in time-lapse microscopy and (b, d, f, h, j, l) fluorescence intensities of ‘positive’ cells in flow cytometry. Pulse amplitudes all vary 20-fold or more within strains or growth conditions. However, median pulse amplitudes do either not vary according to pulse frequencies at all (a, e), or only to a much smaller extent (c, g, i, k) (see Fig. 3f). Pulse amplitude data in (a, c, e, g, i, k) stems from strains/conditions with very different pulse frequencies, dot plots thus show varying numbers of data points and are also plotted as cumulative frequency distributions (right panels, respectively) for easier comparison. The increase in flow cytometry intensities correlating with very high pulse frequencies/fluorescing fractions are not reflected in pulse amplitude data and probably result from consecutive pulses that are still separated by time-lapse analysis, but add up in terms of total fluorescence intensities. Plots in (b, d, f, h, j, l) each show fluorescence data of 4,500 cells assessed as ‘positive’.



Supplementary Figure 12. Effects on the quorum sensing response. **a** Fluorescence microscopy snapshots of microcolonies of a wild-type strain carrying the *mCerulean* fluorophore gene fused to a promoter driving expression of genes involved in exopolysaccharide production (*PwgeA*) illustrate acceleration of the quorum sensing response induced by phosphate starvation. Microcolonies were grown for 24 hours under rich or phosphate starvation conditions, respectively. Scale bars, 10 μm . **b** Means and standard deviations of mean fluorescence intensities per colony from the *PwgeA-mCerulean* fusion of the same 9 wild-type colonies grown as shown in Fig. 4a, here plotted over colony area. **c** Means and standard deviations of mean *PwgeA-mCerulean* intensities per colony of 9 wild-type and *expR*⁻ microcolonies, respectively, both grown under phosphate starvation conditions, plotted (left) over time and (right) colony area, respectively, illustrate that phosphate starvation induces expression of exopolysaccharide genes in *S. meliloti* even in absence of the AHL receptor, albeit with lower speed and intensity. This effect is due to additional direct regulation of the *wge* operon by phosphate starvation¹³. **d** Fluorescence microscopy snapshots of wt, *dgc0* and *pde0* microcolonies, all carrying the *PwgeA-mCerulean* fusion, and **e** means and standard deviations of mean *PwgeA-mCerulean* intensities per colony for 6 of the 9 colonies (rep. 1&2) shown in Fig. 4b plotted over colony area illustrate the onset of the quorum sensing response at different colony sizes depending on c-di-GMP levels. Scale bars, 10 μm . **f** Means and standard deviations of mean *PwgeA-mCerulean* intensities per colony for the third biological replicate for the c-di-GMP effect, plotted (left) over time and (right) colony area show similar relative, but different absolute behaviour. **g** Growth curves of the AHL indicator strain during incubation with supernatants from different strains and optical densities for Fig. 4b, controlling for possible effects of growth differences of the indicator strain on its *sinI* expression levels. The arrow indicates the time of the fluorescence measurement shown in Fig. 4b. **h** Growth curves of the supernatant donor strains for Fig. 4b indicate no effect on growth, i.e., no metabolic burden, by different *sinR* expression levels; donor strains did not carry the *PsinI-mVenus* fusion, i.e., expressed no fluorophore gene and are identical to the control strains for flow cytometry measurements shown in Supplementary Fig. 5b.



Supplementary Figure 13. Gating and quantification of flow cytometry data. **a** Gating was first performed on forward and side scatters (FSC and SSC, respectively) to remove dead cells and debris (SSC-A over FSC-A) and to exclude doublets (SSC-W over SSC-H). Subsequently, the number of samples was reduced to 15,000 events using the FlowJo Exchange DownSample plugin to ensure equal sample size. Strains lacking the *sinI* promoter-fluorophore gene fusion(s) with otherwise identical genetic backgrounds served as negative controls. **b** Cells in the read-out samples with higher fluorescence intensities than those of the respective control cells were assessed as ‘positive’. The fraction of cells per sample assessed as ‘positive’ and their corresponding median fluorescence values were determined with FlowJo. The data shown here were derived from strains with different *sinR* expression levels, from left to right: a *sinR* deletion, the *sinR* promoter mutant, the native *sinR* promoter, the native *sinR* promoter while overproducing its transcription activator NurR, and overproduction of SinR from a plasmid. The scatter plots shown in the second, third, and fourth panel thus correspond to the blue histograms in Supplementary Fig. 5b, the data in the first panel to the blue histogram in Supplementary Fig. 5c (left), and the last panel to the blue histogram in Supplementary Fig. 5d.

Supplementary Table 1. Data summary.

Experiment	Strain / condition	Pulse frequency (1/h)		Flow cytometry fraction		Pulse amplitude (au)			Median flow cytometry intensity (au)		Single molecule microscopy fraction*	
		Mean	SD	Mean	SD	Mean	Median	Q1/Q3	Mean	SD	mean	SD
Titration <i>sinR</i> expression	PsinR*	0.0038	0.0039	0.0154	0.0006	18.87	16.15/40.46	384	10.02	0.1640	0.0301	
	native	0.0254	0.0197	0.0715	0.0023	12.78	8.34/29.40	345	12.34	0.2377	0.0076	
	<i>nurR</i> ⁺⁺	0.0770	0.0114	0.3137	0.0110	16.51	9.67/31.86	355	5.51	0.4743	0.0413	
Phosphate starvation in <i>expR</i>	<i>expR</i> ⁻ rich	0.0283	0.0129	0.0589	0.0025	17.04	10.41/34.19	339	6.66	0.1667	0.0153	
	<i>expR</i> ⁻ P-starv	0.0431	0.0165	0.2937	0.0320	22.44	9.11/47.24	481	21.50	0.4067	0.0451	
Influence of c-di-GMP in <i>expR</i>	<i>expR</i> ⁻	0.0284	0.0219	0.0488	0.0036	15.36	8.34/31.17	313	4.16	0.1667	0.0153	
	<i>expR</i> ⁻ <i>dgc0</i>	0.0652	0.0259	0.1263	0.0075	16.55	8.57/40.50	318	1.00	0.2967	0.0153	
	<i>expR</i> ⁻ <i>pde0</i>	0.0080	0.0054	0.0149	0.0002	26.98	15.38/66.42	300	25.15	0.1300	0.0656	
	<i>expR</i> ⁻ wt	0.0291	0.0263	0.0456	0.0048	17.13	9.38/33.06	301	4.73	0.0926	0.0027	
Phosphate starvation in wt	wt	0.2771	0.0646	0.4173	0.0323	24.90	12.81/44.00	339	17.01	0.1189	0.0141	
	wt rich	0.1891	0.0478	0.6240	0.0667	20.28	10.98/31.49	354	52.17	ND	ND	
	wt P-starv	0.3135	0.0586	0.9667	0.0092	24.44	12.34/44.17	1509	357.10	ND	ND	
Influence of c-di-GMP in wt	wt	0.2288	0.0626	0.5843	0.1060	18.54	10.36/32.33	296	23.43	ND	ND	
	<i>dgc0</i>	0.3462	0.0342	0.9510	0.0046	25.49	12.42/48.59	552	5.51	ND	ND	
	<i>pde0</i>	0.0957	0.0466	0.2880	0.0061	16.16	9.28/27.17	238	0.58	ND	ND	

Measures of central tendency and dispersion of *PsinI-mVenus* expression pulse frequencies, fractions of populations showing fluorescence from the *PsinI-mVenus* fusion in flow cytometry, pulse amplitudes and fluorescence intensities determined by flow cytometry, and of fractions of cells showing fluorescent spots in strains expressing *mScarlet-L-sinR* determined by single molecule microscopy. SD, standard deviation; Q1, first quartile; Q3, third quartile. Data from 3 biological replicates each. * no background subtraction; ND, not determined.

Supplementary Table 2. *P* values for comparisons of pulse frequencies and ‘positive’ fractions in flow cytometry and single molecule microscopy data.

Experiment	Strain / condition	Pulse frequency	Flow cytometry	Single molecule microscopy
Titrating <i>sinR</i> expression	PsinR* vs. native	0.0290	0.0012	0.1119
	PsinR* vs. <i>nurR</i> ⁺⁺	< 0.0001	0.0010	0.0012
	native vs. <i>nurR</i> ⁺⁺	< 0.0001	0.0015	0.0217
Phosphate starvation in <i>expR</i> ⁻	rich vs. P-starv	0.0324	0.0059	0.0066
Influence of c-di-GMP in <i>expR</i> ⁻	<i>expR</i> ⁻ vs. <i>expR</i> ⁻ <i>dgc0</i>	0.0146	0.0012	0.0012
	<i>expR</i> ⁻ vs. <i>expR</i> ⁻ <i>dgc0</i>	0.0661	0.0079	0.7482
	<i>expR</i> ⁻ <i>dgc0</i> vs. <i>expR</i> ⁻ <i>pde0</i>	0.0003	0.0032	0.1039
Influence of ExpR-AHL	<i>expR</i> ⁻ vs. wt	< 0.0001	0.0021	0.1408
Phosphate starvation in wt	rich vs. P-starv	0.0002	0.0112	ND
Influence of c-di-GMP in wt	wt vs. <i>dgc0</i>	0.0010	0.0559	ND
	wt vs. <i>pde0</i>	0.0004	0.0834	ND
	<i>dgc0</i> vs. <i>pde0</i>	< 0.0001	< 0.0001	ND

When comparing two strains or growth conditions in an experiment, two-tailed unpaired t tests with Welch’s correction were performed, i.e., assuming that both groups of data were drawn from Gaussian populations, but not assuming identical standard deviations for the two populations; the indicated *P* values are thus individual *P* values. When comparing three different strains in an experiment, Welch’s ANOVA test with a post-hoc Dunnett’s T3 multiple comparison test was performed, again assuming that all groups of data were drawn from Gaussian populations with individual variances; the *P* values indicated here are multiplicity adjusted *P* values. For both individual and family-wise tests, a 95% confidence interval was chosen. ND, not determined.

Supplementary Table 3. Sample sizes of pulse frequency and single molecule microscopy data.

Experiment	Strain / condition	Pulse frequency	Single molecule microscopy
Titrating <i>sinR</i> expression	PsinR*	3,411	1,260
	native	2,900	1,142
	<i>nurR</i> ⁺⁺	2,440	1,158
Phosphate starvation in <i>expR</i> ⁻	rich	2,639	2,293
	P-starv	2,355	2,321
Influence of c-di-GMP in <i>expR</i> ⁻	<i>expR</i> ⁻	2,517	2,293
	<i>expR</i> ⁻ <i>dgc0</i>	2,518	2,251
	<i>expR</i> ⁻ <i>pde0</i>	2,031	2,761
Influence of ExpR-AHL	<i>expR</i> ⁻	2,331	1,300
	wt	1,506	1,503
Phosphate starvation in wt	rich	1,690	ND
	P-starv	1,240	ND
Influence of c-di-GMP in wt	wt	1,787	ND
	<i>dgc0</i>	2,065	ND
	<i>pde0</i>	1,657	ND

Total numbers of cells analysed per data set (*N*) are given. Each data set was gathered in three independent experiments; for pulse frequency data, three colonies per experiment were analysed. ND, not determined.

Supplementary Table 4. Strains.

Name	Relevant genotype	Figure(s)	Source or reference
<i>E. coli</i>			
DH5 α	F ⁻ <i>endA1 hsdR17(r_K⁻m_K⁺) supE44 thi-1 λ⁻ recA1 gyrA96 relA1 deoR Δ(<i>lacZYA-argF</i>) U169 Φ80d<i>lacZ</i>ΔM15</i>		14
S17-1	<i>E. coli</i> 294 Thi RP4-2-Tc::Mu-Km::Tn7 integrated into the chromosome		15
BL21(DE3)	F ⁻ <i>ompT gal dcm lon hsdS(r_B⁻m_B⁻)</i> λ (DE3 [<i>lacI lacUV5-T7p07 ind1 sam7 nin5</i>])		16
<i>S. meliloti</i>			
Sm2B3001	Wild type (<i>expR</i> restored), Nx ^r , Sm ^r	S2b; S7f, g; S11h, j, l	17
VBSm350	Sm2B3001 pK18 <i>mob3-2xPsinI</i>	1b & S2a	This work
VBSm292	Sm2B3001 <i>PsinI-mScarlet-I</i>	precursor	This work
VBSm295	Sm2B3001 <i>PsinI-mScarlet-I</i> pKE- <i>PsinI-mNeonGreen</i>	S2b	This work
VBSm311	Sm2B3001 pKE- <i>mNeonGreen</i>	S2b	This work
VBSm1	Sm2B3001 <i>PsinI-mVenus</i>	S7f; S11h	This work
VBSm314	Sm2B3001 <i>PsinI-mVenus</i> pK18 <i>mob3-PwgeA-mCerulean</i>	3c; S11g; S12a-f	This work
VBSm43	Sm2B3001 <i>mScarlet-I-sinR</i>	S7g	This work
VBSm191	Sm2B3001 <i>3xflag-sinR</i>	S7i	This work
Rm2011	Wild type <i>expR</i> ⁻ (<i>expR</i> ::IS <i>Rm2011-1</i>), Nx ^r , Sm ^r	S2b; S4a, c, d; S7b, d, f; S11d, f, h	18
VBSm349	Rm2011 pK18 <i>mob3-2xPsinI</i>	1b & S2a	This work
VBSm177	Rm2011 <i>PsinI-mScarlet-I</i>	precursor	This work
VBSm296	Rm2011 <i>PsinI-mScarlet-I</i> pKE- <i>PsinI-mNeonGreen</i>	S2b	This work
VBSm310	Rm2011 pKE- <i>mNeonGreen</i>	S2b	This work
VBSm3	Rm2011 <i>PsinI-mVenus</i>	S5d; S7b, d, f; S11d, f, h	This work
VBSm315	Rm2011 <i>PsinI-mVenus</i> pK18 <i>mob3-PwgeA-mCerulean</i>	1c; 3a-c; S3; S5a, c, e; S11c, e, g; S12c	This work
VBSm237	Rm2011 <i>PsinI-mVenus PsinR</i> [*]	precursor	This work
VBSm248	Rm2011 <i>PsinI-mVenus PsinR</i> [*] pWBT	S5b; S11b	This work
VBSm20	Rm2011 <i>PsinI-mVenus</i> pWBT	S5b; S11b	This work
VBSm21	Rm2011 <i>PsinI-mVenus</i> pWBT- <i>nurR</i>	S5b; S11b	This work
VBSm316	Rm2011 <i>PsinI-Venus PsinR</i> [*] pK18 <i>mob3-PwgeA-mCerulean</i>	precursor	This work
VBSm323	Rm2011 <i>PsinI-mVenus PsinR</i> [*] pK18 <i>mob3-PwgeA-mCerulean</i> pWBT	2d; S5a; S11a	This work
VBSm324	Rm2011 <i>PsinI-mVenus</i> pK18 <i>mob3-PwgeA-mCerulean</i> pWBT	2d; S5a; S11a	This work

VBSm325	Rm2011 <i>PsinI-mVenus</i> pK18 <i>mob3-PwgeA-mCerulean</i> pWBT- <i>nurR</i>	2d; S5a; S11a	This work
VBSm235	Rm2011 <i>PsinR</i> *	precursor	This work
VBSm246	Rm2011 <i>PsinR</i> * pWBT	2d; S5b; S11b; 4b; S12g, h	This work
VBSm201	Rm2011 pWBT	2d; S5b; S11b; 4b; S12g, h	This work
VBSm22	Rm2011 pWBT- <i>nurR</i>	2d; S5b; S11b; 4b; S12g, h	This work
VBSm245	Rm2011 <i>PsinR</i> * pWBT- <i>nurR</i>	S5c	This work
VBSm247	Rm2011 <i>PsinI-mVenus PsinR</i> * pWBT- <i>nurR</i>	S5c	This work
VBSm24	Rm2011 <i>PsinI-mVenus</i> pSRKGm- <i>sinR</i>	S5d	This work
VBSm25	Rm2011 pSRKGm- <i>sinR</i>	S5d; 4b; S12g, h	This work
VBSm351	Rm2011 pK18 <i>mob3-PsinR-mCherry</i>	2a	This work
VBSm353	Rm2011 pK18 <i>mob3-sinR</i> UTR- <i>mCherry</i>	2a	This work
VBSm26	Rm2011 <i>mScarlet-I-sinR</i>	2c; S4c; 3a, b; S7g	This work
VBSm239	Rm2011 <i>PsinR</i> *- <i>mScarlet-I-sinR</i>	precursor	This work
VBSm250	Rm2011 <i>PsinR</i> *- <i>mScarlet-I-sinR</i> pWBT	2d	This work
VBSm30	Rm2011 <i>mScarlet-I-sinR</i> pWBT	2d	This work
VBSm32	Rm2011 <i>mScarlet-I-sinR</i> pWBT- <i>nurR</i>	2d	This work
VBSm242	Rm2011 <i>mScarlet-I-sinR</i> pSRKGm- <i>mScarlet-I-sinR</i>	S4D	This work
VBSm171	Rm2011 3x <i>flag-sinR</i>	2b; S4a, b; S7i	This work
VBSm27	Rm2011 <i>PsinI-mVenus mScarlet-I-sinR</i>	S4d	This work
VBSm302	Rm2011 <i>PsinI-mVenus 3xflag-sinR</i>	S4d	This work
VBSm53	Rm2011 Δ <i>sinR::synTerI</i>	precursor	This work
VBSm251	Rm2011 Δ <i>sinR::synTerI</i> pWBT	S5c; 4b; S12g, h	This work
VBSm217	Rm2011 Δ <i>sinR::synTerI</i> pWBT- <i>nurR</i>	S5c	This work
VBSm55	Rm2011 <i>PsinI-mVenus</i> Δ <i>sinR::synTerI</i>	S7h	This work
VBSm252	Rm2011 <i>PsinI-mVenus</i> Δ <i>sinR::synTerI</i> pWBT	S5c	This work
VBSm218	Rm2011 <i>PsinI-mVenus</i> Δ <i>sinR::synTerI</i> pWBT- <i>nurR</i>	S5c	This work
VBSm215	Rm2011 <i>PsinI-mVenus</i> Δ <i>sinR::synTerI</i> pSRKKm-GB1- <i>sinR</i>	S7h	This work
<i>dgc0</i>	Rm2011 Δ <i>pleD</i> Δ <i>SMc04015</i> Δ <i>SMb20523</i> Δ <i>SMc01464</i> Δ <i>SMA2301</i> Δ <i>SMb20389</i> Δ <i>SMb20447</i> Δ <i>SMb20900</i> Δ <i>SMc00038</i> Δ <i>SMA1548</i> Δ <i>SMc03178</i> Δ <i>SMA0137</i> Δ <i>SMc00992</i> Δ <i>SMc03942</i> Δ <i>SMc00887</i> Δ <i>SMc00033</i>	3b; S7d; S11f	5
VBSm267	<i>dgc0 PsinI-mVenus</i>	S7d; S11f	This work
VBSm317	<i>dgc0 PsinI-mVenus</i> pK18 <i>mob3-PwgeA-mCerulean</i>	3b; S7c; S11e	This work

VBSm271	<i>dgc0 PsinI-mVenus expR⁺</i>	S11l	This work
VBSm319	<i>dgc0 PsinI-mVenus expR⁺ pK18mob3-PwgeA-mCerulean</i>	3d; 4a; S11k; S12d-f	This work
VBSm143	<i>dgc0 mScarlet-I-sinR</i>	3b	This work
VBSm169	<i>dgc0 3xflag-sinR</i>	S7i	This work
<i>pde0</i>	Rm2011 Δ SMb21517 Δ SMc00887 Δ SMc03942 Δ SMb20900 Δ SMc03178 Δ SMc00992 Δ SMc00033 Δ SMc00038 Δ SMb20447 Δ SMa0137 Δ SMa1548 SMc00074(E746A) Δ SMc03141	3b; S7d; S11f	This work
VBSm269	<i>pde0 PsinI-mVenus</i>	S7d; S11f	This work
VBSm318	<i>pde0 PsinI-mVenus pK18mob3-PwgeA-mCerulean</i>	3b; S7c; S11e	This work
VBSm273	<i>pde0 PsinI-mVenus expR⁺</i>	S11l	This work
VBSm320	<i>pde0 PsinI-mVenus expR⁺ pK18mob3-PwgeA-mCerulean</i>	3d; 4a; S11k; S12d-f	This work
VBSm145	<i>pde0 mScarlet-I-sinR</i>	3b	This work
VBSm173	<i>pde0 3xflag-sinR</i>	S7i	This work
Sm2B4001	Sm2B3001 <i>sinI</i>	Precursor	¹⁹
VBSm329	Sm2B4001 pK18mob2-PpstS-mVenus	P-starvation indicator	This work
VBSm168	Sm2B4001 pSRKGm-indicator	4b; S12g	This work

Strains shaded in grey represent precursor strains. ‘S’ in the Figure(s) column refers to Supplementary Figures.

Supplementary Table 5. Plasmids.

Plasmids	Relevant features	Source or reference
pK18 <i>mobsacB</i>	Suicide vector; CAP binding site, <i>lac</i> promoter, <i>lac</i> operator, <i>lacZα</i> , <i>mob</i> , <i>sacB</i> , Km ^r	20
pK18 <i>mob2</i>	Suicide vector; CAP binding site, <i>lac</i> promoter, <i>lac</i> operator, <i>lacZα</i> , <i>mob</i> , Km ^r	20
pK18 <i>mob3</i>	Suicide vector; pK18 <i>mob2</i> derivative lacking CAP binding site, <i>lac</i> promoter, <i>lac</i> operator, <i>lacZα</i> ; containing <i>mob</i> , Km ^r	Courtesy of Marcel Wagner
pKEE	Suicide vector; pK18 <i>mob2</i> derivative containing 3' end of <i>exoP</i> and downstream sequence for integration on pSymB; <i>egfp</i> , Km ^r	Courtesy of Elizaveta Krol
pSRKKm	Expression vector; <i>lacI^q</i> , CAP binding site, <i>lac</i> promoter, <i>lac</i> operator, <i>lacZα</i> , Km ^r	21
pSRKGm	Expression vector; <i>lacI^q</i> , CAP binding site, <i>lac</i> promoter, <i>lac</i> operator, <i>lacZα</i> , Gm ^r	21
pWBT	Expression vector; pSRKGm derivative containing tandem <i>lac</i> and T5 promoters, 3 <i>lac</i> operators	22
pEM-GB1	Expression vector; <i>lacI</i> , T7 promoter, <i>lac</i> operator, N-terminal 6xHis-tag, Factor Xa site, streptococcal protein G B1 domain (GB1), TEV site, Amp ^r	23,24
pET28a	Expression vector; <i>lacI</i> , T7 promoter, <i>lac</i> operator, N-terminal 6xHis-tag, thrombin site, C-terminal 6xHis-tag, Km ^r	Novagen
pK18 <i>mobsacB</i> - <i>PsinI</i> - <i>mVenus</i> - <i>sinI</i>	pK18 <i>mobsacB</i> derivative; containing <i>mVenus</i> w/ stop codon, flanked by <i>PsinI</i> - <i>sinI</i> ₁₋₂₇ and <i>sinI</i> UTR & gene	25
pK18 <i>mobsacB</i> - <i>PsinI</i> - <i>mScarlet-I</i> - <i>sinI</i>	pK18 <i>mobsacB</i> derivative; containing <i>mScarlet-I</i> (codon-optimized) w/ stop codon, flanked by <i>PsinI</i> - <i>sinI</i> ₁₋₂₇ and <i>sinI</i> UTR & gene	This work
pK18 <i>mobsacB</i> - Δ <i>sinR</i> :: <i>synTerI</i>	pK18 <i>mobsacB</i> derivative; containing the synthetic multiple terminator site <i>synTerI</i> flanked by <i>PsinR</i> and the last 21 codons of <i>sinR</i> , downstream <i>PsinI</i> & 5' portion of <i>sinI</i>	This work
pK18 <i>mobsacB</i> - <i>PsinR</i> -3x <i>flag</i> - <i>sinR</i>	pK18 <i>mobsacB</i> derivative; containing 3x <i>flag</i> -tag coding sequence including a linker, flanked by <i>PsinR</i> and <i>sinR</i>	This work
pK18 <i>mobsacB</i> - <i>PsinR</i> - <i>mScarlet</i> - <i>sinR</i>	pK18 <i>mobsacB</i> derivative; containing <i>mScarlet-I</i> w/o stop codon followed by a linker, flanked by <i>PsinR</i> - <i>sinR</i> ₁₋₂₇ and <i>sinR</i>	This work
pK18 <i>mobsacB</i> - <i>PsinR</i> *- <i>sinR</i>	pK18 <i>mobsacB</i> derivative; containing a <i>PsinR</i> w/ mutated NurR binding site, flanked by upstream sequence and <i>sinR</i>	This work
pK18 <i>mobsacB</i> - <i>PsinR</i> *- <i>mScarlet-I</i>	pK18 <i>mobsacB</i> derivative; containing the <i>PsinR</i> w/ mutated NurR binding site, flanked by upstream sequence and <i>sinR</i> ₁₋₂₇ - <i>mScarlet-I</i>	This work

pK18 <i>mobsacB-expR^{ATG}</i>	pK18 <i>mobsacB</i> derivative; containing <i>expR</i> from <i>S. meliloti</i> strain RM8530	17
pK18 <i>mob2-PwgeA-mCer/PT5-mCh/PsinI-mV</i>	pK18 <i>mob2</i> derivative; containing <i>PwgeA-mCerulean</i> , <i>PT5-mCherry</i> , <i>PsinI-mVenus</i>	22
pK18 <i>mob2-PpstS-mVenus</i>	pK18 <i>mob2</i> derivative; containing <i>PsinI-sinI₁₋₂₇-mCerulean</i> , <i>PsinR-mCherry</i> , <i>PpstS-pstS₁₋₉-mVenus</i>	This work
pK18 <i>mob3-2xPsinI</i>	pK18 <i>mob3</i> derivative; containing <i>PsinI-sinI₁₋₂₇-mCerulean</i> , <i>PsinI-sinI₁₋₂₇-mCherry</i> , <i>Plac-mVenus</i>	This work
pK18 <i>mob3-PsinR-mCherry</i>	pK18 <i>mob3</i> derivative; containing <i>PsinI-sinI₁₋₂₇-mCerulean</i> , <i>PsinR-mCherry</i> , <i>Plac-mVenus</i>	This work
pK18 <i>mob3-sinRUTR-mCherry</i>	pK18 <i>mob3</i> derivative; containing <i>PsinI-sinI₁₋₂₇-mCerulean</i> , <i>sinRUTR-mCherry</i> , <i>Plac-mVenus</i>	This work
pK18 <i>mob3-PwgeA-mCerulean</i>	pK18 <i>mob3</i> derivative; containing <i>PwgeA-wgeA₁₋₁₅-mCerulean</i> , <i>Ptp-mCherry</i>	This work
pKE- <i>PsinI-mNeonGreen</i>	pKEE derivative; containing <i>PsinI-sinI₁₋₂₇-mNeonGreen</i> (codon-optimized)	This work
pKE- <i>mNeonGreen</i>	pKEE derivative; containing promoterless <i>mNeonGreen</i> (codon-optimized)	This work
pSRKKm-GB1- <i>sinR</i>	pSRKKm derivative; containing 6xHis-GB1- <i>sinR</i>	This work
pSRKGm-indicator	pSRKGm derivative lacking <i>lacI^q</i> , CAP binding site, <i>lac</i> promoter, <i>lac</i> operator & <i>lacZα</i> ; containing <i>PwgeA-mCerulean</i> , <i>PT5-mCherry</i> , <i>PsinI-mVenus</i>	This work
pSRKGm- <i>sinR</i>	pSRKGm derivative; containing <i>sinR</i>	This work
pSRKGm- <i>mScarlet-I-sinR</i>	pSRKGm derivative; containing <i>sinR₁₋₂₇-mScarlet-I-sinR</i>	This work
pWBT- <i>nurR</i>	pWBT derivative; containing <i>nurR</i>	²⁶
pEM-GB1- <i>sinR</i>	pEMGB1 derivative; containing <i>sinR</i>	This work
pET28a- <i>expR</i>	pET28a derivative; containing <i>expR</i> fused to the N-terminal 6xHis-tag	This work

Supplementary Table 6. Oligonucleotides and synthetic genes.

Name	Sequence (5'-3')	Construct(s)
sinR-X-B-fwd	catctagagatcCATGGCTAATCAACAGGCTGTCCCT	pK18 <i>mobsacB-PsinI-mYenus-sinI</i>
PsinI-X-rev	cattctagaACCGTTCCGTTCACTATCCT	
egfp-X-fwd	cattctagaATGGTGAGCAAGGCGGAGAGCT	
egfp-K-rev	catggtaccTTACTTGTACAGCTCGTCCATGC	
sinI-K+TGA+RBS-fwd	ctaggtaccctaaACGCAATGGAGCGAAAAAATGATC	
sinI+66-E-rev	ctagaattCGTTAAATTCGCAATGCCCCGT	
sinR+209-PstI-f	catctcagGGGCTTTACAGGATCGAC	
PsinI-r-mSc	gccctctgaccatACCGTTTCCGTTCACTATC	
PsinI-mSc	atagtgaaacggaacggtATGGTCAAGCAAGGGC	
mSc-r-sinI	catcgtgattacggatTCACTTATACAGCTCGTCCATG	
sinI-f-mSc	catggacgagctataaggaATCGCGTAATCACGCATG	
sinI+66-X-r	cattctagaGTTAAATTCGCAATGCCCCG	pK18 <i>mobsacB-PsinI-mScarlet-I-sinI</i>
	ATGGTCAAGCAAGGCGGAAAGCCGTCAATAAAGAAATTC	
	TGCGCTTCAAGGTCCACATGGAAGGCTCGATGAAACGG	
	CCACGAGTTCGAGATCGAAAGGCGAAAGGCGCG	
	GCCGTATGAGGGCACCCAGACCCCAAGCTCAAAGGTC	
	ACCAAAGGCGGCGCTGCGTTCTCGTGGGACATCC	
	TTTCGCGGCAATTATGATGGCTCGCGCGCATTCATC	
	AAGCATCCGGCAGACATCCCGGACTATTATAAGCAGT	
	CGTCCCAGAAAGGCTTCAAGTGGGAGCGCGTCATGAA	
	CTTCGAGGATGGCGGCGCATCACCCGTACCGCAGGAC	
	ACCTCGTTGAGGACGGCACCCCTCATCTATAAGGTCA	
	AGCTTCGGGCACGAACTTCCCGCCGGATGGCCCCGGT	
	CATCGAAGAAAAGACCATGGGTGGGAAGCCTCGACC	
	GAGCGGCTCTATCCGGAAGATGGCGTCCCTGAAGGGCG	
	ACATCAAGATGGCCCTCCGCTCAAAGATGGCGGCCG	
	CTACCTCGCGACTTCAAGACCACCTATAAGGCCAAG	
	AAACCGGTCCAGATGCCGGCGCATATAACGTGACCC	
	GCAAAGCTCGACATCACCTCGCACAAACGAGGACTATAC	
mScarlet-I, codon- optimized (Invitrogen)		

	CGTCGTCGAGCAGTATGAGCGCTCGGAAGGCCGCCAT TCGACCGGGCGCATGGACGAGCTGTATAAGTGA	
sinR-up-f	catgaattcGCTCAGCCCTCCTGATCTCAC	
sinR-up-r	ACACCGAAACTTGCCCCAT	
TT-f	TCGGTCAAGTGGAAAGAGTT	
TT-r	GCTTCTCGCCGAGAGTT	
sinR-down-f	GTAGTGTCACAACCGCAAGC	pK18 <i>mobsacB-ΔsinR::synTer1</i>
sinR-down-r	catttagaGCCCCTTCAAGCGACATC	
sinR-up-TT bridg	CAAGTTTCGGTGTTCGGTCAAGTGGGA	
TT-sinR-down bridg	GGCGAGGAAGCGTAGTCCAAC	
PsinR-720-H-f	cataaacttGCCGACCTTCTTCCACCGATA	
PsinR-r-3xFl	tgtaaticgataicgtgaccccttgtaaccacatgcatcctgtaafCCATGCCGTA ACACCGAAACTTG	
sinR-f-3xFl	tcagataicgattacaaggatgacgatgacaaggatccggatccggatccATGGC TAA TCAACAGGCTGT	pK18 <i>mobsacB-PsinR-3xflag-sinR</i>
sinR-E-r	catgaattcTCAGATGGTGGGGATCAGAG	
PsinR-720-H-f	cataaacttGCCGACCTTCTTCCACCGATA	
PsinR+27-Sal-r	catgtegacATTGAGGACAGCCTGTTGATTAG	
mScarlet-I-Sal-f	catgtegacATGGTTTCTAAAGCGGAAGCC	
mScarlet-I-TGA-B-r	catggatccagatccacccttGTACAATTCATCCATACCA	pK18 <i>mobsacB-PsinR-mScarlet-sinR</i>
sinR-X-B-f	cattctagagatccATGGCTAATCAACAGGCTGTCCT	
sinR-E-r	catgaattcTCAGATGGTGGGGATCAGAG	
PsinR-720-Eh-f	gacatgattacgaattcGCCACCTTCTTCCACCGATA	
PsinR*-r	tgcaataaagctggcaGGTGCAGTAATCCCCGTTA	
PsinR*-f	ccaagcttTATTGCACCTAGACAAAAACCGG	pK18 <i>mobsacB-PsinR*-sinR</i>
sinR-Bh-r	tegactctagaggatccTCAGATGGTGGGGATCAGAG	
PsinR-720-Eh-f	gacatgattacgaattcGCCACCTTCTTCCACCGATA	
PsinR*-r	tgcaataaagctggcaGGTGCAGTAATCCCCGTTA	
PsinR*-f	ccaagcttTATTGCACCTAGACAAAAACCGG	pK18 <i>mobsacB-PsinR*-mScarlet-I</i>
mSca-Bh-r	tegactctagaggatccCTTGTACAATTCATCCATACCA	
PpstS-A-F	catgaecttTGCGATCGTCAAGCATATC	
PpstS-S-r	catgtegacAGATTTCATGAA TGTTCTCCC	pK18 <i>mobsacB-PpstS-mVenus</i>

PsinI-M-f	catacggtCAACGATTCTCGGCATATCC	PsinI-mCerulean on pK18mob3-
PsinI-K-r	catggtaccACCGTTTCCGTTCACTATCCT	2xPsinI
PsinI-B-f	catggtaccCAACGATTCTCGGCATATCC	PsinI-mCherry on pK18mob3-2xPsinI
PsinI-X-r	catctagaACCGTTTCCGTTCACTATCCT	
Plac145-AatII-f	catgagctcTTGGCCGATTCAATAATGCAG	Plac-mVenus on pK18mob3-2xPsinI
Plac-rbs-S-r	catgtcaccatttttcgctcaCTGTGTGAAATTGTTATCCGC	
PsinR-B-f	gatgattccCGCATATCTGTCCGCCGT	pK18mob3-PsinR-mCherry
mCh+-S-r	ATTGCGGGAGCTCTTACTTG	
sinRUTR-X-f	catggatccgggtgtacggcatgtctaga	pK18mob3-sinRUTR-mCherry
mCh+-S-r	ATTGCGGGAGCTCTTACTTG	
PwgeA-K-rev	catggtaccTTCCAAAGTGGCCATCTGCTT	pK18mob3-PwgeA-mCerulean
PwgeA-M/Xho-fwd	tagacggttagctcgagTTCCGGGAGGACTGACCTGT	
Ptrp-fwd oligo1	gatccggcggcgaatgagcigtgacaattaatcatcg	Ptrp-mCherry
Ptrp-fwd oligo2	aactagttaactagtagcgaagttcacgtaaaaagggtcacacaggaat	on pK18mob3-PwgeA-mCerulean
Ptrp-rev oligo1	agttcgatgatttaattgcaacagctcatttcggggcggc	
Ptrp-rev oligo2	ctagatttcctgtgtgaccttttaactggaacttgcgtagtagtaact	
Term-exch-Sac-fwd	ataaaacgaaaggctcagtcgaaagacggccttcgfttttaa	Removal of T1 terminators & mVenus
Term-exch-Sac-rev	agctttaaacgaaaggcccagcttctgacgagccttcgftttatagct	on pK18mob3-PwgeA-mCerulean
PsinI-K-f	catggtaccCAACGATTCTCGGCATATCC	
PsinI-r-mN	cgccttctgacaccatACCGTTTCCGTTCACTATC	
mNe-f-sinI	gatagaaacgaaacggtATGGTGTCCGAAAGGCG	
mNe-E-r	catgaattcTCACTTGTAGAGTTTCATCCATG	
	ATGGTGTGAAAGGCGAAAGGACAAACATGGCCCTCGC	
	TTCCGGCAACGCAAGCTGCACATCTTCGGCAGCAT	
	CAACGGGTTCGACTTCGACATGGTCCGCCAAGGCACG	
	GGCAACCCGAACGACGGCTATGAGGAACCTCAACCTCA	
	AGTCGACCAAGGCGACCTCCAGTTCTCGCCGTGGAT	
	CCTCGTCCGCACATCGGCTATGGCTTCCACCCAGTATC	
	TCCCGTATCCGGACGGCATGTCGCCGTCCAGGCAGC	
	CATGGTCGACGGCTCGGGCTATCAGGTCCACCCGACCC	
	ATGCAGTTCGAAAGATGGCGCAAGCCTCACCCGTCAACT	
	ATCGCTATACCTATGAGGGCTCGCACATCAAAAGGCGA	pKE-PsinI-mNeonGreen
mNeonGreen, codon-optimized (Invitrogen)		

	GGCCAGGTCAAAGGCAGGGCTTCCCGGCAGATGGC CCCGTGTGACCAACTCGCTCACCGCAGCCGACTGGT GCCGCTCGAAGAAAACCTATCCGAACGACAAGACCAT CATCTCGACGTTCAAGTGGTGTATACCACCGGCAAC GGCAAAGCGCTATCGCTCGACCGCACGCCACCGTATA CCTTCGCCAAGCCGATGGCAGCCAACTATCTCAAGAA CCAGCCGATGTATGTGTCCCGCAAGACCGAGCTGAAG CACAGCAAGACGGAACCTGAACTTCAAAGAGTGGCAG AAGGCGTTCAACCGACGTCATGGGCATGGATGAACTCT ACAAGTGA	
mN-K-f	catgtaccATGGTGTGAAAAGGCG	pKE- <i>mNeonGreen</i>
mNe-E-r	catgaattcTCACTTGTAGAGTTCATCCATG	
GB1-N-f	catcatatgCATCATCATCATCATCATATCAGCAG	pSRKKm-GB1- <i>sinR</i>
GB1- <i>sinR</i> -S-r	caggagcctcAGATGGTGGGGA	
<i>sinR</i> -N-T5rbs-fwd	tcccatatgaagaggagaataaactATGGCTAAATCAACAGGCTGTC	pSRKGm- <i>sinR</i>
<i>sinR</i> -Sac-rev	catgagctcTCAGATGGTGGGGATCAGA	
<i>sinR</i> -Nh-f	aacaaittcacacaggaacagcatcccatatgaagagagaaataaactATGGCT AATCAACAGGCTGTTCCT	
mScarlet-I-TGA-B-r	catggatccagatccactgcCTTGTACAAATTCATCCATACCA	pSRKGm- <i>mScarlet-I-sinR</i>
<i>sinR</i> -X-B-f	catctagagatccATGGCTAATCAACAGGCTGTTCCT	
<i>sinR</i> -Sh-r	agcgcccccaccggtggagctcTCAGATGGTGGGGATCAGAG	
SmSinR_F	ftaaccATGGCTAAATCAACAGGCT	pEM-GB1- <i>sinR</i>
SmSinR_R	ftaaggatcctTAGATGGTGGGGATCAG	
expR-N-f	catcatATGAATATTACGTTGCTCGTACAGTTTCTG	pET28a- <i>expR</i>
expR+127-H-r	cataagcttACGGGCACAGGAATGAAG	
[Cy3]264f 440r	[Cy3]ACGCTGTTCCGACATGCTCT CGTGATTACCGGATGTAGC	P <i>sinI</i> EMSA fragment

With the exception of synthetic genes, upper case letters indicate bases annealing to the template in PCR, lower case letters indicate tails containing, e.g., restriction sites or linkers. [Cy3], fluorescent dye label.

Supplementary Methods 1. Details on strain constructions.

For the *sinI* promoter-*mVenus* fusion analysed by time-lapse fluorescence microscopy and flow cytometry, a 678 bp fragment containing the *sinI* promoter, 5' untranslated region (UTR) and first nine codons of *sinI*, the *mVenus*²⁷ gene including stop codon, and a 729 bp fragment containing the *sinI* coding sequence preceded by its native ribosome binding site were cloned into pK18*mobsacB*²⁰ in a step-wise fashion using HindIII, XbaI, KpnI and EcoRI restriction enzymes (at one step taking advantage of a HindIII site within the fragment including the *sinI* promoter); the final construct pK18*mobsacB*-P*sinI*-*mVenus*-*sinI* thus carried the *mVenus* gene flanked upstream by the *sinI* promoter and downstream by the *sinI* coding sequence. After conjugation and double homologous recombination in *S. meliloti*, the chromosomal *sinI* locus comprises the native *sinI* promoter, UTR and first nine codons followed by an XbaI site, the *mVenus* gene including a KpnI site immediately preceding the stop codon, and the *sinI* coding sequence preceded by its native ribosome binding site.

The *sinI* promoter-*mScarlet-I* fusion analysed by flow cytometry was constructed in a similar fashion as the *sinI* promoter-*mVenus* fusion. However, here the *sinI* gene is preceded by the entire *sinI* UTR. Fusion of the flanking regions with codon-optimized *mScarlet-I*²⁸ was performed by ligase cycling reaction²⁹, and restriction digestion followed by ligation was only employed for cloning of the preassembled insert into pK18*mobsacB*, resulting in pK18*mobsacB*-P*sinI*-*mScarlet-I*-*sinI*. Thus, *S. meliloti* strains carrying this fusion at the native *sinI* locus have no restriction site introduced by cloning in between the *sinI* promoter, UTR and first nine *sinI* codons and the downstream fluorophore gene, and no restriction site in between the fluorophore gene and the downstream *sinI* UTR and coding sequence.

The *sinI* promoter-*mNeonGreen* fusion likewise analysed by flow cytometry comprises the 259 bp sequence upstream of the *sinI* transcription start site (TSS), again followed by the *sinI* UTR and first nine *sinI* codons, fused to codon-optimized *mNeonGreen*³⁰ via overlap extension PCR³¹. Cutting with KpnI and EcoRI restriction enzymes, the assembled insert was cloned into a suicide vector carrying a 964 bp fragment amplified from *S. meliloti* megaplasmid pSymB, i.e., the 3' 676 bp of the *exoP* gene and the subsequent 288 bp including a terminator sequence immediately downstream of *exoP*. Thus, in *S. meliloti* the final construct pKE-P*sinI*-*mNeonGreen* integrates into the essential megaplasmid pSymB⁴ by homologous recombination, and readthrough of *exoP* transcription into the *sinI* promoter-*mNeonGreen* fusion is blocked by the included terminator sequence (as demonstrated for the analogous promoter probe vector pSRPP18³²). The corresponding control plasmid pKE-*mNeonGreen* carrying a promoterless *mNeonGreen* was obtained by amplification of only the codon-optimized *mNeonGreen* gene with the same reverse primer and an *mNeonGreen* forward primer including a KpnI site.

The construct comprising two identical copies of the *sinI* promoter studied by fluorescence microscopy is based on a modified version of a triple reporter cassette²² allowing for parallel monitoring of the activities of up to three different promoters fused to the *mCerulean*³³, *mCherry*³⁴ and *mVenus* genes, respectively; in contrast to the earlier version, the modified cassette includes the *rpoC/thrA* tandem terminator inserted between the *mCerulean* and *mCherry* genes, and only two copies instead of four of the T1 transcription terminator between the *mCherry* and *mVenus* genes²⁶. Both *sinI* promoter-fluorophore gene fusions comprise the same 259 bp sequence upstream of the *sinI* TSS as the *sinI* promoter-*mNeonGreen* fusion, again followed by the *sinI* UTR and the first nine *sinI* codons; these fragments were cloned in front of *mCerulean* using MluI/KpnI restriction sites and in front of *mCherry* using BamHI/XbaI restriction sites, respectively. The triple reporter cassette was then cut out of its original vector pK18*mob2* by cutting with EcoRI/HindIII restriction enzymes (and additionally with MreI to allow for separation of fragments via gel electrophoresis) and cloned into the EcoRI/HindIII-digested suicide plasmid pK18*mob3*, derived from pK18*mob2*²⁰ by deletion of the *lac* promoter preceding the multiple cloning site. Furthermore, to allow for microscopy image segmentation, a 174 bp fragment

including the *lac* promoter amplified from pSRKGm²¹ combined with the *sinI* ribosome binding site was cloned in front of the *mVenus* gene using AatII/SalI restriction enzymes. In both *S. meliloti* strains carrying the final construct pK18mob3-2xPsinI in this work, the vector had integrated into the chromosome via the *sinI* promoter-*mCherry* fusion, so that the two fusions are separated by approximately 4 kb of plasmid DNA; a third, dark copy of the *sinI* promoter regulates expression of *sinI* in these strains (Fig. 1b & Supplementary Figure 2a).

The *sinR* promoter-*mCherry* construct analysed by fluorescence microscopy in turn is a derivative of the above 2xPsinI construct. The entire *sinR* promoter-*mCherry* fusion (including a 294 bp fragment of *sinR* promoter, UTR and start codon) was amplified from an earlier triple reporter cassette located on pK18mob2²⁶ and used to replace the *sinI* promoter-*mCherry* fusion by cutting both the PCR product and the double *sinI* promoter-fluorophore vector with BamHI/SacI. Thus, this construct pK18mob3-PsinR-*mCherry* likewise carries a *lac* promoter-*mVenus* fusion for microscope image segmentation, and the *sinI* promoter-*mCerulean* fusion. The corresponding control plasmid pK18mob3-*sinR*UTR-*mCherry* lacks the *sinR* promoter, but includes the *sinR* ribosome binding site to enable translation of potential transcriptional readthrough. Both in the *S. meliloti* strain carrying the read-out construct and the *S. meliloti* strain carrying the control construct the plasmid integrated into the chromosome via the *sinI* promoter-*mCerulean* fusion.

The *wgeA* promoter-*mCerulean* construct assayed in long-term time-lapse fluorescence microscopy is a derivative of yet another triple reporter cassette, carrying a 303 bp fragment including the *wgeA* promoter, UTR and the first five *wgeA* codons in front of *mCerulean* inserted via KpnI/MluI restriction sites²⁶. The *trp* promoter and UTR combined with the *lac* ribosome binding site was assembled from oligonucleotides and inserted in front of *mCherry* via BamHI/XbaI restriction sites to allow for microscope image segmentation. The *mVenus* gene and preceding restriction sites and T1 tandem terminators in turn were removed and exchanged for a short terminator sequence in order to allow use of this construct in combination with the chromosomal *sinI* promoter-*mVenus* fusion. The final cassette comprising the *wgeA* promoter-*mCerulean* fusion, the *rpoC/thrA* tandem terminator and the *trp* promoter-*mVenus* fusion was cloned into pK18mob3 via EcoRI and HindIII restriction sites; in *S. meliloti* strains carrying this construct pK18mob3-PwgeA-*mCerulean* the plasmid integrated into pSymB via the *wgeA* promoter-*mCerulean* fusion.

The *pstS* promoter-*mVenus* fusion employed to verify the onset of phosphate starvation in time-lapse fluorescence microscopy experiments likewise is part of a triple reporter construct, albeit on pK18mob2; a 298 bp fragment including the *pstS* promoter and the first three *pstS* codons was cloned in front of the *mVenus* gene using AatII and SalI restriction enzymes. The final plasmid (that also includes the above-described *sinR* promoter-*mCherry* fusion, and the above described *sinI* promoter-*mCerulean* fusion) was integrated into the *S. meliloti sinI* mutant Sm2B4001¹⁹, so that the resulting scavenger/indicator cells do not contribute to AHL levels on the agarose pad during experiments.

The AHL indicator plasmid used in the plate reader experiment was built by cutting both the original pK18mob2-triple reporter cassette²² and pSRKGm²¹ with EcoRI/HindIII, thus removing *lacI*, the *lac* promoter and part of *lacZα* from the latter, and subsequent ligation of the pSRKGm backbone and the triple reporter cassette, yielding pSRKGm-indicator.

For the *mScarlet-sinR* translational fusion employed in single molecule microscopy, a 733 bp fragment containing the *sinR* promoter, UTR and first nine codons, the *mScarlet-1* gene without stop codon, but including a linker (AGGSGS) added via a primer tail, and the *sinR* coding sequence were cloned into pK18mobsacB in a step-wise fashion using SalI/HindIII, EcoRI/XbaI and BamHI/SalI restriction enzymes. After conjugation and double homologous recombination in *S. meliloti*, the fusion protein was expressed from the native *sinR* promoter.

For the N-terminally 3xFLAG-tagged SinR, a 709 bp fragment containing the *sinR* promoter and the *sinR* gene were amplified separately, with the coding sequence for the 3x-FLAG tag (DYKDHDGDYKDHDIDYKDDDDK) and the linker (GSGSGS) comprised as overlapping tails in the inner primers; the two fragments were then fused via overlap extension PCR and cloned into pK18*mobsacB* using PstI (cutting within the *sinR* promoter fragment) and EcoRI. The construct was subsequently integrated into the *S. meliloti* genome via double homologous recombination, replacing the native *sinR* gene, so that strains carrying this construct produced 3xFLAG-tagged SinR from the native *sinR* promoter.

For production and purification of His₆-GB1-SinR, the *sinR* gene was cloned via NcoI/BamHI restriction sites into pEM-GB1; this vector links a 6xHis-tag and the coding sequence of the immunoglobulin-binding domain of streptococcal protein G (GB1 domain) to the N-terminus of the protein of interest^{23,24}, thus enhancing solubility^{35,36}. To examine *in vivo* activity of the His-GB1-SinR fusion protein, the respective coding sequence was amplified from pEM-GB1-*sinR* and cloned into the broad host range expression plasmid pSRKKm which was then conjugated into the *S. meliloti sinR*⁻ mutant ($\Delta sinR::synTer1$) described below.

For production and purification of N-terminally His₆-tagged ExpR, the *expR* gene was amplified via colony PCR from Sm2B3001 and cloned into the expression vector pET28a using NdeI and HindIII restriction sites.

To completely abolish *sinR* expression, a synthetic multiple terminator site (*synTer1*)³⁷ flanked by the *sinR* promoter (up to -7 bp from the *sinR* start codon) and the last 21 codons of *sinR* followed by the *sinI* promoter and most of the *sinI* coding sequence was cloned into pK18*mobsacB*; after integration of the resulting plasmid pK18*mobsacB*- $\Delta sinR::synTer1$ into the *S. meliloti* genome, the resulting *sinR*⁻ strains thus lacked *sinR*, but carried the *sinR* promoter and most of its UTR followed by the terminator sequence blocking potential read-through, the 3' end of *sinR* and the native *sinI* promoter and coding sequence.

To specifically reduce *sinR* expression levels, a mutated version of the *sinR* promoter in which the 5' half of the NurR binding site had been exchanged (GTTTATGAAATATTGCACTA to TGCCAAGCTTTATTGCACTA) according to²⁶ was cloned into pK18*mobsacB* either in front of *sinR*₁₋₂₇-*mScarlet-I* (for the single molecule microscopy strain) or in front of *sinR* (for time-lapse microscopy and flow cytometry strains); due to presence of many restriction sites in the assembled fragment, only the vector was digested with EcoRI and BamHI, while the outer primers were designed with homology to the vector, and fusion of vector and insert was done by aqua cloning³⁸. The mutated promoter was then stably integrated into the genomes of the respective strains by double homologous recombination.

For direct overexpression of *sinR*, the *sinR* coding sequence preceded by the T5 ribosome binding site (added upstream of *sinR* during amplification by means of a primer tail) was cloned into pSRKGm using NdeI/SacI restriction sites.

For overexpression of *mScarlet-I-sinR*, the two genes were amplified separately, *sinR*₁₋₂₇-*mScarlet-I* as described for overexpression of *sinR* with preceding T5 ribosome binding site, and as described for *mScarlet-I-sinR* without stop codon, but including a linker. Both PCR fragments were then digested with BamHI, subsequently ligated, and the product was inserted into the NdeI/SacI-digested pSRKGm via aqua cloning.

The plasmid pK18*mobsacB-expR*^{ATG} was used to restore the AHL receptor in strains derived from *S. meliloti* Rm2011 as these strains carry an insertion sequence in the *expR* locus SMc03899-SMc03896 (*expR::ISRm2011-1*)¹⁷.

Supplementary Methods 2. Construction and characterization of the *pde0 expR*⁻ strain.

The *S. meliloti* Rm2011 genome encodes 22 c-di-GMP-related proteins, 13 of which contain predicted phosphodiesterase (PDE) domains⁵. For the *pde0 expR*⁻ strain, these 13 genes were deleted or, in case of *SMc00074*, replaced with a variant encoding an active site mutation via double homologous recombination using the suicide vector pK18*mobsacB*²⁰.

Gene	Plasmid	Primers / Source
<i>SMb21517</i>	pK18 <i>mobsacB</i> - <i>SMb21517</i>	ataaaagcttAAGATGTACAGCGCGCGG (fwd) ataatctagaATCACGATGCTCTTAGGT (rev) ataatctagaCCGGCGACGCGCCTCGTT (fwd) ataaggatccGGTCTTATTGCGCTTGCG (rev)
<i>SMc00887</i>	pK18 <i>mobsacB</i> - <i>SMc00887</i>	5
<i>SMc03942</i>	pK18 <i>mobsacB</i> - <i>SMc03942</i>	5
<i>SMb20900</i>	pK18 <i>mobsacB</i> - <i>SMb20900</i>	5
<i>SMc03178</i>	pK18 <i>mobsacB</i> - <i>SMc03178</i>	5
<i>SMc00992</i>	pK18 <i>mobsacB</i> - <i>SMc00992</i>	5
<i>SMc00033</i>	pK18 <i>mobsacB</i> - <i>SMc00033</i>	5
<i>SMc00038</i>	pK18 <i>mobsacB</i> - <i>SMc00038</i>	5
<i>SMb20447</i>	pK18 <i>mobsacB</i> - <i>SMb20447</i>	5
<i>SMA0137</i>	pK18 <i>mobsacB</i> - <i>SMA0137</i>	5
<i>SMA1548</i>	pK18 <i>mobsacB</i> - <i>SMA1548</i>	5
<i>SMc00074</i> (<i>rgsP</i>)	pK18 <i>mobsacB</i> - <i>SMc00074</i> -AAL	atattctagaATGCCCTGACCCGTAAG (fwd) ataaaagcttTCAAGCCCGCTTCATCAG (rev) Amplification from pABC- <i>rgsP</i> _{AAL} ³⁹
<i>SMc03141</i>	pK18 <i>mobsacB</i> - <i>SMc03141</i>	atataagcttTGCCGCCATCGAGACATTGTT (fwd) atattctagaGATGAATTCTCGCCGCCATA (rev) atattctagaATCACGATGTTTTAGGGTCG (fwd) atatgatccTTCGGCGGCGTCTGCGGTCCA (rev)

The table lists the *S. meliloti* Rm2011 genes containing PDE domains, the plasmids used for construction of the respective deletion strains, and either the primers used for plasmid construction or the plasmid source. pK18*mobsacB*-*SMc00074*-AAL contains a mutated gene encoding a variant of *SMc00074* in which the ‘EAL’ motif essential for c-di-GMP degradation by PDE domains⁴⁰ is replaced for ‘AAL’ (E746A). All other plasmids contain 600-800 bp-long upstream and downstream flanking regions of the respective gene. Upstream flanking regions include the start codon plus ensuing 27 bp, downstream flanking regions include the last 27 bp plus ensuing stop codon. The primers given were used for amplification of the respective flanking regions from Rm2011 or, in case of *SMc00074*, for amplification of the gene variant from pABC-*rgsP*_{AAL}³⁹. Upper case letters in primer sequences indicate bases annealing to the PCR template, lower case

letters indicate tails containing restriction sites. Deletions and the *SMc00074*-AAL mutation were introduced into Rm2011 (*expR*⁻) sequentially from top to bottom.

Quantification of c-di-GMP levels. Quantification of intracellular c-di-GMP levels was carried out as described by Burhenne and Kaever⁴¹. Briefly, nucleotides were extracted from cell pellets of 5ml TY cultures using 40% (v/v) acetonitrile, 40% (v/v) methanol, and 20% (v/v) water. Samples were then dried and subjected to liquid chromatography-tandem mass spectrometry (LC-MS/MS). Amounts of c-di-GMP detected were normalized to protein mass in the respective sample determined by Bradford assays.

Phenotype assays. Surface attachment was quantified with crystal violet staining as previously described⁵. In short, strains were grown to stationary phase in 30% MOPS-buffered medium (MOPS-buffered medium with nitrogen, carbon and phosphate sources reduced to 30%), diluted 1:10 in the same medium and subsequently grown in 96-well microtiter plates at 30 °C without shaking. After 2 days, cell densities were determined, the medium and unattached cells were removed, and the wells were washed with 200 µl water. Remaining (i.e., attached) cells were stained with 200 µl of aqueous 0.1% (m/v) crystal violet solution for 20 min at room temperature while gently shaking. The staining solution was then discarded, the wells washed twice with water, and the stain dissolved in 200 µl of 20% (v/v) acetone and 80% (v/v) ethanol for 20 minutes at room temperature. Staining of the solution was determined by measuring absorbance at 570 nm (*A*₅₇₀) with an Infinite M Plex microplate reader (Tecan) and normalized to OD₆₀₀.

Motility was quantified by spotting 2 µl of stationary phase cultures on a 1:5 diluted TY agar plate (final agar concentration 0.3% (m/v)). Plates were then incubated at 30 °C and imaged after 2 days. Spot diameters were measured with the Fiji/ImageJ image processing software.

Growth curves were determined by growing 3 biological replicates of each strain in the respective medium in a 96-well microtiter plate shaking at 200 rpm in an Infinite M Plex microplate reader (Tecan) set to 30 °C. Starter cultures had been grown in the same medium to stationary phase and diluted 1:100 for the experiment.

References

1. Zhang, R. *et al.* Structure of a bacterial quorum-sensing transcription factor complexed with pheromone and DNA. *Nature* **417**, 971–974 (2002).
2. Thompson, J. D., Higgins, D. G. & Gibson, T. J. CLUSTAL W: improving the sensitivity of progressive multiple sequence alignment through sequence weighting, position-specific gap penalties and weight matrix choice. *Nucleic Acids Res.* **22**, 4673–4680 (1994).
3. Charoenpanich, P., Meyer, S., Becker, A. & McIntosh, M. Temporal expression program of quorum sensing-based transcription regulation in *Sinorhizobium meliloti*. *J. Bacteriol.* **195**, 3224–3236 (2013).
4. diCenzo, G. C., MacLean, A. M., Milunovic, B., Golding, G. B. & Finan, T. M. Examination of prokaryotic multipartite genome evolution through experimental genome reduction. *PLoS Genet.* **10**, e1004742 (2014).
5. Schäper, S. *et al.* Cyclic di-GMP regulates multiple cellular functions in the symbiotic alphaproteobacterium *Sinorhizobium meliloti*. *J. Bacteriol.* **198**, 521–535 (2016).
6. Krol, E., Schäper, S. & Becker, A. Cyclic di-GMP signaling controlling the free-living lifestyle of alpha-proteobacterial rhizobia. *Biol. Chem.* **401**, 1335–1348 (2020).
7. Schäper, S. *et al.* A bifunctional UDP-sugar 4-epimerase supports biosynthesis of multiple cell surface polysaccharides in *Sinorhizobium meliloti*. *J. Bacteriol.* **201**, 1–15 (2019).
8. Dilanji, G. E., Teplitski, M. & Hagen, S. J. Entropy-driven motility of *Sinorhizobium*

- meliloti* on a semi-solid surface. *Proc. R. Soc. B Biol. Sci.* **281**, 20132575 (2014).
9. Gao, M., Coggin, A., Yagnik, K. & Teplitski, M. Role of specific quorum-sensing signals in the regulation of exopolysaccharide II production within *Sinorhizobium meliloti* spreading colonies. *PLoS One* **7**, e42611-13 (2012).
 10. Nogales, J., Bernabéu-Roda, L., Cuéllar, V. & Soto, M. J. ExpR is not required for swarming but promotes sliding in *Sinorhizobium meliloti*. *J. Bacteriol.* **194**, 2027–2035 (2012).
 11. Pellock, B. J., Teplitski, M., Boinay, R. P., Bauer, W. D. & Walker, G. C. A LuxR homolog controls production of symbiotically active extracellular polysaccharide II by *Sinorhizobium meliloti*. *J. Bacteriol.* **184**, 5067–5076 (2002).
 12. Znacchi, F. C. *et al.* A DNA origami platform for quantifying protein copy number in super-resolution. *Nat. Methods* **14**, 789–792 (2017).
 13. Janczarek, M. Environmental signals and regulatory pathways that influence exopolysaccharide production in Rhizobia. *Int. J. Mol. Sci.* **12**, 7898–7933 (2011).
 14. Grant, S. G. N., Jessee, J., Bloom, F. R. & Hanahan, D. Differential plasmid rescue from transgenic mouse DNAs into *Escherichia coli* methylation-restriction mutants. *Proc. Natl. Acad. Sci.* **87**, 4645–4649 (1990).
 15. Simon, R., Priefer, U. & Pühler, A. A broad host range mobilization system for *in vivo* genetic engineering: Transposon mutagenesis in Gram-negative bacteria. *Bio/Technology* **1**, 784–791 (1983).
 16. Studier, F. W., Rosenberg, A. H., Dunn, J. J. & Dubendorff, J. W. Use of T7 RNA polymerase to direct expression of cloned genes. in 60–89 (1990).
 17. Bahlawane, C., McIntosh, M., Krol, E. & Becker, A. *Sinorhizobium meliloti* regulator MucR couples exopolysaccharide synthesis and motility. *Mol. Plant-Microbe Interact.* **21**, 1498–1509 (2008).
 18. Casse, F., Boucher, C., Julliot, J. S., Michel, M. & Dénarié, J. Identification and characterization of large plasmids in *Rhizobium meliloti* using agarose gel electrophoresis. *J. Gen. Microbiol.* **113**, 229–242 (1979).
 19. McIntosh, M., Meyer, S. & Becker, A. Novel *Sinorhizobium meliloti* quorum sensing positive and negative regulatory feedback mechanisms respond to phosphate availability. *Mol. Microbiol.* **74**, 1238–1256 (2009).
 20. Schäfer, A. *et al.* Small mobilizable multi-purpose cloning vectors derived from the *Escherichia coli* plasmids pK18 and pK19: selection of defined deletions in the chromosome of *Corynebacterium glutamicum*. *Gene* **145**, 69–73 (1994).
 21. Khan, S. R., Gaines, J., Roop, R. M. & Farrand, S. K. Broad-host-range expression vectors with tightly regulated promoters and their use to examine the influence of TraR and TraM expression on Ti plasmid quorum sensing. *Appl. Environ. Microbiol.* **74**, 5053–5062 (2008).
 22. Schlüter, J.-P. *et al.* Classification of phenotypic subpopulations in isogenic bacterial cultures by triple promoter probing at single cell level. *J. Biotechnol.* **198**, 3–14 (2015).
 23. Karniel, A. *et al.* Co-translational folding intermediate dictates membrane targeting of the signal recognition particle receptor. *J. Mol. Biol.* **430**, 1607–1620 (2018).
 24. Michel, E. & Wüthrich, K. High-yield *Escherichia coli*-based cell-free expression of human proteins. *J. Biomol. NMR* **53**, 43–51 (2012).

25. Bettenworth, V., McIntosh, M., Becker, A. & Eckhardt, B. Front-propagation in bacterial inter-colony communication. *Chaos An Interdiscip. J. Nonlinear Sci.* **28**, 106316 (2018).
26. McIntosh, M., Serrania, J. & Lacanna, E. A novel LuxR-type solo of *Sinorhizobium meliloti*, NurR, is regulated by the chromosome replication coordinator, DnaA and activates quorum sensing. *Mol. Microbiol.* **112**, 678–698 (2019).
27. Kremers, G.-J., Goedhart, J., van Munster, E. B. & Gadella, T. W. J. Cyan and yellow super fluorescent proteins with improved brightness, protein folding, and FRET Förster radius. *Biochemistry* **45**, 6570–6580 (2006).
28. Bindels, D. S. *et al.* mScarlet: a bright monomeric red fluorescent protein for cellular imaging. *Nat. Methods* **14**, 53–56 (2017).
29. Kok, S. De *et al.* Rapid and reliable DNA assembly *via* ligase cycling reaction. *ACS Synth. Biol.* **3**, 97–106 (2014).
30. Shaner, N. C. *et al.* A bright monomeric green fluorescent protein derived from *Branchiostoma lanceolatum*. *Nat. Methods* **10**, 407–409 (2013).
31. Ho, S. N., Hunt, H. D., Horton, R. M., Pullen, J. K. & Pease, L. R. Site-directed mutagenesis by overlap extension using the polymerase chain reaction. *Gene* **77**, 51–59 (1989).
32. Bahlawane, C., Baumgarth, B., Serrania, J., Ruberg, S. & Becker, A. Fine-tuning of galactoglucan biosynthesis in *Sinorhizobium meliloti* by differential WggR (ExpG)-, PhoB-, and MucR-dependent regulation of two promoters. *J. Bacteriol.* **190**, 3456–3466 (2008).
33. Rizzo, M. A. & Piston, D. W. High-contrast imaging of fluorescent protein FRET by fluorescence polarization microscopy. *Biophys. J.* **88**, L14–L16 (2005).
34. Shaner, N. C. *et al.* Improved monomeric red, orange and yellow fluorescent proteins derived from *Discosoma* sp. red fluorescent protein. *Nat. Biotechnol.* **22**, 1567–1572 (2004).
35. Huth, J. R. *et al.* Design of an expression system for detecting folded protein domains and mapping macromolecular interactions by NMR. *Protein Sci.* **6**, 2359–2364 (1997).
36. Zhou, P. & Wagner, G. Overcoming the solubility limit with solubility-enhancement tags: successful applications in biomolecular NMR studies. *J. Biomol. NMR* **46**, 23–31 (2010).
37. Döhlemann, J. *et al.* A family of single copy *repABC*-type shuttle vectors stably maintained in the alpha-proteobacterium *Sinorhizobium meliloti*. *ACS Synth. Biol.* **6**, 968–984 (2017).
38. Beyer, H. M. *et al.* AQUA cloning: A versatile and simple enzyme-free cloning approach. *PLoS One* **10**, e0137652-20 (2015).
39. Schäper, S. *et al.* Seven-transmembrane receptor protein RgsP and cell wall-binding protein RgsM promote unipolar growth in Rhizobiales. *PLOS Genet.* **14**, e1007594 (2018).
40. Schmidt, A. J., Ryjenkov, D. A. & Gomelsky, M. The ubiquitous protein domain EAL is a cyclic diguanylate-specific phosphodiesterase: enzymatically active and inactive EAL domains. *J. Bacteriol.* **187**, 4774–4781 (2005).
41. Burhenne, H. & Kaefer, V. Quantification of cyclic dinucleotides by reversed-phase LC-MS/MS. in *Cyclic Nucleotide Signaling in Plants: Methods and Protocols* (ed. Gehring, C.) 27–37 (Humana Press, 2013). doi:10.1007/978-1-62703-441-8_3.

4 Discussion

4.1 Spreading the news: signal propagation over a distance

Bacterial quorum sensing is very often studied in liquid cultures where shaking yields a homogeneous distribution of autoinducers; especially at low cell numbers, this de facto amounts to a dilution of the molecules. In physiological niches like biofilms or the rhizosphere, however, active mixing is negligible, and diffusion is regarded as the most important mechanism of autoinducer dispersal (Stewart, 2003; Stewart & Franklin, 2008). Nevertheless, only few studies have addressed propagation of autoinducer molecules over larger distances by diffusion. In (Bettenworth et al., 2018) we investigated spatiotemporal changes in autoinducer concentrations over a two-dimensional plane – a proxy for the environment – both by mathematical modeling and fluorescence time-lapse microscopy. Developing microcolonies of a wild-type *S. meliloti* sender strain, i.e., a strain capable of both producing and sensing AHLs, served as sources of autoinducers, and distantly located receiver colonies incapable of producing AHLs (*sinI*⁻), but nevertheless able to respond to them, served as indicators for AHL progression over the plane. Both sender and receiver strains carried a *sinI* promoter-fluorophore gene fusion; fluorescence of sender colonies was elevated due to the ExpR-AHL-induced positive feedback on autoinducer synthase gene expression, and fluorescence of receiver colonies increased due to the same feedback mechanisms once the AHL threshold concentration necessary to trigger this feedback reached the respective locations. Of note, fluorescence in this work was not determined at the single-cell level, but as mean fluorescence intensities of the whole colony (Bettenworth et al., 2018).

With a similar setup of sender and receiver strains, Gantner et al. had investigated the reach or “calling distance” of AHLs produced by *P. putida* cells on tomato seedling roots (Gantner et al., 2006). Here, AHL-producing sender cells showed constitutive fluorescence, and non-producing receiver cells carried a fluorophore gene fused to an AHL-responsive promoter. Cell suspensions of the receiver and the sender strain were one after the other applied to seedling root surfaces and the inoculated roots incubated for 24 hours in planter boxes with sand. The next day, the roots were examined by confocal laser scanning microscopy, and calling distances were determined by measuring distances from fluorescing receiver cells to the closest sender cell, which was mostly only 4-5 μm , but in individual cases extended to 37 μm (in the root tip) and 78 μm (in the root hair zone). The authors furthermore used a geostatistical modeling approach to interpolate AHL concentrations based on the distribution of sender cells on the root. Consistent with the experimental data, this analysis suggested that a few sender cells located in close proximity to each other can produce AHL gradients that extend far enough to activate receiver cells located “considerable distances away” (Gantner et al., 2006). However, as far as discernible from the microscopy images presented, sender and receiver cells were very often single cells, suggesting that they either did not grow during incubation, or that they were moved during handling, e.g. while the seedling roots were “being kept moist” with phosphate buffer, or that they were motile, since motility would preclude formation of stable microcolonies (Gantner et al., 2006).

Based on more advanced mathematical modeling of diffusion processes, Alberghini et al. came to a similar conclusion as Gantner et al., namely that autoinducer concentrations in the low nanomolar range – which are in many systems sufficient to induce a positive feedback on autoinducer production – can be reached by adding up the concentration gradients around 2-5 cells, provided these are in close proximity to each other (Alberghini et al., 2009) (Fig. 7A). Indeed, quorum initiation at small cell numbers was observed experimentally in *P. syringae* (Dulla & Lindow, 2008), *P. aeruginosa* (Boedicker et al., 2009) and *A. fischeri* (Hagen et al., 2010) when cells were confined in small volumes; however, this confinement also limited diffusion, linking the studies to “diffusion sensing” as a potential function of autoinducers as proposed by (Redfield, 2002). The number of cells initiating quorum sensing was furthermore highly variable in these studies, possibly indicating heterogeneity in autoinducer production; for *P. syringae*, this was later observed at the single-cell level (Pradhan & Chatterjee, 2014).

Alberghini et al. also simulated the mixing and adding-up of autoinducer gradients for larger numbers of cells both in 2-dimensional and 3-dimensional spheres. Already in the 2-dimensional setting a difference in relative positions – either distantly located or arranged in closely spaced concentric circles – yielded an approximately 300-fold difference in autoinducer levels perceived by a cell in the center (Alberghini et al., 2009). The authors therefore stressed the additive effects of multiple cell proximities and proposed thinking of bacterial cell-to-cell communication in terms of “positional sensing” in which the information conveyed is not the mean density of a well-mixed culture, but the relative topology of the cells (Alberghini et al., 2009), similar to Gantner et al. who had proposed that cell-to-cell communication via AHLs was governed by spatial proximity (Gantner et al., 2006).

In contrast to Alberghini et al. and Gantner et al. who had analyzed autoinducer gradients based on snapshots (Gantner et al., 2006) or by modeling the equilibrium state between constant production and diffusion from single-cell sources (Alberghini et al., 2009), we followed the development of AHL concentration gradients originating from *S. meliloti* sender colonies over time (Bettenworth et al., 2018). The time course of the responses observed in receiver colonies located at increasing distances from the sender colony or colonies then allowed us to quantitatively analyze the progression of a certain AHL concentration – the level necessary to trigger the ExpR-AHL-mediated positive feedback on gene expression from the *sinI* promoter – over the plane. Somewhat surprisingly, this concentration level did not decelerate with increasing distance from the source(s) as might have been expected from diffusive spreading, but instead travelled with constant speed. According to our mathematical model, this effect was due to the exponential growth of the colonies: While these had consisted of only a few cells at the beginning of our microscopy time lapses, they covered 6000-8000 μm^2 at the end of the experiments approximately 24 hours later. Accordingly, the concentration profiles of an exponentially growing number of sender cells had added up over time (Fig. 7B), thus compensating for the thinning effect of diffusive spreading. Mathematical modeling furthermore showed that, likewise in contrast to simple diffusive spreading, the concentration profile originating from an exponentially growing colony is not attenuated, but instead remains well-defined, and thus easy to interpret by distantly located receiver colonies (Bettenworth et al., 2018).

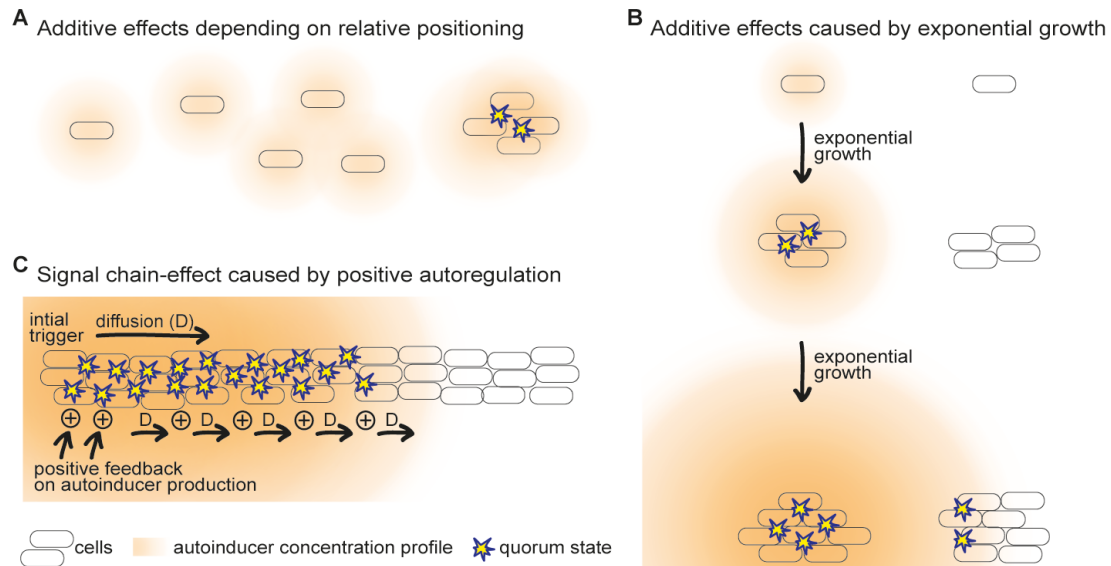


Figure 7. Reach and travelling speed of autoinducers. (A) Relative positioning enables mixing and adding-up of concentration profiles if cells are within sufficient proximity (Alberghini et al., 2009; Gantner et al., 2006). Nevertheless, diffusive spreading from constant sources leads to overall thinning of autoinducer molecules and a deceleration of a specific concentration level with increasing distance from the sources. (B) Exponential growth of sender cells yields additive effects of an exponentially growing number of concentration profiles, counteracting the thinning effect of diffusive spreading and causing a specific concentration level to travel with constant speed over cell-free distances (Bettenworth et al., 2018). (C) A positive feedback loop on autoinducer production yields an iterative process of diffusive spreading and signal amplification in other cells, causing quorum activation to travel in a signal chain-like fashion (Patel et al., 2021; Stabb, 2018). Autoinducer production is furthermore increased since the sensors-turned-producers are exponentially growing cells like the sender cells in (Bettenworth et al., 2018).

A linear least square fit to our data indicated that the positive feedback-inducing AHL concentration moved over the plane at about 1080 $\mu\text{m}/\text{h}$. From this front speed, a diffusion constant of about 1120 $\mu\text{m}^2/\text{s}$ was calculated for the long-chain AHLs produced by *S. meliloti*. Stewart had estimated the diffusion constant of the long-chain AHL 3-oxododecanoyl homoserine lactone (3-oxo-C12-HL) to be 490 $\mu\text{m}^2/\text{s}$ in 25 °C-warm water, and that of the short-chain AHL butyryl-homoserine lactone (C4-HL) to be 720 $\mu\text{m}^2/\text{s}$ (Stewart, 2003); our experimentally determined numbers thus deviate approximately 2-fold from the estimate, but are of a similar order of magnitude. Furthermore, our experiments yielded a calling distance – the maximal distance over which our sender cells elicited a response in receiver cells within the approximately 24 hours observation period – of slightly over 7000 μm , even for a single sender colony (Bettenworth et al., 2018). This number is 2-3 orders of magnitude higher than the calling distances determined by (Gantner et al., 2006), but in good agreement with reports by Flickinger et al. who had observed activity from an AHL-responsive promoter in *P. aeruginosa* receiver cells in hydrogel chambers up to 8000 μm away from the respective sender cells (Flickinger et al., 2011). Surprisingly, however, this was only the case when sender cells were pre-inoculated and pre-incubated for 12 hours, and incubated for further 12 hours after addition of the receivers to the surrounding chambers; in contrast, activation of the AHL-responsive promoter in receiver cells was “nearly undetectable” after 24 hours incubation when sender and receivers were inoculated simultaneously (Flickinger et al., 2011).

Dilanji et al. even observed a response of sensor cells to diffusing autoinducers over a distance of up to 10 000 μm . In their experimental setup, the autoinducers were not produced by sender cells, but externally added in a single drop at one end of a rectangular agar block in which either *E. coli* sensor cells carrying a *luxI* promoter-fluorophore gene fusion (and the *luxR* gene) or *luxI*⁻ *A. fischeri* sensor cells had been uniformly embedded; agar lanes were then monitored by time-lapse microscopy for 20-24 hours, measuring fluorescence or bioluminescence, respectively, emitted by the sensor cells upon AHL-induced expression of the *lux* operon (Dilanji et al., 2012). As expected from diffusive spreading, the magnitude of the response – i.e., either fluorescence or bioluminescence intensity – in the receiver cells decreased with the distance to the AHL droplet. Intriguingly, however, the timing of the response was “surprisingly insensitive” to the distance: Fluorescence from *E. coli* sensor cells, e.g., increased in quick succession after about 2-4 hours and peaked more or less synchronously after about 10-11 hours, regardless of whether the receivers were 100, 2700 or 6700 μm away from the origin of the diffusing autoinducers. Cell growth reached the stationary phase plateau only shortly after this peak, but decelerated already after approximately 7 hours (Dilanji et al., 2012).

With a similar setup as (Dilanji et al., 2012), Patel et al. more recently made a number of interesting observations both with respect to autoinducer dispersal and other aspects of quorum sensing dynamics. For the most part of this work, wild-type *A. fischeri* were embedded in the agar lanes as sensor cells, i.e., cells that had a functional *luxI* gene and thus were capable of AHL production (Patel et al., 2021). At about 10 hours into the initial experiment, weak bioluminescence appeared uniformly throughout all lanes; since this weak luminescence was independent of whether or not an AHL drop had been added as an exogenous stimulus, the authors concluded that it represented an “endogenous” bioluminescence. When they varied the initial density of the embedded cells in a later experiment, ranging from 10^4 to 10^9 colony forming units (cfu) per ml, the highest initial densities yielded a more or less immediate onset of endogenous bioluminescence, and lower densities showed progressively later onsets. From the growth rate, the initial cell densities and the timing of the respective bioluminescence onset the authors calculated that the endogenous bioluminescence always appeared when the embedded cells reached a density of approximately 3×10^8 cfu per ml (Patel et al., 2021).

In the lanes with added AHLs, the uniform endogenous bioluminescence was preceded by a much brighter, propagating bioluminescence; the higher the exogenous stimulus, the earlier this AHL-induced bioluminescence appeared. Analogous to our observations in (Bettenworth et al., 2018), it travelled through the population of wild-type sensor cells with constant speed. In contrast, a likewise AHL-induced propagating bioluminescence observed in a control experiment with *luxI* mutant sensors slowed down continuously with increasing distance to the stimulus (Patel et al., 2021). As in (Dilanji et al., 2012), this control explored a single signal pulse, and the observed attenuation of its concentration profile is in agreement with diffusive spreading of a fixed number of molecules. In the wild-type sensor strain, however, the AHL-induced expression of the *lux* operon not only stimulates bioluminescence, but also AHL synthesis, converting the initially single signal pulse into a signal produced by constant sources. Furthermore, the number of these constant sources should increase perpetually due to two different processes: First, diffusion and positive feedback on AHL synthase gene expression

should concur in an iterative, signal chain-like process, since the sensors-turned-producers will add to the rising AHL levels and allow the positive feedback-inducing concentration to spread further down the agar lane, turning more sensors into producers, and so forth (Fig. 7C). Second, the sensors-turned-producers are exponentially growing cells analogous to the sender cells in (Bettenworth et al., 2018); correspondingly, their exponentially growing number of concentration profiles should also contribute to the progression of bioluminescence at constant speed observed by (Patel et al., 2021).

The mathematical model derived by (Patel et al., 2021) differs in several aspects from the model derived in (Bettenworth et al., 2018). For one thing, diffusion in their experimental setup happened not in two dimensions over a plane, but in one dimension along the agar lane. Furthermore, the *S. meliloti* sender colonies in our experiments had entered the state of elevated AHL-production within the first few hours of colony development, whereas the wild-type *A. fischeri* cells monitored by (Patel et al., 2021) apparently entered this state only in response to an exogenous trigger. The authors therefore included several additional parameters into their equations, namely the basal AHL synthesis rate, the increase in AHL synthesis at full induction, the induction threshold, and a “cooperative term” for the AHL-mediated induction of autoinducer synthesis, i.e., the conversion of sensors into producers. Most importantly, however, their final equation describing the AHL front speed contains the actual population density, whereas the corresponding equation in (Bettenworth et al., 2018) contains the growth rate: According to (Patel et al., 2021), and to theoretical work by (Langebrake et al., 2014), the growth rate itself is unlikely to play an important role, except as the means to reach the cell density sufficient for the wave to travel; the role of this sufficient density in turn is to provide a high enough autoinducer production at the stimulus site “to counteract the diffusive loss of autoinducer [...] and sustain the active state” (Patel et al., 2021). In agreement with this rationale, the experiment with the various initial cell densities described above yielded a “threshold” density also for the propagating, exogenously induced bioluminescence – when sensor cells were embedded at various initial densities, but with the same AHL stimulus, the phenomenon only occurred once the cells reached about 1.5×10^7 cfu per ml (Patel et al., 2021). However, Patel et al. furthermore found that a reduced growth rate (which they achieved by adding chloramphenicol to the agar) not only delayed the onset of the propagating bioluminescence, but also slowed down its speed (Patel et al., 2021). The latter observation would argue for an impact of the growth rate after all, consistent with our findings in (Bettenworth et al., 2018). And even though chloramphenicol very likely affects bacterial physiology also in other aspects than the growth rate, stress is generally considered to stimulate quorum sensing, not to attenuate it (Hense & Schuster, 2015; Papat et al., 2014).

Another experiment in (Patel et al., 2021) yielded very interesting results with respect to the influence of physiological conditions on quorum sensing: The redox-responsive regulator ArcA has been shown to repress *lux* operon expression in its phosphorylated state (Bose et al., 2007); when Patel et al. exchanged the ArcA binding site in the *lux* promoter for a LacI binding site, addition of IPTG was sufficient to induce a propagating bioluminescence even in the absence of an exogenous AHL stimulus – although mechanistically addition of IPTG should only yield a de-repression, but not a stimulation. In contrast, the sensors with the native *lux* promoter had

not shown propagating bioluminescence without exogenous AHLs. It is thus possible that the propagating bioluminescence in the wild type is repressed by ArcA, but that ArcA is displaced at least temporarily by LuxR-AHL when the autoinducer is exogenously added (Septer & Stabb, 2012); this displacement could be more likely – and thus more frequent –, the more AHL is added. Should that be the case, the threshold cell density determined in (Patel et al., 2021) would not be a prerequisite per se, but correspond to a physiological state that renders the cells more receptive to autoinducers – reminiscent of the above-cited conclusion by Fuqua et al. that “first, some external environmental signal other than an autoinducer must be perceived” for target genes to be induced (Fuqua et al., 1994). Point mutations in the ArcA binding site should then relieve this repression and enable a self-induced propagating bioluminescence after a lag phase similar to that observed in the LacI-repressed strain after addition of IPTG; if furthermore stimulated by exogenous AHLs, this lag phase, and the lag phase observed in the initial experiments after addition of AHLs, should be abolished. The same should apply to simultaneous de-repression via IPTG and stimulation via AHLs in the LacI-repressed strain.

4.2 Stochastic pulsing in *sinI* expression

As described in more detail in the Introduction, the prevalent image of quorum sensing is that of a means to determine when a certain cell density – the “quorum” – is reached, and to then change gene expression and behavior in the population in a synchronized fashion (Eickhoff & Bassler, 2018; Mukherjee & Bassler, 2019; Pappenfort & Bassler, 2016; Schauder & Bassler, 2001; Unden, 2014). In order for autoinducers to fulfill this role as proxies for cell density, homogeneity in autoinducer production is more or less explicitly expected (Schauder & Bassler, 2001). Nevertheless, phenotypic heterogeneity was reported for expression of the *agr* operon encoding the *L. monocytogenes* quorum sensing system (Garmyn et al., 2011), for expression of the AHL synthase gene *ahII* in *P. syringae* (Pradhan & Chatterjee, 2014), the AHL synthase genes *traI* and *ngrI* in *S. fredii* (Grote et al., 2014), and the AHL synthase gene *sinI* in *S. meliloti* (Schlüter et al., 2015), all based on single-cell analyses of fluorescence from corresponding promoter-fluorophore gene fusions. Furthermore, phenotypic heterogeneity was reported for AHL production/accumulation in *P. putida* based on single-cell analysis of fluorescence from a *P. aeruginosa lasB* promoter-fluorophore gene fusion serving as an indicator for long-chain AHLs (Cárcamo-Oyarce et al., 2015; Lumjiaktase et al., 2010).

The molecular origins of these heterogeneities were not addressed experimentally; however, in all cases heterogeneity was more pronounced at lower cell densities, with a smaller fraction of cells displaying fluorescence from the respective promoter-fluorophore gene fusions (Cárcamo-Oyarce et al., 2015; Garmyn et al., 2011; Grote et al., 2014; Pradhan & Chatterjee, 2014), or a larger coefficient of variation, a measure of dispersion of the data calculated by division of the standard deviation of single-cell fluorescence intensities by their respective mean (Schlüter et al., 2015). This congruence led to the conclusion that “quorum sensing heterogeneity is a feature associated with the low cell density state of bacterial populations”, and the expectation that, unless environmental conditions favor spatial heterogeneity, at later stages autoinducers would still be produced by the entire population (Mukherjee & Bassler, 2019).

Based on this notion, several explanations have been suggested: For *P. putida*, for instance, a delay of the population-wide cross-induction was proposed, caused by an AHL-triggered synthesis of biosurfactants and the ensuing dispersal of autoinducer-producing cells from the microcolony (Cárcamo-Oyarce et al., 2015; Mukherjee & Bassler, 2019). Furthermore, intermediate, near-threshold autoinducer levels in combination with a bistable and “noisy” gene expression response were put forward based on a modeling approach, since even in well-shaken liquid cultures this combination would activate quorum sensing-related gene expression in some cells, but not in others (Bauer et al., 2017; Mukherjee & Bassler, 2019). Last but not least, according to the same theoretical model, phenotypic heterogeneity in autoinducer production could persist even with monostable feedback regulation on the condition that the response probability is very small, i.e., that cells must respond only rarely to autoinducers in their environment (Bauer et al., 2017).

However, these explanations are not entirely satisfactory. Most importantly, they do not address the actual origin of heterogeneity in autoinducer production, or the origin of initial autoinducer molecules, but instead only focus on the supposed delay in population-wide cross-induction. Yet in none of the studies reporting heterogeneity in autoinducer production all cells turned into contributors even at high cell densities; rather, the fraction of cells showing fluorescence from the reporter fusions only increased to 11-37% of cells in *L. monocytogenes* (depending on the growth medium) (Garmyn et al., 2011), to 78% of cells in *P. syringae* (Pradhan & Chatterjee, 2014), to 74% for *traI* and 84% for *ngrI* in *S. fredii* (Grote et al., 2014), and to “the large majority of cells” in *P. putida* (Cárcamo-Oyarce et al., 2015); in *S. meliloti*, the temporarily high coefficient of variation decreased considerably at later stages of colony development (Schlüter et al., 2015).

When we examined *S. meliloti* strains carrying two identical copies of the *sinI* promoter fused to two different fluorophore genes in (Bettenworth et al., n.d.), comparison of fluorescence intensities from the two fusions revealed that activation of the two promoter copies was only weakly correlated in the wild-type background, and almost entirely uncorrelated in the AHL receptor mutant (*expR*⁻) (Fig. 8A). Such low degrees of correlation in the activation of two identical promoter copies are generally taken as an indication of inherent or “intrinsic” stochasticity in gene expression, i.e., stochastic events in the biochemical reactions – transcription and/or translation – underlying expression of the respective gene (Elowitz et al., 2002; Raj & van Oudenaarden, 2008). When we furthermore examined *sinI* expression in developing microcolonies over time via fluorescence microscopy, tracking of cell lineages and ensuing computational analysis revealed that the observed heterogeneity does not represent subpopulations with distinct stable expression levels, but *sinI* expression in asynchronous pulses over the entire experiment run-time (Fig. 8B). Analysis of one of the colonies from (Schlüter et al., 2015) with the same approach revealed similar pulsatile *sinI* expression over the whole experiment (Fig. 8C). As no *sinI* expression is detectable in early time frames, the coefficient of variation is largest when some cells start pulsing while others are still dark; however, due to the high stability of fluorescent reporters, both current and past expression events contribute to the increasing mean at later time points, and, consequently, the coefficient of variation – calculated by dividing the standard deviation by the mean – decreases.

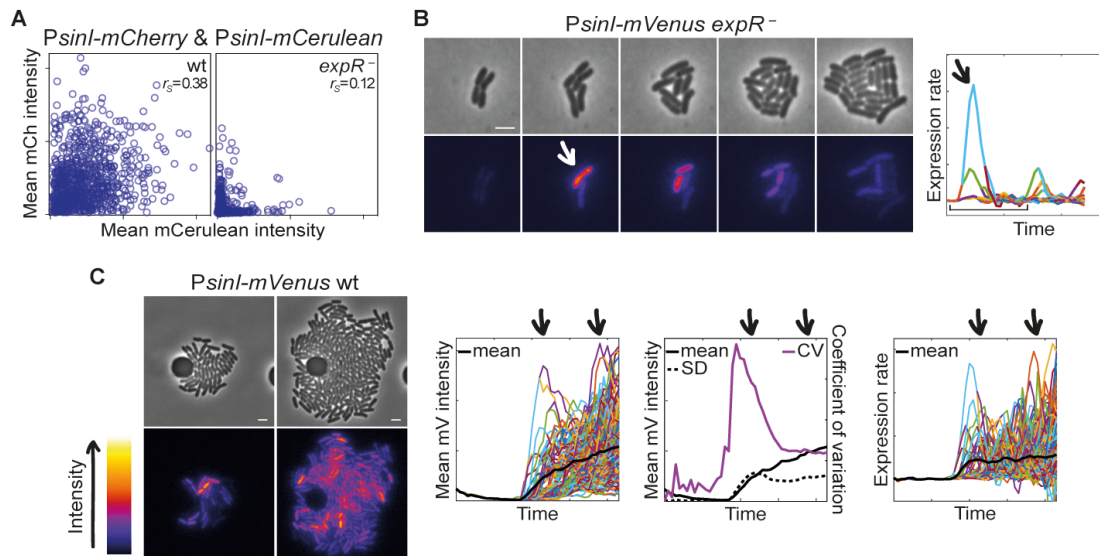


Figure 8. Stochastic pulsing in *sinI* expression. (A) Plots of mean single-cell fluorescence intensities from two *sinI* promoter-fluorophore gene fusions determined by microscopy. The low degree of correlation between mCherry (mCh) and mCerulean intensities within individual cells indicates stochasticity in gene expression. r_s , Spearman's correlation coefficient. (B) Images from a fluorescence time-lapse microscopy movie and the corresponding plot of *sinI* expression rates in a developing $expR^-$ microcolony. Arrows mark the same *sinI* expression pulse, the bracket at the bottom of the plot marks the time covered by the images. (C) Fluorescence time-lapse microscopy images of a wild-type colony from (Schlüter et al., 2015) and the corresponding plots of mean fluorescence intensities displayed by the individual cells (left), of the respective mean, standard deviation (SD) and coefficient of variation (CV) of the population (middle), and of single-cell *sinI* expression rates calculated as in (Bettenworth et al., n.d.) (right). Arrows above the plots mark the time frames of the microscopy images. Microscopy in (C) by Jan-Philip Schlüter. Scale bars, 2 μ m; fluorescence microscopy images, Fiji “fire” lookup table.

Of note, the stochastic pulses in *sinI* expression reported in (Bettenworth et al., n.d.) are distinct from uniform and periodic oscillations like, e.g., the alternating expression of photosynthesis- and nitrogen fixation-related genes in the cyanobacterium *Synechococcus* (Lenz & Søgaard-Andersen, 2011). Likewise, even though stochasticity is clearly involved, they are distinct from mere stochastic fluctuations, since they yield discrete and easily discernible peaks. Rather, pulsatile *sinI* expression is reminiscent of the stochastic pulsing described, e.g., for activity of σ^B and other alternative sigma factors in *Bacillus subtilis* (Locke et al., 2011; Park et al., 2018); for expression of the *lac* operon in absence of inducer (Cai et al., 2006; Yu et al., 2006), of the stress sigma factor σ^S (Patange et al., 2018), and of class II and class III flagella genes in *E. coli* (J. M. Kim et al., 2020); and for activity of several stress-responsive transcription factors in *S. cerevisiae* (Cai et al., 2008; Dalal et al., 2014; Hao & O’Shea, 2012). Similar activity profiles have been furthermore described for higher eukaryotes including mammals, and the terms “transcription pulse” or “transcriptional burst” are sometimes used synonymously to describe such phenomena (Smirnov et al., 2018; Tunnacliffe & Chubb, 2020). In contrast, Levine et al. define “pulsing” as a phenomenon “generated by genetic circuits that activate and deactivate key regulators and modulate pulse characteristics, such as frequencies and amplitudes”, whereas “transcriptional bursting [...] results from the stochastic nature of gene expression” (Levine et al., 2013). However, judging from our findings on AHL synthase gene expression in *S. meliloti*, the roles of the genetic circuit and of the stochastic nature of gene expression are not always clearly distinguishable.

4.3 The mechanism: a regulatory system based on low probabilities

Stochasticity appears to be an integral part of the *S. meliloti* Sin system, originating from the biochemical properties of the key molecule SinR: Whereas a dissociation constant of 40-50 nM for binding of ExpR-AHL to *sinI* promoter DNA was determined in EMSAs (Bamberger, 2020), we could not detect binding of SinR alone to the *sinI* promoter even at 70 μ M with the same method, but only a SinR-dependent supershift when the DNA was simultaneously bound by ExpR-AHL (Bamberger, 2020; Bettenworth et al., n.d.). This supershift was not detectable at SinR concentrations below 20 μ M (Bamberger, 2020). Thus, even when aided by ExpR-AHL, SinR appears to have a very low binding affinity to the *sinI* promoter; in absence of the AHL receptor, this affinity presumably is even lower – so low that it is not detectable at all by our assay.

Consequently, even if present at concentrations in the low micromolar range, SinR would only rarely bind to the *sinI* promoter. However, assuming a volume of approximately 1 μ m³ for a bacterial cell (Milo & Phillips, 2016; Phillips et al., 2009), a 1 μ M concentration would correspond to about 600 molecules per cell, whereas according to our single molecule microscopy data only about 10% of cells in an exponentially growing population display an mScarlet-I-SinR spot (Fig. 9A) (Bettenworth et al., n.d.). Furthermore, this number is very likely still an overestimate, since mScarlet-I-SinR produced much higher fractions of *PsinI-mVenus*-fluorescent cells in flow cytometry measurements than native SinR (Bettenworth et al., n.d.), probably originating from a longer half-life of the fusion protein. Such low protein abundance might seem unusual, but in a quantification of the *E. coli* proteome, about 4% of the proteins assayed could likewise only be detected in 10% or less of the cells (Taniguchi et al., 2010). Hence, scarcity and low binding affinity of SinR make *sinI* transcription initiation an unlikely event and thereby form the biochemical basis for *sinI* expression in a pulsatile rather than a continuous fashion.

In agreement with this conclusion, we found a linear correlation between the fraction of cells displaying mScarlet-I-SinR spots and the frequency of *sinI* expression pulses in the respective strains or under the respective growth conditions in *expR*⁻ backgrounds (Fig. 9B) (Bettenworth et al., n.d.). Furthermore, direct overproduction of SinR in an *expR*⁻ strain abolished heterogeneity in *PsinI-mVenus* flow cytometry data and greatly augmented fluorescence intensities. In *expR*⁺ backgrounds, high-frequency pulses in certain strains or under certain growth conditions were still separable by time-lapse microscopy analysis, but added up in terms of total fluorescence intensities in flow cytometry measurements (Bettenworth et al., n.d.).

Analogous to the gradual modulation of *sinI* expression pulse probabilities by SinR levels, it is to be expected that the AHL receptor-mediated binding of SinR to the *sinI* promoter is likewise not a simple binary switch from “OFF” to “ON”, but instead also gradually shifts probabilities: As mentioned above, a dissociation constant of 40-50 nM for binding of ExpR-AHL to the *sinI* promoter was determined; but in the respective titrations analyzed via EMSAs, a partial shift was already discernible at 5 nM ExpR in presence of 10 μ M AHLs (Fig. 9C), and in analogous assays including 70 μ M SinR, similar fractions of DNA were at once supershifted (Fig. 9D) (Bamberger, 2020). Even ExpR alone, in absence of AHLs, produced a SinR-dependent super-

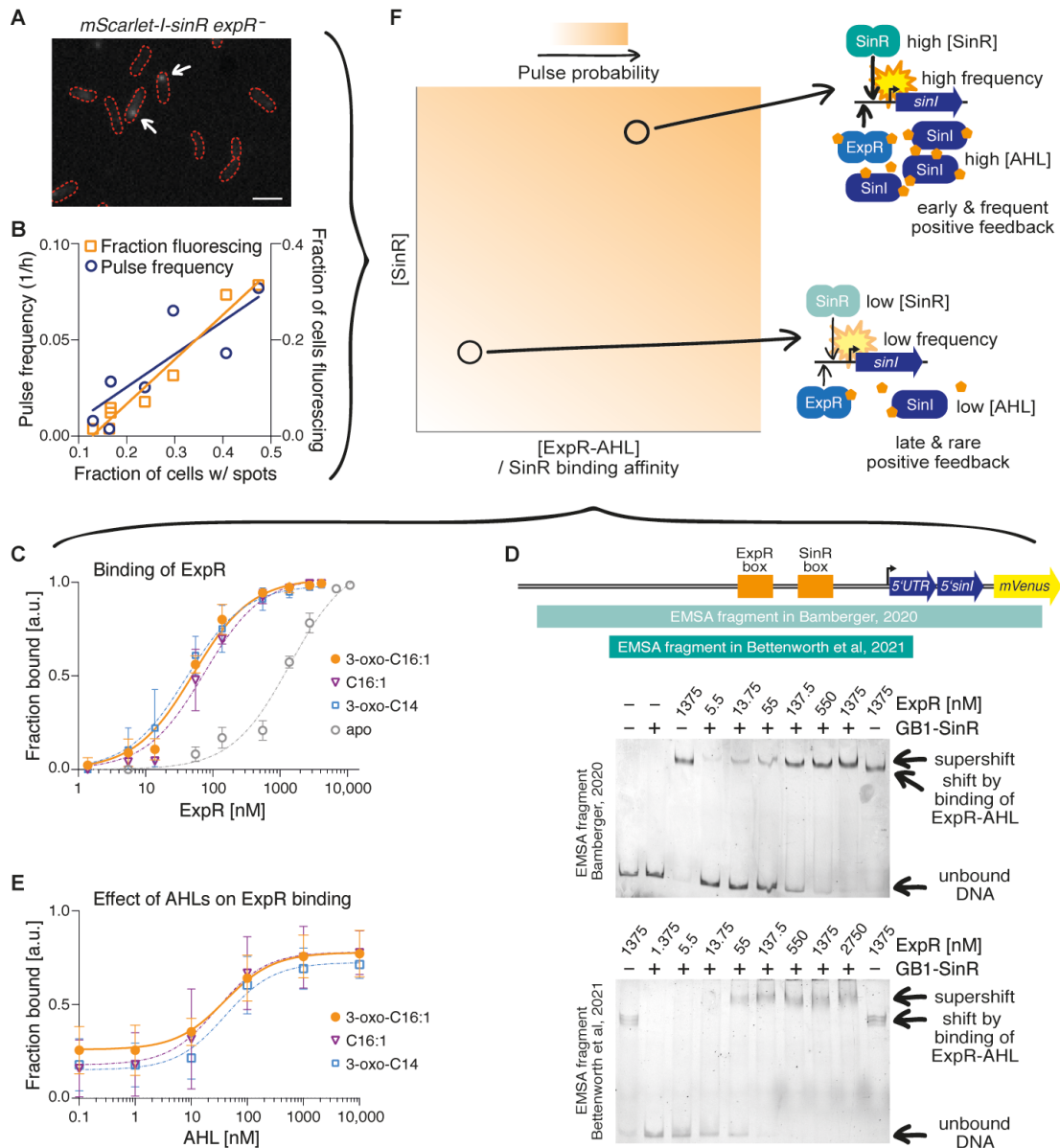


Figure 9. Shaping of *sinI* expression pulse probabilities. (A) Single molecule microscopy image illustrating scarcity of mScarlet-I-SinR fusion proteins. Arrows mark fluorescent spots; scale bar, 2 μm . Microscopy by B. Turkowyd. (B) Plot illustrating the linear correlation between SinR abundance in single molecule microscopy data and *sinI* expression pulse frequency in time-lapse microscopy / flow cytometry data in *expR⁻* strains. (C) Fractions of *sinI* promoter DNA bound by ExpR-AHL or ExpR in EMSAs and corresponding non-linear fits for determination of ExpR dissociation constants. $n=3$; AHLs, 10 μM ; DNA, 2.75 nM. (D) Sketch of the *sinI* promoter and corresponding EMSA fragments (top). The longer fragment (-205 bp to +89 bp from transcription start site (TSS)) used in (Bamberger, 2020) shows only a small, but reproducible SinR-dependent supershift (middle). Analogous EMSAs performed with the fragment from (Bettenworth et al., n.d.) (-163 bp to +14 bp from TSS) produce larger supershifts (bottom). Independent of the fragment, EMSAs reveal the immediate supershift of *sinI* promoter DNA by SinR in presence of increasing amounts of ExpR-AHL. GB1-SinR, 70 μM ; AHL (3-oxo-C16:1), 10 μM ; DNA, 2.75 nM. EMSAs by A. Bamberger. (E) Fractions of *sinI* promoter DNA bound by ExpR-AHL in EMSAs and corresponding non-linear fits for determination of the half maximal effective concentrations of AHLs. $n=3$; ExpR, 80 nM; DNA, 2.75 nM. (C, D (middle), E) Adapted from (Bamberger, 2020). Values for ExpR-AHL dissociation constant and half-maximal effective concentration in the text refer to 3-oxo-C16:1. (F) SinR abundance and binding affinity shape the probability for a *sinI* expression pulse. Very low SinR produces very low *sinI* expression pulse frequency, and consequently low AHL levels and a later and less frequent increase in SinR binding affinity by ExpR-AHL. Higher SinR produces higher pulse frequency, consequently higher AHL levels, an earlier and more frequent ExpR-AHL-mediated increase in SinR binding affinity, and thus a further increase in *sinI* expression pulse frequency.

shift, albeit only at concentrations much above its dissociation constant, i.e., at about 1.4 μM or higher (Bamberger, 2020). Titration of AHLs in presence of both ExpR and SinR was not attempted, but whereas a half maximal effective concentration of 30-40 nM was determined for long-chain AHLs, AHL-facilitated binding of ExpR to the DNA was already observed at 10 nM AHLs, and the plateau was only reached at 1 μM (Fig. 9E) (Bamberger, 2020). It is thus plausible that at concentrations from 10 nM to 1 μM , increasing AHLs will make ExpR-AHL-facilitated binding of SinR to the *sinI* promoter more and more likely.

In conclusion, abundance of ExpR and AHLs shape SinR binding affinity, and SinR binding affinity and SinR abundance in turn shape the probability for a *sinI* expression pulse (Fig. 9F). Since probabilities are low in any case – just more or less so –, it is impossible to predict whether a given cell, at a given moment, will experience *sinI* expression. But despite this clear stochasticity, *sinI* expression is by no means random or arbitrary in terms of “happening without cause or reason”; rather, over a large-enough population, the fraction of cells with a SinR-*sinI* promoter complex and ensuing *sinI* expression is clearly defined by the concentrations of the key players SinR, ExpR and AHLs in the individual cells.

Similarly, the term “noise”, even though widely used as a synonym for stochasticity (Elowitz et al., 2002; Raj & van Oudenaarden, 2008), does not seem appropriate for describing heterogeneity in *sinI* expression: “Noise” – at least in my opinion – has connotations of mere statistical fluctuations or inaccuracies, and furthermore suggests something that might be undesired but unavoidable; the finding by Taniguchi et al. that the cell-to-cell variation in abundance for none of the approximately 1000 *E. coli* proteins analyzed decreased below 30% matches these connotations (Taniguchi et al., 2010). In contrast, the low probabilities described above and the resulting probabilistic switch are an integral part of the Sin system. Without them, regulation of *S. meliloti* quorum sensing would be entirely different: A higher binding affinity of SinR to its promoter, for instance, with everything else unchanged, would considerably increase *sinI* expression rate, and the same is of course true for higher SinR abundance; both would thus strongly increase AHL production in the population and accelerate quorum sensing dynamics. If, on the contrary, the dynamics were to be preserved, a steady *sinI* transcription would have to be compensated for by, e.g., a reduced *sinI* translation rate, a reduced AHL production rate, and/or a reduced sensitivity of the AHL receptor to autoinducers.

Considering the molecular mechanisms underlying other known examples of transcriptional pulsing in bacteria – as far as understood –, low abundance of a key factor might also play a role in pulsatile expression of *E. coli* flagella genes: Flagella gene expression is regulated in a transcriptional cascade, with class I genes *flhDC* encoding the master regulator of class II transcription, and class II genes encoding, amongst others, the alternative sigma factor for class III transcription (Chilcott & Hughes, 2000). As Kim et al. reported, expression of *flhDC* is steady with only small fluctuations, but class II and class III genes are expressed in discrete stochastic pulses (J. M. Kim et al., 2020). The anti-FlhDC factor YdiV apparently plays a central role in pulse generation, since upon deletion of *ydiV* class I and class II promoter activation was much more correlated (J. M. Kim et al., 2020). Based on mathematical modeling it was later concluded that YdiV “creates a monotonic ultrasensitive switch” (Sassi et al., 2020).

However, Sassi et al. only considered sequestration of FlhDC by YdiV as a molecular mechanism in their study, not the YdiV-mediated targeting of FlhDC for ClpXP protease-dependent degradation (Li et al., 2012; Takaya et al., 2012; Wada et al., 2011). Furthermore, the values plotted as “class 1 concentration” against the response curve in (Sassi et al., 2020) are plotted as “class 1 expression” in the original work by (J. M. Kim et al., 2020) and stem from the fluorescent reporter mVenus produced from a transcriptional fusion in the *flhDC* 3' UTR (J. M. Kim et al., 2020). mVenus levels are thus only indicative of *flhDC* transcription, but not of FlhDC degradation, and it is possible that FlhDC levels in wild-type (*ydiV*⁺) cells deviate considerably from those of the reporter.

In fact, several findings suggest that low FlhDC levels might be important for pulsing in flagella class II and class III gene expression: First, expression from the native promoter appears weak, with fluorescence intensities from the transcriptional fusion still slightly overlapping the autofluorescence threshold. Second, pulsing persisted when the native promoter was exchanged for various synthetic constitutive promoters, provided these produced similar (low) expression levels; a very weak synthetic promoter could not trigger class II gene expression even in absence of YdiV, whereas a stronger promoter even in presence of YdiV caused continuous activation of downstream promoters. And third, pulsing in class II and class III gene expression appears to be specific for the isolate used in the study (CGSC #6300). In contrast to this culture, both another isolate (CGSC #7740) of the same strain (MG1655) and strains used for classic chemotaxis studies apparently harbor insertion elements in the *flhDC* regulatory region. Replacing the native *flhDC* regulatory region with the respective region from a chemotaxis strain yielded homogeneous class III (*fliC*) expression at a high level also in CGSC #6300 (J. M. Kim et al., 2020), possibly due to higher transcription either from a promoter within the insertion element, or from a hybrid promoter generated by the insertion (Siguier et al., 2014). Thus, it is possible that YdiV reduces already low FlhDC levels so much that they become limiting – analogous to SinR levels in *S. meliloti* – and only rarely activate class II gene expression. Alternatively, since YdiV levels have been shown to be “extremely low” in *E. coli* (Wada et al., 2012), the anti-FlhDC factor itself might be so rare, or heterogeneously distributed either between cells or within cells over time, that it triggers ClpXP-dependent degradation of FlhDC in some cells, but not in others, thus allowing only the latter to initiate a pulse.

In the case of stochastic pulsing from the *E. coli lac* promoter in absence of inducer, on the other hand, binding affinities appear to play a central role: For a promoter-fluorophore gene fusion based on a reduced promoter version comprising only the *O*₁ and *O*₃ operators, Yu et al. reported expression in stochastic bursts with a mean frequency of 1.2 events per cell cycle (Table 1), producing on average one mRNA molecule per burst and four fluorescent proteins per mRNA (Yu et al., 2006). For the wild-type *lac* promoter comprising all three operators *O*₁, *O*₂ and *O*₃, Cai et al. reported similarly brief bursts with a mean frequency of 0.11 events per cell cycle (Cai et al., 2006). In both cases, the transcriptional bursts were attributed to stochastic and brief dissociation of the *lac* repressor LacI from the respective promoters (Cai et al., 2006; Yu et al., 2006), and the production of only one mRNA molecule per burst observed by Yu et al. was taken to indicate that LacI quickly rebinds the operator region (Yu et al., 2006). Thus, mechanistically, pulsatile *lac* promoter activation is a reversed image of pulsatile *sinI*

expression triggered by stochastic and transient binding of SinR. Furthermore, the differences in burst frequencies reported in the two studies inversely correlate with the differences in repression of the respective promoters by LacI observed in an older population-level study, where a 1300-fold repression was reported for the wild-type *lac* promoter, and a 440-fold repression for a version with only the O_1 and O_3 operators (Oehler et al., 1990). It is thus plausible that both the lower degree of repression at the population level and the higher burst frequency at the single-cell level observed for the O_1 & O_3 *lac* promoter version stem from a lower LacI binding affinity to this promoter, and the higher repression and lower burst frequency of the wild-type version from a higher LacI binding affinity.

	<i>lac</i> promoter w/ O_1 & O_3	<i>sinI</i> promoter in wt	<i>lac</i> promoter w/ O_1 , O_2 & O_3	<i>sinI</i> promoter in <i>expR</i> ⁻
Pulses / cell cycle	1.2 (Yu et al., 2006)	0.42 (This work)	0.11 (Cai et al., 2006)	0.04 (Bettenworth et al., n.d.)

Table 1. Pulse (or burst) frequencies reported for expression from different versions of the *lac* promoter, and for expression from the *sinI* promoter in wild-type (wt) and *expR*⁻ backgrounds. Columns are ordered from highest to lowest frequencies.

The final example of transcriptional pulsing in bacteria to be considered here stems from pulsatile activity of the *B. subtilis* stress response sigma factor σ^B observed by (Locke et al., 2011). Pulses of σ^B activity likewise occur stochastically, and σ^B -mediated expression from the *sigB* promoter – like pulsatile *sinI* expression – exhibits both variability in amplitude and frequency modulation by physiological factors (Locke et al., 2011). However, when Locke et al. monitored cells carrying two *sigB* promoter-fluorophore gene fusions at a high stress level, the results indicated that the underlying mechanism is very different: In agreement with asynchronous pulsatile expression, fluorescence intensities originating from the two *sigB* promoter copies showed considerable cell-to-cell variation; but in strong contrast to the findings for the two *sinI* promoter fusions in (Bettenworth et al., n.d.), fluorescence intensities within single cells were highly correlated. Furthermore, activity of the *sigB* promoter was highly correlated with the activity of other σ^B -regulated promoters within given cells (Locke et al., 2011). These findings indicate that variation in *sigB* promoter activation is due to extrinsic stochasticity or “global [i.e., cell-wide] changes in σ^B activity” (Locke et al., 2011). In other words: Stochasticity appears to be limited to the decision of whether or not, at a given time in a given cell, a pulse is initiated. Pulse initiation according to Locke et al. is triggered by “noise-induced fluctuations” in the ratio of phosphatases and kinases acting on the σ^B anti-anti-sigma factor. Since σ^B via the *sigB* promoter not only controls expression of its own gene, but also of the genes encoding the anti-anti-sigma factor and the corresponding hybrid anti-sigma factor and kinase, this phosphoswitch sets off time-delayed positive and negative feedback loops that then determine pulse characteristics: First, stochastic *sigB* promoter activation yields enough free and active σ^B molecules to simultaneously activate the various target promoters in the respective cell. Later, kinase levels rise, and once kinase activity exceeds phosphatase activity, the anti-anti-sigma factor is re-phosphorylated, resulting in sequestration of σ^B by its anti-sigma factor and termination of the pulse (Locke et al., 2011).

4.4 Postulated roles: information integration and collective decision-making

Since the existence of phenotypic heterogeneity – either in terms of stable subpopulations, or variations over time – is generally taken to indicate a role of the phenomenon in the respective organism’s fitness (Lehner, 2008; Wang & Zhang, 2011), Locke et al. proposed bet hedging as a potential function of pulsing in *B. subtilis* σ^B activity. Pulsing, the authors argued, produced “a broad, but dynamic distribution of states in the population”; this broad distribution might convey fitness advantages in unpredictable environments, and simultaneously balance these advantages with the negative effect of σ^B activity on growth rate (Locke et al., 2011). Likewise, pulsatile class II and class III flagella gene expression according to Kim et al. “would yield a mixed population, with cells favoring either growth or flagella biosynthesis” and “may have evolved as a bet-hedging strategy to minimize cost”, or to “minimize immune responses” when colonizing a host (J. M. Kim et al., 2020). Last but not least, the stochastic pulsing from uninduced *lac* promoters can be viewed as bet hedging, since it generates a subpopulation of cells that are apt to rapidly thrive on lactose as a new carbon source (Cai et al., 2006).

With analogous reasoning, bet hedging was suggested as a function for quorum sensing-related heterogeneities: In case of the heterogeneity in *agr* operon expression in *L. monocytogenes*, e.g., it was stated in a rather general way that the generation of different phenotypes “could facilitate survival of clonal populations to ever-changing environmental conditions” (Garmyn et al., 2011). In case of heterogeneity in *P. syringae* quorum sensing, it was more specifically argued that, since quorum sensing controls lifestyle transitions, it might be advantageous to maintain some members in a population – the quorum sensing-non-responsive cells – adapted for the respective other lifestyle, in case the environment should change yet again (Pradhan & Chatterjee, 2014).

However, in (Bettenworth et al., n.d.) we not only found that the *S. meliloti* AHL synthase gene is expressed in stochastic pulses, but also that different physiological cues modulate the frequency of these pulses. Phosphate starvation and the nucleotide second messenger c-di-GMP produce this effect by altering SinR abundance, whereas the receptor-AHL complex apparently increases SinR binding affinity to the *sinI* promoter. Higher or lower pulse frequencies in *sinI* expression in turn trigger the onset of quorum sensing target gene expression at lower or higher cell numbers, respectively. First, these findings indicate that frequency-modulated pulsing in *S. meliloti* AHL synthase gene expression represents the time-based molecular mechanism actually underlying the effects of phosphate starvation, c-di-GMP and the ExpR-AHL-mediated positive feedback described earlier in population-level studies (McIntosh et al., 2009; Schäper et al., 2016). Second, they also imply that quorum sensing in *S. meliloti* is not so much a matter of cell density sensing, but instead resembles a voting in a local community, or the collective decision making in social insects, for instance during selection of a new nest site by a swarm of honey bees (*Apis mellifera*) (Fig. 10A): Here, so-called scout bees first search the area for potential nest sites. The higher the quality of the site a scout bee has found, the higher the probability that the bee performs a waggle dance once it returns to the swarm. Furthermore, if a bee dances, on average both the frequency – the number of rounds per minute – and the length of the dance increase with the quality of the site. The higher the frequency, and the longer the

dance, the more swarm mates are induced to likewise visit that site and, after examining it themselves, cast their own votes. Since scout bees do not compare different nest sites, but just report on the one site they examined, several putative new homes are initially advertised. However, due to differences in dance rate and length, and the ensuing amplification by recruiting different numbers of new scout bees, a specific site – usually the best – is advertised more and more often, and about an hour after consent has been reached, the swarm lifts off to move in (Seeley, 2010; Seeley & Buhrman, 2001; Seeley & Visscher, 2004, 2008).

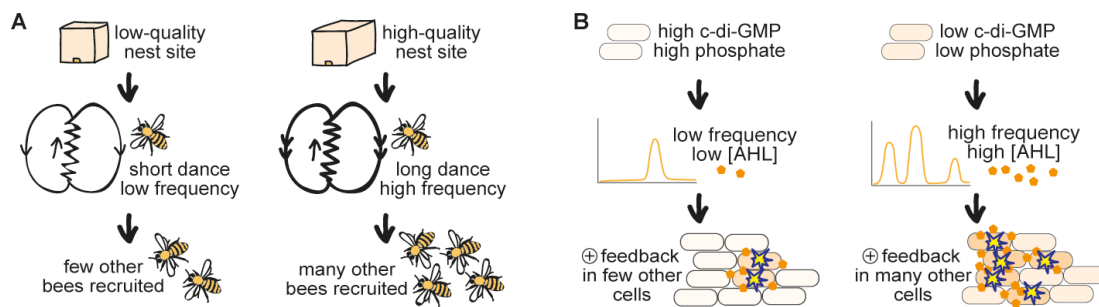


Figure 10. Collective decision-making in *Apis mellifera* and frequency modulation of the quorum sensing response in *S. meliloti*. (A) After examining a potential new nest site, *A. mellifera* scout bees often – but not always – perform a waggle dance. The dance consists of a waggle phase or waggle run (drawn as zigzag) in which the scout bee vigorously waggles her abdomen, and a return phase in which the bee circles back to the starting point of the waggle run, thereby alternating between clockwise and counterclockwise directions. Angle and length of the waggle run, and thus the total number of rounds performed, encode the quality of the site: Scout bees that examined a low-quality nest site have an overall lower probability to dance, and if they do, take longer to return to the starting point of the waggle dance, thus perform fewer rounds per minute, and stop dancing earlier. Scout bees that examined a high-quality nest site have a higher probability to dance, return faster to the starting point if they dance, thus perform more rounds per minute, and continue dancing longer. Altogether, better nest sites thus are advertised more vigorously, and more other bees are recruited to likewise visit them and subsequently cast their own votes (Seeley, 2010; Seeley & Buhrman, 2001; Seeley & Visscher, 2004, 2008). (B) In *S. meliloti*, physiological factors like c-di-GMP or phosphate levels modulate the initial frequency of AHL synthase gene expression pulses, and pulse frequency determines AHL levels in the environment. High AHL levels elicit a positive feedback by increasing pulse probability in neighboring cells. Of note, the neighboring cells' disposition to pulse is still co-shaped by physiological factors, since the latter determine abundance of the essential activator SinR.

In case of *S. meliloti* quorum sensing (Fig. 10B), the pulse frequency with which an individual cell expresses the AHL synthase gene represents its estimate of the current environment and, possibly, its “need” (Hense et al., 2012) for target behaviors like EPS production – the higher the pulse frequency, the more urgently the cell “votes” for the behavioral change. Furthermore, it thereby lowers the activation threshold in its neighbors, since the AHLs it produces, in complex with the receptor, facilitate binding of SinR to the *sinI* promoter. The ExpR-AHL-mediated positive feedback thus represents an amplification process similar to the recruitment of new scout bees: The long, high frequency dance of a given scout bee induces other bees to visit the potential nest site and thereby increases the probability that they will also advertise that site, and the high *sinI* expression rate in a given *S. meliloti* cell makes AHL synthase gene expression in its neighbors more probable. However, whether or not the recruited scout bees do advertise the site upon their return to the swarm still depends on their own judgement of the

site, and whether or not the neighboring *S. meliloti* cells generate a *sinI* expression pulse still depends on their own physiological condition, i.e., on whether or not they have SinR to initiate a pulse.

Of note, effects of growth conditions on the onset of the quorum sensing response have already been observed in a vast number of population-level studies. For instance, Neilson et al. found as early as 1972 that the onset of bioluminescence in *A. fischeri* – the most popular showcase for quorum sensing in Gram-negative bacteria, if not in general – is delayed in the presence of glucose, and that this effect could be compensated for at least partially by addition of cAMP (Neilson et al., 1972); in the 1980s, the effect was traced back to catabolite repression of the autoinducer receptor gene (Dunlap & Greenberg, 1985, 1988; Friedrich & Greenberg, 1983; Lyell et al., 2013). Duan and Surette, after comparing the activity of the *P. aeruginosa las* and *rhl* quorum sensing systems under 46 different growth conditions, summarized that “no correlation could be established between cell densities and the activation of quorum sensing expression [...], indicating the absence of a specific cell density as a prerequisite for quorum sensing activation” (Duan & Surette, 2007). And even though such findings are not included in the prevalent image of quorum sensing as a means “to take a census of the overall cell density and species composition of the vicinal community” (Eickhoff & Bassler, 2018), or “synchronously alter behavior in response to changes in the population density and species composition of the vicinal community” (Mukherjee & Bassler, 2019), many reviewers emphasized the role of physiological cues: E.g., Dunn and Stabb concluded that “by embedding quorum sensing signaling with [such] regulatory systems [like catabolite repression], bacteria are able to modulate the production of autoinducers such that their concentration reflects not only cell density, but also specific parameters of their environment.” (Dunn & Stabb, 2006). And Popat et al. reasoned that “quorum sensing molecules function both as a collective sensing mechanism and as a means of sharing private information on directly sensed environmental variables” (Popat et al., 2014). The frequency-modulated pulsing in AHL synthase gene expression revealed in (Bettenworth et al., n.d.) represents a time-based molecular mechanism for this sharing of private information. It would be curious to see whether the heterogeneities in autoinducer synthase or precursor gene expression in *S. fredii* (Grote et al., 2014), *P. syringae* (Pradhan & Chatterjee, 2014), and *L. monocytogenes* (Garmyn et al., 2011) observed by microscopy snapshots or flow cytometry measurements likewise result from asynchronous stochastic pulsing; since the fractions of quorum sensing-ON and -OFF cells in these studies were also affected by physiological factors, that would make frequency-modulated pulsing a recurring mode of information integration in bacterial quorum sensing.

5 Conclusions

In (Bettenworth et al., n.d.), we have shown that *S. meliloti* quorum sensing is not based on continuous autoinducer production, but on a stochastic regulatory system that encodes each bacterium's physiological state or need for behavioral adaptation in the pulse frequency with which it expresses its AHL synthase gene. Since the pulse frequencies of all members of a population are then integrated in the common pool of autoinducers, and since the response behavior is only initiated once the autoinducer concentration in this common pool exceeds the threshold level, quorum sensing in *S. meliloti* is not so much a matter of cell density sensing, but rather resembles a voting in a local community or the collective decision-making known from social insects (Bettenworth et al., n.d.). In (Bettenworth et al., 2018), we have shown that the threshold autoinducer concentration emanating from a sender colony does not slow down when spreading by diffusion in a two-dimensional environment; instead, the exponential growth of the sender cells compensates for the thinning effect of diffusive spreading and causes the signal to propagate with constant speed. Furthermore, the concentration profile does not wear down, but remains well-defined and thus easy to interpret for distantly located cells of the same species (Bettenworth et al., 2018).

The experimental setup used in (Bettenworth et al., 2018) was based on wild-type sender cells and receiver cells that due to a partial deletion of the AHL synthase gene were incapable of synthesizing their own autoinducers; the work thus established physical parameters like the traveling speed of the respective molecules and their reach, namely that even autoinducers produced by a single sender colony can cover several thousand micrometers in an effective concentration. However, whether or not, or to what extent, incoming autoinducers produced by one wild-type colony affect autoinducer production and response behavior of another, distantly located wild-type colony that itself is capable of autoinducer production is an open question (Fig. 11). Very likely, the answer is again not a simple “yes” or “no”: If, for instance, one colony expresses the AHL synthase gene with high pulse frequency, and another, distantly located colony – be it due to differences in the respective microenvironments – exhibits low AHL synthase gene expression pulse frequency, autoinducers produced by the first colony will at some point reach the second colony at the concentration necessary to trigger the positive feedback on AHL synthase gene expression. However, since the probability for AHL synthase gene expression is co-shaped by abundance of the essential activator SinR (Bettenworth et al., n.d.), this effect of the incoming autoinducers should be limited as long as microenvironmental conditions at the second location make for relatively low abundance of this key molecule. In addition to this limited increase in actual pulse frequency, the cells in the second colony – figuratively speaking – should be put on alert by the external autoinducers, able to immediately boost their own AHL synthase gene expression should their SinR levels rise accordingly. In fact Stabb suggested a similar role for diffusing autoinducers based on work on *A. fischeri lux* operon expression (Septer & Stabb, 2012), hypothesizing that “if a key environmental cue is spreading into the population, then pheromone sensing might prime cells for its arrival, serving as a warning alarm or dinner bell” (Stabb, 2018).

Since – unlike in case of the *A. fischeri* bioluminescence genes – *S. meliloti* quorum sensing target genes are not encoded in the same operon as the AHL synthase gene, but at other locations in the genome (Charoenpanich et al., 2013), and since their expression is not controlled by SinR, it is even conceivable that the increased production of “own” inducers in the second colony is skipped, and the quorum sensing response launched immediately in response to incoming autoinducers. However, to achieve this immediate response, the concentration of incoming autoinducers would have to be about 20-fold higher than for induction of the positive feedback on AHL synthase gene expression (Charoenpanich et al., 2013). Whether or not this is possible, and how incoming autoinducers exactly affect AHL synthase gene expression in an *S. meliloti* colony that is itself capable of autoinducer production could be tested, e.g., by following gene expression from both the *sinI* and the *wgeA* promoter by time-lapse microscopy in *dgc0* colonies mimicking the high-frequency condition and wild-type or *pde0* colonies mimicking the low-frequency condition.

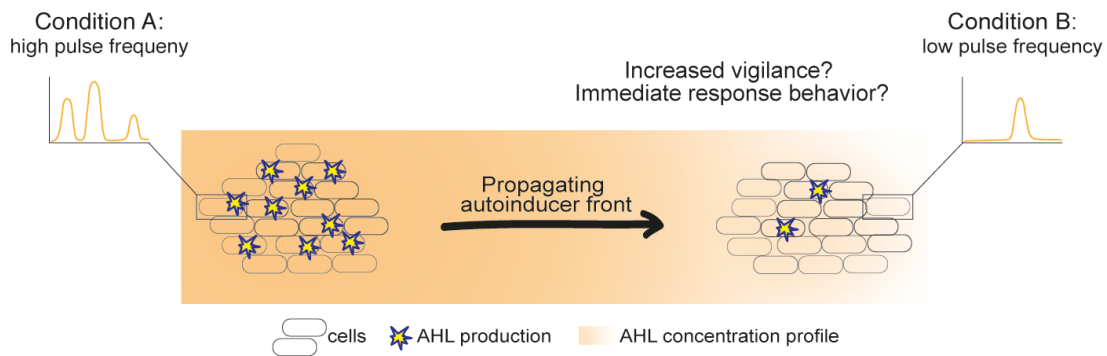


Figure 11. Quorum sensing dynamics at the single-cell and population level in *S. meliloti*. Physiological conditions determine the pulse frequency with which individual *S. meliloti* cells express their AHL synthase gene. Pulse frequencies of all cells of a colony are then integrated in the common pool of autoinducers and determine when the quorum sensing response behavior is initiated (Bettenworth et al., n.d.). Autoinducers emanating from such colonies travel with constant speed in a two-dimensional environment, comparable to propagating fronts in pattern-forming systems (Bettenworth et al., 2018). However, whether or not, or to what extent autoinducers originating from one colony influence the behavior of distantly located colonies that are themselves capable of autoinducer production is an open question. It is possible that they raise AHL synthase gene expression pulse frequencies only to a certain extent and furthermore create a state of alert or increased vigilance, enabling “receiver” colonies to quickly boost their own production if microenvironmental changes at the respective location increase SinR abundance. Since quorum sensing target genes in *S. meliloti* are not encoded in the same operon as the AHL synthase gene, and since their expression is not controlled by SinR, it is furthermore conceivable that the response behavior is immediately triggered by the incoming autoinducers, albeit the concentration necessary to trigger, e.g., EPS production is about 20-fold higher than the concentration necessary to trigger the positive feedback on AHL synthase gene expression.

6 References

- Ackermann, M. (2015). A functional perspective on phenotypic heterogeneity in microorganisms. *Nature Reviews Microbiology*, *13*(8), 497–508. <https://doi.org/10.1038/nrmicro3491>
- Alberghini, S., Polone, E., Corich, V., Carlot, M., Seno, F., Trovato, A., & Squartini, A. (2009). Consequences of relative cellular positioning on quorum sensing and bacterial cell-to-cell communication. *FEMS Microbiology Letters*, *292*(2), 149–161. <https://doi.org/10.1111/j.1574-6968.2008.01478.x>
- Alloing, G., Martin, B., Granadel, C., & Claverys, J. (1998). Development of competence in *Streptococcus pneumoniae*: pheromone autoinduction and control of quorum sensing by the oligopeptide permease. *Molecular Microbiology*, *29*(1), 75–83. <https://doi.org/10.1046/j.1365-2958.1998.00904.x>
- Anetzberger, C., Jung, K., Schell, U., & Jung, K. (2012). Single cell analysis of *Vibrio harveyi* uncovers functional heterogeneity in response to quorum sensing signals. *BMC Microbiology*, *12*(1), 209. <https://doi.org/10.1186/1471-2180-12-209>
- Anetzberger, C., Pirch, T., & Jung, K. (2009). Heterogeneity in quorum sensing-regulated bioluminescence of *Vibrio harveyi*. *Molecular Microbiology*, *73*(2), 267–277.
- Bahlawane, C., McIntosh, M., Krol, E., & Becker, A. (2008). *Sinorhizobium meliloti* regulator MucR couples exopolysaccharide synthesis and motility. *Molecular Plant-Microbe Interactions*, *21*(11), 1498–1509.
- Bamberger, A. (2020). Charakterisierung des ExpR-vermittelten positiven Feedbacks in der Quorum-Sensing-Antwort von *Sinorhizobium meliloti*. *Masterarbeit*.
- Bartels, F. W., McIntosh, M., Fuhrmann, A., Metzendorf, C., Plattner, P., Sewald, N., Anselmetti, D., Ros, R., & Becker, A. (2007). Effector-stimulated single molecule protein-DNA interactions of a quorum-sensing system in *Sinorhizobium meliloti*. *Biophysical Journal*, *92*(12), 4391–4400. <https://doi.org/10.1529/biophysj.106.082016>
- Bassler, B. L., & Losick, R. M. (2006). Bacterially Speaking. *Cell*, *125*(2), 237–246.
- Bauer, M., Knebel, J., Lechner, M., Pickl, P., & Frey, E. (2017). Ecological feedback in quorum-sensing microbial populations can induce heterogeneous production of autoinducers. *ELife*, *6*, 438–471.
- Baumgardt, K., Charoenpanich, P., McIntosh, M., Schikora, A., Stein, E., Thalmann, S., Kogel, K.-H., Klug, G., Becker, A., & Evguenieva-Hackenberg, E. (2014). RNase E affects the expression of the acyl-homoserine lactone synthase gene *sinI* in *Sinorhizobium meliloti*. *Journal of Bacteriology*, *196*(7), 1435–1447.
- Baumgardt, K., Smídová, K., Rahn, H., Lochnit, G., Robledo, M., & Evguenieva-Hackenberg, E. (2016). The stress-related, rhizobial small RNA RcsR1 destabilizes the autoinducer synthase encoding mRNA *sinI* in *Sinorhizobium meliloti*. *RNA Biology*, *13*(5), 486–499.

- Bettenworth, V., McIntosh, M., Becker, A., & Eckhardt, B. (2018). Front-propagation in bacterial inter-colony communication. *Chaos: An Interdisciplinary Journal of Nonlinear Science*, 28(10), 106316. <https://doi.org/10.1063/1.5040068>
- Bettenworth, V., Steinfeld, B., Duin, H., Petersen, K., Streit, W. R. W. R., Bischofs, I. B., & Becker, A. (2019). Phenotypic heterogeneity in bacterial quorum sensing systems. *Journal of Molecular Biology*, 431(23). <https://doi.org/10.1016/j.jmb.2019.04.036>
- Bettenworth, V., van Vliet, S., Turkowyd, B., Bamberger, A., Wendt, H., McIntosh, M., Steinchen, W., & Becker, A. (n.d.). Frequency modulation of a bacterial quorum sensing response. *Under Review at Nature Communications*.
- Bischofs, I. B., Hug, J. A., Liu, A. W., Wolf, D. M., & Arkin, A. P. (2009). Complexity in bacterial cell-cell communication: Quorum signal integration and subpopulation signaling in the *Bacillus subtilis* phosphorelay. *Proceedings of the National Academy of Sciences*, 106(16), 6459–6464. <https://doi.org/10.1073/pnas.0810878106>
- Boedicker, J. Q., Vincent, M. E., & Ismagilov, R. F. (2009). Microfluidic confinement of single cells of bacteria in small volumes initiates high-density behavior of quorum sensing and growth and reveals its variability. *Angewandte Chemie - International Edition*, 48(32), 5908–5911. <https://doi.org/10.1002/anie.200901550>
- Bose, J. L., Kim, U., Bartkowski, W., Gunsalus, R. P., Overley, A. M., Lyell, N. L., Visick, K. L., & Stabb, E. V. (2007). Bioluminescence in *Vibrio fischeri* is controlled by the redox-responsive regulator ArcA. *Molecular Microbiology*, 65(2), 538–553. <https://doi.org/10.1111/j.1365-2958.2007.05809.x>
- Botsford, J. L., & Harman, J. G. (1992). Cyclic AMP in prokaryotes. *Microbiological Reviews*, 56(1), 100–122. <https://doi.org/10.1128/mr.56.1.100-122.1992>
- Boyer, M., & Wisniewski-Dyé, F. (2009). Cell-cell signalling in bacteria: not simply a matter of quorum. *FEMS Microbiology Ecology*, 70(1), 1–19.
- Byers, J. T., Lucas, C., Salmond, G. P. C., & Welch, M. (2002). Nonenzymatic turnover of an *Erwinia carotovora* quorum-sensing signaling molecule. *Journal of Bacteriology*, 184(4), 1163–1171. <https://doi.org/10.1128/jb.184.4.1163-1171.2002>
- Cai, L., Dalal, C. K., & Elowitz, M. B. (2008). Frequency-modulated nuclear localization bursts coordinate gene regulation. *Nature*, 455(7212), 485–490. <https://doi.org/10.1038/nature07292>
- Cai, L., Friedman, N., & Xie, X. S. (2006). Stochastic protein expression in individual cells at the single molecule level. *Nature*, 440(7082), 358–362.
- Cárcamo-Oyarce, G., Lumjiaktase, P., Kümmerli, R., & Eberl, L. (2015). Quorum sensing triggers the stochastic escape of individual cells from *Pseudomonas putida* biofilms. *Nature Communications*, 6, 5945.
- Carlsaw, H. S., & Jaeger, J. C. (1959). *Conduction of Heat in Solids*. Oxford University Press, London.

- Case, R. J., Labbate, M., & Kjelleberg, S. (2008). AHL-driven quorum-sensing circuits: their frequency and function among the Proteobacteria. *The ISME Journal*, 2(4), 345–349. <https://doi.org/10.1038/ismej.2008.13>
- Charoenpanich, P. (2015). Regulatory mechanisms of the Sin quorum sensing system and its impact on survival of the soil-dwelling bacterium *Sinorhizobium meliloti*. *Dissertation*.
- Charoenpanich, P., Meyer, S., Becker, A., & McIntosh, M. (2013). Temporal expression program of quorum sensing-based transcription regulation in *Sinorhizobium meliloti*. *Journal of Bacteriology*, 195(14), 3224–3236.
- Chilcott, G. S., & Hughes, K. T. (2000). Coupling of flagellar gene expression to flagellar assembly in *Salmonella enterica* Serovar Typhimurium and *Escherichia coli*. *Microbiology and Molecular Biology Reviews*, 64(4), 694–708. <https://doi.org/10.1128/MMBR.64.4.694-708.2000>
- Churchill, M. E. A., & Chen, L. (2011). Structural basis of acyl-homoserine lactone-dependent signaling. *Chemical Reviews*, 111(1), 68–85. <https://doi.org/10.1021/cr1000817>
- Claverys, J., Grossiord, B., & Alloing, G. (2000). Is the Ami-AliA/B oligopeptide permease of *Streptococcus pneumoniae* involved in sensing environmental conditions? *Research in Microbiology*, 151(6), 457–463. [https://doi.org/10.1016/S0923-2508\(00\)00169-8](https://doi.org/10.1016/S0923-2508(00)00169-8)
- Cohen, D. (1966). Optimizing reproduction in a randomly varying environment. *Journal of Theoretical Biology*, 12(1), 119–129. [https://doi.org/10.1016/0022-5193\(66\)90188-3](https://doi.org/10.1016/0022-5193(66)90188-3)
- Dalal, C. K., Cai, L., Lin, Y., Rahbar, K., & Elowitz, M. B. (2014). Pulsatile dynamics in the yeast proteome. *Current Biology*, 24(18), 2189–2194. <https://doi.org/10.1016/j.cub.2014.07.076>
- Dangeard, P.-A. (1926). Recherches sur les tubercules radicaux des Légumineuses. In *Botaniste* (Vol. 16, pp. 1–275).
- De Lajudie, P., Willems, A., Pot, B., Dewettinck, D., Maestrojuan, G., Neyra, M., Collins, M. D., Dreyfus, B., Kersters, K., & Gillis, M. (1994). Polyphasic taxonomy of Rhizobia: emendation of the genus *Sinorhizobium* and description of *Sinorhizobium meliloti* comb. nov., *Sinorhizobium saheli* sp. nov., and *Sinorhizobium teranga* sp. nov. *International Journal of Systematic Bacteriology*, 44(4), 715–733. <https://doi.org/10.1099/00207713-44-4-715>
- Decho, A. W., Norman, R. S., & Visscher, P. T. (2010). Quorum sensing in natural environments: emerging views from microbial mats. *Trends in Microbiology*, 18(2), 73–80.
- Dilanji, G. E., Langebrake, J. B., De Leenheer, P., & Hagen, S. J. (2012). Quorum activation at a distance: spatiotemporal patterns of gene regulation from diffusion of an autoinducer signal. *Journal of the American Chemical Society*, 134(12), 5618–5626.
- Dilanji, G. E., Teplitski, M., & Hagen, S. J. (2014). Entropy-driven motility of *Sinorhizobium meliloti* on a semi-solid surface. *Proceedings of the Royal Society B: Biological Sciences*,

- 281(1784), 20132575.
- Duan, K., & Surette, M. G. (2007). Environmental regulation of *Pseudomonas aeruginosa* PAO1 Las and Rhl quorum-sensing systems. *Journal of Bacteriology*, 189(13), 4827–4836. <https://doi.org/10.1128/JB.00043-07>
- Dulla, G., & Lindow, S. E. (2008). Quorum size of *Pseudomonas syringae* is small and dictated by water availability on the leaf surface. *Proceedings of the National Academy of Sciences*, 105(8), 3082–3087. <https://doi.org/10.1073/pnas.0711723105>
- Dunlap, P. V. (1999). Quorum regulation of luminescence in *Vibrio fischeri*. *Journal of Molecular Microbiology and Biotechnology*, 1(1), 5–12.
- Dunlap, P. V., & Greenberg, E. P. (1985). Control of *Vibrio fischeri* luminescence gene expression in *Escherichia coli* by cyclic AMP and cyclic AMP receptor protein. *Journal of Bacteriology*, 164(1), 45–50.
- Dunlap, P. V., & Greenberg, E. P. (1988). Control of *Vibrio fischeri lux* gene transcription by a cyclic AMP receptor protein-LuxR protein regulatory circuit. *Journal of Bacteriology*, 170(9), 4040–4046. <https://doi.org/10.1128/JB.170.9.4040-4046.1988>
- Dunn, A. K., & Stabb, E. V. (2006). Beyond quorum sensing: the complexities of prokaryotic parliamentary procedures. *Analytical and Bioanalytical Chemistry*, 387(2), 391–398.
- Eberhard, A. (1972). Inhibition and activation of bacterial luciferase synthesis. *Journal of Bacteriology*, 109(3), 1101–1105. <https://doi.org/10.1128/jb.109.3.1101-1105.1972>
- Egland, P. G., Palmer, R. J., & Kolenbrander, P. E. (2004). Interspecies communication in *Streptococcus gordonii-Veillonella atypica* biofilms: Signaling in flow conditions requires juxtaposition. *Proceedings of the National Academy of Sciences*, 101(48), 16917–16922. <https://doi.org/10.1073/pnas.0407457101>
- Eickhoff, M. J., & Bassler, B. L. (2018). SnapShot: Bacterial quorum sensing. *Cell*, 174(5), 1328–1328.e1. <https://doi.org/10.1016/j.cell.2018.08.003>
- Elowitz, M. B., Levine, A. J., Siggia, E. D., & Swain, P. S. (2002). Stochastic gene expression in a single cell. *Science*, 297(5584), 1183–1186. <https://doi.org/10.1126/science.1070919>
- Feklistov, A., Sharon, B. D., Darst, S. A., & Gross, C. A. (2014). Bacterial sigma factors: A historical, structural, and genomic perspective. *Annual Review of Microbiology*, 68(1), 357–376. <https://doi.org/10.1146/annurev-micro-092412-155737>
- Flickinger, S. T., Copeland, M. F., Downes, E. M., Braasch, A. T., Tuson, H. H., Eun, Y.-J., & Weibel, D. B. (2011). Quorum sensing between *Pseudomonas aeruginosa* biofilms accelerates cell growth. *Journal of the American Chemical Society*, 133(15), 5966–5975. <https://doi.org/10.1021/ja111131f>
- Frederix, M., & Downie, J. A. (2011). Quorum sensing. In *Advances in Microbial Physiology* (1st ed., Vol. 58, pp. 23–80). Elsevier Ltd. <https://doi.org/10.1016/B978-0-12-381043-4.00002-7>

- Friedrich, W. F., & Greenberg, E. P. (1983). Glucose repression of luminescence and luciferase in *Vibrio fischeri*. *Archives of Microbiology*, 134(2), 87–91. <https://doi.org/10.1007/BF00407937>
- Fuqua, W. C., & Winans, S. C. (1994). A LuxR-LuxI type regulatory system activates *Agrobacterium* Ti plasmid conjugal transfer in the presence of a plant tumor metabolite. *Journal of Bacteriology*, 176(10), 2796–2806. <https://doi.org/10.1128/jb.176.10.2796-2806.1994>
- Fuqua, W. C., Winans, S. C., & Greenberg, E. P. (1994). Quorum sensing in bacteria: the LuxR-LuxI family of cell density-responsive transcriptional regulators. *Journal of Bacteriology*, 176(2), 269–275.
- Galibert, F., Finan, T. M., Long, S. R., Pühler, A., Abola, P., Ampe, F., Barloy-Hubler, F., Barnett, M. J., Becker, A., Boistard, P., Bothe, G., Boutry, M., Bowser, L., Buhrmester, J., Cadieu, E., Capela, D., Chain, P., Cowie, A., Davis, R. W., ... Batut, J. (2001). The composite genome of the legume symbiont *Sinorhizobium meliloti*. *Science*, 293(5530), 668–672. <https://doi.org/10.1126/science.1060966>
- Gancedo, J. M. (2013). Biological roles of cAMP: variations on a theme in the different kingdoms of life. *Biological Reviews*, 88(3), 645–668. <https://doi.org/10.1111/brv.12020>
- Gantner, S., Schmid, M., Dürr, C., Schuegger, R., Steidle, A., Hutzler, P., Langebartels, C., Eberl, L., Hartmann, A., & Dazzo, F. B. (2006). *In situ* quantitation of the spatial scale of calling distances and population density-independent N-acylhomoserine lactone-mediated communication by rhizobacteria colonized on plant roots. *FEMS Microbiology Ecology*, 56(2), 188–194. <https://doi.org/10.1111/j.1574-6941.2005.00037.x>
- Gao, M., Chen, H., Eberhard, A., Gronquist, M. R., Robinson, J. B., Rolfe, B. G., & Bauer, W. D. (2005). *sinI*- and *expR*-dependent quorum sensing in *Sinorhizobium meliloti*. *Journal of Bacteriology*, 187(23), 7931–7944. <https://doi.org/10.1128/JB.187.23.7931-7944.2005>
- Gao, M., Coggin, A., Yagnik, K., & Teplitski, M. (2012). Role of specific quorum-sensing signals in the regulation of exopolysaccharide II production within *Sinorhizobium meliloti* spreading colonies. *PLOS ONE*, 7(8), e42611-13.
- Gao, M., Tang, M., Guerich, L., Salas-Gonzalez, I., & Teplitski, M. (2015). Modulation of *Sinorhizobium meliloti* quorum sensing by Hfq-mediated post-transcriptional regulation of ExpR. *Environmental Microbiology Reports*, 7(1), 148–154.
- García-Betancur, J.-C., Goñi-Moreno, Á., Horger, T., Schott, M., Sharan, M., Eikmeier, J., Wohlmuth, B., Zerneck, A., Ohlsen, K., Kuttler, C., & López, D. (2017). Cell differentiation defines acute and chronic infection cell types in *Staphylococcus aureus*. *ELife*, 6, e28023-39.
- Garmyn, D., Gal, L., Briandet, R., Guilbaud, M., Lemaitre, J. P., Hartmann, A., & Piveteau, P. (2011). Evidence of autoinduction heterogeneity via expression of the Agr system of *Listeria monocytogenes* at the single-cell level. *Applied and Environmental Microbiology*, 77(17), 6286–6289.

- Grandclément, C., Tannières, M., Moréra, S., Dessaux, Y., & Faure, D. (2016). Quorum quenching: role in nature and applied developments. *FEMS Microbiology Reviews*, *40*(1), 86–116. <https://doi.org/10.1093/femsre/fuv038>
- Grote, J., Krysciak, D., Schorn, A., Dahlke, R. I., Soonvald, L., Muller, J., Hense, B. A., Schwarzfischer, M., Sauter, M., Schmeisser, C., & Streit, W. R. (2014). Evidence of autoinducer-dependent and -independent heterogeneous gene expression in *Sinorhizobium fredii* NGR234. *Applied and Environmental Microbiology*, *80*(18), 5572–5582.
- Grote, J., Krysciak, D., & Streit, W. R. (2015). Phenotypic heterogeneity, a phenomenon that may explain why quorum sensing does not always result in truly homogenous cell behavior. *Applied and Environmental Microbiology*, *81*(16), 5280–5289.
- Gurich, N., & González, J. E. (2009). Role of quorum sensing in *Sinorhizobium meliloti*-alfalfa symbiosis. *Journal of Bacteriology*, *191*(13), 4372–4382. <https://doi.org/10.1128/JB.00376-09>
- Ha, J. H., Hauk, P., Cho, K., Eo, Y., Ma, X., Stephens, K., Cha, S., Jeong, M., Suh, J. Y., Sintim, H. O., Bentley, W. E., & Ryu, K. S. (2018). Evidence of link between quorum sensing and sugar metabolism in *Escherichia coli* revealed via cocystal structures of LsrK and HPr. *Science Advances*, *4*(6), eaar7063-12. <https://doi.org/10.1126/sciadv.aar7063>
- Hagen, S. J., Son, M., Weiss, J. T., & Young, J. H. (2010). Bacterium in a box: sensing of quorum and environment by the LuxI/LuxR gene regulatory circuit. *Journal of Biological Physics*, *36*(3), 317–327. <https://doi.org/10.1007/s10867-010-9186-4>
- Hao, N., & O’Shea, E. K. (2012). Signal-dependent dynamics of transcription factor translocation controls gene expression. *Nature Structural & Molecular Biology*, *19*(1), 31–39. <https://doi.org/10.1038/nsmb.2192>
- Hardie, K. R., & Heurlier, K. (2008). Establishing bacterial communities by “word of mouth”: LuxS and autoinducer 2 in biofilm development. *Nature Reviews Microbiology*. <https://doi.org/10.1038/nrmicro1916>
- Hense, B. A., Kuttler, C., Müller, J., Rothballer, M., Hartmann, A., & Kreft, J.-U. (2007). Does efficiency sensing unify diffusion and quorum sensing? *Nature Reviews Microbiology*, *5*(3), 230–239.
- Hense, B. A., Müller, J., Kuttler, C., & Hartmann, A. (2012). Spatial heterogeneity of autoinducer regulation systems. *Sensors*, *12*(12), 4156–4171. <https://doi.org/10.3390/s120404156>
- Hense, B. A., & Schuster, M. (2015). Core principles of bacterial autoinducer systems. *Microbiology and Molecular Biology Reviews*, *79*(1), 153–169. <https://doi.org/10.1128/mnbr.00024-14>
- Hoang, H. H., Becker, A., & González, J. E. (2004). The LuxR homolog ExpR, in combination with the Sin quorum sensing system, plays a central role in *Sinorhizobium meliloti* gene expression. *Journal of Bacteriology*, *186*(16), 5460–5472.

- <https://doi.org/10.1128/JB.186.16.5460-5472.2004>
- Horswill, A. R., Stoodley, P., Stewart, P. S., & Parsek, M. R. (2007). The effect of the chemical, biological, and physical environment on quorum sensing in structured microbial communities. *Analytical and Bioanalytical Chemistry*, 387(2), 371–380. <https://doi.org/10.1007/s00216-006-0720-y>
- Irving, S. E., Choudhury, N. R., & Corrigan, R. M. (2020). The stringent response and physiological roles of (pp)pGpp in bacteria. *Nature Reviews Microbiology*, 19(4), 256–271. <https://doi.org/10.1038/s41579-020-00470-y>
- Jenal, U., Reinders, A., & Lori, C. (2017). Cyclic di-GMP: second messenger extraordinaire. *Nature Reviews Microbiology*, 15(5), 271–284. <https://doi.org/10.1038/nrmicro.2016.190>
- Jones, K. M., Kobayashi, H., Davies, B. W., Taga, M. E., & Walker, G. C. (2007). How rhizobial symbionts invade plants: the *Sinorhizobium - Medicago* model. *Nature Reviews Microbiology*, 5(8), 619–633. <https://doi.org/10.1038/nrmicro1705>
- Joshi, J. R., Khazanov, N., Charkowski, A., Faigenboim, A., Senderowitz, H., & Yedidia, I. (2021). Interkingdom signaling interference: the effect of plant-derived small molecules on quorum sensing in plant-pathogenic bacteria. *Annual Review of Phytopathology*, 59(1), 153–190. <https://doi.org/10.1146/annurev-phyto-020620-095740>
- Kaplan, H. B., & Greenberg, E. P. (1985). Diffusion of autoinducer is involved in regulation of the *Vibrio fischeri* luminescence system. *Journal of Bacteriology*, 163(3), 1210–1214.
- Keller, L., & Surette, M. G. (2006). Communication in bacteria: an ecological and evolutionary perspective. *Nature Reviews Microbiology*, 4(4), 249–258.
- Kempner, E. S., & Hanson, F. E. (1968). Aspects of light production by *Photobacterium fischeri*. *Journal of Bacteriology*, 95(3), 975–979. <https://doi.org/10.1128/jb.95.3.975-979.1968>
- Kim, J. M., Garcia-Alcala, M., Balleza, E., & Cluzel, P. (2020). Stochastic transcriptional pulses orchestrate flagellar biosynthesis in *Escherichia coli*. *Science Advances*, 6(6), eaax0947. <https://doi.org/10.1126/sciadv.aax0947>
- Kim, M. K., Ingremeau, F., Zhao, A., Bassler, B. L., & Stone, H. A. (2016). Local and global consequences of flow on bacterial quorum sensing. *Nature Microbiology*, 1(1), 15005–15012.
- Kirisits, M. J., Margolis, J. J., Purevdorj-Gage, B. L., Vaughan, B., Chopp, D. L., Stoodley, P., & Parsek, M. R. (2007). Influence of the hydrodynamic environment on quorum sensing in *Pseudomonas aeruginosa* biofilms. *Journal of Bacteriology*, 189(22), 8357–8360. <https://doi.org/10.1128/JB.01040-07>
- Kleerebezem, M., Quadri, L. E. N., Kuipers, O. P., & De Vos, W. M. (1997). Quorum sensing by peptide pheromones and two-component signal-transduction systems in Gram-positive bacteria. *Molecular Microbiology*, 24(5), 895–904. <https://doi.org/10.1046/j.1365-2958.1997.4251782.x>

- Krol, E., & Becker, A. (2004). Global transcriptional analysis of the phosphate starvation response in *Sinorhizobium meliloti* strains 1021 and 2011. *Molecular Genetics and Genomics*, 272(1), 1–17. <https://doi.org/10.1007/s00438-004-1030-8>
- Krol, E., & Becker, A. (2011). ppGpp in *Sinorhizobium meliloti*: biosynthesis in response to sudden nutritional downshifts and modulation of the transcriptome. *Molecular Microbiology*, 81(5), 1233–1254.
- Krol, E., & Becker, A. (2014). Rhizobial homologs of the fatty acid transporter FadL facilitate perception of long-chain acyl-homoserine lactone signals. *Proceedings of the National Academy of Sciences*, 111(29), 10702–10707.
- Lang, J., & Faure, D. (2014). Functions and regulation of quorum-sensing in *Agrobacterium tumefaciens*. *Frontiers in Plant Science*, 5, 1–13. <https://doi.org/10.3389/fpls.2014.00014>
- Langebrake, J. B., Dilanji, G. E., Hagen, S. J., & De Leenheer, P. (2014). Traveling waves in response to a diffusing quorum sensing signal in spatially-extended bacterial colonies. *Journal of Theoretical Biology*, 363, 53–61.
- Lehner, B. (2008). Selection to minimise noise in living systems and its implications for the evolution of gene expression. *Molecular Systems Biology*, 4(1), 170. <https://doi.org/10.1038/msb.2008.11>
- Lenz, P., & Søgaard-Andersen, L. (2011). Temporal and spatial oscillations in bacteria. *Nature Reviews Microbiology*, 9(8), 565–577. <https://doi.org/10.1038/nrmicro2612>
- Levine, J. H., Lin, Y., & Elowitz, M. B. (2013). Functional roles of pulsing in genetic circuits. *Science*, 342(6163), 1193–1200.
- Li, B., Li, N., Wang, F., Guo, L., Huang, Y., Liu, X., Wei, T., Zhu, D., Liu, C., Pan, H., Xu, S., Wang, H.-W., & Gu, L. (2012). Structural insight of a concentration-dependent mechanism by which YdiV inhibits *Escherichia coli* flagellum biogenesis and motility. *Nucleic Acids Research*, 40(21), 11073–11085. <https://doi.org/10.1093/nar/gks869>
- Locke, J. C. W., Young, J. W., Fontes, M., Jimenez, M. J. H., & Elowitz, M. B. (2011). Stochastic pulse regulation in bacterial stress response. *Science*, 334(6054), 366–369. <https://doi.org/10.1126/science.1208144>
- Lonetto, M. A., Donohue, T. J., Gross, C. A., & Buttner, M. J. (2019). Discovery of the extracytoplasmic function σ factors. *Molecular Microbiology*, 112(2), 348–355. <https://doi.org/10.1111/mmi.14307>
- Lumjiaktase, P., Aguilar, C., Battin, T., Riedel, K., & Eberl, L. (2010). Construction of self-transmissible green fluorescent protein-based biosensor plasmids and their use for identification of N-acyl homoserine-producing bacteria in lake sediments. *Applied and Environmental Microbiology*, 76(18), 6119–6127. <https://doi.org/10.1128/AEM.00677-10>
- Lyell, N. L., Colton, D. M., Bose, J. L., Tumen-Velasquez, M. P., Kimbrough, J. H., & Stabb, E. V. (2013). Cyclic AMP receptor protein regulates pheromone-mediated

- bioluminescence at multiple levels in *Vibrio fischeri* ES114. *Journal of Bacteriology*, *195*(22), 5051–5063. <https://doi.org/10.1128/JB.00751-13>
- Maamar, H., & Dubnau, D. (2005). Bistability in the *Bacillus subtilis* K-state (competence) system requires a positive feedback loop. *Molecular Microbiology*, *56*(3), 615–624. <https://doi.org/10.1111/j.1365-2958.2005.04592.x>
- Marketon, M. M., Gronquist, M. R., Eberhard, A., & González, J. E. (2002). Characterization of the *Sinorhizobium meliloti* *sinR/sinI* locus and the production of novel N-acyl homoserine lactones. *Journal of Bacteriology*, *184*(20), 5686–5695. <https://doi.org/10.1128/JB.184.20.5686-5695.2002>
- McIntosh, M., Krol, E., & Becker, A. (2008). Competitive and cooperative effects in quorum-sensing-regulated galactoglucan biosynthesis in *Sinorhizobium meliloti*. *Journal of Bacteriology*, *190*(15), 5308–5317. <https://doi.org/10.1128/JB.00063-08>
- McIntosh, M., Meyer, S., & Becker, A. (2009). Novel *Sinorhizobium meliloti* quorum sensing positive and negative regulatory feedback mechanisms respond to phosphate availability. *Molecular Microbiology*, *74*(5), 1238–1256.
- Meyer, A., Megerle, J. A., Kuttler, C., Müller, J., Aguilar, C., Eberl, L., Hense, B. A., & Rädler, J. O. (2012). Dynamics of AHL mediated quorum sensing under flow and non-flow conditions. *Physical Biology*, *50*(13), 133001–133011.
- Milo, R., & Phillips, R. (2016). Cell biology by the numbers. Garland Science, Taylor & Francis Group, LLC.
- Milton, D. L. (2006). Quorum sensing in vibrios: Complexity for diversification. *International Journal of Medical Microbiology*, *296*(2–3), 61–71. <https://doi.org/10.1016/j.ijmm.2006.01.044>
- Monnet, V., Juillard, V., & Gardan, R. (2014). Peptide conversations in Gram-positive bacteria. *Critical Reviews in Microbiology*, *42*(3), 1–13. <https://doi.org/10.3109/1040841X.2014.948804>
- Mukherjee, S., & Bassler, B. L. (2019). Bacterial quorum sensing in complex and dynamically changing environments. *Nature Reviews Microbiology*, *17*(6), 371–382. <https://doi.org/10.1038/s41579-019-0186-5>
- Müller, J., Kuttler, C., Hense, B. A., Rothballer, M., & Hartmann, A. (2006). Cell–cell communication by quorum sensing and dimension-reduction. *Journal of Mathematical Biology*, *53*(4), 672–702.
- Mutlu, A., Trauth, S., Ziesack, M., Nagler, K., Bergeest, J. P., Rohr, K., Becker, N., Höfer, T., & Bischofs, I. B. (2018). Phenotypic memory in *Bacillus subtilis* links dormancy entry and exit by a spore quantity-quality tradeoff. *Nature Communications*, *9*(1), 69. <https://doi.org/10.1038/s41467-017-02477-1>
- Nealson, K. H. (1977). Autoinduction of bacterial luciferase. *Archives of Microbiology*, *112*(1), 73–79. <https://doi.org/10.1007/BF00446657>

- Nealson, K. H., Eberhard, A., & Hastings, J. W. (1972). Catabolite repression of bacterial bioluminescence: functional implications. *Proceedings of the National Academy of Sciences*, *69*(5), 1073–1076. <https://doi.org/10.1073/pnas.69.5.1073>
- Nealson, K. H., Platt, T., & Hastings, J. W. (1970). Cellular control of the synthesis and activity of the bacterial luminescent system. *Journal of Bacteriology*, *104*(1), 313–322.
- Neiditch, M. B., Capodagli, G. C., Prehna, G., & Federle, M. J. (2017). Genetic and structural analyses of RRNPP intercellular peptide signaling of Gram-positive bacteria. *Annual Review of Genetics*, *51*(1), 311–333.
- Newman, J. R. S., Ghaemmighami, S., Ihmels, J., Breslow, D. K., Noble, M., DeRisi, J. L., & Weissman, J. S. (2006). Single-cell proteomic analysis of *S. cerevisiae* reveals the architecture of biological noise. *Nature*, *441*(7095), 840–846. <https://doi.org/10.1038/nature04785>
- Oehler, S., Eismann, E. R., Krämer, H., & Müller-Hill, B. (1990). The three operators of the *lac* operon cooperate in repression. *The EMBO Journal*, *9*(4), 973–979. <https://doi.org/10.1002/j.1460-2075.1990.tb08199.x>
- Paczkowski, J. E., Mukherjee, S., McCready, A. R., Cong, J.-P., Aquino, C. J., Kim, H., Henke, B. R., Smith, C. D., & Bassler, B. L. (2017). Flavonoids suppress *Pseudomonas aeruginosa* virulence through allosteric inhibition of quorum-sensing receptors. *Journal of Biological Chemistry*, *292*(10), 4064–4076. <https://doi.org/10.1074/jbc.M116.770552>
- Paget, M. S. (2015). Bacterial sigma factors and anti-sigma factors: Structure, function and distribution. *Biomolecules*, *5*(3), 1245–1265. <https://doi.org/10.3390/biom5031245>
- Pakula, R., & Walczak, W. (1963). On the nature of competence of transformable streptococci. *Journal of General Microbiology*, *31*(1), 125–133. <https://doi.org/10.1099/00221287-31-1-125>
- Papenfort, K., & Bassler, B. L. (2016). Quorum sensing signal–response systems in Gram-negative bacteria. *Nature Reviews Microbiology*, *14*(9), 576–588. <https://doi.org/10.1038/nrmicro.2016.89>
- Park, J., Dies, M., Lin, Y., Hormoz, S., Smith-Unna, S. E., Quinodoz, S., Hernández-Jiménez, M. J., Garcia-Ojalvo, J., Locke, J. C. W., & Elowitz, M. B. (2018). Molecular time sharing through dynamic pulsing in single cells. *Cell Systems*, *6*(2), 216–229.e15. <https://doi.org/10.1016/j.cels.2018.01.011>
- Patange, O., Schwall, C., Jones, M., Villava, C., Griffith, D. A., Phillips, A., & Locke, J. C. W. (2018). *Escherichia coli* can survive stress by noisy growth modulation. *Nature Communications*, *9*(1), 5333. <https://doi.org/10.1038/s41467-018-07702-z>
- Patel, K., Rodriguez, C., Stabb, E. V., & Hagen, S. J. (2021). Wavelike propagation of quorum activation through a spatially distributed bacterial population under natural regulation. *Physical Biology*, *18*(4), 046008. <https://doi.org/10.1088/1478-3975/ac02ac>
- Pearson, J. P., Van Delden, C., & Iglewski, B. H. (1999). Active efflux and diffusion are

- involved in transport of *Pseudomonas aeruginosa* cell-to-cell signals. *Journal of Bacteriology*, *181*(4), 1203–1210. <https://doi.org/10.1128/jb.181.4.1203-1210.1999>
- Pedraza, J. H., & Van Oudenaarden, A. (2005). Noise propagations in gene networks. *Science*, *307*(5717), 1965–1969. <https://doi.org/10.1126/science.1109090>
- Pellock, B. J., Teplitski, M., Boinay, R. P., Bauer, W. D., & Walker, G. C. (2002). A LuxR homolog controls production of symbiotically active extracellular polysaccharide II by *Sinorhizobium meliloti*. *Journal of Bacteriology*, *184*(18), 5067–5076. <https://doi.org/10.1128/JB.184.18.5067-5076.2002>
- Pérez, J., Jiménez-Zurdo, J. I., Martínez-Abarca, F., Millán, V., Shimkets, L. J., & Muñoz-Dorado, J. (2014). Rhizobial galactoglucan determines the predatory pattern of *Myxococcus xanthus* and protects *Sinorhizobium meliloti* from predation. *Environmental Microbiology*, *16*(7), 2341–2350.
- Phillips, R., Kondev, J., & Theriot, J. (2009). *Physical Biology of the Cell*. Garland Science, Taylor & Francis Group, LLC.
- Piper, K. R., Beck Von Bodman, S., Hwang, I., & Farrand, S. K. (1999). Hierarchical gene regulatory systems arising from fortuitous gene associations: controlling quorum sensing by the opine regulon in *Agrobacterium*. *Molecular Microbiology*, *32*(5), 1077–1089. <https://doi.org/10.1046/j.1365-2958.1999.01422.x>
- Platt, T. G., & Fuqua, W. C. (2010). What's in a name? The semantics of quorum sensing. *Trends in Microbiology*, *18*(9), 383–387. <https://doi.org/10.1016/j.tim.2010.05.003>
- Popat, R., Cornforth, D. M., McNally, L., & Brown, S. P. (2014). Collective sensing and collective responses in quorum-sensing bacteria. *Journal of The Royal Society Interface*, *12*(103), 20140882. <https://doi.org/10.1098/rsif.2014.0882>
- Pradhan, B. B., & Chatterjee, S. (2014). Reversible non-genetic phenotypic heterogeneity in bacterial quorum sensing. *Molecular Microbiology*, *92*(3), 557–569.
- Prudhomme, M., Attaiech, L., Sanchez, G., Martin, B., & Claverys, J. P. (2006). Antibiotic stress induces genetic transformability in the human pathogen *Streptococcus pneumoniae*. *Science*, *313*(5783), 89–92. <https://doi.org/10.1126/science.1127912>
- Raj, A., & van Oudenaarden, A. (2008). Nature, nurture, or chance: stochastic gene expression and its consequences. *Cell*, *135*(2), 216–226.
- Raser, J. M., & O'Shea, E. K. (2005). Noise in gene expression: origins, consequences, and control. *Science*, *309*(5743), 2010–2013. <https://doi.org/10.1126/science.1105891>
- Redfield, R. J. (2002). Is quorum sensing a side effect of diffusion sensing? *Trends in Microbiology*, *10*(8), 365–370.
- Römling, U., Galperin, M. Y., & Gomelsky, M. (2013). Cyclic di-GMP: the first 25 years of a universal bacterial second messenger. *Microbiology and Molecular Biology Reviews*, *77*(1), 1–52. <https://doi.org/10.1128/mnbr.00043-12>

- Ruby, E. G., & McFall-Ngai, M. J. (1992). A squid that glows in the night: development of an animal-bacterial mutualism. *Journal of Bacteriology*, *174*(15), 4865–4870. <https://doi.org/10.1128/jb.174.15.4865-4870.1992>
- Sallet, E., Roux, B., Sauviac, L., Jardinaud, M. F., Carrère, S., Faraut, T., De Carvalho-Niebel, F., Gouzy, J., Gamas, P., Capela, D., Bruand, C., & Schiex, T. (2013). Next-generation annotation of prokaryotic genomes with EuGene-P: application to *Sinorhizobium meliloti* 2011. *DNA Research*, *20*(4), 339–353. <https://doi.org/10.1093/dnares/dst014>
- Sassi, A. S., Garcia-Alcala, M., Kim, J. M., Cluzel, P., & Tu, Y. (2020). Filtering input fluctuations in intensity and in time underlies stochastic transcriptional pulses without feedback. *Proceedings of the National Academy of Sciences*, *117*(43), 26608–26615. <https://doi.org/10.1073/pnas.2010849117>
- Schäper, S., Krol, E., Skotnicka, D., Kaefer, V., Hilker, R., Søgaard-Andersen, L., & Becker, A. (2016). Cyclic di-GMP regulates multiple cellular functions in the symbiotic alphaproteobacterium *Sinorhizobium meliloti*. *Journal of Bacteriology*, *198*(3), 521–535.
- Schauder, S., & Bassler, B. L. (2001). The languages of bacteria. *Genes & Development*, *15*(12), 1468–1480.
- Schlüter, J.-P., Czuppon, P., Schauer, O., Pfaffelhuber, P., McIntosh, M., & Becker, A. (2015). Classification of phenotypic subpopulations in isogenic bacterial cultures by triple promoter probing at single cell level. *Journal of Biotechnology*, *198*, 3–14.
- Seeley, T. D. (2010). *Honeybee Democracy*. Princeton University Press, Princeton and Oxford.
- Seeley, T. D., & Buhrman, S. C. (2001). Nest-site selection in honey bees: how well do swarms implement the "best-of- N " decision rule? *Behavioral Ecology and Sociobiology*, *49*(5), 416–427. <https://doi.org/10.1007/s002650000299>
- Seeley, T. D., & Visscher, P. K. (2004). Group decision making in nest-site selection by honey bees. *Apidologie*, *35*(2), 101–116. <https://doi.org/10.1051/apido:2004004>
- Seeley, T. D., & Visscher, P. K. (2008). Sensory coding of nest-site value in honeybee swarms. *Journal of Experimental Biology*, *211*(23), 3691–3697. <https://doi.org/10.1242/jeb.021071>
- Septer, A. N., & Stabb, E. V. (2012). Coordination of the Arc regulatory system and pheromone-mediated positive feedback in controlling the *Vibrio fischeri lux* operon. *PLoS ONE*, *7*(11), e49590. <https://doi.org/10.1371/journal.pone.0049590>
- Siguier, P., Gourgouyere, E., & Chandler, M. (2014). Bacterial insertion sequences: their genomic impact and diversity. *FEMS Microbiology Reviews*, *38*(5), 865–891. <https://doi.org/10.1111/1574-6976.12067>
- Silander, O. K., Nikolic, N., Zaslaver, A., Bren, A., Kikoin, I., Alon, U., & Ackermann, M. (2012). A genome-wide analysis of promoter-mediated phenotypic noise in *Escherichia coli*. *PLoS Genetics*, *8*(1), e1002443.
- Smirnov, E., Hornáček, M., Vacík, T., Cmarko, D., & Raška, I. (2018). Discontinuous

- transcription. *Nucleus*, 9(1), 149–160. <https://doi.org/10.1080/19491034.2017.1419112>
- Smith, J. L., Fratamico, P. M., & Novak, J. S. (2004). Quorum sensing: a primer for food microbiologists. *Journal of Food Protection*, 67(5), 1053–1070. <https://doi.org/10.4315/0362-028X-67.5.1053>
- Smits, W. K., Eschevins, C. C., Susanna, K. A., Bron, S., Kuipers, O. P., & Hamoen, L. W. (2005). Stripping *Bacillus* : ComK auto-stimulation is responsible for the bistable response in competence development. *Molecular Microbiology*, 56(3), 604–614. <https://doi.org/10.1111/j.1365-2958.2005.04488.x>
- Smits, W. K., Kuipers, O. P., & Veening, J.-W. (2006). Phenotypic variation in bacteria: the role of feedback regulation. *Nature Reviews Microbiology*, 4(4), 259–271.
- Stabb, E. V. (2018). Could positive feedback enable bacterial pheromone signaling to coordinate behaviors in response to heterogeneous environmental cues? *MBio*, 9(3). <https://doi.org/10.1128/mBio.00098-18>
- Steinchen, W., & Bange, G. (2016). The magic dance of the alarmones (p)ppGpp. *Molecular Microbiology*, 101(4), 531–544. <https://doi.org/10.1111/mmi.13412>
- Stewart, P. S. (2003). Diffusion in biofilms. *Journal of Bacteriology*, 185(5), 1485–1491.
- Stewart, P. S., & Franklin, M. J. (2008). Physiological heterogeneity in biofilms. *Nature Reviews Microbiology*, 6(3), 199–210.
- Swain, P. S., Elowitz, M. B., & Siggia, E. D. (2002). Intrinsic and extrinsic contributions to stochasticity in gene expression. *Proceedings of the National Academy of Sciences*, 99(20), 12795–12800. <https://doi.org/10.1073/pnas.162041399>
- Takaya, A., Erhardt, M., Karata, K., Winterberg, K., Yamamoto, T., & Hughes, K. T. (2012). YdiV: a dual function protein that targets FlhDC for ClpXP-dependent degradation by promoting release of DNA-bound FlhDC complex. *Molecular Microbiology*, 83(6), 1268–1284. <https://doi.org/10.1111/j.1365-2958.2012.08007.x>
- Taniguchi, Y., Choi, P. J., Li, G.-W., Chen, H., Babu, M., Hearn, J., Emili, A., & Xie, X. S. (2010). Quantifying *E. coli* proteome and transcriptome with single-molecule sensitivity in single cells. *Science*, 329(5991), 533–538. <https://doi.org/10.1126/science.1188308>
- Teplitski, M., Eberhard, A., Gronquist, M. R., Gao, M., Robinson, J. B., & Bauer, W. D. (2003). Chemical identification of N-acyl homoserine lactone quorum-sensing signals produced by *Sinorhizobium meliloti* strains in defined medium. *Archives of Microbiology*, 180(6), 494–497. <https://doi.org/10.1007/s00203-003-0612-x>
- Tomasz, A. (1965). Control of the competent state in *Pneumococcus* by a hormone-like cell product: an example for a new type of regulatory mechanism in bacteria. *Nature*, 208, 155–159.
- Tomasz, A., & Hotchkiss, R. D. (1964). Regulation of the transformability of pneumococcal cultures by macromolecular cell products. *Proceedings of the National Academy of Sciences*, 51(3), 480–487. <https://doi.org/10.1073/pnas.51.3.480>

- Tunnacliffe, E., & Chubb, J. R. (2020). What is a transcriptional burst? *Trends in Genetics*, 36(4), 288–297. <https://doi.org/10.1016/j.tig.2020.01.003>
- Uden, G. (2014). Regulation des Stoffwechsels und des Zellaufbaus von Bakterien. In G. Fuchs (Ed.), *Allgemeine Mikrobiologie*. Georg Thieme Verlag.
- van Gestel, J., Vlamakis, H., & Kolter, R. (2015). From cell differentiation to cell collectives: *Bacillus subtilis* uses division of labor to migrate. *PLoS Biology*, 13(4), e1002141. <https://doi.org/10.1371/journal.pbio.1002141>
- Vannini, A. (2002). The crystal structure of the quorum sensing protein TraR bound to its autoinducer and target DNA. *The EMBO Journal*, 21(17), 4393–4401. <https://doi.org/10.1093/emboj/cdf459>
- Veening, J.-W., Hamoen, L. W., & Kuipers, O. P. (2005). Phosphatases modulate the bistable sporulation gene expression pattern in *Bacillus subtilis*. *Molecular Microbiology*, 56(6), 1481–1494. <https://doi.org/10.1111/j.1365-2958.2005.04659.x>
- Veening, J.-W., Smits, W. K., & Kuipers, O. P. (2008). Bistability, epigenetics, and bet-hedging in bacteria. *Annual Review of Microbiology*, 62(1), 193–210. <https://doi.org/10.1146/annurev.micro.62.081307.163002>
- Wada, T., Hatamoto, Y., & Kutsukake, K. (2012). Functional and expressional analyses of the anti-FlhD₄C₂ factor gene *ydiV* in *Escherichia coli*. *Microbiology (United Kingdom)*, 158(6), 1533–1542. <https://doi.org/10.1099/mic.0.056036-0>
- Wada, T., Morizane, T., Abo, T., Tominaga, A., Inoue-Tanaka, K., & Kutsukake, K. (2011). EAL domain protein YdiV acts as an anti-FlhD₄C₂ factor responsible for nutritional control of the flagellar regulon in *Salmonella enterica* Serovar Typhimurium. *Journal of Bacteriology*, 193(7), 1600–1611. <https://doi.org/10.1128/JB.01494-10>
- Wang, Z., & Zhang, J. (2011). Impact of gene expression noise on organismal fitness and the efficacy of natural selection. *Proceedings of the National Academy of Sciences*, 108(16), E67–E76.
- Watson, W. T., Minogue, T. D., Val, D. L., von Bodman, S. B., & Churchill, M. E. A. (2002). Structural basis and specificity of acyl-homoserine lactone signal production in bacterial quorum sensing. *Molecular Cell*, 9(3), 685–694. [https://doi.org/10.1016/S1097-2765\(02\)00480-X](https://doi.org/10.1016/S1097-2765(02)00480-X)
- West, S. A., & Cooper, G. A. (2016). Division of labour in microorganisms: an evolutionary perspective. *Nature Reviews Microbiology*, 14(11), 716–723. <https://doi.org/10.1038/nrmicro.2016.111>
- West, S. A., Griffin, A. S., Gardner, A., & Diggle, S. P. (2006). Social evolution theory for microorganisms. *Nature Reviews Microbiology*, 4(8), 597–607.
- Whiteley, M., Diggle, S. P., & Greenberg, E. P. (2017). Progress in and promise of bacterial quorum sensing research. *Nature*, 551(7680), 313–320. <https://doi.org/10.1038/nature24624>

- Xavier, K. B., & Bassler, B. L. (2005). Regulation of uptake and processing of the quorum-sensing autoinducer AI-2 in *Escherichia coli*. *Journal of Bacteriology*, *187*(1), 238–248. <https://doi.org/10.1128/JB.187.1.238-248.2005>
- Yates, E. A., Philipp, B., Buckley, C., Atkinson, S., Chhabra, S. R., Sockett, R. E., Goldner, M., Dessaux, Y., Cámara, M., Smith, H., & Williams, P. (2002). N -Acylhomoserine lactones undergo lactonolysis in a pH-, temperature-, and acyl chain length-dependent manner during growth of *Yersinia pseudotuberculosis* and *Pseudomonas aeruginosa*. *Infection and Immunity*, *70*(10), 5635–5646. <https://doi.org/10.1128/IAI.70.10.5635-5646.2002>
- Yu, J., Xiao, J., Ren, X., Lao, K., & Xie, X. S. (2006). Probing gene expression in live cells, one protein molecule at a time. *Science*, *311*(5767), 1600–1603.
- Zatakia, H. M., Nelson, C. E., Syed, U. J., & Scharf, B. E. (2014). ExpR coordinates the expression of symbiotically important, bundle-forming Flp pili with quorum sensing in *Sinorhizobium meliloti*. *Applied and Environmental Microbiology*, *80*(8), 2429–2439. <https://doi.org/10.1128/AEM.04088-13>
- Zhang, R., Pappas, K. M., Brace, J. L., Miller, P. C., Oulmassov, T., Molyneaux, J. M., Anderson, J. C., Bashkin, J. K., Winans, S. C., & Joachimiak, A. (2002). Structure of a bacterial quorum-sensing transcription factor complexed with pheromone and DNA. *Nature*, *417*(6892), 971–974. <https://doi.org/10.1038/nature00833>
- Zhang, Z., Claessen, D., & Rozen, D. E. (2016). Understanding microbial divisions of labor. *Frontiers in Microbiology*, *7*(DEC), 1–8. <https://doi.org/10.3389/fmicb.2016.02070>

Appendix

Eidesstattliche Erklärung / *Statutory declaration*

Ich versichere, dass ich die hier vorgelegte Dissertation mit dem Titel

I declare that I have composed the here-submitted thesis entitled

„Quorum sensing dynamics in the α -proteobacterium *Sinorhizobium meliloti* at the single-cell and population level“

selbstständig und ohne unerlaubte Hilfe angefertigt, mich dabei keiner anderen als der von mir ausdrücklich bezeichneten Quellen und Hilfsmittel bedient und, wenn Bezug auf die Arbeit anderer genommen wird, dies entsprechend gekennzeichnet habe. Meine Beiträge zu Arbeiten, die gemeinsam mit anderen Autoren veröffentlicht wurden, werden explizit aufgeführt.

by myself and without external assistance, that I have not used other sources than those indicated, and that I have given appropriate credit where reference is made to the work of others. My contributions to jointly-authored publications are explicitly stated.

Diese Dissertation wurde in der jetzigen oder einer ähnlichen Form noch bei keiner anderen Hochschule eingereicht und hat keinen sonstigen Prüfungszwecken gedient.

This thesis, in its current or a similar version, has not been submitted to any other university and did not serve for any other academic degree.

Marburg, 1. March 2022

Vera Bettenworth

Acknowledgements

First and foremost, I want to thank Anke Becker and Matthew McIntosh for the opportunity to conduct my doctorate in the Becker laboratory and on this exciting topic; as a single mum of three small kids I am sure I was not the most obvious candidate. Furthermore, I am very grateful for the freedom they gave me to follow my own interests and ideas.

I also want to express my profound gratitude to Bruno Eckhardt – for numerous helpful and inspiring discussions, for the confidence he had in me, and for his friendship.

I am very grateful to my wonderful collaborators: Simon van Vliet who enabled me to quantitatively analyze what until then I could only see and describe, but not count or measure; Bartosz Turkowyd and Ulrike Endesfelder who enabled me to count such a difficult molecule as SinR – this information was extremely helpful; Annika Bamberger who showed great endurance in performing what felt like innumerable EMSAs; and Wieland Steinchen who provided me with many insights into protein biochemistry and enabled me to test my hypotheses on the ExpR-AHL-mediated positive feedback.

Similarly, I want to thank all former and present members of the Becker laboratory, in particular Matthew McIntosh and Elizaveta Krol, for sharing strains and plasmids, for advice on experiments, for nice discussions, and generally for the friendly atmosphere in the lab; special thanks go to Matthew McIntosh for introducing me to *S. meliloti* and the Sin quorum sensing system, to Andreas Kautz and Patrick Manz for introducing me to fluorescence microscopy, and to Stephan Ringshandl for introducing me to some more sophisticated Excel tools.

Moreover, I want to thank Martin Ackermann, Florian Altegoer, Alexander Anders, Ilka Bischofs, Moritz Bünemann, Alma dal Co, Gert Bange, Knut Drescher, Silvia González Sierra, Peter Graumann, Raimo Hartmann, Rogelio Hernandez-Tamayo, Georg Hochberg, Hannah Jeckel, Peter Lenz, Gabriele Malengo, Christoph Mayer, Manuel Osorio-Valeriano, Dorota Skotnicka, Victor Sourjik, Martin Thanbichler, Lucia Vidakovic, Bastian Vögeli and Barbara Waidner for fruitful discussions and/or help with methods. I am grateful to Fabienne Chevance and Kelly T. Hughes for proof-reading the paragraphs discussing pulsatile *E. coli* flagellar gene expression, and to Wieland Steinchen for general proof-reading.

I also want to thank my former superior at the “Neue Zürcher Zeitung”, Heidi Blattmann, for her enthusiasm on my decision to do a doctorate after all – that was very encouraging.

I am exceedingly grateful to my family, neighbors and friends – Marlies & Siegfried Bettenworth, Gisela & Ulrike Hensch, Anne & Michael Haas, the whole von Kanitz family, Anastasia Demir and Wieland Steinchen – for being so wonderful with my children. Without their help, this work would not have been possible.

My deepest gratitude belongs to my daughters, for enduring my frequent absence and absentmindedness, for nevertheless turning out so wonderful, and for their unwavering love.

Curriculum vitae

Diese Seite enthält persönliche Daten. Sie ist deshalb nicht Bestandteil der Online-Veröffentlichung.